

Developing Peptide Modified Novel Bioactive Materials for Bone Tissue Engineering Applications

Submitted to the Graduate School of Natural and Applied Sciences
in partial fulfillment of the requirements for the degree of

Doctor of Philosophy

in Biomedical Technologies

by

Günnur Pulat

ORCID 0000-0003-0895-4768

June, 2021

This is to certify that we have read the thesis **Developing Peptide Modified Novel Bioactive Materials for Bone Tissue Engineering Applications** submitted by **Günnur Pulat**, and it has been judged to be successful, in scope and in quality, at the defense exam and accepted by our jury as a DOCTORAL THESIS.

APPROVED BY:

Advisor: **Assoc. Prof. Dr. Ozan Karaman**
İzmir Kâtip Çelebi University

Committee Members:

Assoc. Prof. Dr. Utku Kürşat Ercan
İzmir Kâtip Çelebi University

Assoc. Prof. Dr. Aylin Şendemir
Ege University

Assoc. Prof. Sinan Güven
Dokuz Eylül University

Assist. Prof. Dr. Didem Şen Karaman
İzmir Kâtip Çelebi University

Date of Defense: June 14, 2021

Declaration of Authorship

I, **Günnur Pulat**, declare that this thesis titled **Developing Peptide Modified Novel Bioactive Materials for Bone Tissue Engineering Applications** and the work presented in it are my own. I confirm that:

- This work was done wholly or mainly while in candidature for the Master's / Doctoral degree at this university.
- Where any part of this thesis has previously been submitted for a degree or any other qualification at this university or any other institution, this has been clearly stated.
- Where I have consulted the published work of others, this is always clearly attributed.
- Where I have quoted from the work of others, the source is always given. This thesis is entirely my own work, with the exception of such quotations.
- I have acknowledged all major sources of assistance.
- Where the thesis is based on work done by myself jointly with others, I have made clear exactly what was done by others and what I have contributed myself.

Signature:

Date: 14.06.2021

Developing Peptide Modified Novel Bioactive Materials for Bone Tissue Engineering Applications

Abstract

In bone tissue engineering, biomimetic scaffolds that can generate a specific cellular response and form bone tissue through biological recognition can be developed by using extracellular matrix (ECM) mimetic peptides. The main focus of this dissertation is the development of a peptide-modified novel biomimetic approach to design scaffolds for bone tissue engineering. In the first part, the surface of electrospun poly (lactide-co-glycolide) (PLGA) scaffolds was modified with cold atmospheric plasma (CAP) to induce more carboxylic groups and increase the biomineralization of NFs by increase glutamic acid (GLU) peptide conjugation. Mineralization, surface roughness, and wettability of CAP treated and GLU peptide conjugated NFs and the effect of surface modification on human mesenchymal stem cells (hMSC) proliferation were investigated. Consequently, CAP treatment-induced bio-functional peptide conjugation and biomineralization. In the second part, KLD (KLDLKLDLKLDL) self-assembled peptide (SAP) hydrogels with short bioactive motif O1 (EEGGC) and O2 (EEEEEE) were self-assembled in different concentrations (0.5%, 1%, and 2%) to enhance osteogenesis and biomineralization of injectable SAP hydrogels with the capability of being injected to bone defects. Compared to the KLD scaffold, we found that these designed bioactive peptide scaffolds significantly promoted key osteogenic markers expression levels determined by real-time PCR and immunofluorescence analysis. In the third part, we aimed to develop biomimetic SAP hydrogels that allow

the rapid formation of a vascular structure and determine the efficacy of IKVAV (V1) and YIGSR (V2) bioactive peptides integrated KLD SAP hydrogel on in vitro vascularization. Two SAP hydrogels which are KLD-V1 and KLD-V2 were designed and produced at 0.5% and 1% concentrations. The proliferation of hMSC/HUVEC co-culture increased with the addition of laminin-derived peptides to KLD. The immunofluorescent staining and RT-qPCR were performed to analyze PECAM, vWf, and Ve-cadherin proteins and gene expression, respectively. Laminin-derived peptide-functionalized SAP improved the vasculogenesis potential. KLD-V2 sharply increased proliferation and vascularization compared to KLD-V1. In the fourth part, a novel multifunctional scaffold that can induce both bone tissue and vascular formation and take the defect shape via injection was developed by SAP hydrogels for osseointegration of dental implants. The efficacy of using multi-functional SAP hydrogel on dental implant osseointegration was determined with resonance frequency analysis, reverse torque right after in-vivo study. Injectable multifunctional scaffolds accelerated dental implant osseointegration. In the last chapter, a vascularized bone tissue model by using GLU peptide conjugated stem cell-laden electrospun nanofibers reinforced SAP hydrogels with a vasculogenic epitope (YIGSR), which can support osteogenic and vasculogenic differentiation in vitro was proposed for bone defects. After physical characterizations, the osteogenic differentiation was evaluated by DNA quantification, calcium and ALP assay, q-PCR, immunofluorescent staining, and vasculogenic differentiation were evaluated by performing q-PCR and immunofluorescent staining. The developed bone model has been shown to significantly increase osteogenic and vasculogenic differentiation. Overall, the findings in this thesis will aid in further optimization of biofunctionalized biomaterials to support stem cell-based bone repair and regeneration. It is also believed that such findings will help researchers to design better biomimetic scaffolds to be translated into the clinic to improve bone healing processes.

Keywords: Bone tissue engineering, Nanofibers, Self-Assembled peptide, Hydrogels, Osseointegration

Kemik Doku Mühendisliği Uygulamaları için Peptit ile Modifiye Edilmiş Özgün Biyoaktif Malzemelerin Geliştirilmesi

ÖZ

Kemik doku mühendisliğinde, hücre dışı matris (HDM) benzeri peptitler kullanılarak biyolojik tanıma yoluyla belirli bir hücresel yanıt ve kemik dokusu oluşturabilen biyobenzer yapı iskeleleri geliştirilebilir. Bu tezin ana odak noktası, kemik dokusu mühendisliği için yapı iskeleleri tasarlamak üzere peptit ile modifiye edilmiş yeni bir biyobenzer yaklaşımın geliştirilmesidir. İlk bölümde, elektro-eğirme yöntemi ile üretilmiş poli (laktid-ko-glikolid) (PLGA) NF (nanofiber) yapı iskelelerinin yüzeyi, daha fazla karboksilik grup oluşturmak ve glutamik asit (GLU) peptit konjugasyonunu artırarak NF'lerin biyomineralizasyonunu artırmak üzere soğuk atmosferik plazma (SAP) ile modifiye edilmiştir. SAP ile muamele edilmiş ve GLU peptit konjuge NF'lerin mineralizasyonu, yüzey pürüzlülüğü ve ıslanabilirliği ve insan mezenkimal kök hücreleri (hMSC) proliferasyonu üzerindeki etkisi araştırılmıştır. Sonuç olarak, SAP muamelesi biyofonksiyonel peptit konjugasyonunu ve biyomineralizasyonu indüklemiştir. İkinci bölümde, kısa biyoaktif motifli O1 (EEGGC) ve O2 (EEEE) ile KLD (KLDLKLKLDL) kendiliğinden yapılanan peptiti (KYP) entegre edilerek, farklı konsantrasyonlarda (% 0,5, % 1 ve % 2) kendiliğinden yapılan hidrojeller elde edilmiştir. Kemik kusurlarına enjekte edilebilen KYP hidrojellerinin osteogenezi ve biyomineralizasyonu KLD iskelesi ile karşılaştırıldığında, tasarlanan biyoaktif peptit

iskelelerinin, gerçek zamanlı PCR ve immüno Floresan analizi ile belirlenen temel osteojenik belirteçlerin ekspresyon seviyelerini önemli ölçüde desteklediği bulunmuştur. Üçüncü bölümde, hızlı bir vasküler yapı oluşumuna izin veren ve KLD KYP hidrojeline entegre edilen IKVAV (V1) ve YIGSR (V2) biyoaktif peptitlerin in vitro vaskülarizasyon üzerindeki etkinliğini belirleyen biyomimetik KYP hidrojellerinin geliştirmesi hedeflenmiştir. KLD-V1 ve KLD-V2 olmak üzere iki KYP hidrojel, %0.5 ve %1 konsantrasyonlarda tasarlanmış ve üretilmiştir. hMSC/HUVEC ortak kültürünün çoğalması, KLD'ye laminin türevli peptitlerin eklenmesiyle artmıştır. PECAM, vWf ve Ve-cadherin proteinlerini ve gen ekspresyonunu analiz etmek için sırasıyla immüno Floresan boyama ve RT-qPCR yapılmıştır. Laminin türevli peptit modifiye KYP hidrojeller, vaskülojen potansiyelini arttırmıştır. KLD-V2, KLD-V1'e kıyasla proliferasyonu ve vaskülarizasyonu keskin bir şekilde arttırmıştır. Dördüncü bölümde, dental implantların osseointegrasyonuna yönelik KYP hidrojelleri ile hem kemik dokusu hem de damar oluşumunu indükleyebilen ve enjeksiyon yoluyla defekt şeklini alabilen çok işlevli yeni bir iskele geliştirilmiştir. Dental implant osseointegrasyonunda çok fonksiyonlu KYP hidrojel kullanımının etkinliği in-vivo çalışmanın hemen ardından rezonans frekans analizi, ters tork ile belirlenmiştir. Enjekte edilebilir çok işlevli iskeleler, dental implant osseointegrasyonunu hızlandırmıştır. Son bölümde, kemik defektleri için in vitro osteojenik ve vaskülojenik farklılaşmayı destekleyebilen vaskülojenik epitop (YIGSR) ile güçlendirilmiş KYP hidrojelleri ile GLU peptit konjuge kök hücre yüklü elektrospun NF'ler kullanılarak vaskülarize bir kemik doku modeli önerilmiştir. Fiziksel karakterizasyonlardan sonra, osteojenik farklılaşma için DNA, kalsiyum ve ALP kantifikasyonu, q-PCR, immüno Floresan boyama ve vaskülojenik farklılaşma q-PCR ve immüno Floresan boyama yapılarak değerlendirilmiştir. Geliştirilen kemik modelinin osteojenik ve vaskülojenik farklılaşmayı önemli ölçüde arttırdığı gösterilmiştir. Genel olarak, bu tezdeki bulgular, kök hücre bazlı kemik onarımını ve rejenerasyonunu desteklemek için biyofonksiyonelleştirilmiş biyomateryallerin daha fazla optimizasyonuna yardımcı olacaktır. Ayrıca, bu tür bulguların, araştırmacıların kemik iyileşme süreçlerini iyileştirmek için kliniğe çevrilecek daha iyi biyomimetik yapı iskeleleri tasarımlarına yardımcı olacağına inanılmaktadır.

Anahtar Kelimeler: Kemik doku mühendisliği, Nanofiberler, Kendiliğinden yapılan peptid, Hidrojel, Osseointegrasyon

To my family and my grandfather İsmail Hakkı Yasalı, who was always proud of our achievements. . .

Acknowledgment

This thesis was supported by TÜBİTAK within the scope of “Development and evaluation in vitro and in vivo efficacy of multifunctional self-assembled peptide hydrogel for accelerating the osseointegration period of dental implants” Project No. 117S429. I would like to thank TÜBİTAK for their support. I would like to thank İzmir Katip Çelebi University Coordination Office of Scientific Research Projects, for their support through the Research Project 2021-TDR-FEBE-0001.

Foremost, I would like to thank my advisor, Assoc. Prof. Dr. Ozan Karaman. I am deeply thankful to him, for all the time he invested to teach me how to be a researcher. I would like to thank Assoc. Prof. Dr. Utku Kürşat Ercan and Assoc. Prof. Dr. Aylin Şendemir for their support and contribution to the progression of my Ph.D. thesis. I also want to thank to Oğuzhan Gökmen, and Ziyşan Buse Çevik, Assoc. Prof. Dr. Murat Ulu, Yusuf Ercan, Ömer Ankaya and Kutay Arkoç for their support. I wish to express my sincere thanks to the committee members, Assoc. Prof. Dr. Sinan Güven and Assist. Prof. Dr. Didem Şen Karaman.

I would like to thank my beloved husband Hasan Fırat Pulat, who always supports me and shows patience and understanding. I would like to thank my dear mother Fahriye Onak, my father Ali Rifat Onak, my brother Onur Onak and my sister Canan Onak, whose support I always feel. I am very grateful to my nephew Batur Onak, who is my biggest source of motivation.

Table of Contents

Declaration of Authorship.....	ii
Abstract	iii
Öz	v
Acknowledgment	viii
List of Figures	xiv
List of Tables.....	xxi
List of Abbreviations.....	xxii
List of Symbols	xxvi
1 Background.....	1
1.1 Bone Tissue.....	1
1.1.1 Bone Structure and Functions	2
1.1.2 Bone Cells	4
1.1.3 Formation of Bone Tissue.....	5
1.1.3.1 Osseointegration.....	6
1.1.3.2 Blood Vessel Formation in Bone Tissue.....	10
1.2 Bone Tissue Engineering.....	11
1.2.1 Biomaterials for Bone Tissue Engineering	12
1.2.1.1 Key Factors for Biomaterials	12
1.2.1.2 Types of Biomaterials	16
1.2.2 Types of Scaffolds	20
1.2.3 Fabrication Techniques for Biomimetic Scaffolds	21
1.2.4 Scaffold Modification Techniques.....	26
1.2.5 Development of Bioactive Surfaces	28

2 Aims of the Thesis	31
3 Accelerated Mineralization on Nanofibers via Cold Atmospheric Plasma Assisted Glutamic Acid Templated Peptide Conjugation	32
3.1 Introduction	32
3.2 Materials and Methods	35
3.2.1 Peptide Synthesis	35
3.2.2 Fabrication of Nanofibers	36
3.2.3 Peptide Conjugation of Nanofibers.....	36
3.2.4 Calcium Phosphate Crystals Nucleation of Nanofibers.....	36
3.2.5 Characterization of Nanofibers	37
3.2.6 Cell Attachment and Proliferation Analysis	38
3.2.7 Statistical Analysis.....	39
3.3 Results	39
3.3.1 Characterization of Peptide Conjugated Nanofibers.....	39
3.3.2 Biomineralization of Peptide Conjugated Nanofibers	43
3.3.3 Cell Proliferation and Morphology on Nanofibers	44
3.4 Discussion	46
3.5 Conclusion	50
4 Enhanced Osteogenesis of Human Mesenchymal Stem Cells by Self-assembled Peptide Hydrogel Functionalized with Glutamic Acid Templated Peptides	51
4.1 Introduction	51
4.2 Materials and Methods	54
4.2.1 Peptide Synthesis.....	54
4.2.2 Self-assembled Hydrogel Fabrication	55
4.2.3 Cell Culture and Hydrogel Encapsulation.....	55
4.2.4 Osteogenic Differentiation of hMSCs in Hydrogels	56
4.2.4.1 Quantitative Real-time PCR Analysis.....	56
4.2.4.2 Immunofluorescent Staining	57

4.2.5 Alizarin Red Staining.....	57
4.2.6 Statistical Analysis.....	57
4.3 Results	58
4.3.1 Osteogenic Differentiation of hMSCs in Self-assembled Hydrogels .	58
4.3.2 Alizarin Red Staining.....	60
4.4 Discussion	61
4.5 Conclusion	64
5 Role of Functionalized Self-Assembled Peptide Hydrogel on In Vitro Vasculogenesis	65
5.1 Introduction	65
5.2 Materials and Methods	69
5.2.1 Peptide Synthesis	69
5.2.2 Self-assembled Hydrogel Fabrication and Characterization.....	70
5.2.3 Cell Culture and Proliferation Analysis	72
5.2.4 Quantitative Real-time PCR Analysis	72
5.2.5 In vitro Angiogenesis Assay	73
5.2.6 Immunofluorescent Staining	74
5.2.7 Statistical Analysis.....	74
5.3 Results	75
5.3.1 Characterization of Hydrogels	75
5.3.2 Proliferation of HUVEC/MSK in SAP Hydrogels.....	78
5.3.3 Quantitative Real-time PCR Analysis	78
5.3.4 In vitro Angiogenesis Assay	79
5.3.5 Immunofluorescent Staining	80
5.4 Discussion	81
5.5 Conclusion.....	87
6 Self-assembled peptide Hydrogel for Accelerating the Osseointegration Period of Dental Implants.....	88

6.1	Introduction	88
6.2	Materials and Methods	90
6.2.1	Peptide Synthesis	90
6.2.2	Self-assembled Hydrogel Fabrication.....	91
6.2.3	In vitro Cell Differentiation	91
6.2.3.1	Cell Seeding and Proliferation Analysis	91
6.2.3.2	Osteogenic differentiation in multifunctional hydrogels	92
6.2.3.3	Vasculogenic differentiation of in multifunctional hydrogels	94
6.2.4	In vivo Evaluation.....	95
6.2.4.1	Replacement of the Dental Implants	95
6.2.4.2	Resonance Frequency Analysis	96
6.2.4.3	Reverse Torque Test	97
6.2.5	Statistical Analysis.....	97
6.3	Results	98
6.3.1	Proliferation of HUVEC/hMSC in SAP Hydrogels.....	98
6.3.2	Osteogenic Differentiation in Multifunctional Hydrogels.....	99
6.3.3	Vasculogenic Differentiation of SAP Hydrogels.....	103
6.3.4	In vivo Evaluation.....	105
6.4	Discussion	106
6.5	Conclusion.....	109
7	Peptide Conjugated Nanofiber Reinforced Self-assembled peptide Hydrogel for Bone Regeneration	110
7.1	Introduction	110
7.2	Materials and Methods	113
7.2.1	Peptide Synthesis	113
7.2.2	Fabrication and Characterization of Nanofibers	113
7.2.3	Fabrication of Nanofiber Reinforced Hydrogels	114

7.2.4 Mechanical Properties.....	114
7.2.5 Cell Culture.....	115
7.2.6 In vitro Osteogenic Differentiation.....	115
7.2.7 Quantitative Real-time PCR Analysis	116
7.2.8 Immunofluorescence Staining	117
7.2.9 Statistical Analysis.....	118
7.3 Results	118
7.3.1 Characterization of Fiber Reinforced Hydrogels.....	118
7.3.2 Osteogenic Differentiation in Hydrogels	121
7.3.3 Vasculogenic Differentiation in Hydrogels	124
7.4 Discussion	126
7.5 Conclusion.....	130
8 Concluding Remarks	131
Appendices	1676
Appendix A The Characterization Data of Peptides	167
Appendix B Publications from the Thesis.....	170
Appendix C Ethical Committee Approval	171
Curriculum Vitae	173

List of Figures

Figure 1.1 The classification of bones based on shape	2
Figure 1.2 The organization of different elements within the long bone.....	3
Figure 1.3 Schematic representation of bone cells	5
Figure 1.4 Basic electrospinning setup	23
Figure 3.1 Schematic diagram of NTAP assisted conjugation of glutamic (E) acid templated peptides on PLGA nanofibers with EDC/NHS chemistry. Experimental groups are neat NF, NTAP treated NF (pNF), GLU peptide conjugated NF (without NTAP treatment) (GLU-NF) and NTAP treated GLU peptide conjugated NF (GLU-pNF).....	40
Figure 3.2 Scanning electron microscopy images of (a) PLGA nanofibers (NF) (scale bar represents 1 μ m), (b) histogram showing nanofiber diameters distribution, (c) mineralized neat NF (NF), (d) mineralized NTAP treated NF (pNF), (e) mineralized GLU peptide conjugated NF (without NTAP treatment) (GLU-NF), (f) mineralized NTAP treated GLU peptide conjugated NF (GLU-pNF) (scale bar represents 1 μ m).....	41
Figure 3.3 (a) Mean of Fluorescence Intensity of neat NF, pNF, GLU-NF, and GLU-pNF after dissolving in DMSO. Measurement of contact angle of (b) NF, (c) pNF, (d) GLU-NF (e) GLU-pNF.....	42
Figure 3.4 Representative 3D topographical view of (a) neat NF, (b) NTAP treated NF (pNF), (c) GLU peptide conjugated NF (without NTAP treatment) (GLU-NF), (d) NTAP treated GLU peptide conjugated NF (GLU-pNF) obtained by AFM	43
Figure 3.5 (a) Calcium content of calcium phosphate (CaP) deposited on NF, pNF, GLU-NF, and GLU-pNF within 7 days incubation in 1.5xSBF, (b) X-ray diffraction spectrum of NF, pNF, GLU-NF and GLU-pNF for CaP deposition after 7 days incubation in 1.5xSBF (c) Tensile modulus of neat NF, NTAP treated NF (pNF), GLU peptide conjugated NF (without NTAP	

treatment) (GLU-NF) and NTAP treated GLU peptide conjugated NF (GLU-pNF).....	44
Figure 3.6 (a) The percentage of increase in cell number at 1, 3, and 7 days after seeding cells on neat NF, NTAP treated NF (pNF), GLU peptide conjugated NF (without NTAP treatment) (GLU-NF), and NTAP treated GLU peptide conjugated NF (GLU-pNF). Morphology of human marrow stromal cells (hMSCs) seeded on (b) NF, (c) pNF, (d) GLU-NF, and (e) GLU-pNF (BIV). PLGA NF incubated in basal media for 7 days. Phalloidin (red) and 4,6-diamidino-2-phenylindole (DAPI; blue) represent cytoskeletal actin and cell nuclei in the image (Scale bar represents 50µm)	45
Figure 4.1 RT-PCR analysis of gene expression of osteogenic markers of (a) alkaline phosphatase (ALPase), (b) type 1 collagen (COL-1), (c) osteopontin (OPN), (d) osteocalcin (OCN) for hMSCs encapsulated in 0.5%, 1%, 2% KLD, KLD-O1, KLD-O2, and Biogelx and incubated in osteogenic medium for up to 28 days. The error bars indicate the mean SE (n = 3) of the data. [One-way ANOVA was used to assess significant differences.] [($p < 0.05$, $**p < 0.01$, $***p < 0.001$) Newman–Keuls multiple contrast test]	59
Figure 4.2 Immunofluorescent staining revealed the expression of osteogenic markers COL-I (first column: green), OPN (second column: red) and OCN (third column: green) in 2% (a) KLD, (b) Biogelx, (c) KLD-O1, (d) KLD (O2) after 28 days incubation. 4',6-diamidino-2-phenylindole (DAPI; blue) was used to indicate cell nuclei (Scale bar represents 50 µm)	60
Figure 4.3 Alizarin red staining for mineral deposition of hMSCs encapsulated in 0.5 % (first column), 1% (second column) and 2% (third column) (a) Biogelx, (b) KLD, (c) KLD-O1, (d) KLD-O2 after 28 days' incubation in osteogenic medium. (Scale bar represents 50 µm).....	611
Figure 5.1 Laminin derived peptide integrated Self-assembled peptide hydrogels significantly enhanced vascularisation of human umbilical vein endothelial cells (HUVECs) and human mesenchymal stem cells (hMSCs) coculture	69

Figure 5.2 Representative 3D topographical view of (a) KLD-V1, (b) KLD-V2 Self-assembled peptide (SAP) nanofibers obtained by Atomic Force Microscopy.....	75
Figure 5.3 Scanning electron microscopy images of (a) KLD-V1, (b) KLD-V2 Self-assembled peptide (SAP) nanofibers (scale bar represents 200 nm).	76
Figure 5.4 Rheology analysis of 0.5%, and 1% (a) KLD-V1, (b) KLD-V2 Self-assembled peptide (SAP) hydrogels. G' and G'' represents storage and loss modulus, respectively.....	77
Figure 5.5 Biodegradation of 0.5% and 1% KLD-V1, KLD-V2 Self-assembled peptide (SAP) hydrogels (Time periods: 7,14,21,28, 35,42,49,56, and 63 days)	77
Figure 5.6 Cell number of HUVEC/hMSC encapsulated in 0.5% (A), 1% (B) KLD-V1, KLD+V1, KLD-V2, KLD+V2 and Biogelx and incubated in vasculogenic medium for up to 7 days. The error bars indicate the mean SE (n = 3) of the data. [One-way ANOVA was used to assess significant differences.] [($*p < 0.05$, $**p < 0.01$, $***p < 0.001$) Newman–Keuls multiple contrast test]	78
Figure 5.7 The mRNA expression levels (as fold difference) of (a) PECAM-1, (b) VE-Cadherin, (c) vWF, in 0.5 % and (d) PECAM-1, (e) VE-Cadherin, (f) vWF in 1 % KLD, KLD-V1, KLD-V2, and Biogelx after HUVEC/hMSC encapsulation and incubation in vasculogenic medium for up to 7 days. The error bars indicate the mean SE (n = 3) of the data. [One-way ANOVA was used to assess significant differences.] [($*p < 0.05$, $**p < 0.01$, $***p < 0.001$) Newman–Keuls multiple contrast test].....	79
Figure 5.8 Capillary-like tube formation assay. Representative microscopic images of the capillary network of 1 % (a) KLD, (b) KLD-V1, (c) KLD-V2, (d) Biogelx after HUVEC/hMSC encapsulation and incubation in vasculogenic medium for up to 7 days. (Scale bar represents 200 μ m). Histogram representing (e) Mesh mean size (f) Total tube length (g) Number of meshes (h) Number of junctions (i) Total mesh area (J) Number of nodes of the capillary-like network as calculated from image the analysis. The error bars indicate the mean SE (n = 3) of the data. [One-way ANOVA was used to assess significant differences.] [($*p < 0.05$, $**p < 0.01$, $***p < 0.001$) Newman–Keuls multiple contrast test].....	80

Figure 5.9 Expression pattern of vasculogenic markers PECAM-1(red), and vWF (green) for HUVEC/hMSC encapsulated in 1% (a) Biogelx, (b) KLD, (c) KLD-V1 (d) KLD-V2 after 7 days' incubation in vasculogenic medium. (Scale bar represents 100 μ m).....	81
Figure 6.1 Schematic illustration of multifunctional self-assembled peptide (SAP) hydrogel for dental implant osseointegration.....	90
Figure 6.2 Implantation of titanium into the tibia of a New Zealand. (a) SAP hydrogel insertation, (b) installation of titanium dental implants into the tibia.....	96
Figure 6.3 (a) Resonance frequency analysis (b) Reverse torque measurements of dental implants before the removal	97
Figure 6.4 Cell number of HUVEC/hMSC encapsulated in KLD, KLD-O, KLD-O/KLD-V, and Biogelx and incubated in osteogenic/vasculogenic (1:1) medium for up to 28 days. The error bars indicate the mean SE (n = 3) of the data. [One-way ANOVA was used to assess significant differences.] [($*p < 0.05$, $**p < 0.01$, $***p < 0.001$) Newman–Keuls multiple contrast test]	98
Figure 6.5 (a) DNA content, (b) ALP activity, (c) Calcium content of HUVEC/hMSCs encapsulated in KLD, KLD-O, KLD-O/KLD-V and Biogelx and incubated in osteogenic/vasculogenic (1:1) medium for up to 28 days. The error bars indicate the mean SE (n = 3) of the data. [One-way ANOVA was used to assess significant differences.] [($*p < 0.05$, $**p < 0.01$, $***p < 0.001$) Newman–Keuls multiple contrast test].....	100
Figure 6.6 The mRNA expression levels (as fold difference) of (a) alkaline phosphatase (ALPase), (b) type 1 collagen (COL-1), (c) osteopontin (OP), (d) osteocalcin (OC) for HUVEC/hMSCs encapsulated in KLD, KLD-O, KLD-O/KLD-V and Biogelx and incubated in osteogenic/vasculogenic (1:1) medium for up to 28 days. The error bars indicate the mean SE (n = 3) of the data. [One-way ANOVA was used to assess significant differences.] [($*p < 0.05$, $**p < 0.01$, $***p < 0.001$) Newman–Keuls multiple contrast test]	101
Figure 6.7 Expression pattern of osteogenic markers type 1 collagen (COL-I) (green, first column), osteopontin (OP) (red, second column) and osteocalcin (OC) (green, third column) for HUVEC/hMSCs encapsulated in (a) KLD-	

	O/KLD-V (a 1-3), (b) KLD-O (b1-3), (c) KLD (1-3) and (d) Biogelx (d 1-3) after 28 days' incubation in osteogenic/vasculogenic (1:1) medium. Cell nuclei in the images are stained with 4',6-diamidino-2-phenylindole (DAPI; blue) (Scale bar represents 100 μ m).....	102
Figure 6.8	Alizarin red staining for mineral deposition of HUVEC/hMSCs encapsulated in (a) Biogelx, (b) KLD, (c) KLD-O (C) and KLD-O/KLD-V (D) after 28 days' incubation in osteogenic/vasculogenic (1:1) medium. (Scale bar represents 50 μ m).....	103
Figure 6.9	The mRNA expression levels (as fold difference) of (a) Ve-Cadherin, (b) vWF, (c) Pecam-1 for HUVEC/hMSCs encapsulated in KLD, KLD-O, KLD-O/KLD-V and Biogelx and incubated in osteogenic/vasculogenic (1:1) medium for up to 28 days. The error bars indicate the mean SE (n = 3) of the data. [One-way ANOVA was used to assess significant differences.] [($*p < 0.05$, $**p < 0.01$, $***p < 0.001$) Newman–Keuls multiple contrast test]	104
Figure 6.10	Expression pattern of vasculogenic markers PECAM-1(red), and vWF (green) for HUVEC/hMSC encapsulated in (a) Biogelx, (b) KLD, (c) KLD-V1, (d) KLD-V2 after 7 days' incubation in osteogenic/vasculogenic (1:1) medium. (Scale bar represents 100 μ m).....	105
Figure 6.11	(a) Resonance frequency analysis (RFA) (b) Reverse Torque values comparing control and KLD-O/KLD-V hydrogel treated implants at surgery and after 8 weeks healing	106
Figure 7.1	Schematic diagram of PLGA electrospun nanofiber reinforced self-assembled hydrogel with increased mechanical properties, osteogenesis, and vascularization.....	113
Figure 7.2	Scanning electron microscopy images of (a) KLD-V self-assembled peptide (SAP) (b) electrospun PLGA nanofiber (NF) Fluorescent microscopy images of (c) PLGA NF (d) fluorescein isothiocyanate (FITC) labeled glutamic acid peptide conjugated NF (GLU-NF)	119
Figure 7.3	(a) Picture of electrospun PLGA nanofiber (NF) reinforced SAP hydrogel (d=38 mm, h=20 mm) (b) Young's modulus of hydrogels under compression, (c) Compression stress-strain curves of KLD-V, (d) KLD-V/NF (e) KLD-V/ GLU-NF hydrogels	120

Figure 7.4 Biodegradation of KLD-V, KLD-V/NF, and KLD-V/GLU-NF hydrogels (Periods: 7,14,21,28, 35,42,49).....	120
Figure 7.5 (a) DNA content (b) ALP activity (c) Calcium content of HUVEC/hMSCs encapsulated in KLD-V, KLD-V/NF, KLD-V/GLU-NF incubated in osteogenic/vasculogenic (1:1) medium for up to 28 days. The error bars indicate the mean SE (n = 3) of the data. [One-way ANOVA was used to assess significant differences.] [($p < 0.05$, $p < 0.01$, $p < 0.001$) Newman– Keuls multiple contrast test].....	121
Figure 7.6 The mRNA expression levels (as fold difference) of (a) alkaline phosphatase (ALPase) (b) type 1 collagen (COL-1) (c) osteopontin (OP) (d) osteocalcin (OC) (D) for HUVEC/hMSCs encapsulated in KLD-V, KLD-V/NF, KLD-V/GLU-NF and incubated in osteogenic/vasculogenic (1:1) medium for up to 28 days. The error bars indicate the mean SE (n = 3) of the data. [One-way ANOVA was used to assess significant differences.] [($p < 0.05$, $p < 0.01$, $p < 0.001$) Newman–Keuls multiple contrast test]	123
Figure 7.7 Expression pattern of osteogenic markers type 1 collagen (COL-I)(green, first column), osteopontin (OP) (red, second column), and osteocalcin (OC) (green, third column) for HUVEC/hMSCs encapsulated in KLD- V/GLU-NF (AI–III), KLD-V/NF (BI–III), KLD (CI–III) after 28 days’ incubation in osteogenic/vasculogenic (1:1) medium. Cell nuclei in the images are stained with 4’,6-diamidino-2-phenylindole (DAPI; blue) (Scale bar represents 100 μ m).....	124
Figure 7.8 The mRNA expression levels (as fold difference) of (a) Ve-Cadherin (b) vWF (c) osteopontin (OP) Pecam-1 for HUVEC/hMSCs encapsulated in KLD-V, KLD-V/NF, KLD-V/GLU-NF and incubated in osteogenic/vasculogenic (1:1) medium for up to 28 days. The error bars indicate the mean SE (n = 3) of the data. [One-way ANOVA was used to assess significant differences.] [($p < 0.05$, $p < 0.01$, $p < 0.001$) Newman– Keuls multiple contrast test].....	125
Figure 7.9 Expression pattern of vasculogenic markers PECAM-1(red), and vWF (green) for HUVEC/hMSC encapsulated in (a) KLD-V/GLU-NF (b)	

<p style="text-align: center;">KLD-V/NF (c) KLD-V (C) after 7 days' incubation in osteogenic/vasculogenic (1:1) medium (Scale bar represents 100 μm)</p>	126
<p>Figure A.1 Liquid chromatography spectra of A) GLU, B) KLD, C) KLD-O1, D) KLD-O2, E) KLD-V1, and F) KLD-V2</p>	168
<p>Figure A.2 Ionization mass spectra of A) GLU, B) KLD, C) KLD-O1, D) KLD-O2, E) KLD-V1, and F) KLD-V2.....</p>	169
<p>Figure C.1 Ethical Committee Approval</p>	171

List of Tables

Table 4.1 Forward and reverse primers. Alkaline phosphatase (ALP), Collagen Type I (Col-1), Osteopontin (OPN), Osteocalcin (OCN), and glyceraldehyde 3-phosphate dehydrogenase (GAPDH; housekeeping gene) (GAPDH) used to asses hMSCs differentiation in qRT-PCR amplification	56
Table 5.1 Forward and reverse primers. PECAM-1, Ve-Cadherin, vWF, and glyceraldehyde 3-phosphate dehydrogenase (GAPDH; housekeeping gene) (GAPDH) used to asses vasculogenic differentiation in qRT-PCR amplification.....	73
Table A.1 Sequences, observed and calculated molecular weight of synthesized peptides.....	167

List of Abbreviations

2D	Two-Dimensional
3D	Three-Dimensional
AFM	Atomic Force Microscopy
Al ₂ O ₃	Alumina
ALP	Alkaline Phosphatase
Boc	tert-butyloxycarbonyl
BSA	Bovine Serum Albumin
BSP	Bone Sialoprotein
Ca	Calcium
CAD	Computer-Aided Design Model
CAP	Cold Atmospheric Plasma
CaP	Calcium Phosphate
COL-1	Collagen Type-I
COOH	Carboxyl
cpTi	Commercially Pure Titanium
DAPI	4',6-Diamidino-2-Phenylindole
DCM	Dichloromethane
DIEA	N, N-Diisopropylethylamine
DMSO	Dimethyl Sulfoxide
ECM	Extracellular Matrix
ECs	Endothelial Cells
EDC	1-Ethyl-3-(3-Dimethylaminopropyl)-Carbodiimide

EPCs	Endothelial Progenitor Cells
FBS	Fetal Bovine Serum
FDM	Fused Deposition Modeling
Fmoc	9-fluorenylmethyloxycarbonyl
FITC	Fluorescein Isothiocyanate
GAPDH	Glyceraldehyde 3-Phosphate Dehydrogenase
GLU	Glutamic Acid
G'	Storage Modulus
G''	Loss Modulus
H ₂ O	Water
HA	Hydroxyapatite
HBTU	2-(1H-benzotriazol-1-yl)-1,1,3,3-tetramethyluronium hexafluorophosphate
HCl	Hydrochloric Acid
hEGF	Human Epidermal Growth Factor
HEPES	4-(2-Hydroxyethyl)-1-Piperazineethanesulfonic Acid
HFP	1,1,1,3,3,3-Hexafluoro-2-Propanol
HOBt	Hydroxybenzotriazole
HPLC	High-Pressure Liquid Chromatography
HUVECs	Human Umbilical Vein Endothelial Cells
MBHA	4-Methylbenzhydramine
mSBF	Modified SBF
MSCs	Mesenchymal Stem Cells
MTT	3-(4,5-Dimethylthiazol-2-yl)-2,5-Diphenyltetrazolium Bromide
NaHCO ₃	Sodium Bicarbonate
NF	Nanofiber
NH ₂	Amine
NHS	N-Hydroxysuccinimide

NTAP	Non-Thermal Atmospheric Plasma
NVP	N-Vinyl-2-Pyrrolidone
OCN	Osteocalcin
OD	Optical Density
ON	Osteonectin
OPN	Osteopontin
P	Phosphorus
PA	Peptide Amphiphilic
PBS	Phosphate Buffered Saline
PCL	Poly (ϵ -Caprolactone)
PDGF	Platelet-Derived Growth Factor
PECAM-1	Platelet/Endothelial Cell Adhesion Molecule-1
PEGDA	Poly Ethylene Glycol Diacrylate
PET	Polyethylene Terephthalate
PGA	Poly (glycolic Acid)
PLA	Poly (lactic Acid)
PLAA	poly (L-lactide)
PLEOF	Poly Lactic Ethylene Oxide Fumarate
PLGA	Poly Lactic-Co-Glycolic Acid
PMN	Polymorphonuclear leukocytes
<i>p</i> NPP	P-Nitrophenylphosphate
RFA	Resonance Frequency Analysis
RNS	Reactive Nitrogen Species
ROS	Reactive Oxygen Species
RTT	Reverse Torque Tests
SAP	Self-assembled peptide
SBF	Simulated Body Fluid

SEM	Scanning Electron Microscope
SEM	Scanning Electron Microscopy
SLS	Selective Laser Sintering
TFA	Trifluoroacetic Acid
TGF- β	Transforming Growth Factor-Beta
TIPS	Triisopropylsilane
VE-cadherin	Vascular Endothelial Cadherin
VEGF	Vascular Endothelial Growth Factor
vWF	Von Willebrand Factor
XRD	X-ray Diffractometer
ZrO ₂	Zirconia

List of Symbols

g	Gram
Hz	Hertz
kV	Kilo Volt
MPa	Mega Pascal
ml	Milliliter
Mw	Molecular Weight
°C	Degree Celsius
μl	Microliter
θ	Contact Angle

Chapter 1

Background

1.1 Bone Tissue

The tissue consists of the cells that similarly function in the body. There are roughly 200 different cell types that are systematized into four major tissues: nervous, epithelial, muscle tissue, connective. One of the connective tissue is bone tissue, which consists of the extracellular matrix (ECM) and the cells. The majority of the connective tissue consists of blood supply, nerves, and scattered cells submerged in the ECM. Bone, which is a type of connective tissue, has a hierarchically organized and dynamic structure and is continuously being replaced through the process of bone remodeling [1]. The bone tissue composed of organic composite fibrous protein and collagen network (30-35% of the weight) covered with a stiff matrix of inorganic calcium/phosphate (65-70% of the weight) and cells, blood vessels [2-4]. The organic matrix in the bone mostly contains collagen type-I (COL-1), bone cells, lipid, non-collagenous, and cell attachment proteins such as osteopontin (OPN), osteocalcin (OCN), bone sialoprotein (BSP), osteonectin (ON), and proteoglycans [5, 6]. Collagen which is the major component in organic bone ECM provides flexibility and resistance. Inorganic components are mainly composed of calcium (Ca) and phosphorus (P) in the form of small hydroxyapatite (HA) crystals and create the major characteristic function by giving the matrix compression strength. Spherical nano HA crystals contained partly calcium and phosphorous. The formation of these HA crystals increases passively calcium and phosphate levels. Nevertheless, HA formation is a cell-mediated process that is regulated by specific proteins which enhance or inhibit calcification similar to osteogenesis. Chondrocytes or apoptotic cells provide an ECM which promotes the initial steps for the generation of HA crystals after the release of membrane vesicles by osteoblasts and initiates the deposition of extracellular mineral.

Mineralized collagen fibrils are the major component of bone material. The quantity, integrity, and relation of organic and inorganic components determine the structural and mechanical behavior of bone, such as elasticity and strength [5-9].

Bone contributes to an adult human body by a total of 213 bones, made from two distinct types: spongy and compact, and categorized in 4 groups which are: spongy and compact, and categorized in 4 groups which are: short, long, irregular, and flat bone [10] (see Figure 1.1).

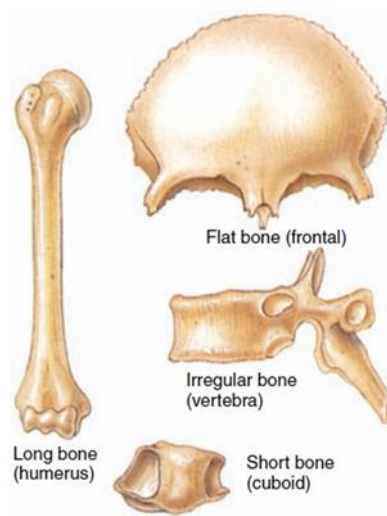


Figure 1.1: The classification of bones based on the shape [10]

1.1.1 Bone Structure and Functions

The uniqueness of the bone tissue makes the skeletal system multifunctional and assists six basic functions: providing mineral homeostasis, movement, protection, support, hemopoiesis, and triglyceride storage. Bone supports the body by providing a framework that creates a space for soft tissue to attach. Protection and assistance for movement are achieved with the help of the bone tissue by absorbing any force applied to the body and making soft tissue move synchronized with hard tissue. Bone tissue also provides mineral balance throughout the body by storing and releasing the minerals such as calcium and phosphorus when it is needed. Moreover, bone tissue

contains a part of connective tissue named red bone marrow which is the center for red blood cell production within the human body throughout hemopoiesis. In the skeleton, each bone has two types of structure: spongy bone and compact bone. Trabecular bone, or cancellous (spongy bone), is a form of bone that contains a trabeculated structure with a porous formation, composed of osteocytes that are trapped within the lacuna and rods that are dispersed within the bone marrow. It makes up almost 20% of the human skeleton and can be found at the edge of long bones throughout the body [10]. Also, the void spaces within the porous structure consist of the red bone marrow where mesenchymal stem cells (MSCs) are produced. Compact or cortical bone is a type of dense and solid bone that contains a system called Haversian with packed osteons with small spaces (see Figure 1.2). The Haversian system is a cylindrical shape, formed by an osteogenic canal that is surrounded by lamellae and lacunae which is the space between the osteocytes that are located within the lacunae and the lamellae (rings of a matrix). Also, the osteogenic channels contain blood vessels that supply metabolic supplements such as oxygen, glucose that can reach the bone surface [11]. The bone surface contains two layers which are the outer periosteal, a fibrous connective tissue layer that contains nerve fibers, vessels, osteoblast, and osteocytes, and inner endosteal surface, a membrane-like layer that is connected with bone marrow, also with vessel channels and trabecular bone [10].

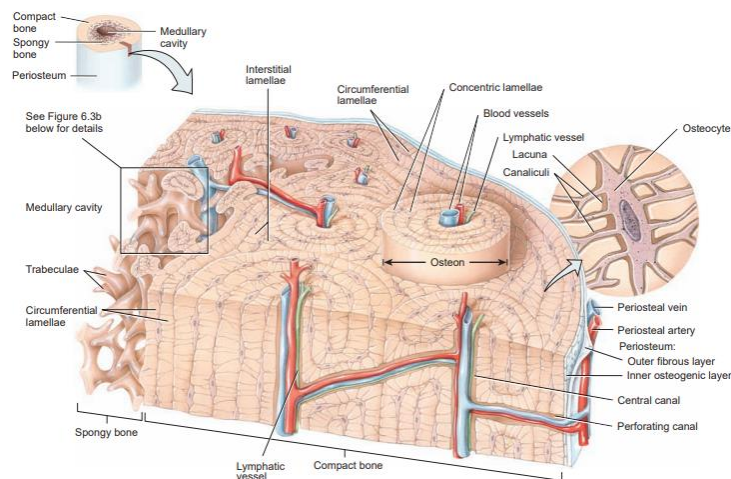


Figure 1.2: The organization of different elements within the long bone [12]

1.1.2 Bone Cells

Bone tissue cells which are fundamental elements of bone tissue have a major role during the osteogenesis (development of new bone tissue) and regeneration of a defected area of the bone tissue. The bone cells are osteoblasts, osteoclasts, and osteocytes (see Figure 1.3). Osteoblasts are completely differentiated cells originating from pre-osteoblasts or osteoprogenitor cells [13]. Osteoblasts are bone-forming cells that are uninuclear, specialized, and not terminally differentiated. They synthesize the organic compound of the bone matrix such as COL-1, proteoglycans, glycoproteins, and form osteoid tissue in bone formation regions. They initiate the calcification process then, differentiate into osteocytes by covering their surroundings with ECM matrix [12, 14]. Osteoids are formed by bone matrix, newly synthesized, and not yet calcified by osteoblasts [15]. Calcification starts with the alkaline phosphatase (ALP) enzyme secretion and then mineralization begins in the bone tissue. ALP enzyme plays role in the calcification of the matrix by allowing calcium to precipitate into the matrix as calcium phosphate [12, 16, 17]. When the bone formation is completed, osteoblasts turn into osteocytes or undergo apoptosis.

Osteocytes are located within the calcified bone matrix. Osteocytes are the core cells which are originated from osteoblasts, which comprise 90% of mature bone tissue and regulate the main metabolism within the bone tissue such as detection of damages and the remodeling of the bone tissue. They are differentiated from osteoblast bone cells whose metabolic activity decreases and cannot divide. They are generally enclosed by the lacuna and have either a stellate shape or a dendritic cell. Since the bone matrix is calcified, substance transport occurs via osteocytes and they keep bone tissue alive [18].

Osteoclasts, which are developed from hematopoietic cells within the blood circulation, are the main cell type that takes place during the maintenance of the defected tissue especially after bone tissue resorption [19]. They release enzymes and acids to break down the components within the ECM (proteins and mineral components) for remodeling [12]. During bone construction, osteoclasts settle on the surfaces of the trabeculae or the inner surfaces of the compact parts. Osteoclasts, resorb the inner surface of cortical bone and the surface of trabeculae while osteoblasts are

building new bone tissue. The bone tissue can extend and expand and the wearing parts can be removed and replaced [29, 30]. Bone is built by the collapse of the bone matrix (endochondral ossification) on the existing cartilage matrix or by direct mineralization (intramembranous ossification) of the matrix secreted by osteoblasts [31].

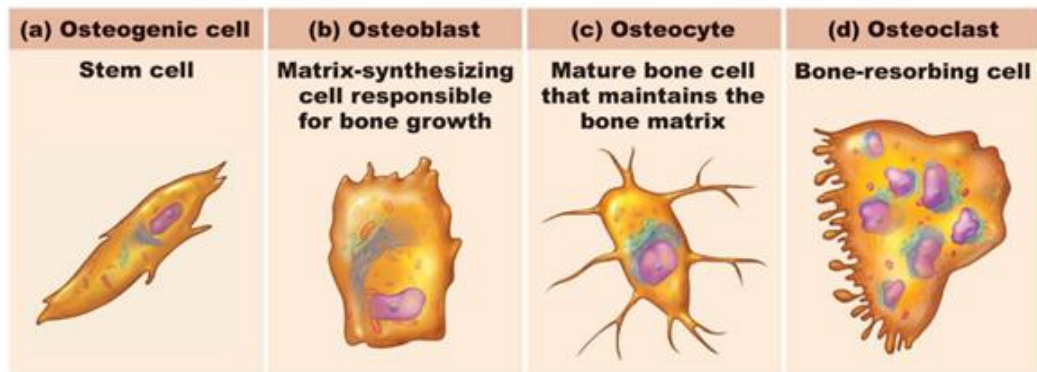


Figure 1.3: Schematic representation of bone cells [20]

1.1.3 Formation of Bone Tissue

Bone structure is formed by two diverse development processes (osteogenesis) called endochondral and intramembranous ossification [21]. Endochondral ossification is an essential progression that occurs in five stages during the fetal development of long bones. It starts with a formation of cartilage tissue and results in the long bones [22]. In the first phase, mesenchymal stem cells become cartilage cells due to the presence of paracrine factors which makes mesodermal cells produce transcription factors [23]. In the second phase, mesenchymal cells become condensed to form compact nodules then differentiate into chondrocytes and form the pattern of long bone by rapidly proliferating and increasing their number in the third phase. In the fourth phase, they stop producing their copies but continue expanding their volume, as a result, they become hypertrophic chondrocytes and alter their matrix to reach the mineralized environment of bone tissue. In the last phase, hypertrophic chondrocytes will create a space that will eventually become bone marrow by dying through apoptosis. The cells which surround the formed model will differentiate into osteoblast to replace all the

cartilage part, produce a bone matrix thus form the bone tissue [22]. Intramembranous ossification occurs during the formation of cranium flat bones, facial bones, mandible and clavicle bones which are fetal flat bones via a developmental process in which mesenchymal cells differentiate into osteoblasts in a region called calcification center which the certain points at flat bones that consists of embryonic connective tissue and infused calcium salts. During this process, a bond between osteoblast and calcified fiber region occurs as a result of secretion of collagenous proteoglycan matrix by osteoblasts. As a result of this binding osteoid matrix is calcified and the first true bone formation is completed [22, 24]. Following this, the transformation of the calcification center into an ossification center and then the formation of osteocytes which are enclosed between lamellae also occurs. Then osteocytes form structures called spicules which are structural elements of spongy bone. Spicules come together to form the spongy bone and cover the inner and outer sides by a layer of compact mesenchymal cells which is named as periosteum [24]. Even though both types of developmental processes of the bone structure have their distinctive ways of forming osteon either directly or through an extra middle step, they both start with the presence of mesenchyme and eventually form a composite material which contains four types of cells, inorganic and organic components and distinctive structures formed within the material, that called calcified osteon tissue [21].

1.1.3.1 Osseointegration

The osseointegration concept was first presented by Brånemark *et al.* has been presented to the literature, afterward, many researchers made important progress on this subject. Consequently, osseointegration has been defined as "the direct structural and functional connection between the surface of living bone tissue adjacent to the implant and the implant surface under loading without fibrous tissue" [25]. When an osseointegrated dental implant is examined by electron microscope, it is observed that the bone and the implant surface are directly connected with no soft tissue formation. A series of biological events develop in the surrounding spongiosis and cortical bone in the process of completing the bone apposition formed on the implant material placed in the socket prepared in the bone. The successive processes of osseointegration, such as bone resorption and bone apposition, have been described in detail histologically in human and animal studies. In 2012, Terheyden *et al.* distinguished osseointegration in

four phases; exudative (hemostasis), inflammatory, proliferative, remodeling phases [26].

The exudative phase is a process that begins with the preparation of the socket with implant drills and the implant is placed and lasts between minutes and hours. The differentiation and growth factors are released into the implant by the mechanical devastating of the bone ECM. The blood coming out of the cut vessels in the bone establishes the infrastructure of fibrinogen polymerization to create the first ECM in the defect area. As soon as the implant is replaced, the load pattern of the surface changes by the interaction of the implant surface with water molecules and ions. Divalent positively charged ions such as calcium are equally potentially bound to their negatively charged equivalents. Following ions, especially high concentration of albumin first adheres to the surface, and then vitronectin and fibronectin are adsorbed by the surface. Cell attachment to the implant surface occurs due to protein adsorption. Therefore, especially adhesion proteins such as fibronectin interact with cell-binding regions such as the RGD sequence. The activated integrins interact with fibrinogen to form a platelet plug. At the same time, platelets bind to collagen to form collagen fibrils towards the implant surface and allow them to attach to the surface like a network. Cytokines released from platelets degranulated as a result of binding.

The inflammatory phase begins approximately 10 minutes after implant placement and lasts until the first day after surgery. The release of growth factors such as transforming growth factor-beta (TGF- β), and platelet-derived growth factor (PDGF) initiates degranulation of platelets. Vascular permeability of white blood cells and serum proteins is increased by Bradykinin derived from degranulated platelets. Vasodilatory histamine is secreted from platelets. Vasodilatory histamine causes hyperemia by increasing the flow of histamine and decreasing the blood circulation rate. In the hemostatic phase, initial vasoconstriction occurs and causes vasodilation, swelling, and warming in the skin surrounding the wound. Polymorphonuclear leukocytes (PMN) and macrophages are released from the vessels into the environment as the first response of the host defense. First of all, PMNs, which dominate the environment, release reactive radicals to the environment to eliminate bacteria in the environment through the release of reactive oxygen species. It also releases digestive enzymes such as collagenase and elastase. These enzymes also digest and damage injured and healthy

tissues around the implant. When the acute period passes, lymphocytes and macrophages dominate the environment. While removing bacteria, debris, and neutrophils from the environment, they terminate the inflammatory phase with proinflammatory cytokines, FGF, PDGF, and vascular endothelial growth factor (VEGF). The fibrogenic and angiogenic growth factors released from macrophages initiate the proliferative phase. Another issue that is as important as antibiotics and local disinfectants in limiting the inflammatory phase is to terminate the surgical procedure with the cleanest possible form of the surgical area and thus provide the lowest bacterial inoculation [26]. The wound then proceeds to a stage of the healing process. The tissue debris is biochemically degraded and underwent phagocytosis by macrophages. The macrophages synthesize proinflammatory cytokines and proteases using antigenic inhibitors for digesting proteases and stop the tissue degradation started by PMNs. This will, in turn, produce growth factors by matrix proteins and proteoglycans.

The proliferative phase begins with the regeneration of ECM degraded in the acute phase of the inflammatory phase and angiogenesis. The granulation tissue is formed. The period of the proliferative phase is between a few days to weeks. Fibroblasts appear on the third or fourth day. They migrate into the wound by amoeboid movements. They synthesize the protective and stabilizing components of the ECM such as proteoglycans, collagen, and elastin. The precursors of endothelial cells are stimulated and angiogenesis is induced due to the low oxygen concentration with the help of VEGF, PDGF, and FGF secreted by macrophages. Pericytes released from the vessel walls in response to VEGF turn into endothelial progenitor cells and progress in the form of a tube by clustering towards areas where oxygen is low. New vascular loops that are formed by the union of the vascular tubes with the existing vessels restart blood flow and angiogenesis occurs. Consequently, angiogenesis restores the oxygen supply, which is a necessary condition for osteogenesis. Newly formed bone tissue is located only in the areas near blood vessels. Briefly, activated osteoclasts adhere themselves to the fracture areas of the residue of bone, resorb and create space for bone healing. However, it will influence the primary stability of implants. Osteoclasts dissolve the bone by the action of hydrochloric acid (HCl) and proteases and release BMP, TGF- β , PDGF from the bone ECM, which initiates the formation of new bone. Perivascular cells (osteoprogenitor cells) proliferate through the implant surface and

differentiate into new osteoblasts under the influence of BMPs. Osteoprogenitor cells attach to the implant surface via integrins which have RGD motifs that allow them to attach to ECM proteins. The osteoblasts are not attached directly to the metal surface. The osteoblasts bind to the outermost protein layer of the implant. Bone precursor cells prepare the environment required for cellular attachment by producing fibronectin on the implant surface. After firmly attached to the implant surface, osteoprogenitor cells turn into osteoblasts active for bone production, and osteoblasts begin to synthesize osteocalcin and alkaline phosphatase as molecular markers, along with calcium phosphate. Towards the end of 2 weeks, woven bone is formed at the implant surfaces, this will create a secondary stabilization. When the implant is first placed, it gains primary stability due to the friction between the threads and the bone. On the first day, primary stability is very vital after implant placement. Under normal circumstances, the first week is the weakest stage since primary stability can drop to crucial levels. Within a week, the implant is placed, new bone formation begins, and primary bone contacts are replaced by new secondary bone connections. In the socket, the first bone formed after the bone is injured with a drill is called a woven bone. Woven bone formation is from the existing bone between the implant threads. With the synthesis of the Type 3 collagen matrix by osteoblasts, new bone formation starts with intramembranous ossification in the alveolar bone. At the end of the process, Type 1 collagen takes its place in the bone under any circumstances. This matrix is then mineralized by hydroxyapatite. During primary bone formation, mineralization occurs more rapidly; it is not fully organized and does not integrate with collagen (extra fibrils).

In the remodeling phase, parallel bone formed is structured perpendicular to the peak of implant threads. The organization of the bone becomes more trabecular. This process happened by the coupling action of osteoclasts and osteoblasts. Osteoclasts activated by osteoblast messenger RANKL resorbs the woven bone and the osteoblasts lay down highly organized lamellar bone. This simultaneous action of osteoblasts and osteoclasts is coordinated by the osteocyte and its messenger sclerostin. In the latter case, the Haversian system which is a new unit is formed containing a central blood vessel.

1.1.3.2 Blood Vessel Formation in Bone Tissue

Blood vessels consist of various cell types. Endothelial cells (ECs) and mural (or perivascular) cells cover the outer and inner layer of blood vessels, respectively. The mural cells might be categorized as vascular smooth muscle cells and pericytes based. Blood vessels can be formed through two processes, angiogenesis and vasculogenesis. Angiogenesis occurs in early embryogenesis by differentiation of mesodermal cells to the progenitors of blood cells and ECs. These cells move to defined places in a process called vasculogenesis and cluster together for the formation of the primitive vessels. As a result, most new blood vessels arise through angiogenesis and continues through a series of processes such as the expansion of existing vascular networks, EC branching, migration, proliferation, and vascular anastomosis. Angiogenesis resulting from extensive communication between various vascular cells ensures that the newly formed vessel is completely stable and functional. For example, the arteriovenous specification of an EC subset causes the capillary beds to expand and the development of veins and arteries. Undifferentiated mesenchymal cells called pericytes, and smooth muscle cells and in the connective tissue, are particularly necessary for vascular remodeling, stabilization, and maturation. In addition, depending on the organ involved in vasculogenesis, vasculogenesis is controlled by local microenvironmental signals that blood vessels are formed and specialized. This leads to certain molecular signatures in ECs. This signature is also valid for the bone vasculature.

Bone contains bone marrow which is a nucleus of hematopoietic cells and adipocytes. Bone is rich in the calcified matrix. Except for the growth plate and articular cartilage, all parts of the skeletal system are highly vascularized and have blood vessels. Similar to other organs, there is a hierarchical organization in the vascular system of the bone where an arterial branch feeds the capillary network at the center of the diaphysis. The marrow is located in the main shaft of the bone. There are two lower bone capillaries, Type H and Type L [27]. Although these capillaries are interconnected as a single network, they differ depending on functional properties and marker expression. The metaphysis contains type H capillaries are found in. The metaphysis region is where the avascular growth plate is located, and located close to the growth plate. These capillaries extend at their distal ends in the form of interconnecting vessel columns, and the H capillaries close to the compact bone are associated with osteoprogenitor

cells that aid in the release of the perivascular osteoblasts. High levels of CD31 (PECAM1) are expressed by H-type capillaries. The H-type capillaries running along the distal long bone are densely linked close to the growth plate. Unlike type H capillaries, type L vessels are densely located in the bone marrow cavity of the diaphysis. Type L capillaries form a highly branched capillary network, expressing lower levels of the markers CD31. Densely packed hematopoietic cells surround type L capillaries which are connected to the central vein. Arteries deliver blood directly to H-type vessels in the endosteum and metaphysis instead of type L sinusoidal capillaries. Due to the bone vasculature, blood flows from the arteries to the H-type capillaries and then to the L-type sinusoidal network at the interface between the diaphysis and metaphysis. Finally, it is drained into the large central vein.

1.2 Bone Tissue Engineering

Tissue engineering is the combination of different scientific fields, such as engineering principles and biology, to mimic human tissues. Bone tissue engineering is also an interdisciplinary field that uses synthetic grafts as alternatives to allografts and autografts to support tissue regeneration. Bone tissue engineering aims to produce 3-D scaffolds that resemble an extracellular matrix, mechanically support the bone and enable the formation of bone tissue. Scaffolds are given osteoinductive, osteoconductive, and osteogenic properties to increase cell adhesion, proliferation, and spread of cells by this approach. In addition, these scaffolds facilitate differentiation into osteoblastic strains by activating biological and chemical factors. Scaffolds with suitable structures for cells cause cell attachment, proliferation, and differentiation. Scaffolds should degrade after the new bone tissue formation. Moreover, the surface of these scaffold biomaterials must be suitable for the regeneration and mineralization of damaged bone tissue. Biomaterials used for bone regeneration such as ceramics, composites, and polymers. Also, techniques for scaffold preparation are available to gain properties such as high surface/volume ratio, durability, and morphological similarity to ECM. Surface modification techniques are being studied for optimal bone tissue regeneration. The surfaces of the scaffolds can be changed to improve chemical and physical properties without losing their integrity.

1.2.1 Biomaterials for Bone Tissue Engineering

Biomaterials possess various characteristics and properties depending on the intention of usage and possessing duration to assist, help and replace the targeted tissue without any rejection [28]. Some specific properties make materials considered as in the “biomaterials” category. The terms such as biocompatibility, bifunctionality, bioinertness, biodegradability, bioactivity, non-toxic, and non-inflammatory are considered critical for biomaterials [29, 30].

1.2.1.1 Key Factors for Biomaterials

Biocompatibility is one of the characteristics that a biomaterial should possess not to create an inflammatory response, not to cause any toxic effect on tissue, and be accepted by the host tissue after the implementation [31]. It is the “ability of a material to perform with an appropriate host response in a specific application” [32]. In tissue engineering, biocompatibility is very important for scaffolds and matrices that can support the regeneration process by having a suitable environment for cell-cell communication, cellular metabolism, and supporting optimum ECM conditions. Bifunctionality indicates biochemical, biophysical, and biological functionality and the ability of a material to initiate regeneration of the tissue via different biological cues [31, 33]. Bioinert materials do not cause any chemical reaction or biological response in the host tissue and release any potentially reactive compounds [31]. A fibrous capsule is formed around the bioinert material. The biological functionality of materials is critical and based on tissue integration through implants. Bioinert biomaterials such as zirconia, alumina, titanium, and carbon are generally used as implant materials. The interaction between the host tissue and the material is directly related to bioactivity, the property of the material that can cause biological activity such as modulation of metabolic processes [34, 35]. Bioactive materials create a chemical bond with the bone tissue. This interaction results in the osteointegration process [31]. The non-toxic and inflammatory properties of the material are the ability to not cause any scar tissue formation or side effects caused by small compounds released from the biomaterial or from the material itself.

Physical, chemical, biological, and mechanical characteristics are critical for biomaterials [31]. The physical properties of materials directly affect the ability of cells to adhere to the material surface. Among such properties, wettability and roughness are generally critical surface properties [31]. Wettability can be defined as the ability of such a material that can maintain its contact with a liquid-like material for a certain period [36]. It depends on the hydrophobic or hydrophilic nature of the material. The potential friction between surfaces has a major influence on biological responses such as protein absorption [37]. Heavily polar water molecules close to the surface exhibit enhanced relationships with water molecules around hydrophobic surfaces. Because of the entropy, energetically unfavorable losses occur. The hydrophobic parts of the protein structure resulting from the dehydration of the protein structure have weak hydrophobic reactions with the surface, except for water molecules to compensate for this energy loss. The interaction leads to a rise in water entropy in the solution while increasing the protein adsorption of the biomaterial surface [38]. To obtain wettability, the contact angle of the material surface is measured and considered as the main indicator [39]. Roughness, whether *in vivo* or *in vitro*, is an important property that affects the success of more behaviors such as cellular binding, proliferation [40]. Surface roughness is defined as the indicator of fine-spaced micro-sized irregularities on the material surface [41]. Depending on whether the surfaces are soft or rough, the behavior of the cells changes, and this surface property has a direct effect on the cell-material bond within the tissue [31, 40, 42]. Material composition, particle size, crystallinity, and porosity are also important physical properties. Material composition is the main property of a biomaterial that can be changed according to its purpose, and it also affects the cell material behavior in the surrounding tissue, its properties such as biocompatibility, biodegradability [43]. Particle size used as porogen determines the surface-area-volume ratio and porosity of biomaterials. Porosity affects the material's cell permeability, efficacy, and ability to induce an immune response after degradation. [44]. Scaffolds used for bone defects require a highly porous scaffold higher than 90% and a porosity higher than 80% for effective cell transmission. Mechanical properties, interconnectivity, and pore size are affected by the molecular weight of the polymer. The discrepancies in the mechanical properties that occurred between *in vitro* and *in vivo* studies might be caused affected by different cell types requiring different pore sizes for localization in the scaffold after

implantation. For instance, bone cells choose larger pores while fibroblasts choose to be placed in slighter pores [45]. Crystallinity is another property that depends mostly on polymer composition and environmental factors. It is defined as a measure of the number of crystal parts within a material on a percentile scale [46]. As the crystallinity of a material increases, the solubility decreases, and the structural integrity changes. For bone tissue, crystallinity property comes from the mineral within and it is considered to correlate with age and the crystallinity degree [47].

Mechanical properties of a material are considered as a building block during the production of a structure to replace or support the biological activity within the host tissue. Researchers aim to produce this structure by mimicking the mechanical properties of the host tissue by using specific materials. The materials are selected by considering the mechanical properties such as young's modulus, tensile and yield strength, ductility and toughness, compression strength, fatigue, and wear [31]. Young's modulus, or modulus of elasticity, is considered to be a measure of a material's ability to resist any changes in its original dimensions when a force is applied to the material's surface. It is calculated by dividing the force per square meter by its fractional change in length [48]. For bone regeneration, biomaterials with a similar young's modulus are usually preferred to provide a homogeneous distribution of any tensile and compression stress and avoid any fracture or stress shielding [49]. Tensile and yield strength is the defined stress value of a material that may or may not have gone through a structural change permanently at that stress level. Those values of any material are observed through a stress and strain curve and the points define the cumulative areas which the material can return to its original shape (elastic region) and can not return (plastic region). Until the yield strength point, materials can resist the applied force and can return their shape easily, while at tensile strength it loses its elastic future and goes through the plastic phase that will eventually result in fracture. The Compressive strength of a material indicates its resistance to an axial pressure per unit area [50]. For bone regeneration, the biomaterials tensile, yield strength points, and compressive strength are considered to have a structure that can resist the pressure for enough period for an efficient recovery. Ductility is another important property for a material that faces pressure constantly like bone tissue and is defined as the material's ability to go through plastic deformation without any fracture formation. It is also considered as an indicator of how much a material can be malleable or soft [51].

Toughness, on the other hand, which is also defined as a material's ability to go through a plastic deformation without rupture, can also be defined as a material's capacity to absorb energy and can be found throughout the entire area under a material's stress-strain curve [48, 52]. Fatigue of materials is defined as the constant pressure that results in progressive plastic deformations which is a result of repeated high stress and strain. The concept named "fatigue life" is considered while developing the material, which is the number of stress cycles that such material can preserve its character without any rupture. Especially while developing a biomaterial for bone tissue regeneration, researchers prefer having good resistance to fatigue [53]. The wear of material is more related to the environmental forces that it faces rather than the material directly. However, the characteristics of the material surface can be a result of its components or structural conformation which is directly related to the material. Wear is defined as the process that is caused by the contact between surfaces of two substances that results in a decrement or structural deformation within the surface.

The biological properties of a biomaterial are considered as the main element that decides such materials fate within the host tissue. Whether creating new material or developing a structure, researchers prefer using specific materials that have the desired biological properties. Some of those properties can be also considered as the chemical properties which are already explained in the chemical properties part. However, some additional biological properties are needed especially for bone tissue regenerations. Those properties are osteoconductivity, osteoinductivity, and osteointegration. Osteoinductivity is material's ability to trigger the development of bone-forming cell lineage or in other words induction of osteogenesis [54]. When osteoinductive materials are placed within the defected host tissue, it triggers the enrollment of undeveloped cells to differentiate into preosteoblasts. Especially for bone regenerations that aim at the fractured structure, osteoinduction is the main elements that should be considered. Osteoconductivity is the material's ability to allow preosteoblast or osteoblasts to grow on its surface or within the pores without causing any inflammatory response. Especially while developing implants researchers prefer osteoconductive materials to have a better healing process.

1.2.1.2 Types of Biomaterials

Metals are usually used as a part of implants to replace the function of defected tissue permanently. Metallic biomaterials with high mechanical features due to their crystal structures and strong metallic bonds have several areas of usage in bone tissue engineering. However, biocompatible metal or alloys are preferred instead of other materials which have some disadvantages such as the release of metal ions due to corrosion that can cause immunological tissue reaction. Metal alloys are frequently used in joint and bone implants due to their good physical features such as high strength, toughness, and ductility. Metallic biomaterials with good corrosion resistance and mechanical properties are used in the construction of tools such as plates, screws, nails used for fixing hip, knee, spine implants, and broken structures. Metal prostheses must be tested in buffer solutions to assess biocompatibility [55]. such as tantalum, magnesium, titanium, and more [56]. Titanium is an ideal implant material due to its excellent biocompatibility [57]. The biocompatibility of titanium is determined by its ability to form a stable and nanometer-thick layer of TiO_2 , which forms spontaneously on its surface, protecting pure titanium from corrosion even during wear [58]. Commercially pure titanium (cpTi) is classified according to its oxygen content and divided into four groups. Grade 4, which contains 0.4% oxygen, is the maximum oxygen-containing group, whereas Grade 1 which has 0.18% oxygen, minimum oxygen-containing group. There are mechanical differences between the different classes, and these differences are mainly due to the number of contaminants. Iron is introduced to improve the corrosion resistance of titanium. To increase durability and reduce density, aluminum is introduced to titanium. Vanadium is used as an aluminum cleaner to avoid corrosion. α -Ti (α -phase) is the hexagonal closed packed cage of titanium. When (α -phase is heated to 883 °C, it turns into β phase. Titanium sustains the reactivity until it spontaneously creates a dense oxide layer on the surface. Under 882.5 °C, titanium is a biphasic metal and transforms into α -phase into β -phase in the temperature higher than 882.5 °C. Titanium has been the material of choice in intra-bone applications due to its high passivation, controlled thickness, elasticity module close to the bone, resistance to chemical attack, catalytic activity in chemical reactions [49]. Titanium helps the osseointegration of implants. The success of titanium implants in osseointegration makes them an ideal candidate for dental and orthopedic implants. Grade 4 implants have been used for a long time in clinical dating back to the 1965s

[59]. However, in some cases, Grade 4 titanium has insufficient mechanical and tensile strength. For example, in cases where an implant is required to complete a single tooth deficiency and the implant needs to be placed in a narrow area, implants smaller than a diameter of 3.5 mm are preferred [60-62]. In this case, the implant with a reduced diameter faces an increased risk of fracture [61, 63]. Therefore, it has become necessary to develop titanium alloys instead of pure titanium to improve the mechanical strength of small diameter implants. The aesthetic properties of titanium bring some disadvantages. Especially in patients with thin gum biotype in the aesthetic area, the gray color is reflected from the neck of the implant to the gingiva, and even if the implant is successful, the result is not satisfactory and success is limited. In such cases using titanium implants may require soft tissue grafts [64].

Ceramics are inorganic and non-metallic solid materials containing metal, nonmetal, or semi-metal atoms held by ionic and covalent bonds. Ceramics specially designed for the repair, reconstruction, or replacement of the organs of the body that are damaged or lose their function are called bioceramics. Bioceramic materials are common in use because they are biocompatible, have no immune system triggering effects, and are not allergic and carcinogenic [65]. Bioceramics are resistant to abrasion and very light. Bioceramics are made of polycrystalline and resist microorganisms, temperature, solvents, and pH changes due to their stable chemical structure. Ceramic biomaterials can be divided into three groups according to tissue response: bioinert ceramics, bioactive ceramics, and bioresorbable ceramics [66]. Bioinert materials retain their physical and mechanical properties when they interact with tissue. Therefore, they are not biologically active. In this way, they resist corrosion and wear. Live cells adjacent to the tissue in bioinert materials do not react, but they usually grow protective fibrous cells in areas close to the implant surface to protect local cells from mechanical damage [67]. The most commonly used bioinert ceramics is alumina (Al_2O_3). Alumina, which belongs to the group of bioinert ceramics, has high chemical stability and does not show toxic properties. It is commonly used in load-bearing applications [68]. Zirconia (ZrO_2) is more durable, dense than alumina, and better surface quality can be achieved. However, new zirconia-alumina composites have been developed with stronger strength and fracture toughness than alumina alone [69]. Bioactive ceramics are a type of material that creates direct chemical bonds with the bone or soft tissue of the organism. Two

examples of bioactive materials are bioglasses and HA. Bioglasses are biomaterials containing low amounts of silica and high amounts of sodium and calcium. The biggest advantage of bioactive glasses is the high surface reaction rate that allows quick tissue binding. The most important disadvantage is mechanical weakness and low fracture toughness caused by a two-dimensional amorphous glass structure. Therefore, these glasses are not appropriate for use in applications requiring load-bearing [70]. Hydroxyapatite ($\text{Ca}_{10}(\text{PO}_4)_6(\text{OH})_2$) is suitable for biomedical applications because they are biocompatible and bioactive. It is the basic mineral composition of natural bone. HA is also an osteoconductive and non-toxic substance. However, its mechanical properties are not sufficient for various applications. Therefore, HA ceramics cannot be used alone in areas exposed to heavy loads [71]. In addition, it was observed that these biomaterials had slower degradation rates in the body than the rate of bone formation. In some studies, it has been shown that HA is not resorbed in the body and stays as a foreign substance for a while [72].

Natural polymers are divided into two groups either polysaccharide-based or protein-based [73]. Protein-based biomaterials that are used in bone tissue engineering are fibrin, silk, and collagen [74]. Polysaccharide-based biomaterials that are used in bone tissue engineering chitosan, alginate, hyaluronan, and agarose [73]. Fibrin is a type of natural protein-based polymer found in the blood, composed of fibronectins and having a cross-linked, net-like structure. It is used in tissue engineering applications to enhance the wound healing process and in the form of scaffolds. For bone tissue regeneration, it has become an important biomaterial due to its high biocompatibility, easily controlled biodegradable structure and ability to be used for biomolecule and cell delivery [75]. Silk is a type of protein-based natural polymer that has properties such as long-term degradation, improved hydrophilicity, biocompatibility, and fine mechanical strength that makes it a good participant in bone tissue application [73, 76]. For bone tissue regeneration, it is usually used in the form of electrospun scaffolds. However, it is found to have a poor osteoinduction property, so generally used in a combination with other biomaterials and factors [77]. Collagen is a biomaterial found in the human body in bone, cartilage, dentin, and cement, also within the ECM to provide mechanical stability to cell and tissue structure. It also accounts for 89% of the organic matrix and 32% of the volume of the composition. For bone regeneration, it is used in various forms such as injectable hydrogel, membranes, and

films or scaffolds, in addition to being combined with other materials to overcome its poor mechanical properties [78, 79]. Chitosan is defined as a type of polysaccharide that is formed through the deacetylation of chitin molecule and usually found within the shells of marine creatures, fungi cell walls and insect shells[80]. It is considered as a promising biomaterial in bone tissue engineering applications due to its biocompatible, biodegradable, and non-toxic properties. Chitosan is used in the form of scaffolds and hydrogels [81]. Alginate is another biomaterial that is polysaccharide-based that can be found in brown seaweeds [81]. For bone tissue engineering, it is generally used in form of a scaffold by combining alginate with other biomaterials or as hydrogel one research group used it to provide a delivery system for growth factors to the host tissue [82, 83]. Agarose is algae and seaweed-based natural polymer that is generally used in cell culture applications to replace the cell medium. It is used in the form of a scaffold to promote cells and help them differentiate to the target cell line [84]. Hyaluronan is naturally found within the tissues of skin and cartilage, usually used as a treatment for osteoarthritis, glaucoma, and corneal transplantation [73]. For bone regeneration, it is used in the form of hydrogels[85], grafts[86], and as delivery vehicles [87]. Synthetic polymers such as polyglycolic acid (PGA), polylactide (PLA), and poly(lactic-co-glycolic) acid (PLGA) are mostly used biomaterials. They have good mechanical strength and they are cheap when compared with synthetic polymers. Synthetic polymers can be fabricated with desired architecture and also, their degradation rate can be controlled by controlling the composition of the synthetic polymer. Despite these advantages, synthetic polymers have poor cell distribution and adhesion since they have hydrophobic surfaces and because of that fewer cell-recognition signals. Also, because of their acidic degradation products, they cause systemic or local reactions in the body. They have less bioactivity when compared with natural polymers. Because of that, there is an immune rejection possibility with synthetic polymers [88, 89]. PLGA is a type of biodegradable and biocompatible FDA-approved copolymer that is used in various applications such as drug delivery, tissue engineering applications and sutures [90, 91]. PLGA is synthesized by the chemical reaction between lactic acid and glycolic acid monomers at different ratios. It has a good solubility range, can be easily shaped, semi crystalline, hydrophobic, altered in size and can be degraded via hydrolysis of the ester linkages [92]. The degradation of PLGA occurs in 4 steps: first water penetrates the amorphous part, disrupts the

hydrogen and van der Waals bonds (hydration), then the covalent bonds between the monomers begin to cleave, then the carboxylic end groups begin to autocatalyze and mass loss occurs within the covalent bonds of the backbone, and finally the final cleavage of segments in the solvent and their dispersion occurs [93].

1.2.2 Types of Scaffolds

Hydrogels can be defined as 3D crosslinked networks of polymers, which can swell in water and keep huge liquid volumes within the swollen state. Hydrogels, which have a porous structure, can be modified with certain bioactive molecules such as growth factors, peptides, and proteins for the aim of providing functionality biochemically, and they are capable to mimic the 3D environment of tissue structures. The water ingredient of hydrogels is at elevated levels reaching up to 99% based on the concentration of polymeric composition of hydrogels [94]. Due to their high water holding capacity, they are highly hydrophilic and have viscoelastic mechanical properties [95]. The source and composition of polymers source denote whether the hydrogel is natural, synthetic. Natural hydrogels might be obtained from naturally occurring polysaccharides and their structure is similar to natural ECM. Hydrogels can be synthesis in 3 ways: by using a crosslinking agent, by crosslinking the polymers that already exist, or by combining both methods. Their performance is influenced and can be controlled by several properties. These properties are being sensitive to pH and temperature, having visco-elastic properties, percentage of porosity and pore size, presence of any functional groups, allowance to be shaped, sterilization capacity level, stability degree to reactions like hydrolysis, oxidation, and chemical behavior of crosslinks and backbone of the hydrogel. Hydrogels are generally used in bone regeneration applications due to their similarity with ECM structure, biodegradability, ability to use it to produce scaffold, and their ability to act as a carrier for cells and bioactive molecules [96].

Scaffolding materials with a nanofibrous structure are available to be used in the field of tissue engineering since they have a huge surface-area-to-volume rate and imitate the structure of natural ECM at the nano dimensions. Nanofibrous scaffolds have micro-scale porosity inside them which makes the cellular activities, adhesion, and differentiation easy. ECM has collagen filaments nearly 50-500 nm in diameter, and

nanofibrous scaffolds have similarities to the natural ECM collagen filaments [97]. Furthermore, the nanostructures produced via self-assembly can be turned into functional materials when some specific desired bioactive sequences are introduced, encouraging activeness and molecular selectiveness of these structures in this way [98, 99]. The functionalization of self-assembled nanofibrous scaffolds is a good strategy to control cell behaviors such as cell attachment, spreading, migration, and differentiation. Researchers recently have focused on Self-assembled peptide functionalization through direct solid-phase synthesis extension at the amino-terminal to alter its biological activity as hydrogel scaffolds.

1.2.3 Fabrication Techniques for Biomimetic Scaffolds

The material and porous structure of the scaffold is important for tissue reengineering applications. To form a functional tissue, a scaffold should be fabricated with the proper method to promote cellular distribution and growth into three-dimensional space [100]. The conventional method of tissue engineering is the autograft which depends on the availability of donor tissues. Because of side effects such as pain and risks to patients, scaffold fabrication becomes prominent. There are several scaffold fabrication techniques. Commonly used scaffold fabrication techniques are solvent casting/particulate leaching, freeze-drying, gas foaming, phase separation, rapid prototyping, and electrospinning.

In the solvent casting/ particulate leaching technique, salts are spilled in a mold. Then, the salt-filled mold is cast by the polymer-solvent solution. Then, the solvent evaporates. Salt particles are leached away by submerging the remaining matrix into the water to obtain porous scaffolds. This technique is low cost and the fabricated scaffolds have high porosity of up to 90%. However, this fabrication technique is time-consuming and the solvents are very toxic [101, 102].

In the freeze-drying technique, also called lyophilization, first a proper solvent is used to dissolve the polymer. The solution is cooled to a temperature that is less than its freezing point and then, evaporated. Finally, a solid scaffold with an interconnected structure is obtained. By changing the freezing method, the pore sizes can be controlled. Disadvantages of the freeze-drying technique are high energy consumption, usage of cytotoxic solvents generation of pores with irregular size [103].

In the gas foaming technique, firstly polymeric solution is prepared with water or fluorophore. Then, the polymeric solution is pressurized with carbon dioxide or nitrogen until the polymer is saturated. After the saturation of polymers, nucleation and gas bubbles occur. This situation causes to pore formation inside the fabricated scaffold. The obtained scaffold structures have high porosity up to %85 [104].

In phase separation, the polymer is dissolved in the solvent and a polymer solution is formed. Then the temperature is lowered and the polymer solution is separated into two phases: the low polymer phase and the high polymer phase. After the solvent portion is removed, the high polymer phase solidifies and a relatively porous framework structure is obtained. The phase separation technique is operated at low temperatures. The frameworks obtained by this technique have high porosity up to 98% [105].

Rapid prototyping which is a computerized fabrication technique enables the rapid fabrication of framework structures using a computer-aided design model (CAD). This method allows the fabrication of scaffolds with control over the polymer structure to overcome some of the disadvantages of other fabrication techniques. Customized and patient-specific scaffolds can be fabricated using this technique. Rapid prototyping techniques include selective laser sintering (SLS), stereolithography, fused deposition modeling (FDM), and 3D printing [106].

Electrospinning technology can produce polymer nanofibers with diameters ranging from 3 nm to 5 μm . A basic electrospinning system consists of a collector, syringe pump, high voltage source, and syringe. First, a polymer solution is prepared using a suitable solvent. The polymer solution is pumped and results in a drop of the solution. Then, a high electric field is applied to the polymer solution, resulting in charge repulsion within the polymer solution. When the charge repulsion overcomes the surface tension of the polymer solution, the jet of polymer solution begins and is ejected from the tip of the needle. At the same time, the solvent portion evaporates and the polymer nanofibers are collected by the collector. Finally, a scaffold structure is obtained. The electrospinning technique can be used to produce nanofibrous scaffolds. However, obtaining scaffolds with sufficient pore size can be problematic. In addition, the solvents used to form the polymer solution can be toxic [107].

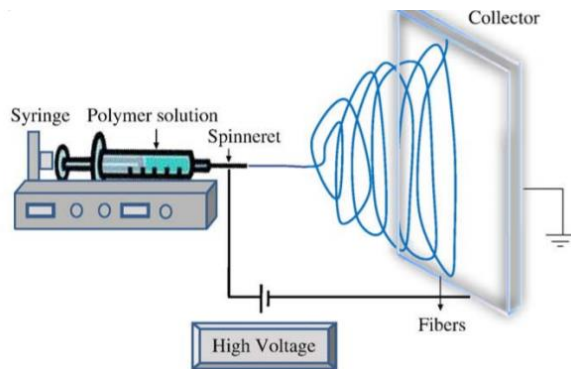


Figure 1.4: Basic electrospinning setup [108]

Self-assembly can be defined as a process in which disordered molecules, atoms, or components of a system are spontaneously organized into more ordered, defined structures through certain modes of interaction occurring between them [97, 109-111]. Self-assembly which is a dynamic procedure is a spontaneous phenomenon that occurred in nature for years. Small atoms or molecules interplay with each other and are put in order and so that supramolecular constructs are formed [97, 112]. Living systems and nature are very important for providing sources to create novel matters [113]. Nature provides an infinite resource to humans for designing and producing original substances and creating inventions [109]. It is well known that nature has mastered producing many nanostructures by using only twenty amino acids. Self-assembly plays a crucial role in natural construct formation. Therefore self-assembly processes are good chances for humans to develop countless materials and substances at nano dimensions by mimicking the nature and natural procedures [98]. Assembly of collagen, silk, and keratin can be some samples for the self-assembly of molecules in nature [114]. Nowadays self-assembly can be considered an important method for the fabrication of nanostructures or structures containing nanofibers. It provides to produce useful and operational materials, especially the biomaterials and scaffolds for tissue engineering.

Self-assembly is included in bottom-up systems. Self-assembly as a bottom-up process has many advantages over top-down processes in that it allows 3D assembly, achievement of near-atomic property sizes, manufacturing on a large scale with

effective cost [98]. To obtain supramolecular practical systems and constructs, the process of self-assembly of small building blocks exists everywhere in nature. Peptide amphiphilic (PA) molecules and their self-assembly are good examples of such supramolecular biological constructs [115]. PA is the most important self-assembling substance known, it includes a peptide region and forms hydrogen bonds to form β -sheets, and a hydrophobic region containing only a carbon tail [95, 110]. This peptide part is connected to a hydrophobic alkyl tail with a peptide bond [115]. PAs are biocompatible and biodegradable. Under physiological circumstances, PA molecules self-assemble into nanoscale one-dimensional constructs by forming nanofibers, and they are also known to be capable of forming hydrogels by water encapsulation and the self-assembly of PAs provides nanofiber production with a high-aspect-ratio [116]. This fiber system, which contains large water in its structure, can mimic the natural ECM. Biologically effective and active nanostructures can be formed with the addition of epitopes by the exchange of amino acid series. PAs have enormous potential for some interventions in the biomedical field, such as point-of-need drug delivery, wound healing, and processes for tissue engineering and regenerative medicine, and materials created by self-assembly of PA molecules are also finding a place in technology, materials science, and electronics [95]. PAs can also self assemble into cylindrical nanofibers, globular micelles, or flat strips [113]. The final structure formed by the self-assembly of PAs can be diverse, such as nanofiber, nanoribbon, nanosphere, etc., and this diversity is due to the concentration, type, and sequence of the peptide. PAs have enormous potential for some interventions in the biomedical field, such as point-of-need drug delivery, wound healing, and processes for tissue engineering and regenerative medicine, and materials generated by self-assembly of PA molecules are also finding a place in technology, materials science, and electronics and nanotechnology [111]. Moreover, PA molecules have the ability to make signs that induce a biological effect, and they could usher in the innovations for the future of medicine by enabling the production of gel-like meshes that entrap cells within the tissues into which they are injected by self-assembly of peptide segments [117].

Molecular self-assembly scaffolds mimic the structure and functions of the native ECM as in the body. The main point of self-assembly is molecular recognition. Self-assembly can be used as a tool to generate synthetic compounds with specific properties and gradual structure. In the mechanism of self-assembly, disorganized

molecules organize themselves into some larger and ordered structures that have hierarchical arrangement and complication. The most essential features of the self-assembly process are the complementary chemical and also structural compatibility via some interactions that are weak and non-covalent. Molecular self-assembly is a method that includes some non-covalent interactions such as hydrogen bonding, ionic bonding, metal-ligand interactions, water-mediated hydrogen bonding, electrostatic, hydrophobic, and van der Waals interactions to produce new materials. All these interactions and bonds are weak, dynamic, and sensitive, but when they come together and go into action, they can form structures that have good stability and they can manage the 3D arrangement of molecules such as proteins and determine their communication with other particles [117-119].

In the practice of tissue engineering science, self-assembly products behave like 3D synthetic scaffolds. They have important utilities; for example, they have an adaptable structure, they ensure gel media that are biologically suitable and degradable, that have a porous structure and biological activity when used in tissue regeneration studies. Moreover, these gels prepared by peptide self-assembly can be used as injectable gel substances. These cell-based injectable gel scaffolds can be used to transfer required cells into the defective part of the damaged tissue to accelerate tissue regeneration [120]. Peptide hydrogels prepared by self-assembly of PAs through cross-linking are biocompatible, conformable, invertible, and have favorable properties and the addition of biologically active peptide epitopes to the structures allows mimicking the ECM of the desired tissue [99]. Although various molecules may be available in self-assembly processes, peptides are very appealing due to their biodegradability, versatility, and biocompatibility, and scientists can control them to adopt different secondary structures. Peptide molecules are crucial for functional self-assembly because they have a more basic structure and different physical and chemical properties. The fact that they are very simple, adaptable or versatile, and purchasable makes peptide models good systems for self-assembly. It is well known that the two basic sources of peptide molecules are the naturally derived peptides and the chemically produced peptides. Naturally derived peptides have some limitations such as difficult availability, risk of contamination, and variability. On the other hand, peptides obtained by chemical synthesis do not have these problems and can be manipulated according to the desired necessities [109, 112, 121].

1.2.4 Scaffold Modification Techniques

Scaffold interactions with cells are very crucial in tissue engineering. The property of the surface directly affects the cellular response and the rate and quality of new tissue formation may be affected. Surface chemistry and topography define whether protein molecules are adsorbed and the protein adsorption affects the way cells attach and proliferate. One disadvantage of biodegradable synthetic polymers for scaffolding materials is that they do not contain bioactive recognition molecules. Hydrophobic polymers cannot create an ideal environment for cell-biomaterial interactions. Therefore, surface modification of polymeric scaffolds is a recent important field of study.

Chemical surface modification is used when conventional physical methods are inadequate to improve surface properties without changing the surface roughness. In chemical surface modification methods, the polymer is dipped in chemical, coated, or chemical pustules to improve the surface properties of the polymer. These wet procedures also eliminate germs and debris to sterilize for biomedical applications. Wet chemical etching induces the functional groups on the surface and thus increases the surface energy. Wet chemical etching is effective because the solvent penetrates deeply into the pores of the polymer matrix. In addition, materials can be processed selectively thanks to wet chemicals. For example, wet chemicals such as potassium permanganate and 2- (2-butoxyethoxy) ethanol increase the biomaterial surface roughness, while exhibiting additional etching of the surface [122]. The surface adhesion of nylon is increased by iodine-potassium iodide solution by increasing the crystallinity [123]. Sodium hydroxide, a strong base, was used to modify polypropylene networks without compromising their mechanical properties, and this modification increased cell attachment [124]. Polyethylene terephthalate (PET) films are modified using acetonitrile-permanganate-sulfuric acid, respectively, to form new carboxylic groups on the surface. While traditional wet chemical etching approaches can be economical and practical, they require expertise as the reaction rate depends on the material composition, the processing time, and the power of the reagent. In addition, these processes always exceed the amount of hazardous waste generated by additional procedures such as washing and drying.

Due to changes in surface chemistry, modification of polymer substrates with a laser by fluency under the ablation threshold improves cell attachment. Reactive radicals are revealed by the chemical bonds broken by laser irradiation. The formation of these radicals occurs after the rapid reaction of the broken bonds with the surrounding atmosphere. As a result of oxidization of the polymer surface, it is formed in new functional groups such as new COOH and OH groups as well as reactive nitrogen species with a smaller number of amino groups [125]. As a result of changing the surface energy of polymers with laser, attachment, and proliferation of cells increase [126]. However, the fact that the excessive functional groups added to the surface and the reduction of attached cells by increasing the processing time indicates that this method is contra-efficient. Another disadvantage is that the material is deformed and lost as a result of increasing the fluidity above the ablation threshold during laser application. The purpose of the ablation process is to generate a groove where the cells line up themselves during attachment. Since the surface of these grooves becomes functional thanks to the oxygen groups and the roughness rises, it increases cell adhesion in the modified areas [127].

Free radicals and electrons, electrically excited species, reactive nitrogen (RNS) and oxygen species (ROS), and photons from the fourth state of matter, plasma. During plasma formation, ionization of the gas occurs due to the energy given to the gas. Electrical energy is usually applied to the gas to create plasma. When an external electric field created under high voltage is applied to the gas, the applied electric field accelerates the free electrons. Electrons accelerated by gas atoms and molecules allow electrons to be removed from gas molecule structures, causing electron avalanche and gas ionization. When the externally applied electric field accelerates free electrons and the free electrons acquire kinetic energy, their temperature can rise to thousands of Kelvins. The kinetic energy of free electrons is transferred to gas molecules during collisions between free electrons and gas molecules. Depending on the efficiency of energy transfer from electrons to heavier ions and neutral gas atoms and/or molecules, plasmas are classified as thermal (or hot or equilibrium) and non-thermal plasma (or cold or unstable). In a thermal plasma, there is a thermal equilibrium as the temperature is relatively homogeneous across electrons and heavy particles such as molecules, atoms, and ions. The underlying reason for this is that when thermal plasmas are produced, electrons perform fast and elastic collisions without loss of energy, and

heavy particles and electrons are given electrical energy due to their high mobility and high numbers [128]. In cold plasma, the cooling of heavier ions and neutral gas atoms and molecules occurs faster than the transfer of energy from electrons to them. Thus, the plasma remains at room temperature and therefore cold plasma heat-sensitive biological substrates and biomaterials can be applied. Cold atmospheric plasma (CAP) therapy is an emerging technique, and its various applications, including antimicrobial and anticancer activity, together with biomaterial modifications, have been reported in the literature due to its applicability on biological materials and biomaterials [129]. Along with free radicals generated during CAP formation, ROS and RNS can react with treated materials to achieve surface modification with no or minimal damage to the surface. Plasma-assisted surface modification has been shown to improve cell attachment due to increased hydrophilicity.

1.2.5 Development of Bioactive Surfaces

To improve the properties of native ECM, the development of bioactive surfaces on biomaterials is important to increase the capacity of biomaterials to support cell adhesion. Surface modification and development affect host response to biomaterial and cell interactions [130]. Proteins are the basic constituent of living organisms. It has various effects on cells. Proteins in the basal membrane play an important role in the behavior of cells. Usage of peptides is very popular in tissue engineering studies. Peptides allow for easier observation of the effects of the short active sequences in the long protein chains. They are effective on cell attachment, proliferation, growth, migration, adhesion, and differentiation. These effects can be stimulant or inhibitor, depending on the used cell and peptide type. Because of the wide impact scale of peptides, they have become the focus of different studies. Peptides are used in the research of new treatment methods and the development of existing methods. They are mostly used on nerve, cartilage, bone, vascularization, biomaterial surface and scaffold functionalization, and cancer therapy research areas [131, 132].

An amino acid is an organic substance that contains an amine ($-NH_2$) and a carboxyl ($-COOH$) group throughout a side chain (R group). In nature, 20 amino acids are used to create proteins and peptides. Amino acids have an amino group attached to the carbon atom of the carboxyl group. Peptides are made by connecting these amino acids

by peptide bonds [133]. When more than 100 amino acids come together, they form proteins. Peptides can be synthesized in a solution utilizing a solid phase processor. In a solid phase peptide synthesis system, the protecting group is insoluble resin, while in the liquid phase peptide synthesis system, the protecting group has a soluble form in the solution in which the reaction occurs [134].

The introduction and use of the technique called “Solid Phase Peptide Synthesis” began in 1963 with R. B. Merrifield. R. B. Merrifield used this technique to produce a tetrapeptide molecule by separately adding benzyloxy carbonyl amino acids to the polystyrene resin step by step. The benefits of solid-phase peptide synthesis are simplicity of the process, cheapness, and speed. [117, 135]. The starting point for peptide synthesis by this method is based on the binding of the first amino acid to the resin which is solid support containing a linker. Other amino acids are then added to lengthen the peptide chain [134]. To couple the first amino acid, structures called linkers with active and functional groups can be added to the structure of the resin used in the synthesis. The resin material should be able to swell in solutions used during peptide synthesis [133]. Solid-phase peptide synthesis mainly consists of three stages, deprotection, activation of carboxyl groups, coupling of amino acids via peptide bond creation [133]. First, deprotection of the resin is performed with chemicals such as piperidine, cyclo-hexylamine to remove protecting groups [117]. In the solid phase synthesis, Fmoc (9-fluorenylmethyloxycarbonyl) and Boc (tert-butyloxycarbonyl) are utilized mainly as protecting groups which are found in amino acids in the form of protecting group. Fmoc protecting group as a base labile group is temporary. In the deprotection step for creating the free amino groups, Fmoc is eliminated at every stages of peptide synthesis by using the piperidine [136]. In order to produce peptide bonding, this amino group interacts with the carboxyl group that is activated. Sidechains and N-terminus in the structure of amino acids can be protected by protecting groups that prevent the amino acid side chains from reacting with each other and allows the synthesis of the desired sequence of peptides accurately. Unlike the Fmoc group of amine groups, side chains of amino acid residues also have protecting permanent groups. These permanent protecting groups are kept attached during the synthesis, but they are merely cleared in the final step in which cleavage takes place [133, 136]. Following the deprotection process, the initial amino acid is coupled to resin. Attachment of first amino acid to resin structure can be achieved over C-

terminus. Solid-phase peptide synthesis that is notified by Merrifield is conducted from C-terminus to N-terminus. The N-protected amino acid is attached to resin with the carboxylic group and the C-terminus of that amino acid is attached to a solid support. After the coupling of the first amino acid to resin, other amino acids can be coupled and the sequence of the desired peptide is extended from C-terminus to N-terminus through a repeated sequence of deprotection and coupling of amino acids [134, 137]. Then, deprotection is performed to remove the protecting group in the structure of the lastly added amino acid, thereby releasing the N-terminus. Also, acetylation can be performed as the final step to preserve the N-end of the peptide molecule. Lastly, the resulting peptide is separated from resin by cleavage [117, 133].

Chapter 2

Aims of the Thesis

The main focus of this dissertation is the development of a peptide-modified novel biomimetic approach to design scaffolds for bone tissue engineering. Biomimetic peptides were used as a tool to facilitate the bioactivity of engineered synthetic scaffolds for bone tissue engineering applications. For this purpose, biomimetic peptides were synthesized by the solid-phase peptide synthesis method according to the desired bioactivity such as osteogenic and vasculogenic differentiation. The effect of these peptides was examined after integrating the scaffolds produced with different fabrication techniques. The specific aims of the study were to (i) accelerate mineralization on nanofibers via cold atmospheric plasma assisted glutamic acid templated peptide conjugation (ii) enhance osteogenesis of human mesenchymal stem cells by self-assembled peptide hydrogel functionalized with glutamic acid templated peptides (iii) investigate the role of functionalized self-assembled peptide hydrogel on in vitro vasculogenesis (iv) develop self-assembled peptide hydrogel for accelerating the osseointegration period of dental implants by inducing both osteogenic and vasculogenic differentiation (v) develop peptide conjugated nanofiber reinforced self-assembled peptide hydrogel for bone regeneration by inducing both osteogenic and vasculogenic differentiation

The overall hypothesis is thus: bioactive peptides can be integrated into scaffolds and improve their osteogenic potential. These bioactive peptides have an impact on facilitating their usage in tissue engineering. Overall, the findings in this thesis will aid in further optimization of biofunctionalized biomaterials to support stem cell-based bone repair and regeneration. It is also believed that such findings will help researchers to design better biomimetic scaffolds to be translated into the clinic to improve bone healing processes.

Chapter 3

Accelerated Mineralization on Nanofibers via Cold Atmospheric Plasma Assisted Glutamic Acid Templated Peptide Conjugation

3.1 Introduction

Scaffolds composed of hydroxyapatite (HA) and natural or synthetic polymers with tunable mechanical, chemical and physical properties can successfully mimic mineralized collagen nanofibers (NF) [138, 139]. To fabricate such biomimetic scaffold, many fabrication techniques have been utilized including electrospinning, solvent casting, freeze-drying, laser sintering, and 3D printing [140-142]. Among those techniques, electrospinning has been extensively used for developing bone ECM mimetic nanofibrous scaffolds by using natural or synthetic polymers [138, 143, 144]. Nanofibrous scaffolds not only resemble the assembly of bone ECM but also provide sufficient surface area for cell proliferation and differentiation [145, 146]. However, the major drawback of using electrospun nanofibrous scaffolds on bone tissue engineering is their inadequate mechanical properties [147, 148]. To overcome this limitation and also better imitate the mineralized bone tissue, composite scaffolds have been developed by combining HA with electrospun scaffolds by generally using blending electrospinning and biomineralizing in simulated body fluid (SBF) [149]. In the blending electrospinning technique, HA crystals can only bind physically on the surface of the NF and could be dissociated right after the fabrication of the scaffolds. It was previously reported that no significant difference was observed in the

mechanical properties of the electrospun scaffolds developed by blending electrospinning [149, 150]. However, in the biomineralization technique, composite nanofibrous scaffolds showed better biocompatibility and significantly higher mechanical properties of scaffolds due to the growth of nano-HA crystals that strongly attached to the surface of the NF [151, 152]. To initiate nano-HA growth on the surface of NF, biological cues that initiate the first step of the biomineralization known as the calcium chelating process should be present on the NF surface [145, 153].

Although natural polymers have biological cues that highly support scaffold mineralization as well as cell attachment and proliferation [154], there are some disadvantages such as less control over their mechanical properties and fast biodegradability [155, 156]. To address this issue some unmodified synthetic polymers have been preferred as scaffold material, but the absence of biological recognition cues on their surface limits their efficient use [157]. Therefore, the surface of the synthetic polymers needs to be modified to provide functional groups that initiate binding of biological cues that are known to induce biomineralization [158].

There are several surface modification methods to associate biological function into synthetic NF scaffolds [159]. Typically, these methods are based on the chemical integration of cell directive molecules such as growth factors and peptides into the scaffold. The mechanical properties of the polymer should retain while biochemical signals ensure the activity following chemical modification [160]. Surface modification of the scaffolds by using bioactive proteins or peptides can induce the desired signaling pathways in cells. The diversity of functional groups on ECM proteins makes peptides a great choice for tissue engineering applications. Nucleation and growth of HA crystals on collagen NF are mediated via bone sialoprotein (BSP) and osteocalcin which are constituent of bone ECM. These non-collagenous protein structure involve ranging from 2 to 10 residues of acid (GLU) sequences mediate nucleation and growth of HA [161]. In a previous study, Osteogenic differentiation and the effect of HA deposition to aligned NF were investigated on 2-mer GLU peptide on PLGA NF by using rat marrow stromal cells (MSCs). Herein, to conjugate biomimetic peptide sequence to accelerate biomineralization, we synthesized low molecular weight acrylate poly (L-lactide) (PLAA), conjugate 2-mer GLU peptide to acrylate groups of PLAA and electrospun high molecular weight PLGA blended low

molecular weight PLAA-2-mer GLU compound. The results demonstrated that 2-mer GLU peptide on the surface of PLGA NF enhanced nucleation and growth of HA crystals resulting in accelerated osteogenic differentiation of MSCs and mineralization [152]. Moreover, Barati *et al.* added organic acids into modified SBF (mSBF) and investigated biomineralization content on GLU peptide modified Polylactic Acid (PLA) based nanofibers. It was reported that mineralized CaP content on NF was significantly increased by the addition of organic acids to mSBF [162].

Synthetic polymers can be modified chemically with high reactive functional groups, such as carboxyl groups, for direct conjugation of bioactive peptide molecules [163]. Different polymer modification techniques such as pulsed laser deposition, ion beam deposition, covalent immobilization, photochemical modification, and oxygen plasma treatment have been carried out to enhance hydrophilicity and introduce functional groups on the polymeric scaffold surface to act as biological cues [164-166]. Several plasma-based technologies have provided an alternative approach to create thin porous coatings in the nanometre-thickness range that could promote cell attachment and proliferation [167, 168]. Non-Thermal atmospheric plasma (NTAP) or cold atmospheric plasma produces oxygen-containing functional groups on the polymer surface, mainly hydroxyl and carboxyl groups by reacting with polymers without altering mechanical properties [169]. Remarkably, when oxygen is inserted into the polymer matrix with NTAP treatment, the wettability of the polymer surface dramatically increases whereas no surface topography change is observed [170]. The introduction of carboxyl functional groups on the polymer surface can be useful for further conjugation with biofunctional peptides [171]. Therefore, we considered that it could be used as a pre-surface modification technique to effectively immobilize BSP mimetic GLU templated peptide onto the NF.

In this study, we used NTAP treatment as a surface functionalization methodology for effectively conjugating GLU peptide directly to PLGA nanofiber instead of blending electrospinning which is then mineralized in SBF to resemble the biomineralization process and structure of bone. This study comprehensively investigated for the first time in the literature the following: (i) determine the effect of NTAP treatment on GLU peptide conjugation and biomineralizing in SBF to form composite scaffolds; (ii) characterization of the morphology, structure, and mechanical properties of these

surface-modified and mineralized scaffolds; (iii) observing MSCs morphology and proliferation capability on the composite scaffolds.

3.2 Materials and Methods

3.2.1 Peptide Synthesis

All the peptide synthesis chemicals were provided from AAPPTEC (Louisville, KY, USA). EEEEEEE (Glu-Glu-Glu-Glu-Glu-Glu) peptide was synthesized on 4-Methylbenzhydrylamine (MBHA) resin (0.67mmol/g loading capacity) via Fmoc-based solid-phase peptide synthesis manually as previously described [152, 168]. Briefly, amino acid coupling based on the loading capacity of the resin was done with the Fmoc-protected amino acid (2 equiv), hydroxybenzotriazole (HOBt, 2 equiv), and 2-(1H-benzotriazol-1-yl)-1,1,3,3-tetramethyluronium hexafluorophosphate (HBTU, 4 equiv) in DMF for 3 hours. After each coupling reaction, remaining free amine groups were removed by adding to the resin with 10% acetic anhydride/DMF solution for 30 minutes. Fmoc removal was performed by using 20% piperidine in DMF for 30 minutes. Each coupling and deprotection reaction was controlled by the ninhydrin test. For fluorescein isothiocyanate (FITC) conjugation, Lysin (-Lys) was coupled to EEEEEEE sequence to enhance the reaction of amino groups to isothiocyanates groups of FITC. After removing Fmoc protecting group of -Lys from EEEEEEEK peptide (GLUK), the resins were treated with 5% (v/v) N,N-Diisopropylethylamine (DIEA) in dichloromethane (DCM). The FITC coupling solution containing 389.4 mg (FITC; Sigma Aldrich, St. Louis, MO, USA) and 256.8 μ L DIEA in 3.0 mL DMF was added to the reaction vessel. The peptide was cleaved from the resin by using trifluoroacetic acid (TFA): triisopropylsilane (TIPS): water (H₂O) solution at a ratio of 95:2.5:2.5. DCM and TFA were removed by using the rotary evaporator. The peptide was triturated with ice-cold diethyl ether three times and freeze-dried. The peptide was then characterized and purified by LCMS with preparative high-pressure liquid chromatography (HPLC, Agilent 1260 Quaternary LC) equipped with mass spectrometry (Agilent 6530 Q-TOF) with an electrospray ionization (ESI) source as previously described [168] (see liquid chromatography and mass spectra for GLU, in Figure A.1 , Figure A.2 and Table A.1, Appendix A).

3.2.2 Fabrication of Nanofibers

The 50:50 poly (lactic-co-glycolic acid) (PLGA) (Mw ~ 90 kDa; Purasorb PDLG5010, Corbion Purac Biomaterials, Gorinchem, Netherlands) was used for electrospinning as described previously [152]. In brief, a blend of 7wt % PLGA in 1,1,1,3,3,3-hexafluoro-2-propanol (HFP; Matrix Scientific; Columbia) was prepared as solvent. The polymer solution was transferred to a 10-ml syringe equipped with a 21-gauge needle by using a syringe pump. Aluminum foil was wrapped around the drum and coverslips in 13 mm diameter were attached to the rotating wheel to collect aligned NF. The aligned NF were collected by an aluminum rotating wheel with previously optimized electrospinning conditions such as a syringe flow rate of a distance of 15 cm, 20 kV electrical potential, 1.0 ml/h, and rotation speed of 1200 rpm [152].

3.2.3 Peptide Conjugation of Nanofibers

Surface modification of the scaffolds was performed using 1-ethyl-3-(3-dimethylaminopropyl)-carbodiimide and N-hydroxysuccinimide (EDC/NHS) chemistry after NTAP treatment. Briefly, NTAP was applied on electrospun NF at 31kV of output voltage and 1.5 kHz frequency for 45 seconds with a fixed 1 mm discharge gap. After NTAP treatment, scaffolds were washed with distilled water three times. A solution containing EDC (2 mM) and NHS (5 mM) in 0.1 M MES buffer (pH 5.3) was poured into NF and kept at 37 °C for 40 minutes. The activated NF were immersed with DI water three times to eliminate the unreacted solution. The NF were then treated with EEEEEEE peptide solutions at a concentration of 1 mM in sterile PBS, followed by incubation at 4 °C for 24 h. The NF are rinsed with PBS before characterization.

3.2.4 Calcium Phosphate Crystals Nucleation of Nanofibers

All the chemicals used for simulated body fluid (SBF) preparation were purchased from Sigma-Aldrich (St. Louis, MO, USA). NFs were incubated in a modified 1.5-fold concentrated SBF (1.5x SBF) for 1, 4, and 7 days. The SBF solution (pH 4.2) was prepared as previously described [172] by adding monosodium phosphate (NaH_2PO_4), sodium bicarbonate (NaHCO_3), magnesium chloride hexahydrate ($\text{MgCl}_2 \cdot 6\text{H}_2\text{O}$),

calcium chloride monohydrate ($\text{CaCl}_2 \cdot \text{H}_2\text{O}$), potassium chloride, and sodium chloride in deionized water. The NF were washed three times with deionized water after incubation.

3.2.5 Characterization of Nanofibers

Scanning electron microscope (SEM; Carl Zeiss Microscopy, Germany) was used to characterize the fiber diameter of electrospun PLGA NF. The NF were acquired with 3 kV accelerating voltage after coating with gold (QUORUM; Q150 RES; East Sussex; United Kingdom) for 60 seconds at 20 mA. NFs were analyzed with ImageJ software to measure the average fiber size by using the scale bars in the images obtained from the SEM software.

Peptide conjugation on nanofibers was assessed as previously described [152]. Briefly, NF, NTAP treated NF (pNF), GLU peptide conjugated NF (GLU-NF), and NTAP treated and peptide conjugated NF (GLU-pNF) were treated with 5 mg/ml FITC solution prepared in phosphate-buffered saline for 4 hours. FITC can chemically couple with only reactive amine side chains of GLUK peptide due to the reaction of primary amine groups of GLUK peptide with carboxyl groups of NFs which are exposed via NTAP treatment. After conjugation, all groups were dissolved in dimethylsulphoxide (DMSO; Sigma-Aldrich, St. Louis, Missouri, USA) and emission wavelength of 520 nm and excitation wavelength of 495 nm was used to measure fluorescent intensity by Microplate Reader (Synergy™ HTX Multi-Mode, BioTek, Winooski, VT, USA).

Effect of GLU peptide conjugation and NTAP treatment on the hydrophilicity of NF, pNF, GLU-NF, and GLU-pNF surface was evaluated by contact angle measurements using KSV Attension Theta goniometer (Biolin Scientific, Stockholm, Sweden). Briefly, 4 μl deionized water was dropped to the NF, pNF, GLU-NF, and GLU-pNF surface, photographed. The average of the measurements was defined as the contact angle (θ).

The surface topography of NF, pNF, GLU-NF, and GLU-pNF were analyzed by an Easyscan 2 (Nanosurf AG, Liestal, Switzerland) Atomic Force Microscopy (AFM) with the Nanosurf Easyscan 2 software operating in tapping mode employing a silicon

cantilever probe Tap190Al-G (Buced Sensors, Sofia, Bulgaria) with a constant force of 48 N/m and resonance frequency of 190 kHz. In dry conditions, fibers were directly deposited on a mica substrate and scanned.

The calcium phosphate (CaP) nucleation amount on the NF was assessed by calcium assay (QuantiChrom, Bioassay Systems, Hayward, CA, USA). Briefly, the NF contained calcium was dissolved in 1 M HCl. Next, the sample was added to the working solution. The wavelength of 612 nm was used to measure absorbance. A calibration curve was created with reference calcium solutions and the intensity values were associated with the equivalent calcium values. The quantity of CaP content based on NF mass (wt%) was calculated as described previously [152, 162]. Total CaP mineralized deposition on NFs was calculated at 1., 4. and 7 days. On day 7, the CaP crystal structure on mineralized NF, pNF, GLU-NF, and GLU-pNF was investigated by X-ray diffractometer (XRD; X'Pert Pro, Philips, Eindhoven, The Netherlands) with CuK α radiation source at 30 kV as previously demonstrated [152]. The background spectra of neat PLGA NF were subtracted from each group to better identify CaP peaks. Commercial nano HA (Sigma Aldrich, St. Louis, MO, USA) was also analyzed with XRD.

The tensile modulus of CaP nucleated NF, pNF, GLU-NF, GLU-pNF (20 \times 5 mm) was measured with a testing machine (Autograph 194 AG-IC Series, Shimadzu Corp., Kanagawa, Japan) as previously described [152]. The strain rate was defined as 0.03 s⁻¹. The linear region in the stress-strain curve was used to calculate the slope which was defined as tensile modulus.

3.2.6 Cell Attachment and Proliferation Analysis

hMSC cell line (HMSC-AD-500, Lot#102) was purchased from CLS cell lines Service (Eppelheim, Germany) and cultivated in DMEM containing Fetal Bovine Serum (FBS;10%), penicillin-streptomycin (100 units/mL), amphotericin-B (250 ng/mL), and gentamicin (50 μ g/mL). Cell culture medium was replaced with fresh medium at intervals of two days. UV radiation exposed to the NF for 1 hour and inserted in 70% ethanol for 30 minutes for sterilization [152]. The hMSC suspension was seeded on NFs which were attached to 13 mm circular glass coverslips (1 \times 10⁵ cells/cm²) and cultivated in 5% CO₂ for up to 7 d.

For the cell proliferation analysis of hMSCs that were seeded on the NFs, 3-(4, 5-dimethylthiazol-2-yl)-2, 5-diphenyltetrazolium bromide (MTT) (Vybrant® MTT Cell Proliferation Assay Kit, Invitrogen, Waltham, MA, USA) was performed at 1 d, 4 d, and 7 d [173]. First, cell medium was removed and 10% MTT solution in DMEM was added to each sample. The procedures with MTT were carried out in the dark. Encapsulated cells were incubated in the MTT for 4 hours at 37°C and 5% CO₂. Then, MTT dye was removed from the samples, and dimethyl sulfoxide (DMSO, Sigma-Aldrich, Steinheim, Germany) was added for dissolving formazan crystals. A microplate reader (Biotek Synergy HTX, Winooski, VT, USA) was used to measure the absorbance value by setting the wavelength to 570 nm. Focal adhesion staining (FAK100, Merck Millipore, Billerica, MA, USA) was carried out to observe actin filaments and nuclei in hMSCs by using phalloidin and 4',6-Diamidino-2-Phenylindole (DAPI), respectively [168]. hMSCs seeded NFs were rinsed with Phosphate Buffered Saline (PBS). The fixation was performed by 4% paraformaldehyde. 0.1% Triton X-100 in PBS was used to permeabilize to allow DAPI and phalloidin to access intracellular epitopes. 1.5% bovine serum albumin (BSA) in PBS was used to eliminate unspecific binding within the cell. Then, NFs were incubated in phalloidin in PBS for 1h and DAPI for 5 min. The fluorescent microscope was used for imaging.

3.2.7 Statistical Analysis

All obtained data were statistically analyzed using two-way ANOVA (SPSS 12.0, SPSS GmbH, Germany) and the Student-Newman-Keuls technique as a post hoc test. At least three samples from each experimental group ($n = 3$) were tested, and each experiment had at least three replicates. All the average values, standard deviations, and standard error values were calculated. p values were used to define meaningful group distinctions ($***p < 0.001$, $**p < 0.01$, $*p < 0.05$).

3.3 Results

3.3.1 Characterization of Peptide Conjugated Nanofibers

GLU peptide conjugation onto the surface of NTAP treated and non-treated NF was schematically shown in Figure 3.1. The SEM photomicrograph of PGLA electrospun

NF is given in Figure 3.2a. NF diameter distribution histogram (see Figure 3.2b) was calculated by using ImageJ. The diameter of NF used throughout the study ranged from 76 nm to 374 nm and the mean diameter was calculated as 266 ± 14 nm. After incubation in 1.5x SBF for 7 d, the images of the NF, pNF, GLU-NF, and GLU-pNF are depicted in Figure 3.2c, d, e, and f, respectively. Although CaP crystals were observed in both groups, maximum CaP deposition was achieved in GLU-pNF.

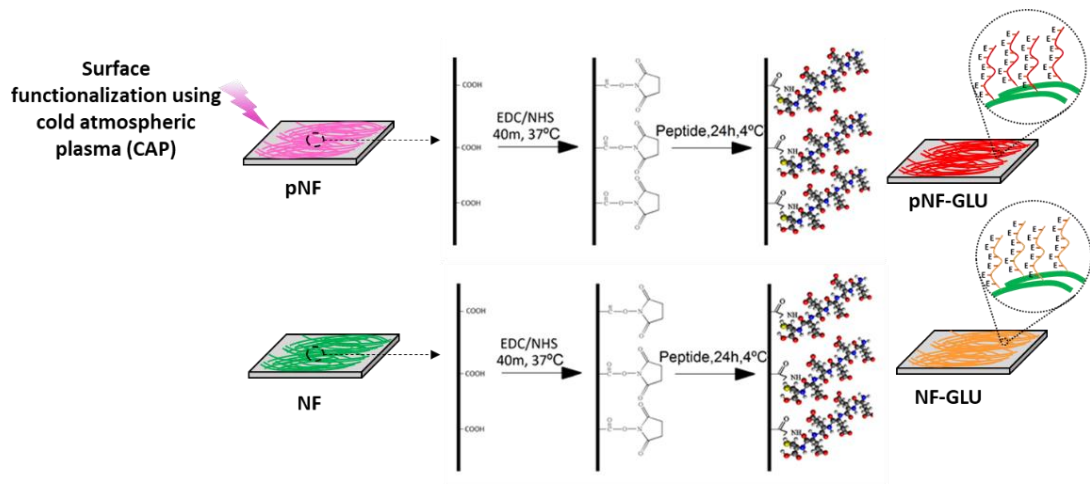


Figure 3.1: Schematic diagram of NTAP assisted conjugation of glutamic (E) acid templated peptides on PLGA nanofibers with EDC/NHS chemistry. Experimental groups are neat NF, NTAP treated NF (pNF), GLU peptide conjugated NF (without NTAP treatment) (GLU-NF) and NTAP treated GLU peptide conjugated NF (GLU-pNF)

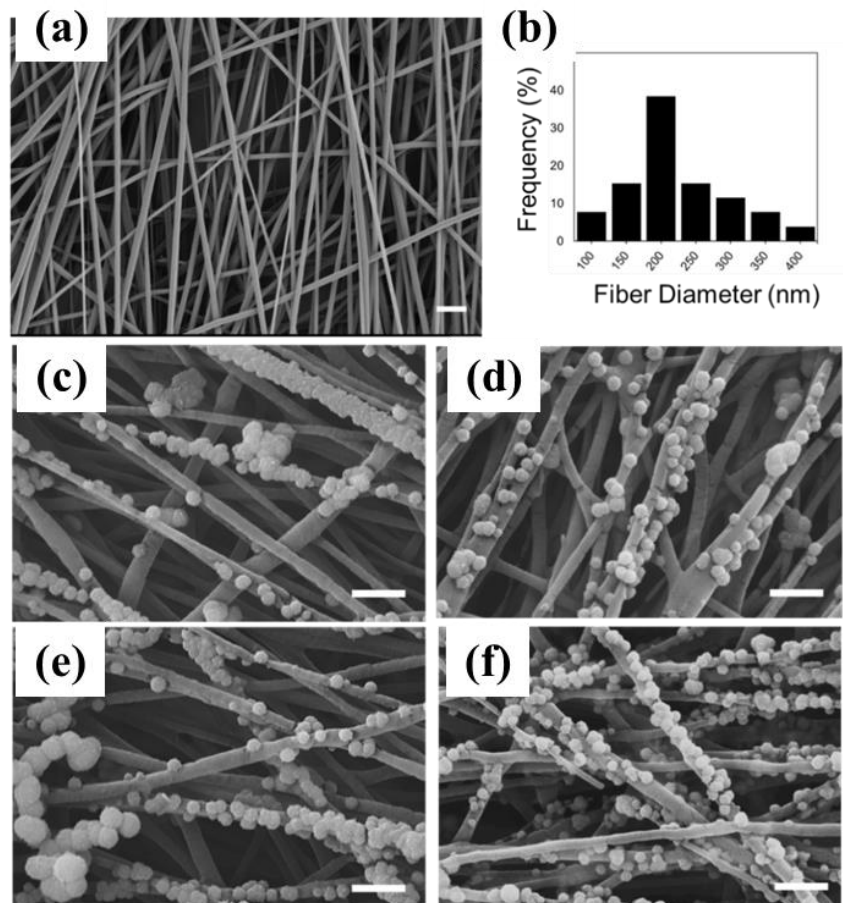


Figure 3.2: Scanning electron microscopy images of (a) PLGA nanofibers (NF) (scale bar represents 1 μm), (b) histogram showing nanofiber diameters distribution, (c) mineralized neat NF (NF), (d) mineralized NTAP treated NF (pNF), (e) mineralized GLU peptide conjugated NF (without NTAP treatment) (GLU-NF), (f) mineralized NTAP treated GLU peptide conjugated NF (GLU-pNF) (scale bar represents 1 μm)

The peptide conjugation efficacy on NF surface was compared by measuring the FITC intensity of dissolved FITC labeled GLU peptide. Briefly, FITC labeled GLU peptides were conjugated on the electrospun NF and NTAP treated NF to show the amount of peptide coverage. Then, fibers were dissolved, and FITC intensities of NF, pNF, GLU-NF, and GLU-pNF were measured. The mean fluorescence intensity of each sample was also measured by using three different samples. As shown in Figure 3.3a, the maximum fluorescence intensity was observed with GLU-pNF, whereas no fluorescence was observed in negative controls (NF and pNF).

Water contact angle (θ) measurement was evaluated to indicate the impact of peptide conjugation on NTAP treated and non-treated PLGA NF on hydrophilicity. The contact angle measurements were conducted on NF, pNF, GLU-NF, and GLU-pNF (see Figure 3.3b-e). Results demonstrated that after NTAP treatment the water contact angle of NF dropped from $123.70 \pm 5.73^\circ$ to $71.78 \pm 2.41^\circ$. Furthermore, after conjugation of GLU peptide, the water contact angle (θ) of non-NTAP treated NF decreased from $123.70 \pm 5.73^\circ$ to $74.81 \pm 8.54^\circ$, while NTAP treated NF dropped from $71.78 \pm 2.41^\circ$ to $54.50^\circ \pm 3.49^\circ$.

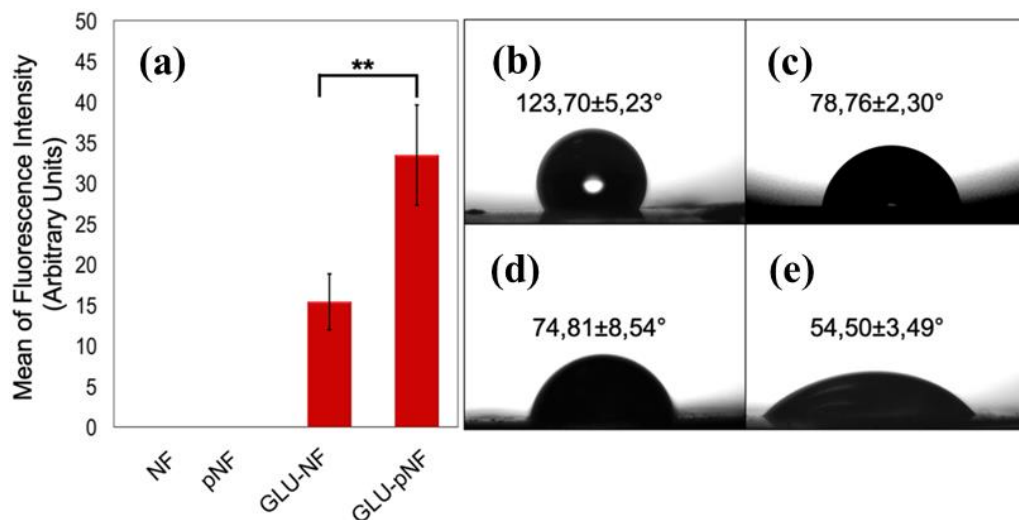


Figure 3.3: (a) Mean of Fluorescence Intensity of neat NF, pNF, GLU-NF, and GLU-pNF after dissolving in DMSO. Measurement of contact angle of (b) NF, (c) pNF, (d) GLU-NF (e) GLU-pNF

Roughness analysis of NF, pNF, GLU-NF, and GLU-pNF was conducted by using AFM. The mean surface roughness (S_a) for NF group was 199.5 ± 2.4 nm (see Figure 3.4a). After NTAP treatment, the surface roughness dramatically increased to 304.3 ± 11.6 nm (see Figure 3.4b). Additionally, GLU peptide conjugation on NF showed a slight increase in roughness (251.1 ± 9.6) (see Figure 3.4c). Similarly, GLU peptide conjugation after NTAP treatment increased the S_a value from 304.3 ± 11.6 nm to 381.1 ± 8.2 nm (see Figure 3.4d).

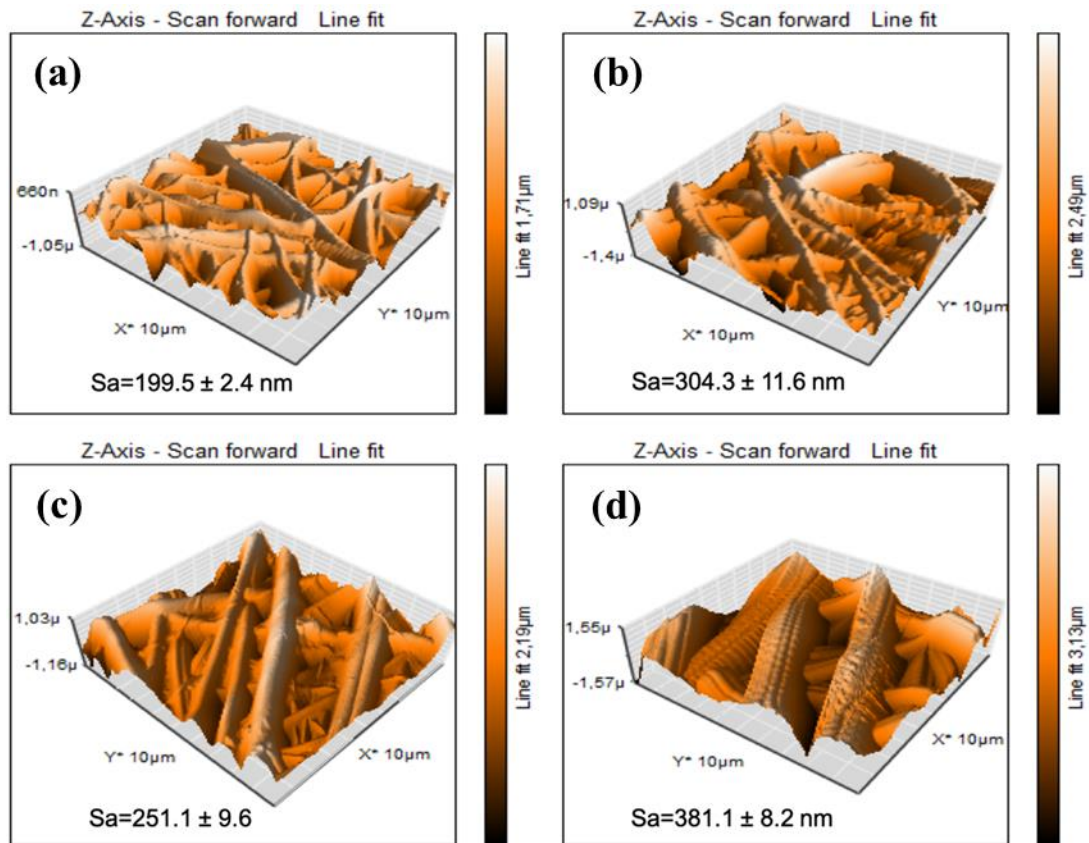


Figure 3.4: Representative 3D topographical view of (a) neat NF, (b) NTAP treated NF (pNF), (c) GLU peptide conjugated NF (without NTAP treatment) (GLU-NF), (d) NTAP treated GLU peptide conjugated NF (GLU-pNF) obtained by AFM

3.3.2 Biomineralization of Peptide Conjugated Nanofibers

Calcium content deposited on NF, pNF, GLU-NF, and GLU-pNF after incubation in 1.5x SBF for 1, 4, and 7 days is shown in Figure 3.5a. CaP content wt% on both groups constantly increased as incubation time changed from 1 to 4 and 7 days and similar patterns were observed on each time point. In detail, calcium content on GLU-pNF at day 1 (53.1 ± 4.8 wt%) was significantly high compared to NF (9.9 ± 2.1 wt%; $p < 0.001$), GLU-NF (17.5 ± 4.7 wt%; $p < 0.001$), and pNF (22.1 ± 1.1 wt%; $p < 0.001$). A similar pattern was found at 4 d where GLU-pNF (67.3 ± 2.1 wt%) had significantly high calcium content compared to NF (16.8 ± 1.7 wt%; $p < 0.001$), GLU-NF (30.7 ± 2.1 wt%; $p < 0.001$), and pNF (33.5 ± 2.8 wt%; $p < 0.001$), respectively. At day 7, the calcium content on pNF (41.7 ± 1.6 wt%; $p < 0.001$), GLU-NF (34.9 ± 2.3 wt%; $p < 0.001$), and GLU-pNF (81.7 ± 5.1 wt%; $p < 0.001$) significantly higher than NF (23.2

± 2.1 wt%). It was also observed that GLU-pNF had a significantly high content of calcium at day 7 compared to NF ($p < 0.001$), pNF ($p < 0.001$), and GLU-NF ($p < 0.001$).

The XRD spectra of commercial HA (red), NF (purple), pNF (blue), GLU-NF (orange), and GLU-pNF (green) after 7 days of incubation in 1.5x SBF are shown in Figure 3.5b. Results showed that the crystal deposition only in GLU-pNF showed characteristics of HA which peak centered at 25.8° and 31.8° [174] while NF, pNF, and GLU-NF showed slight peaks that did not match specific HA peaks.

Mechanical characterization of CaP deposited NF, pNF, GLU-NF, and GLU-pNF was conducted and the tensile modulus of each group is presented in Figure 3.5c. The tensile modulus of CaP deposited NF, pNF, GLU-NF, and GLU-pNF were measured as 206 ± 14 MPa, 426 ± 23 MPa, 433 ± 69 MPa, and 742 ± 41 MPa, respectively.

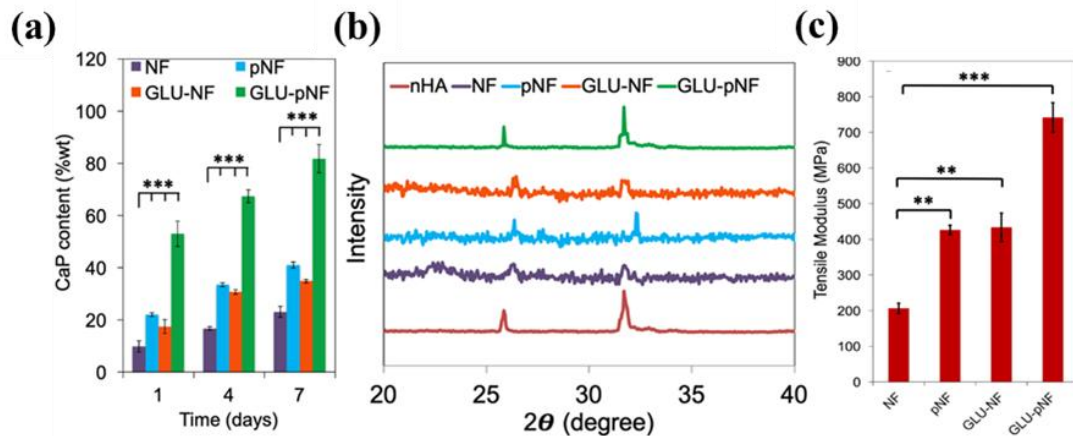


Figure 3.5: (a) Calcium content of calcium phosphate (CaP) deposited on NF, pNF, GLU-NF, and GLU-pNF within 7 days incubation in 1.5xSBF, (b) X-ray diffraction spectrum of NF, pNF, GLU-NF and GLU-pNF for CaP deposition after 7 days incubation in 1.5xSBF (c) Tensile modulus of neat NF, NTAP treated NF (pNF), GLU peptide conjugated NF (without NTAP treatment) (GLU-NF) and NTAP treated GLU peptide conjugated NF (GLU-pNF)

3.3.3 Cell Proliferation and Morphology on Nanofibers

At 1d, 4d, and 7d, an MTT assay was performed to evaluate cell proliferation on CaP nucleated NFs (see Figure 3.6a). The percentage of cell number raised on NF ($5 \pm 3\%$), GLU-NF ($55 \pm 8\%$), pNF ($106 \pm 2\%$) and GLU-pNF ($130 \pm 4\%$) at 1 day. The ratio

of cell number was increased on GLU-pNF, pNF, GLU-NF, and NF groups to $168 \pm 11\%$, $139 \pm 14\%$, $87 \pm 2\%$, and $37 \pm 6\%$ at day 4. Additionally, cell number increase on GLU-pNF ($209 \pm 3\%$; $p < 0.001$) were significantly higher than pNF (170 ± 5), GLU-NF (110 ± 11), and NF (55 ± 14) at day 7.

The morphology of the hMSCs on CaP nucleated NF, pNF, GLU-NF, and GLU-pNF was examined after culturing in basal medium for 7 days using fluorescence microscopy (see Figure 3.6b-e). Fluorescence microscope images showed that hMSCs effectively attached and spread on each group. Although the number of cells changed within groups and with respect to culture time, there was no difference observed in hMSCs morphology when seeded on CaP deposited NF, pNF, GLU-NF, and GLU-pNF.

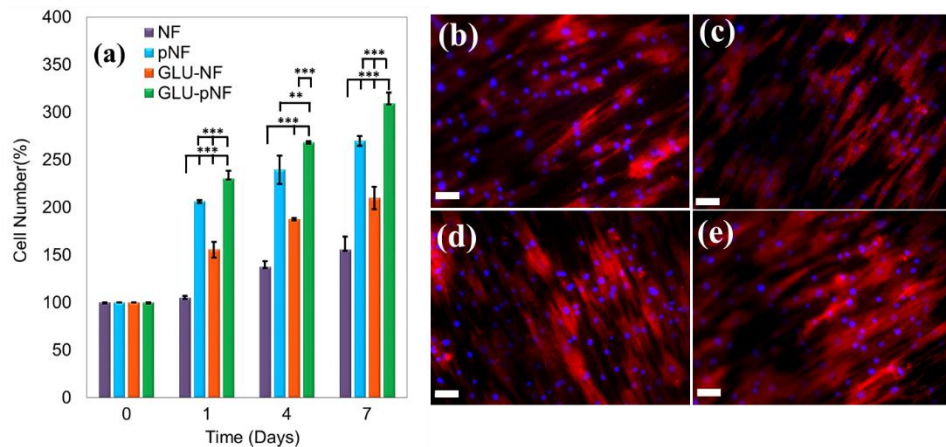


Figure 3.6: (a) The percentage of increase in cell number at 1, 3, and 7 days after seeding cells on neat NF, NTAP treated NF (pNF), GLU peptide conjugated NF (without NTAP treatment) (GLU-NF), and NTAP treated GLU peptide conjugated NF (GLU-pNF). Morphology of human marrow stromal cells (hMSCs) seeded on (b) NF, (c) pNF, (d) GLU-NF, and (e) GLU-pNF (BIV). PLGA NF incubated in basal media for 7 days. Phalloidin (red) and 4,6-diamidino-2-phenylindole (DAPI; blue) represent cytoskeletal actin and cell nuclei in the image (Scale bar represents $50\mu\text{m}$)

3.4 Discussion

There is a growing demand for biomimetic synthetic scaffolds with improved biological properties for accelerated bone regeneration due to the requirement of enhanced differentiation as well as cell adhesion, proliferation [175, 176]. Composite nanofibrous scaffolds have been extensively used for bone tissue engineering applications and named as one of the most ideal scaffolds since they can mimic the structure of bone and presents an extensive surface area for cell adhesion [177, 178]. One of the important drawbacks defined for synthetic nanofibrous scaffolds is the difficulty of CaP nucleation exactly on the structure of nanofibers which directly affects mechanical properties and biological response [179]. Herein, the PLGA NF surface was modified with NTAP treatment to increase GLU peptide conjugation and characterize the influence of such modification on biomineralization as well as hMSCs adhesion, proliferation, and morphology.

Micrographs of NF, pNF, GLU-NF, and GLU-pNF after biomineralization are shown in Figure 3.2b-e. The results demonstrated that CaP crystals were in the average size of $110 \text{ nm} \pm 12$ and increased by conjugation of GLU peptide on the NF. It was also observed that NTAP treatment caused a higher deposition of CaP on NF. Our results were consistent with Kim *et al.* where they reported increased mineralization of CaP crystals via NTAP treatment on poly(ϵ -caprolactone) (PCL) scaffolds [180]. GLU-pNF group showed high content of CaP crystals compared to NF, pNF, and GLU-NF groups. Moreover, it could be observed from the SEM micrographs that GLU peptides act as nano-CaP crystals nucleation points as in biomineralization.

The fluorescence intensity of GLU-pNF group showed significantly high fluorescence intensity compared to GLU-NF due to facilitated peptide conjugation (see Figure 3.3a). It is speculated that increased carboxyl groups on the NF surface following NTAP treatment resulted in higher peptide conjugation. These results are also consistent with contact angle measurements. Contact angle results indicated that surface hydrophilicity increased by NTAP treatment and negatively charged GLU peptide conjugation. As shown in Figure 3.3b-e, the contact angle (θ) dropped from $123,70 \pm 5,23^\circ$ to $54,50 \pm 3,49^\circ$ in NTAP treated NF, whereas the contact angle (θ) following GLU peptide conjugation dropped from $123,70 \pm 5,23^\circ$ to $74,81 \pm 8,54^\circ$. It

was considered that a lower contact angle could directly be related to higher GLU peptide conjugation with the help of NTAP treatment. These results were confirmed by Rezaei *et al.* who observed that oxygen DBD plasma treatment resulted in the breakdown of C-C and C-H bonds on the PMMA surface leading to the introduction of carbon radicals and production of functional oxygen-containing groups such as COOH and O-H on the PMMA surface [181]. It is important to maximize the introduction of –COOH groups to polymer surfaces to enhance peptide conjugation. For that purpose, NTAP treatment increased peptide conjugation by producing functional oxygen-containing groups such as COOH and OH. Hence, effective peptide conjugation might have resulted in increased hydrophilicity in addition to NTAP related functional oxygen groups on the surface. Similar to our results, Yang *et al.* and Karaman *et al.* demonstrated that peptide immobilized NF became more hydrophilic [152, 182]. Therefore, with the support of these results, it is speculated that NTAP assisted GLU peptide conjugation significantly increased GLU peptide content on NF leading to increased CaP content.

Surface topographies of NF, pNF, GLU-NF, and GLU-pNF were demonstrated in Figure 3.4 a–d, respectively. According to the results, NTAP application and GLU peptide conjugation improved the surface roughness of NF. In addition, the surface roughness increase is higher on pNF to GLU-pNF than NF to GLU-NF. It might be considered that NTAP treatment resulted in efficient peptide conjugation on NF surface. In a recent study, Man *et al.* fabricated peptide conjugated electrospun fibers using a polyvinyl pyrrolidone/bovine serum albumin/rhTGF- β 1 composite solution and PCL to develop a co-delivery system of rhTGF- β 1 and MSCs affinity peptide. They reported that peptide conjugation on scaffolds resulted in increased roughness [183, 184]. In another study, Deng *et al.* prepared a peptide-decorated PCL nanofibrous microenvironment with electrospinning technique and conjugated it with vitronectin peptide to enhance the osteogenic potential of hPSCs *in vitro*. Their results demonstrated that the addition of peptides also increased the surface roughness of the modified PCL substrates [183, 184].

Calcium assay results suggested that GLU-pNF showed significantly higher CaP deposition than NF, pNF, and GLU-NF (see Figure 3.5a). It was speculated that enhanced negatively charged functional groups produced after NTAP treatment

following with GLU conjugation caused a sharp increase in calcium content. In our previous study, PLAA-GLU peptide conjugate was blended with high MW PLGA and electrospun fibers were fabricated. CaP content ratio based on NF mass results indicated that on single layer GLU-NF nanofibers maximum of 49.2 ± 2.1 % CaP content was obtained [152]. However, with NTAP assisted conjugation we conducted in this study, significantly higher CaP content (81.7 ± 5.1 %) was determined. These results confirmed that effective peptide conjugation with initial NTAP treatment significantly increased the amount of CaP content mineralized on the surface of the NF.

NTAP treatment of synthetic nanofibers exposes a variety of functional groups on them, including amino, carboxyl, and hydroxyl groups [185]. Cui *et al.* reported that among developed functional amino, carboxyl, and hydroxyl groups on Poly(DL-lactide) (PDLA) fibers, carboxyl groups have a more potent influence on HA nucleation and growth in SBF due to the strong electrostatic attraction of carboxyl groups and calcium ions [186]. Our results are consistent with Sarvestani *et al.*, where they investigated the effect of 6-mer glutamic acid peptide (Glu6) conjugated to synthetic hydrogel to improve mechanical properties by enhancing interaction with CaP nanocrystals. The results indicated that conjugation of Glu6 peptide increased carboxylic groups on the hydrogels due to the available carboxyl group on each glutamic acid and higher interaction of Glu6 peptide with CaP crystals enhanced shear modulus of composite hydrogel [187]. All these studies and our results suggest that GLU peptide conjugation after NTAP treatment causes the formation of a significantly higher number of carboxyl groups on NF compared to NF, pNF, and GLU-NF groups, which enhances interaction with calcium ions in SBF and CaP mineralization.

The CaP crystal characteristics were determined via XRD analysis. The results demonstrated that only GLU-pNF group resembled HA characteristic CaP crystals on the nanofibers (see Figure 3.5b). Based on these findings we considered that enhanced GLU peptide conjugation not only increased the content of CaP crystals but also guide the calcium ions adhesion and further reaction to transform into HA crystals known to be the stoichiometrically stable phase of CaP and major content of bone inorganic phase. Although GLU-NF and GLU-pNF groups theoretically directed mineralization through conjugated GLU peptides, limited GLU peptide conjugation was observed on

GLU-NF group due to the lack of available carboxyl groups (see Figure 3.3a). Therefore, CaP crystal characteristics were influenced and shifted the HA-specific XRD spectrum to brushite [188]. As already stated, the substrate surface adsorbs calcium ions and initial nucleation sites are aggregated near the surface during mineralization [189]. It is speculated that limited carboxyl groups due to less GLU peptide conjugation inhibit the formation of HA which is a stoichiometrically stable form of CaP crystals [152]. In a previous study, Tavafoghi *et al.* investigated the effect of a negatively charged Glutamic acid and positively charged Arginine. It was reported that negatively charged functional groups were more effective than neutral and positive groups in HA precipitation of due to hydrogen bond, carboxyl groups, and electrostatic attraction [190].

Tensile modulus of CaP deposited NF, pNF, GLU-NF, and GLU-pNF are presented in Figure 3.5c. Results showed that increased nano-CaP deposition on GLU-pNF significantly enhanced tensile modulus compared to NF, pNF, and GLU-NF. It was also indicated that CaP deposited pNF and GLU-NF significantly higher tensile modulus levels than NF. One possible explanation for such a trend is the increase and homogenous deposition of nano-CaP influence mechanical properties of NF [191, 192]. Compared to the direct addition of CaP into electrospinning solution to develop CaP deposited NF scaffolds, nucleating the nano-CaP on NF was reported as a more effective technique due to the cause of immediate precipitation of nano-CaP before ejection [193, 194]. For instance, a negatively charged surface enhances the nucleation of CaP, leading to a more uniform, thick, dense coating and subsequently improved mechanical properties which are considered important for bone tissue engineering applications.

The proliferation of hMSCs on CaP nucleated NF, pNF, GLU-NF, and GLU-pNF was presented in Figure 3.6a. The faster proliferation of hMSCs was observed with increasing the CaP content on NF. It could be related to higher CaP content by modifying the surface with NTAP treatment and GLU peptide conjugation following with mineralization formed the better biomimetic surface structure of bone ECM. It was previously noted that surface properties of scaffolds including wettability, roughness, and chemical functionalities with bioactive molecules directly affect cell attachment and proliferation [195]. Our results were consistent with those of Birhanu

et al. where they applied NTAP treatment following CaP deposition on electrospun composite PLLA/P123 NF and demonstrated that increased hydrophobicity and roughness positively influence cellular adhesion and proliferation [196]. The higher surface area created by rough surfaces improves the interaction between integrin-binding points of the cells and NF surface [197]. Although different proliferation profiles were observed on NF, pNF, GLU-NF, and GLU-pNF, there was no significant difference in morphology of hMSCs suggesting that hMSCs kept their stemness ability and most likely did not start differentiation when cultured in basal media.

Promoting biomineralization via effective conjugation of biomimetic peptides on synthetic nanofibers could potentially be a strong alternative to scaffolds for guided bone regeneration in tibial and mandibular defects [198]. Mesenchymal stem cells seeded mineralized electrospun scaffolds would be acting as a barrier to prevent invasion of soft tissue towards bone defect at the same time accelerate bone regeneration due to biocomposite structure of the scaffold.

3.5 Conclusion

In this study, the effect of NTAP treatment mainly on GLU peptide conjugation, mineralization of NF, mechanical properties, and hMSC proliferation were investigated. NTAP treated and non-treated PLGA NF were conjugated with GLU peptide and mineralized in the SBF. The results revealed that NTAP treatment significantly increased GLU peptide conjugation which further enhanced CaP nucleation on NF. Mechanical properties of NF improved by increasing the deposition of nano-CaP on NF. In addition, increasing the CaP content on NF NTAP treatment and GLU peptide conjugation enhanced the proliferation of hMSCs. All these results together implied that NTAP application and GLU peptide conjugation can be a potentially promising method to develop efficient CaP nucleated NF for bone tissue engineering applications.

Chapter 4

Enhanced Osteogenesis of Human Mesenchymal Stem Cells by Self-assembled Peptide Hydrogel Functionalized with Glutamic Acid Templated Peptides

4.1 Introduction

Successful bone tissue repair or replacement is a major ongoing challenge in the regenerative medicine field. Tissue engineering has been proposed approaches by making use of synthetic scaffolds for replacement or regeneration of the damaged tissue come through the insufficiencies of current tissue repair strategies. The highly hierarchical and complex structure of bone requires scaffolds that provide architectural support and form mineral phases. Extracellular matrix (ECM) proteins such as osteonectin, osteopontin, and bone sialoprotein play an essential role in mineralization by regulating bone development. Although soluble ECM proteins have been implicated in tissue scaffolds, the lack of knowledge about the function and the distribution of these proteins incorporated in the biological mineralization of bone tissue is considered a limitation [199]. Furthermore, ECM proteins which have multiple functions and whose function may change in different distribution, have limitations such as the risk of triggering an immune response and transmitting diseases [200]. As an alternate approach, the incorporation of small peptides within a scaffold that can guide biomineralization has been proposed due to these peptides' capability

of high resistance to pH or temperature changes and precise control over the chemical composition. A glutamic acid-rich peptide (sequences of glutamic acids) derived from bone ECM proteins such as osteonectin, osteocalcin, osteopontin, and bone sialoprotein, mimics the terminal region of the glycoprotein of bone and acts as a calcium ion nucleation point [187, 201]. Furthermore, glutamic acid-rich peptide conjugated electrospun nanofibers significantly enhanced the osteogenic differentiation of human bone marrow-derived mesenchymal stem cells (hMSCs) [152, 201]. Since the relatively two-dimensional (2D) structure of nanofibers has been reported to remain an insufficient environment for bone tissue regeneration, researchers have been focused to develop three-dimensional(3D) scaffolds that enhance the precise formation and mineralization of functional bone tissues.

Hydrogels with 3D interconnected porous structure and high-water content mimic trabecular bone extracellular matrix and have been widely used in bone tissue engineering. Hydrogels can be classified into two groups based on their natural or synthetic origins. Natural hydrogels remain incapable of cell-matrix interaction to enhance cell adhesion, proliferation, and differentiation into specific lineage osteogenesis as well due to the absence of bioactive factors. Thus, it is an urge to develop a bioactive synthetic hydrogel scaffold that can induce osteogenesis. Although inadequate mechanical properties of hydrogels became a major problem for bone tissue engineering, hydrogels are promising injectable scaffolds which are used for regeneration of non-load bearing trabecular bone defects [202]. Self-assembled peptide (SAP) hydrogels mimicking the structural and functional properties have considerable potential for bone tissue engineering applications. SAP hydrogels are emergent biomaterials for bone regeneration due to the spontaneous formation in the absence of chemical crosslinkers or physical stimulation such as heat and UV exposure. SAP hydrogels can not only provide a temporary 3D network but also guide bone repairing and increase the bioactivity of the matrix by functionalizing with different peptide epitopes [203].

The regeneration capacity of the bone may be insufficient in large defects and multi-part fractures. In such cases, the filling of the bone defect with hydrogels gains great importance in terms of triggering bone healing and providing structural and mechanical support in this process. SAP hydrogel has been recently used as injectable

material for tissue repair. Kisiday *et al.*, designed and synthesized KLD (KLDLKLDLKLDL-NH₂, K: Lysin, L: Leucine, D: Aspartic acid) peptide consisting of a short sequence of 12 amino acids which is easy to modify and able to be used in an injectable form by self-assembling at different concentrations with tunable mechanical properties [204, 205]. Furthermore, the potential of KLD SAP hydrogels in the promotion of chondrogenesis and osteogenesis has been reported [206]. The functionalization of SAP hydrogels is a good strategy to control cell behaviors such as cell attachment, spreading, migration, and differentiation. Researchers recently have focused on SAP functionalization through direct solid-phase synthesis extension at the amino-terminal to alter its biological activity as hydrogel scaffolds. Many self-assembling peptides, such as E1Y9 (Ac-EYKYKYKY-NH₂), RADA16, and KLD have been used to functionalized with a biological motif for tissue regeneration. Tsutsumi *et al.* constructed peptide hydrogels using E1Y9 that were functionalized with bioactive sequences DGR (DGRDSVAYG) selected from osteopontin, PRG (PRGDSGYRGDS) selected from type IV collagen, RGD (RGDS) selected from fibronectin and all of the E1Y9/E1Y9-derivative mixed hydrogels exhibited a good adhesion ability and compatibility for MC3T3-E1 cells, a mouse pre-osteoblast cell line [207]. He *et al.* was applied the functional motif RGD to modify peptide d-RADA16 for designing peptide d-RADA16-RGD and reported that d-RADA16-RGD were found to significantly promote bone regeneration [203]. Bian *et al.* created a fusion of the N-cadherin mimetic peptide (HAVDI) and KLD and referred to as “KLD-Cad”, to fabricate self-assembled hydrogels that promote chondrogenesis of human mesenchymal stem cells (hMSCs) [208]. Biom mineralization and osteoinductive capability of synthetic SAPs can be increased by the functionalization of bioactive motifs of EEEEE and EEGGC. Even though some studies are showing the individual osteoinductive capacity of EEGGC and EEEEE templated peptides when conjugated with synthetic scaffolds, no study in the literature compares the osteoinductive capacity of the two peptides integrated on 3D SAP hydrogels to the best of our knowledge. In this study, first the functional glutamic acid peptides (EEGGC and EEEEE) were applied to modify KLD peptide for designing and fabricating KLD-EEGGC and KLD-EEEEE and self-assembled in different concentrations (0.5%, 1%, and 2%). The performance of functionalization of KLD Self-assembled peptide with different glutamic acid templated peptides in different concentrations was investigated

and then, the influence of the EEGGC and EEEEE peptide sequences which are previously reported as osteogenesis and biomineralization inducing epitopes [201]. Next, the concentration of hydrogels on bone regeneration was evaluated with respect to mRNA expression and immunofluorescence analysis. The incorporation of glutamic acid peptides in SAP hydrogels significantly increases the expression of osteogenic markers and the production of bone ECM matrix by encapsulated hMSCs. The conjugated glutamic acid peptide increases the expression of osteogenic markers and biomineralization, according to our findings from q-PCR, and immunofluorescence staining, alizarin red assay.

4.2 Materials and Methods

4.2.1 Peptide Synthesis

KLD (the peptide with the sequence of Ac-Lys-Leu-Asp-Leu-Lys-Leu-Asp-Leu-Lys-Leu-Asp-Leu-NH₂), KLD-EEGGC (the peptide with the sequence of Ac- Lys-Leu-Asp-Leu-Lys-Leu-Asp-Leu-Lys-Leu-Asp-Leu-Glu-Glu-Gly-Gly-Cys-NH₂), and KLD-EEEE (the peptide with the sequence of Ac- Lys-Leu-Asp-Leu-Lys-Leu-Asp-Leu-Lys-Leu-Asp-Leu-Glu-Glu-Glu-Glu-Glu-NH₂) were synthesized on 4-Methylbenzhydrylamine (MBHA) resin (0.67mmol/g loading capacity) by using 9-fluorenylmethoxycarbonyl (Fmoc) chemistry as previously described by using the automated peptide synthesis device (AAPPTEC Focus Xi, Louisville, KY, USA) [201]. All amino acid was coupled with 2 equivalents (based on the loading capacity of resin) of Fmoc-protected amino acid, 2-(1H-benzotriazol-1-yl)-1,1,3,3-tetramethyluronium hexafluorophosphate (HBTU; 2 equiv), hydroxybenzotriazole (HOBt; 2 equiv) and *N,N*-diisopropylethylamine (4equiv; DIEA) HBTU in *N,N*-Dimethylformamide (DMF) for 3 hours. The Fmoc-protecting group was removed for 30 minutes with 20 percent piperidine in DMF. To acetylate the unreacted amine groups in each coupling step, a 10% acetic anhydride-DMF solution was used. The ninhydrin test was used to verify each coupling and deprotection reaction. The peptide was cleaved from the resin by using trifluoroacetic acid (TFA): triisopropylsilane (TIPS): H₂O solution at a ratio of 95:2.5:2.5. TFA was evaporated on the rotary evaporator. The peptide was washed with ice-cold diethyl ether three times and then

the suspension was centrifuged to discard the supernatant following with lyophilization of the peptide at -80 °C (Biobase Biodustry Bk-FD10P, Shandong, China). Further, purification of peptides was conducted via preparative high-performance liquid chromatography (HPLC, Agilent 1200 series) system equipped with Zorbax Extend-C18 2.1 × 50 mm column. The gradient of 0.1% TFA/water and 0.1% TFA/acetonitrile were used with the mobile phase and the detection wavelength was selected as 220 nm. Mass spectrums of KLD, KLD-EEGGC (KLD-O1), and KLD-EEEEEE (KLD-O2) peptides were characterized via mass spectrometry (Agilent 6530 Q-TOF) with an electrospray ionization (ESI) source (see liquid chromatography and mass spectra for KLD, KLD-O1, and KLD-O2 in Figure A.1, Figure A.2 and Table A.1, Appendix A).

4.2.2 Self-assembled Hydrogel Fabrication

KLD, KLD-EEGGC, and KLD-EEEEEE, Biogelx (Biogelx Inc., Scotland, UK) peptide powders were separately dissolved in sterilized deionized water (0.5%, 1%, and 2% w/v), and sonicated for 30 minutes prior to use. To prepare the KLD hydrogel, KLD solution was mixed with sterilized Dulbecco's Modified Eagle's Medium (DMEM) cell culture medium with 25 mM 4-(2-hydroxyethyl)-1-piperazineethanesulfonic acid (HEPES) buffer without Fetal Bovine Serum (FBS). It should be noted that 2% w/v concentration was selected as the highest concentration due to the complete solubility problem of KLD, KLD-EEGGC, and KLD-EEEEEE peptides over 2% w/v in sterilized deionized water.

4.2.3 Cell Culture and Hydrogel Encapsulation

hMSC cell line (HMSC-AD-500, Lot#102) was purchased from CLS cell lines Service (Eppelheim, Germany) and cultivated in DMEM containing FBS (10%), penicillin-streptomycin (100 units/mL), gentamicin (50 µg/mL) and, amphotericin-B (250 ng/mL). Cell culture medium was replaced with fresh medium at intervals of two days. The hMSCs suspension was encapsulated in hydrogel (5×10^6 cells/ml) in a basal medium. After incubation for 24 hours, the medium was changed by using osteogenic media which contains basal media consisting of dexamethasone (100 nM), ascorbic acid (50 µg/mL), β-glycerophosphate (10 mM) and cultivated in a humidified 5% CO₂

incubator for 28 d. MSCs encapsulated KLD incubated in the osteogenic medium were used as the negative control group.

4.2.4 Osteogenic Differentiation of hMSCs in Hydrogels

4.2.4.1 Quantitative Real-time PCR Analysis

Total cellular RNA isolation was carried out by using the Blood/Cell Total RNA Mini Kit (Geneaid, Sijhih City, Taiwan) at each time point (7, 14, 21, and 28 d). Then, the purified RNA extraction was converted to cDNA with M-MuLV First Strand cDNA Synthesis Kit (Biomatik, Ontario, Canada). The cDNA obtained was subjected to Step One Plus Real-time PCR system (Applied Biosystems, Foster City, USA) amplification with gene-specific primers. Forward and reverse primers for RT-qPCR, including alkaline phosphatase (ALP), Collagen type I (COL-1), osteopontin (OPN), osteocalcin (OCN), and glyceraldehyde 3-phosphate dehydrogenase (GAPDH) demonstrated in Table 4.1 were purchased from Sentegen Biotechnology (Ankara, TURKEY) and used to evaluate gene expression [209]. The differential expression of genes ALP, COL-1, OPN, and OCN were quantified by StepOne Software v2.3 and Ct values were classified by the $2^{(-\Delta\Delta C_t)}$ method described elsewhere [210]. Every group was experimented with in qPCR as doublet and repeated as triplicate (n = 6).

Table 4.1: Forward and reverse primers. Alkaline phosphatase (ALP), Collagen Type I (Col-1), Osteopontin (OPN), Osteocalcin (OCN), and glyceraldehyde 3-phosphate dehydrogenase (GAPDH; housekeeping gene) (GAPDH) used to assess hMSCs differentiation in qRT-PCR amplification

GENES	Forward Primer	Reverse Primer
Alkaline Phosphatase	5'- GTG GAG TAT GAG AGT GAC GAG AA- 3'	5'-AGA TGA AGT GGG AGT GCT TGT AT-3'
Collagen Type I	5'-TGA CGA GAC CAA GAA CTG-3'	5'-TCA GCC TTA GAC GCC TCA AT-3'
Osteopontin	5'-ATG AGA TTG GCA GTG ATT-3'	5'-TTC AAT CAG AAA CTG GAA-3'
Osteocalcin	5'-TGT GAG CTC AAT CCG GAC TGT-3'	5'-CCG ATA GGC CTC CTG AAG C-3'
GAPDH	5'-AAA TCC CAT CAC CAT CTT CC-3'	5'-CCA GCA TCG CCC CAC TT-3'

4.2.4.2 Immunofluorescent Staining

Immunofluorescence staining was carried out to observe protein expression and nuclei in hMSCs by using primary and secondary antibodies and phalloidin and 4',6-Diamidino-2-Phenylindole (DAPI), respectively [197]. Cell-encapsulated KLD SAP hydrogels and Biogelx were rinsed with PBS. The fixation was performed by 4% paraformaldehyde. 0.1% Triton X-100 in PBS was used to permeabilize to allow DAPI and antibodies to access intracellular epitopes. 1.5% bovine serum albumin (BSA) in PBS was used to eliminate unspecific binding within the cell. Then, samples were incubated in primary antibodies in PBS containing 1% BSA overnight at 4°C. Primary antibodies (Santa Cruz Biotechnology Inc., Santa Cruz, California, USA) were used included mouse monoclonal antibody against COL-1 (cat. no sc-59772; 1:50), mouse monoclonal against OPN antibody (cat. no. sc-21742; 1:50), and mouse monoclonal antibody against OCN (cat. no. sc-365797; 1:500). Fluorescence secondary antibodies (Santa Cruz Biotechnology Inc., Santa Cruz, California, USA) included m-IgG kappa BP-FITC (cat. no. sc-516140; 1:200) and m-IgG kappa BP-PE (cat. no. sc-21742; 1:200) were diluted with 1% BSA. The fluorescent microscope (Olympus CKX41, Tokyo, Japan) was used for imaging.

4.2.5 Alizarin Red Staining

Calcium deposition on hMSCs encapsulated hydrogels over 28 d were evaluated by Alizarin Red staining (Alizarin Red S, Sigma Aldrich, St. Louis, MO, USA). Briefly, hMSCs were fixed for 15 minutes using 4 % PFA followed by wash steps using PBS (1x), and the staining solution (1% Alizarin Red S in ddH₂O) was applied for 30 minutes followed by imaging using the inverted microscope (Olympus CKX41, Tokyo, Japan).

4.2.6 Statistical Analysis

All the data that are obtained, were statistically analyzed with two-way ANOVA (SPSS 12.0, SPSS GmbH, Germany) and the Student-Newman-Keuls technique as a post hoc test. At least three samples from all experimental groups were tested (n = 3) and experiments were at least three replicates. Average values, standard deviations,

and standard error values of all results were determined. Meaningful distinctions among groups were defined at p values ($***p < 0.001$, $**p < 0.01$, $*p < 0.05$).

4.3 Results

4.3.1 Osteogenic Differentiation of hMSCs in Self-assembled Hydrogels

Expression of osteogenic markers ALP, Col-1, OPN, and OCN with incubation time for MSC-encapsulated peptide hydrogels is shown in Figures 4.1a-d, respectively. For the KLD control group, expression of ALP, Col-1, OPN, and OCN was significantly less than for all groups. ALP mRNA expression for all groups followed their corresponding ALP activity, peaking at day 14 and returning to the baseline level at day 28. mRNA expression for OPN, OCN, and Col-1 increased gradually with incubation time. Expression of osteogenic markers ALP, Col-1, OPN, and OCN increased with a concentration in all groups. Furthermore, ALP, Col-1, OPN, and OCN expression was highest for 2% KLD-O2 at each time point. For example, Col-1 expression for 2% KLD-O2 at day 28 was $46,32 \pm 1,57$ while that for KLD, Biogelx and KLD-O1 was $12,35 \pm 0,64$, $15,6 \pm 1,32$, and $24,67 \pm 2,24$ ($p^{***} < 0.001$) respectively; OPN expression for 2% KLD-O2 at day 28 was $53,29 \pm 1,32$ while that for KLD, Biogelx and KLD-O1 $9,02 \pm 0,27$, $13,8 \pm 1,92$, $33,33 \pm 0,68$ and ($p^{***} < 0.001$) respectively; and OCN expression for 2% KLD-O2 at day 28 was $26,06 \pm 1,33$ while that for KLD, Biogelx and KLD-O1 $3,44 \pm 0,25$, $7,6 \pm 1,23$ and $13,94 \pm 0,84$ ($p^{***} < 0.001$) respectively; expression of ALP for KLD-O2 at day 14 was $38,51 \pm 4,31$ while that for KLD, Biogelx and KLD-O1 was $7,24 \pm 2$, $11,13 \pm 3$, and $28,80 \pm 3,05$ ($p^{***} < 0.001$) respectively.

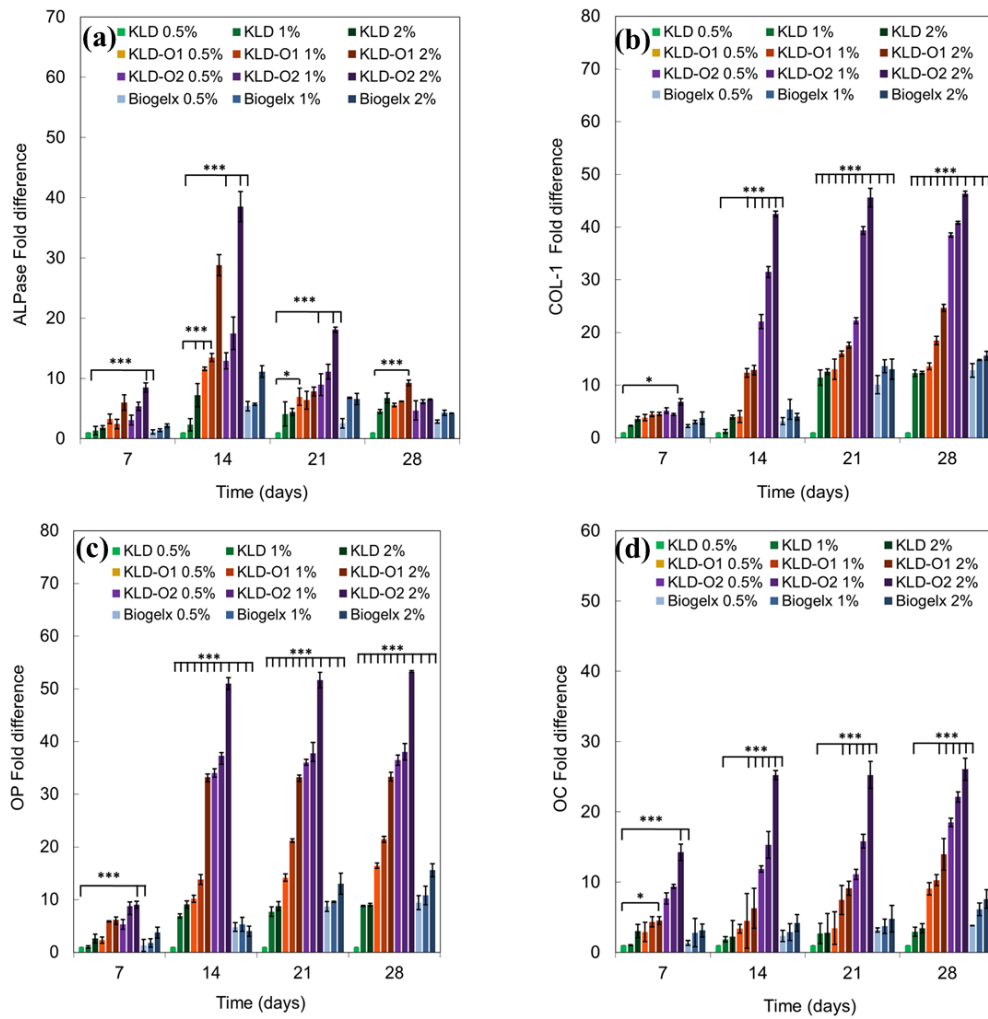


Figure 4.1: RT-PCR analysis of gene expression of osteogenic markers of (a) alkaline phosphatase (ALPase), (b) type 1 collagen (COL-1), (c) osteopontin (OPN), (d) osteocalcin (OCN) for hMSCs encapsulated in 0.5%, 1%, 2% KLD, KLD-O1, KLD-O2, and Biogelx and incubated in osteogenic medium for up to 28 days. The error bars indicate the mean SE (n = 3) of the data. [One-way ANOVA was used to assess significant differences.] [(*p<0.05, **p<0.01, ***p<0.001) Newman–Keuls multiple contrast test]

Immunostained images of hMSCs encapsulated 2% KLD, KLD-O1, KLD-O2, and Biogelx are depicted in Figure 4.2. Briefly, cells were incubated in an osteogenic medium for 28 d and then chemically fixed for immunostaining. Lastly, proteins were stained using first primary antibodies against and then labeled with secondary antibodies to be visualized using inverted fluorescence microscopy. Columns a to c are COL-1(green), OCN (red), and OCN (green), respectively, and rows 1–4 are Biogelx as a positive control, KLD as a negative control, KLD-O1 and KLD-O2. The

expression of these osteogenic maturation-related proteins was drastically higher for hMSCs on KLD-O2 than those on KLD-O2, Biogelx, and KLD, respectively. Immunofluorescence staining of differentiated hMSCs also confirmed q-PCR results.

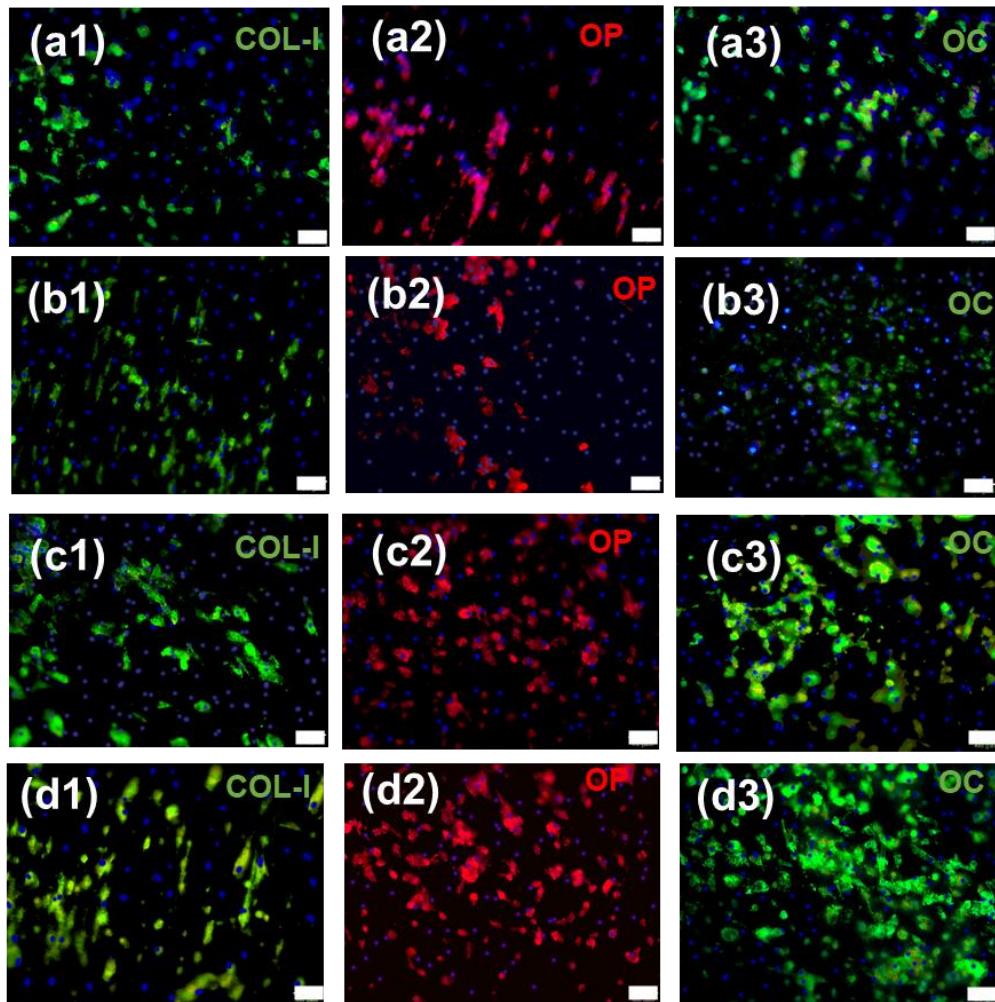


Figure 4.2: Immunofluorescent staining revealed the expression of osteogenic markers COL-I (first column: green), OPN (second column: red) and OCN (third column: green) in 2% (a) KLD, (b) Biogelx, (c) KLD-O1, (d) KLD (O2) after 28 days incubation. 4',6-diamidino-2-phenylindole (DAPI; blue) was used to indicate cell nuclei (Scale bar represents 50 μ m)

4.3.2 Alizarin Red Staining

Sections of the hydrogel's culture matrix on the 28th day showed matrix nodules stained with Alizarin Red and markedly mineralized (see Figure 4.5). Although the sign of mineralization in control cultures is less than in the other groups, the color

intensity in the KLD-O2 group shows that the mineralization is more than in the other groups. Overall, the 2% KLD-O2 group showed the greatest staining for Alizarin Red.

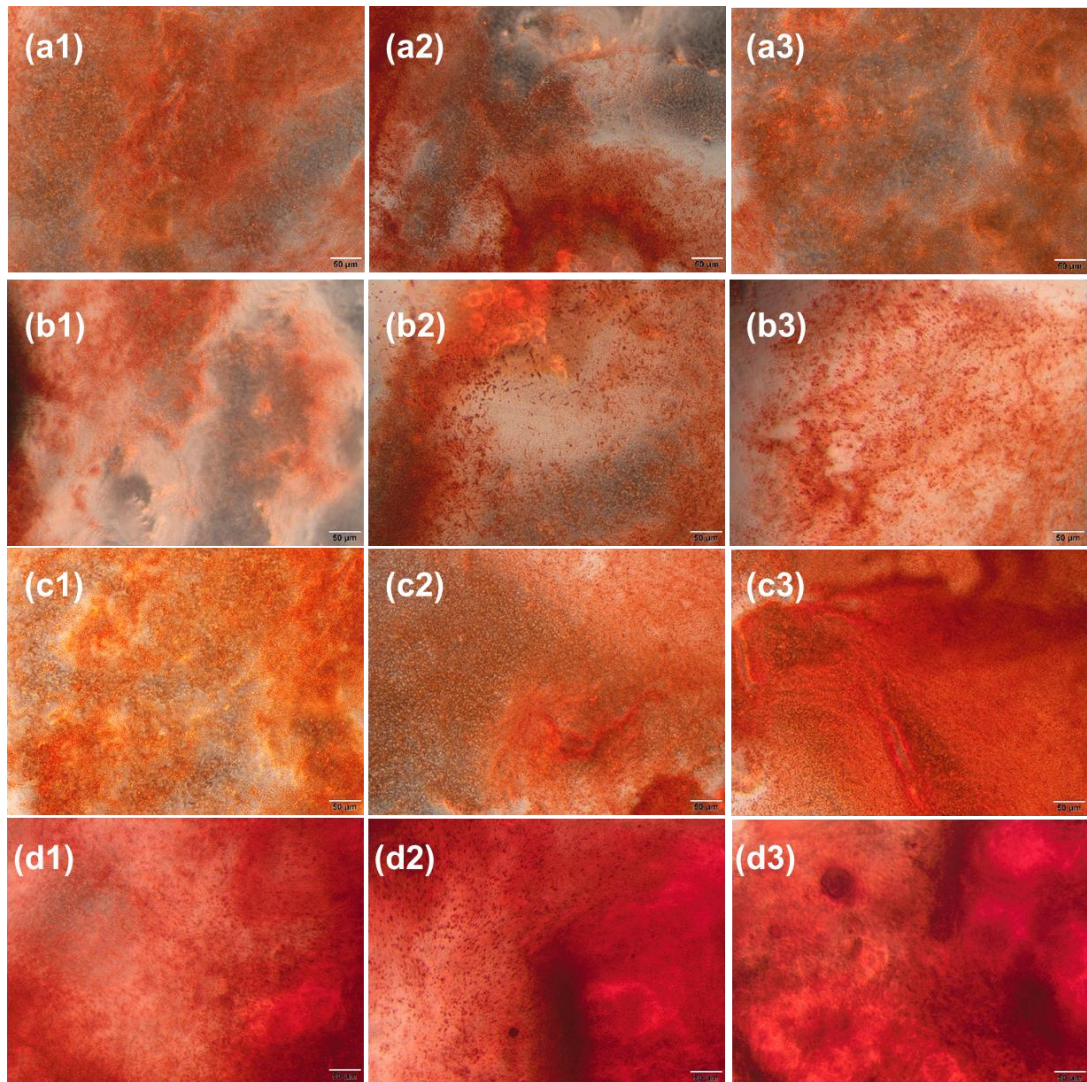


Figure 4.3: Alizarin red staining for mineral deposition of hMSCs encapsulated in 0.5 % (first column), 1% (second column) and 2% (third column) (a) Biogelx, (b) KLD, (c) KLD-O1, (d) KLD-O2 after 28 days' incubation in osteogenic medium. (Scale bar represents 50 μm)

4.4 Discussion

Short SAPs as essential nano-biomaterials are being applied to integrated biological processes in living systems [211, 212]. KLD can self-assemble to form nanofibers and this property has been utilized in bone and cartilage tissue engineering [213]. Herein,

our objective was to enhance osteogenesis and biomineralization of injectable SAP hydrogels with controlled mechanical properties so that the peptide also becomes capable of being injected into bone defects which commonly occur acutely because of trauma, infection, or surgical resection. For this purpose, we have designed two variants of KLD that contained variable numbers of glutamic acid which are O1 (EEGGC) and O2 (EEEEEE), and produced the hydrogels in different concentrations (0.5%, 1%, and 2%). The major findings of this study include: (1) addition of glutamic acid residues to KLD did not affect self-assembling process (2) addition of glutamic acid residues to KLD significantly enhanced osteogenesis and biomineralization of hMSCs (3) KLD-O1 and KLD-O2 induced osteogenic gene (ALP, Col-1, OPN, and OCN) expression.

Molecular self-assembly is a spontaneous process that includes disordering molecules or systems and the formation of more defined structures as a result of intermolecular interactions [214]. To form a SAP hydrogel, intermolecular interactions and balance between hydrophobicity and hydrophilicity of a peptide often play a significant role [215]. The functionalization of SAP hydrogels is a good strategy to control cell behaviors such as cell attachment, spreading, migration, and differentiation. Furthermore, the addition of functional peptide group charge at the N-terminus of SAP may influence peptide self-assembly into nanofibers which is essential for hydrogel formation [216]. Herein, the addition of negatively charged glutamic residues to KLD sequence increased its net negative charge resulting in an introduction of hydrophilic groups to its variants. Even after the addition of glutamic acid residues at the N-terminus of KLD, the ability of hydrogel formation of the peptides was not affected.

Differentiation of hMSCs into osteoblast is a complex process, which includes hMSCs proliferation, differentiation, maturation, and mineralization. During osteogenic differentiation, COL-1 mineralizes in the presence of calcium ions into calcium phosphate which makes up approximately 70% of bone matrix, whereas ALP enzyme, OPN, and OCN proteins mediate nucleation and stabilization of calcium phosphate crystals [217]. ALP is a key enzyme in the bone matrix that supplies mineral nucleation sites with free phosphate ions by cleaving organic phosphate esters [218]. ALP expression profile is generally associated with a peak during the early differentiation of progenitor cells into immature osteoblasts. Increasing ALP level up to the 14th day

supports bone formation and osteoblast activation. As that the progenitor cells are matured, the ALP level typically decreases and COL-1, OPN, OCN expression increases, indicating a late-osteoblast state [219]. The expressions of COL-1, OPN, and OCN are expected to rise throughout the 28 days of incubation considering their crucial role in bone mineralization [220]. Herein, osteogenic differentiation was also evaluated with respect to the expression of osteogenic markers including ALP, COL-1, OPN, and OCN using real-time PCR. The results demonstrated KLD-O2 significantly induced expression of these markers as compared to KLD-O1, Biogelx, and KLD indicating that five glutamic acids containing O2 peptide are more effective on osteogenic differentiation of hMSCs compared to two glutamic acids containing O1 peptide. The expression of all the markers on KLD only was the lowest, indicating the positive impact of the two glutamic acid peptides for bone mineralization. Nudelman *et al.* indicated that negatively charged glutamic acid peptides act as a calcium ion nucleation points in collagen nanofibers during biomineralization and significantly promoted the interaction with positively charged calcium ions [221]. Ca^{2+} with varying affinity depending on pH ions can bind to amino acids. Therefore, it could be indicated that increased glutamic acid in the SAP hydrogel stabilized more CaP resulting in higher ALP activity, Ca content as well as higher expression of osteogenic gene markers [221]. Considering the inductive effect of mineralization on osteogenic differentiation, this might be one of the reasons for a higher level of osteogenic gene marker expression with KLD-O2 than KLD-O1. Immunofluorescence staining of differentiated hMSCs also confirmed gene expression results. The expression of these osteogenic maturation-related proteins such as COL-1, OPN, and OCN, was drastically higher for hMSCs in KLD-O2 than those in KLD-O1, Biogelx, and KLD, respectively. In consistent with real-time PCR results, cells on KLD-O1 showed an elevated expression of these markers compared to those on KLD, highlighting the osteogenic inductive effect of glutamic acid residue. In our previous study, we demonstrated that two and six glutamic acid sequences including ECM mimetic peptides facilitated the mineralization process and significantly increased gene expression and secretion of COL-I, OCN, and OPN [152].

The calcium deposition during biomineralization was examined using alizarin red S staining analysis because it can specifically bind with calcium ions at low pH. After 28 days, darker red dots and red ribbons, which indicated higher calcium deposition

inside of hydrogel, were observed in 2% KLD-O2 groups. In contrast, KLD exhibited poor calcium deposition. It could be related to higher CaP content by modifying KLD SAP with glutamic acid templated peptide conjugation formed the better biomimetic surface structure of bone ECM. Promoting biomineralization via functional bioactive peptides on synthetic SAP could potentially be a strong alternative to hydrogel scaffolds for guided bone regeneration.

4.5 Conclusion

In summary, KLD SAP was successfully functionalized with biomimetic glutamic acid templated peptides through direct solid-phase synthesis extension at the amino-terminal. We found that although the addition of glutamic acid templated peptide to KLD SAP increases hydrophilicity, SAP hydrogel was successfully formed. Glutamic acid templated peptides improved the osteoinductive capacity of the KLD SAPs. Moreover, five glutamic acids templated peptides containing KLD sharply increased ALP activity, calcium content, and expression of key osteogenic markers of ALP, COL-1, OPN, and OCN compared to two glutamic acids templated peptide containing KLD. It was further depicted that glutamic acid residue is the major fragment that influences mineralization and osteogenic differentiation in non-collagenous proteins of bone extracellular matrix. Our findings revealed that KLD SAP functionalized with EEEEE templated peptides had more potential for inducing osteogenesis. Several studies are emphasizing the importance of enhancing the bioactivity of synthetic SAP hydrogels for better bone tissue regeneration. It is believed that such findings will aid in further optimization of biofunctionalized biomaterials to support stem cell-based bone repair and regeneration.

Chapter 5

Role of Functionalized Self-Assembled Peptide Hydrogel on In Vitro Vasculogenesis

5.1 Introduction

Most successes in regenerative medicine have been limited due to unassisted delivery of oxygen and nutrients removal of the waste products in avascular tissue constructs when it is implanted to the patient [222]. Developing larger and complex tissues requires rapid and stable vascular formation for sustaining cell viability and function [223]. The majority of the tissue construct with inadequate vascular network fails because the nutrient diffusion is limited up to 100–200 μm from the host vasculature [224]. The process of vascularization is based upon the complicated interactions between endothelial cells (ECs), the interstitial extracellular matrix (ECM), and the neighboring mural cell types such as mesenchymal stromal cells (MSCs) via various growth factors which enable regeneration [225]. The matrix interplay is crucial for the ECs to develop blood vessels by the proliferation, migration, and differentiation. Synthetic scaffolds might be tailored to provide a micro-environment to cells for guiding and supporting blood vessel formation in clinically relevant tissues based on this interaction [226].

One strategy for improving the survival of tissue-engineered construct involves the coculture of ECs with MSCs [227]. Although the interaction between ECs and MSCs and their functions in-building cellular networks are not clearly understood, ECs have been reported to form microcapillary structures *in vitro* [228]. Initially, vascular

endothelial growth factor (VEGF) activates ECs for proliferation and secretion of various enzymes to degrade ECM and the basement membrane. Tubular structures were built by migration of ECs and stabilized by the enrolment of mural cells such as MSCs, which deposit new ECM proteins form basal lamina by differentiation into pericytes [225]. A range of coculture systems of the ECs and MSCs were investigated since they are inherently linked during vasculogenesis [227, 229]. For instance, Liu *et al* encapsulated human bone marrow stromal cells (hMSCs) and human umbilical vein endothelial cells (HUVECs) in a 3D gelatin-methacrylate (Gel-MA) hydrogels with microspheres and observed that hMSC/HUVEC co-culture enhanced vascularization compared to HUVEC or hMSC monoculture [227].

ECM proteins such as collagen, fibronectin, and laminin, play an essential role in vasculogenesis [230]. Laminins, which compose the basement membrane between the endothelial cell layer and mural cells in vascular lumen, make up a heterotrimeric glycoprotein family, with each protein-containing one α , β , and γ subunit [231]. These subunits determine the properties and functions of the laminin proteins [232]. Integrin ligand interaction is determined by the α chain, while multiple signaling pathways in focal adhesion are affected by the β subunit connection to the cytoskeleton. Several laminin-derived peptides such as IKVAV, and YIGSR amino acid sequences, have been investigated for modulation of cell attachment and migration to the surrounding ECM in the microvascular matrix during physiological vasculogenesis. One of the α -chain of laminin-derived peptides IKVAV has been reported to improve endothelial cell attachment, following tubule formation including capillary branching, and vessel formation [233]. YIGSR peptide derived from the laminin β chain has been widely considered as a mediator of cell adhesion [234]. Recent studies have depicted that YIGSR improves endothelial cell attachment and tubule formation. Many researchers focused on the integration of laminin-derived peptides to synthetic scaffolds to achieve extensive vascularization as an alternative approach to protein loading, since these functional peptides are specifically intended to stimulate significant regulation cascades by binding to the same receptor as their originated protein [235, 236].

Self-assembled peptide (SAP) hydrogels have significant potential for tissue engineering applications since robust gels are formed through supramolecular interactions and crosslinked physically like natural proteins in ECM without

comprehensive chemical cross-linking to form a nanofibrous structure. Ease of fabrication, the capability of biofunctionalization, and superior biocompatibility properties make SAP hydrogels an ideal tissue engineering scaffold compared to synthetic polymeric hydrogels, which do not bear any functional biological motifs. Furthermore, by altering SAP composition, the mechanical, chemical, and biological properties can be tuned to improve the utility in a variety of applications. Peptides can also be incorporated into the hydrogels and released to facilitate vascularization.

Hydrogels have been used to engineer vascularized tissue constructs to assemble into micro-capillary networks with co-cultured ECs and MSCs by drawing the evolutionary memory of ECs. Bioactive peptide incorporation into the hydrogels has great potentials to improve vascularization and develop vascular structure. Self-assembled peptides (SAP) are capable of functionalization with bioactive peptides by attachment to the N-terminal and SAP hydrogels are formed through supramolecular interactions without any chemical cross-linking procedure consist of UV exposure and additional crosslinkers which are toxic for the cells. Therefore, SAP hydrogels which are crosslinked physically like natural proteins in ECM, are ideal candidates for tissue engineering scaffold compared to synthetic polymeric hydrogels, which need a chemical cross-linking procedure. However, hydrogel formation of biofunctionalized SAPs might be challenging since the addition of functional peptide group charge at the N-terminus of peptide might have the negative effect of the peptide on water solubility and self-assembly process. Therefore, appropriate bioactive epitopes should be selected for the appropriate SAP peptides. For instance, Kim *et al.* developed substance P (GRPQPQFFGLM) modified KLD SAP hydrogel and confirmed that cell migration capacity of MSCs in the KLD12-SP was higher than KLD-12 group [206]. Although, the best-recruiting ability of KLD12-SP was stated compared to KLD12 and related with wound-healing processes, the angiogenic potential of KLD12-SP just considered by comparing SP-modified RADA16 peptide hydrogel which enhanced angiogenesis and prevented fibrosis and apoptosis in the injured site after the application to a mouse hind limb ischemia model and the tendency of KLD-12 SP to angiogenesis was not evaluated. Although there is no gold standard motif to functionalize SAPs for vasculogenic differentiation, short functional sequences similar to vascular ECM might be effective.

Herein, we functionalized KLD Self-assembled peptide hydrogel (hereafter denoted KLD hydrogel) with laminin-derived short peptides which are IKVAV (V1) and YIGSR (V2), and self-assembled in different concentration to mimic the laminin in native ECM. To the best of our knowledge, the potential of KLD SAP on hydrogel formation after functionalization with IKVAV and YIGSR peptides by attachment to the N-terminal has not been reported. This is a comparative study that evaluates the effect of IKVAV and YIGSR on vasculogenesis when used to modify the KLD SAP was performed after successful hydrogel formation as an alternative to the other IKVAV and YIGSR functionalized synthetic polymers exist in the literature (for the schematic of the study see Figure 5.1). In our previous study, KLD (KLDLKLKLDL-NH₂, K: Lysin, L: Leucine, D: Aspartic acid) peptide consisting of a short sequence of 12 amino acids was modified by osteogenic epitopes and improved osteogenic differentiation-inducing characteristic [237]. In this study, we functionalized KLD Self-assembled peptide hydrogel (hereafter denoted KLD hydrogel) with laminin-derived short peptides which are IKVAV (V1) and YIGSR (V2), and self-assembled in different concentration to mimic the laminin in native ECM. Biogelx, which is sold in Biogelx Ltd., a UK-based biomaterials company, was preferred as a positive control due to its bioactivity and short structure as reported to compare with KLD hydrogels [238]. To the best of our knowledge, it is the first-time approach for a combination of short KLD SAP hydrogels and two different bioactive short bioactive peptides and assessing the efficacy of this functionalization on vasculogenesis. We have designed two SAP which is KLD-V1 and KLD-V2 and produced the hydrogels 0.5% and 1% concentrations. The proliferation of hMSC/HUVEC co-culture increased with the addition of laminin derived peptides to KLD. The immunofluorescent staining and RT-qPCR were performed to analyses PECAM, and vWf proteins and genes expression, respectively. The results revealed that KLD-V2 hydrogel significantly improved vasculogenesis in hMSC/HUVEC co-culture compared to KLD-V1, Biogelx and KLD because YIGSR in KLD-V2 increased cell population and ECM secretion by the interaction with cells and induced vasculogenesis.

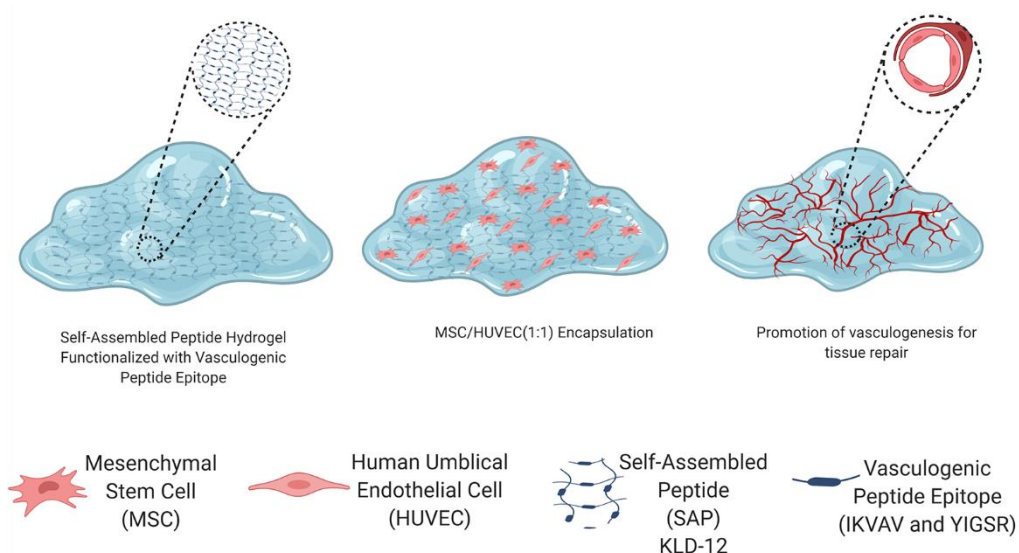


Figure 5.1: Laminin derived peptide integrated Self-assembled peptide hydrogels significantly enhanced vascularisation of human umbilical vein endothelial cells (HUVECs) and human mesenchymal stem cells (hMSCs) coculture

5.2 Materials and Methods

5.2.1 Peptide Synthesis

The peptide synthesis chemicals were obtained from AAPPTEC (Louisville, KY, USA). KLD (Ac-Lys-Leu-Asp-Leu-Lys-Leu-Asp-Leu-Lys-Leu-Asp-Leu-NH₂), KLD-IKVAV (Ac-Lys-Leu-Asp-Leu-Lys-Leu-Asp-Leu-Lys-Leu-Asp-Leu-Ile-Lys-Val-Ala-Val-NH₂) and KLD-YIGSR (Ac-Lys-Leu-Asp-Leu-Lys-Leu-Asp-Leu-Lys-Leu-Asp-Leu-Tyr-Ile-Gly-Ser-Arg-NH₂), IKVAV (Ile-Lys-Val-Ala-Val-NH₂) and Tyr-Ile-Gly-Ser-Arg-NH₂) were synthesized on 4-Methylbenzhydrylamine (MBHA) resin (0.67mmol/g loading capacity) by using 9-fluorenylmethoxycarbonyl (Fmoc) chemistry at the automated peptide synthesis device (AAPPTEC Focus Xi, Louisville, KY, USA) as previously described [237]. Briefly, Fmoc-protected amino acids (2 equiv), hydroxybenzotriazole (HOBt; 2 equiv), 2-(1H-benzotriazol-1-yl)-1,1,3,3-tetramethyluronium hexafluorophosphate (HBTU; 2 equiv), and *N,N*-diisopropylethylamine (4equiv; DIEA) HBTU in *N,N*-Dimethylformamide (DMF) were reacted with resins for 3 hours. 20% piperidine was used for the removal of Fmoc-protecting group. 10% acetic anhydride/DMF solution was used for acetylation

of unreacted amine groups for each coupling stage during peptide synthesis. For the amino acid coupling and deprotection steps, a ninhydrin test was conducted to check and control each coupling and deprotection reaction. The subsequent amino acids were also coupled using the same method until the desired sequence was completed. When all amino acids were coupled, the cleavage solution including trifluoroacetic acid (TFA): triisopropylsilane (TIPS): water (H₂O) at a ratio of 95:2.5:2.5 was poured into the resins. After two hours, the solution was poured into cold diethyl ether and the peptide was filtered. After that step, the peptide suspension was centrifuged and the supernatant was discarded. The remaining ether was removed with the rotary evaporator. Finally, the peptide was lyophilized by freeze-drying method at -80 °C (Biobase Biodustry BkFD10P, Shandong, China). The peptides were purified by using a preparative high-performance liquid chromatography system (HPLC, Agilent 1200 series). Agilent Zorbax 300SB-C18 4.6 × 150 mm column was used together with mixture of two different solutions of 0.1% (v/v) TFA/water and 0.1% (v/v) TFA/acetonitrile for mobile phase and detection wavelength was selected as 220 nm [237]. Mass spectrums of KLD, KLD-IKVAV (KLD-V1), and KLD-YIGSR (KLD-V2) peptides were characterized via mass spectrometry (Agilent 6530 Q-TOF) with an electrospray ionization (ESI) source. (see liquid chromatography and mass spectra for KLD, KLD-V1, and KLD-V2 in Figures A1 and 2 and Table A1, Supporting Information).

5.2.2 Self-assembled Hydrogel Fabrication and Characterization

0.5% and 1% w/v KLD, KLD-IKVAV, and KLD-YIGSR, Biogelx (Biogelx Inc., Scotland, UK) hydrogels were produced by dissolving peptide powders in sterilized deionized water prior to use. Peptide solutions were mixed with sterilized Dulbecco's Modified Eagle's Medium (DMEM) cell culture medium with 25 mM 4-(2-hydroxyethyl)-1-piperazineethanesulfonic acid (HEPES) buffer containing no Fetal Bovine Serum (FBS). To highlight the importance of anchoring peptides onto SAP hydrogel for the cell proliferation, we performed MTT assay additionally for KLD-unconjugated V1 and KLD-unconjugated V2 by adding unconjugated (IKVAV) V1 and V2 (YIGSR) in KLD with the same molar ratio in peptide conjugated hydrogel (hereafter KLD-unconjugated V1 and KLD-unconjugated V2 denoted as KLD+V1 and KLD+V2, respectively).

The hydrogel samples completely degraded *in vitro* at 37°C in simulated body fluid (SBF) which was prepared by dissolving NaHCO₃ (4.2 mM), K₂HPO₄ (1.0 mM), NaCl (136.8 mM), KCl (3.0 mM), CaCl₂ (2.5 mM), MgCl₂.6H₂O (1.5 mM) and NaSO₄ (0.5 mM) in deionized water [239]. The pH of SBF was arranged to 7.4 with 60 mM NaHCO₃ solution. After the SAP hydrogels with a diameter of 12 mm were shaken continuously in an orbital shaker at 100 rpm in SBF, the hydrogels were lyophilized and weighed at intervals of 7 days and mass losses were measured [240]

The nanofiber surface topography of SAP hydrogels was investigated by Atomic Force Microscopy (AFM) (Easyscan 2, Nanosurf AG, Liestal, Switzerland) via the Nanosurf Easyscan 2 software. The scanning procedure was operated in tapping mode using a silicon cantilever probe Tap190Al-G (Baged Sensors, Sofia, Bulgaria) with the following parameters; a force constant of 48 N/m and resonance frequency of 65 kHz. For the sample preparation, 1 µL of hydrogels were mixed with 19 µL deionized water and the samples were spread on the mica substrate. After the samples were gelled, SAPs were dried by lyophilization. Self-assembled nanofibers were scanned in dry conditions.

The self-assembled nanofibrous structure was observed with a Scanning Electron Microscope (SEM; Carl Zeiss Microscopy, Germany) with an accelerating voltage of 3kV after coating with gold in the rotary pumped coater (QUORUM; Q150 RES; East Sussex; United Kingdom) at 20 mA for 60 seconds. The SAP structures were prepared with the sample preparation method for AFM imaging. After the scale bars of images were obtained from SEM software and the average fiber size were calculated with 100 different peptide fiber diameter in the image with ImageJ software (National Institutes of Health, Bethesda, MD, USA).

Disk-shaped hydrogel samples were cut with a 20-mm cork borer and put on discovery hybrid rheometer-2 (HR2, TA Instruments, New Castle, DE). The storage (G') and loss moduli (G'') were recorded with the parameters following parameters: the gap of 0.5 cm, a shear strain of 1%, and angular frequency of 0,1-10 rad/s, as previously described [240].

5.2.3 Cell Culture and Proliferation Analysis

hMSCs (HMSC-AD-500, CLS cell lines Service, Lot#102, Eppelheim, Germany) and HUVECs (kindly donated from Ege University Research Group of Animal Cell Culture and Tissue Engineering Laboratory) were cultivated in DMEM containing FBS (10%), penicillin-streptomycin (100 units/mL), amphotericin-B (250 ng/mL), and gentamicin (50 µg/mL). Cell culture medium was replaced with fresh medium with intervals of two days. The hMSCs/HUVECs (1:1) suspension was encapsulated in hydrogel (5×10^6 cells/ml). After incubation for 24 hours for cell adhesion, the medium was replaced with vasculogenic medium (EGM-2 Bullet Kit (Lonza, Walkersville, USA) contained hydrocortisone, epidermal growth factor (hEGF), fibroblast growth factor (hFGF-B), ascorbic acid, insulin-like growth factor (R3-IGF-1), heparin, ascorbic acid, GA-1000 (gentamicin, amphotericin-B), with 10% FBS) and cultured in a humidified 5% CO₂ incubator for up to 7 d. The negative control group was determined as hMSCs/HUVECs (1:1) encapsulated KLD incubated in the vasculogenic medium.

For the cell proliferation analysis of HUVECs/MSCs that were encapsulated into the hydrogels, 3-(4, 5-dimethylthiazol-2-yl)-2, 5-diphenyltetrazolium bromide (MTT) (Vybrant® MTT Cell Proliferation Assay Kit, Invitrogen, Waltham, MA, USA) assay was performed at 1., 4. and 7. days of the culture as previously described [201]. First, the cell medium was removed and 10% MTT dye in the culture medium was added to each sample. The procedures with MTT were carried out in the dark. Encapsulated cells were incubated in the MTT dye for 4 hours at 37°C and 5% CO₂. Then, MTT dye was removed from the samples, and 500 µl dimethyl sulfoxide (DMSO, Sigma-Aldrich, Steinheim, Germany) was added for dissolving formazan crystals. Hydrogel structures were smashed by pipetting and the absorbance was measured at 570 nm using a microplate reader (Biotek Synergy HTX, Winooski, VT, USA).

5.2.4 Quantitative Real-time PCR Analysis

Total cellular RNA in each sample was isolated at each time point (1, 4, and, 7d) by using the Blood/Cell Total RNA Mini Kit (Geneaid, Sijhih City, Taiwan). cDNA was converted from the extracted purified RNA by using M-MuLV First Strand cDNA

Synthesis Kit (Biomatik, Ontario, Canada). The cDNA was subjected to Step One Plus Real-time PCR system (Applied Biosystems, Foster City, USA) amplification with gene-specific primers. Forward and reverse primers for RT-qPCR, shown in Table 5.1, including platelet/endothelial cell adhesion molecule-1 (PECAM-1) [241], von Willebrand factor (vWF)[242], vascular endothelial cadherin (VE-cadherin) [241], and glyceraldehyde 3-phosphate dehydrogenase (GAPDH) were purchased from Sentegen Biotechnology (Ankara, TURKEY) and used to evaluate gene expression [209]. The differential expression of genes PECAM-1, vWF, and VE-cadherin was quantified by StepOne Software v2.3 and Ct values were classified by the $2^{(-\Delta\Delta Ct)}$ method described elsewhere [210, 243]. Every group was experimented with in qPCR as doublet and repeated as triplicate (n = 6).

Table 5.1: Forward and reverse primers. PECAM-1, Ve-Cadherin, vWF, and glyceraldehyde 3-phosphate dehydrogenase (GAPDH; housekeeping gene) (GAPDH) used to assess vasculogenic differentiation in qRT-PCR amplification

GENES	Forward Primer	Reverse Primer
PECAM-1	GCTGACCCTTCTGCTCT GTT	TGAGAGGTGGTGCTGACA TC
VE-Cadherin	TCACCTGGTCGCCAATC C	AGGCCACATCTTGGGTTC CT
vWF	CCCATTTGCTGAGCCTT GT	GGATGACCACCGCCTTTG
GAPDH	GAAATCCCATCACCAT CTTCC	CCAGCATCGCCCCACTT

5.2.5 In vitro Angiogenesis Assay

To determine the pro-angiogenic activity of SAP hydrogels, in vitro angiogenesis assay was performed to examine the inducing angiogenesis effect of SAP hydrogels. The 100 μ L of 1% (w/v) KLD-V1, KLD-V2, KLD, and Biogelx peptide solution was poured into wells of 96-well multi-well plate. 200 μ L DMEM cell culture medium with 25 mM 4-(2-hydroxyethyl)-1-piperazineethanesulfonic acid (HEPES) buffer containing no Fetal Bovine Serum (FBS) was gently added on the top of peptide solution for 2 hours gelation. After the excess DMEM was removed, 10^4

hMSCs/HUVECs (1:1) suspension was seed on SAP hydrogels and cultured with EGM-2 in a humidified 5% CO₂ to enable capillary-like formation in the hydrogels for 7 d. Cells were then fixed with PBS containing 0.2% glutaraldehyde and 1% paraformaldehyde. The images were acquired using an inverted microscope and analyzed using a program developed for the ImageJ software with the “Angiogenesis Analyzer” plugin [244, 245].

5.2.6 Immunofluorescent Staining

Immunofluorescence staining was carried out to observe protein expression and nuclei in HUVEC/hMSC by using primary and secondary antibodies and phalloidin and 4',6-Diamidino-2-Phenylindole (DAPI), respectively [197]. Cell-encapsulated KLD SAP hydrogels and Biogelx were rinsed with PBS. The fixation was performed by 4% paraformaldehyde. 0.1% Triton X-100 in PBS was used to permeabilize to allow DAPI and antibodies to access intracellular epitopes. 1.5% bovine serum albumin (BSA) in PBS was used to eliminate unspecific binding within the cell. Then, samples were incubated in primary antibodies in PBS containing 1% BSA overnight at 4°C. Primary antibodies (Santa Cruz Biotechnology Inc., Santa Cruz, California, USA) were used included mouse monoclonal antibody against PECAM-1 (cat. no. sc-376764; 1:50), and mouse monoclonal antibody against vWF antibody (cat. no. sc-365712; 1:50). Fluorescence secondary antibodies (Santa Cruz Biotechnology Inc., Santa Cruz, California, USA) included m-IgG kappa BP-FITC (cat. no. sc-516140; 1:200) and m-IgG kappa BP-PE (cat. no. sc-21742; 1:200) were diluted with 1% BSA. The fluorescent microscope (Olympus CKX41, Tokyo, Japan) was used for imaging.

5.2.7 Statistical Analysis

All the data that are obtained, were statistically analyzed with two-way ANOVA (SPSS 12.0, SPSS GmbH, Germany) and the Student-Newman-Keuls technique as a post hoc test. At least three samples from all experimental groups were tested (n = 3) and experiments were at least three replicates. Average values, standard deviations, and standard error values of all results were determined. Meaningful distinctions among groups were defined at p values (***p < 0.001, **p < 0.01, *p < 0.05).

5.3 Results

5.3.1 Characterization of Hydrogels

KLD, KLD-IKVAV, KLD-YIGSR, and Biogelx hydrogels were produced and characterized on KLD, KLD-IKVAV (KLD-V1), and KLD-YIGSR (KLD-V2) groups. Vasculogenic differentiation of HUVECs/hMSCs was assessed on 0.5% and 1% w/v KLD (control), KLD-IKVAV (KLD-V1), and KLD-YIGSR (KLD-V2), Biogelx (positive control) groups.

AFM analyses were assessed for the topography of SAP structures (see Figure 5.2). Moreover, SEM imaging was used to confirm the self-assembled nanofiber network in the SAP hydrogel structures (see Figure 5.3). 0.5 % KLD, KLD-V1, and KLD-V2 were used to observe structure because the hydrogels in higher concentration disabled to observe the fiber topography morphology in both AFM and SEM imaging. The average diameter of nanofibers was approximately 19 ± 3 , 19 ± 1 , and 18 ± 1 nm in the KLD, KLD-V1, and KLD-V2, respectively in the AFM and SEM images.

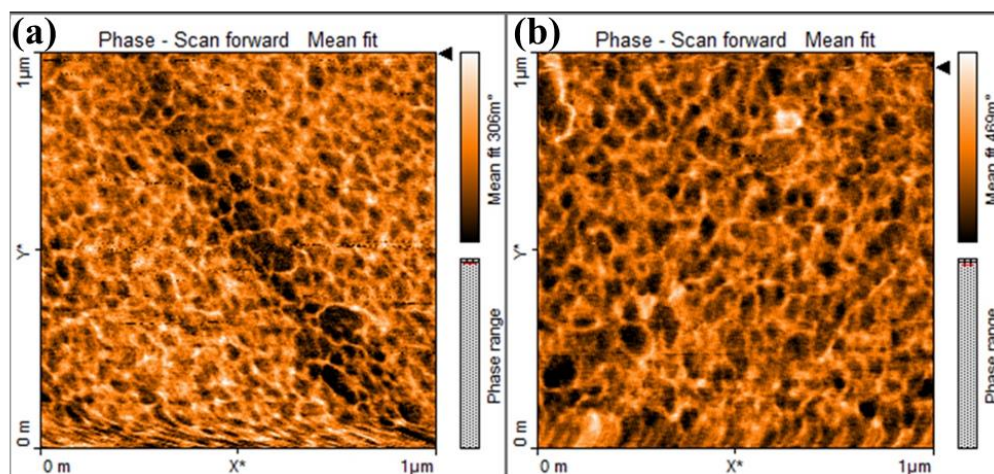


Figure 5.2: Representative 3D topographical view of (a) KLD-V1, (b) KLD-V2 Self-assembled peptide (SAP) nanofibers obtained by Atomic Force Microscopy

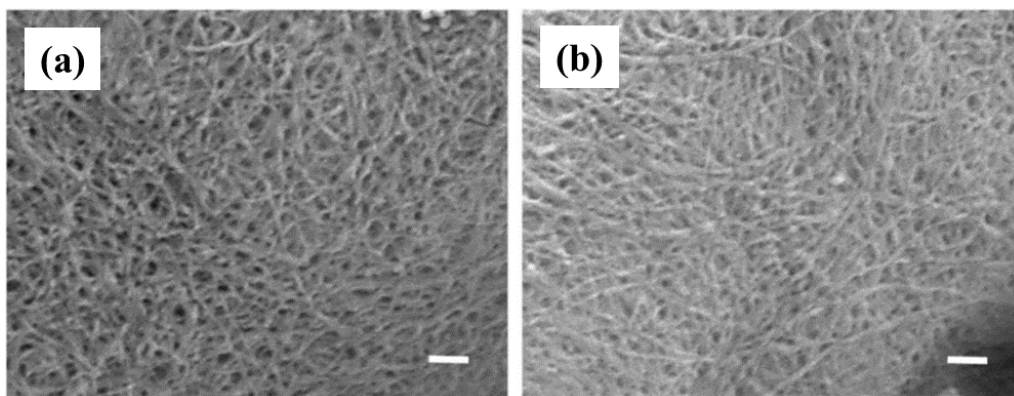


Figure 5.3: Scanning electron microscopy images of (a) KLD-V1, (b) KLD-V2 Self-assembled peptide (SAP) nanofibers (scale bar represents 200 nm).

The macroscopic properties of SAP hydrogels were evaluated by rheology measurements (see Figure 5.4). The same rheological properties were observed in KLD-V1 and KLD-V2. The crossover points between the storage modulus (G') and the loss modulus (G'') observed at the same frequencies in equal peptide concentrations. The maximum storage modulus remained below 1000 Pa for all solutions. G' and G'' has increased with concentration and remained relatively constant as a function of frequency. In rheology analysis, KLD hydrogels containing two different vasculogenic epitopes (IKVAV and YIGSR) are expressed in the form of KLD-V as they are rheologically similar. The value of storage modulus (G') was observed in 1% KLD-V1 and 0.5% KLD-V1 as between 215-260 Pa and 160-200 Pa, respectively. The value of loss modulus (G'') was observed in 1% KLD-V1 and 0.5% KLD-V1 as between 30-60 Pa and 20-35 Pa, respectively.

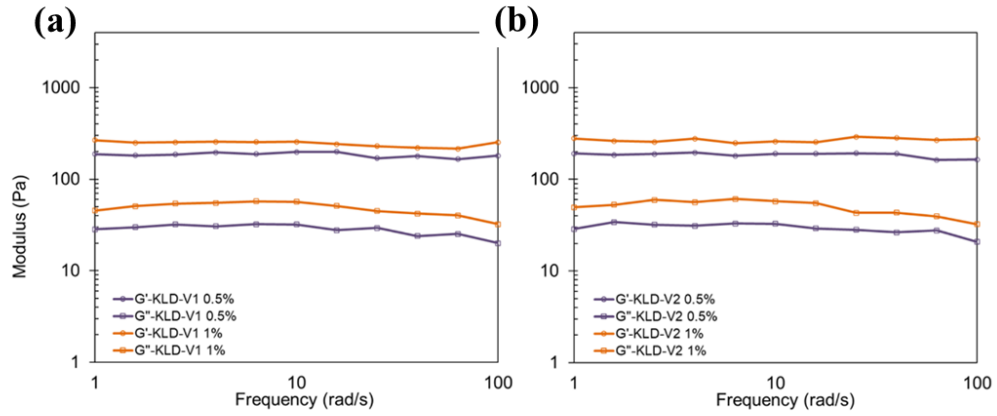


Figure 5.4: Rheology analysis of 0.5%, and 1% (a) KLD-V1, (b) KLD-V2 Self-assembled peptide (SAP) hydrogels. G' and G'' represents storage and loss modulus, respectively

The biodegradation of hydrogels was calculated every 7 d (see Figure 5.5). The duration required for complete degradation was similar in KLD, KLD-V1, and KLD-V2 groups in equal concentration. 0.5% and 1% hydrogels completely degraded after 35 d and 42 d respectively. The difference in biodegradation time was not statistically significant between KLD, KLD-V1, and KLD-V2 groups.

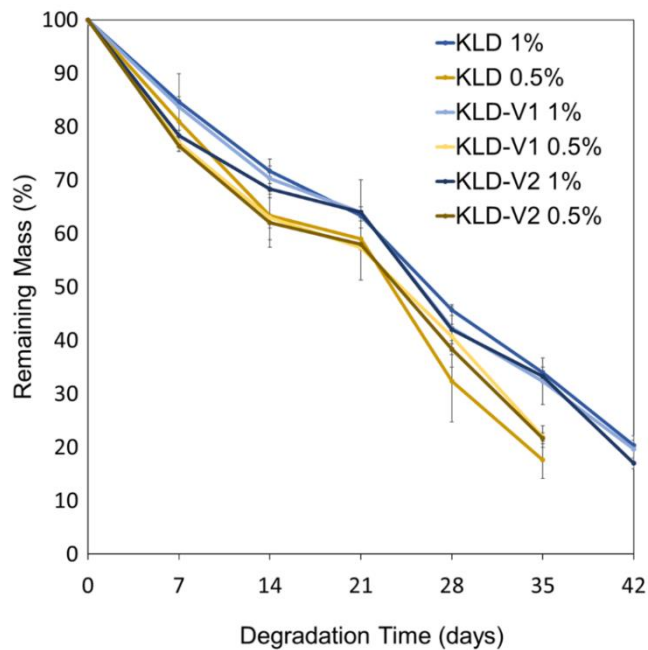


Figure 5.5: Biodegradation of 0.5% and 1% KLD-V1, KLD-V2 Self-assembled peptide (SAP) hydrogels (Time periods: 7,14,21,28, 35,42,49,56, and 63 days)

5.3.2 Proliferation of HUVEC/MSC in SAP Hydrogels

The viability and proliferation of HUVEC/hMSC in KLD, KLD-V1, KLD-V2, KLD+V1, KLD+V2, and Biogelx peptide hydrogels were assessed by MTT assay with respect to incubation time of 1, 4, and 7 d (see Figure 5.6). The cell number of 0.5% and 1% KLD, KLD-V1, KLD-V2 KLD+V1, KLD+V2, and Biogelx increased slightly with incubation time. The cell number of the 1% KLD-V2 group was significantly higher than KLD, KLD-V1, and Biogelx at each time point. At Day 7, the ratio of cell number in 1% KLD-V2 was $7,393,333 \pm 89,876$ while $3,630,000 \pm 116,237$ ($p^{***} < 0,001$), $2,280,000 \pm 51,316$ ($p^{***} < 0,001$), and $2,165,000 \pm 147,460$ ($p^{***} < 0,001$) in KLD-V1, Biogelx and KLD, respectively.

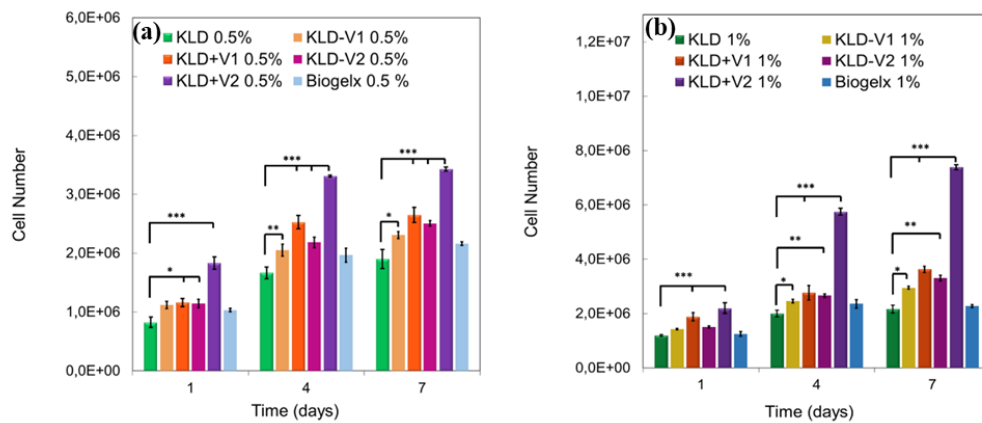


Figure 5.5: Cell number of HUVEC/hMSC encapsulated in 0.5% (A), 1% (B) KLD-V1, KLD+V1, KLD-V2, KLD+V2, and Biogelx and incubated in vasculogenic medium for up to 7 days. The error bars indicate the mean SE ($n = 3$) of the data. [One-way ANOVA was used to assess significant differences.] [$*p \leq 0.05$, $**p \leq 0.01$, $***p \leq 0.001$] Newman–Keuls multiple contrast test]

5.3.3 Quantitative Real-time PCR Analysis

Expression of PECAM-1, vWF, and VE-cadherin as vasculogenic markers with incubation time for HUVEC/MSC-encapsulated SAP hydrogels is depicted in Figures 5.7a-f, respectively. Expression of PECAM-1, vWF, and VE-cadherin in the KLD control group was significantly lower than for Biogelx, KLD-V1, and KLD-V2. PECAM-1 expression, peaking at day 1 and 4, returning to the baseline level at day 7. vWF and VE-cadherin expression increased gradually with incubation time. Higher

expression of vasculogenic markers PECAM-1, vWF, and VE-cadherin was observed in 1% concentration for all groups. Furthermore, PECAM-1, vWF, and VE-cadherin expression was highest for 1% KLD-V2 for each time point. For instance, vWF expression for 1% KLD-V2 at day 7 was $28,80 \pm 1,52$ while that for KLD, Biogelx and KLD-V1 was $2,25 \pm 1,06$, $7,93 \pm 0,03$, and $11,58 \pm 0,28$ ($p^{***} < 0,001$) respectively; VE-cadherin expression for 1% KLD-V2 at day 7 was $17,57 \pm 0,98$ while that for KLD, Biogelx and KLD-V1 $11,42 \pm 0,80$, $11,73 \pm 1,05$, $11,42 \pm 0,50$ and ($p^{***} < 0,001$) respectively; and expression of PECAM-1 for KLD-V2 at day 4 was $33,26 \pm 0,57$ while that for KLD, Biogelx and KLD-V1 was $7,72 \pm 1,45$, $8,55 \pm 0,18$, and $14,16 \pm 1,93$ ($p^{***} < 0,001$) respectively.

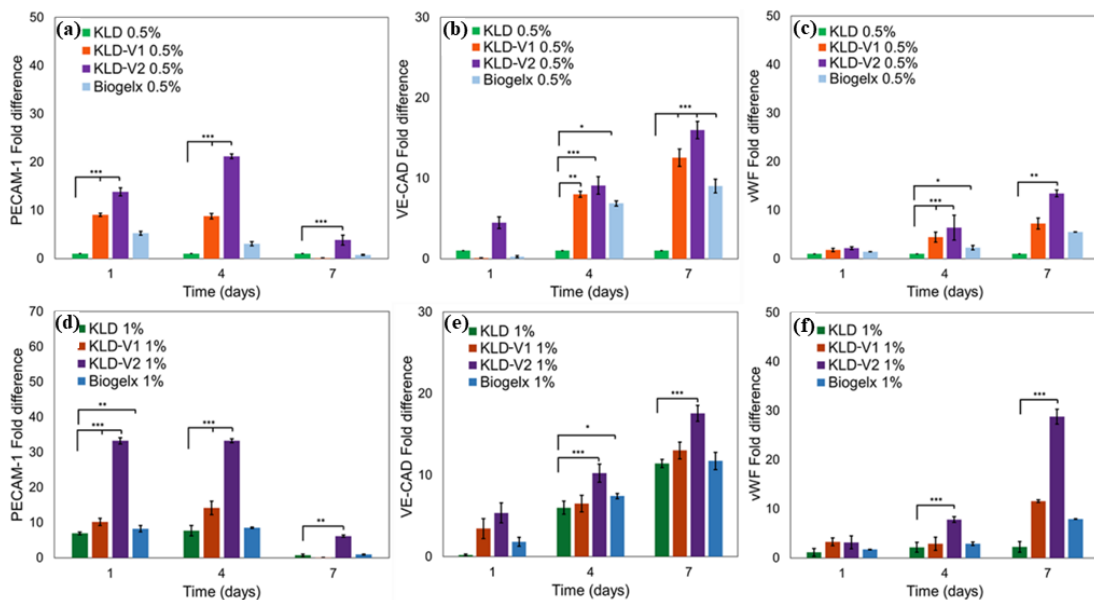


Figure 5.6: The mRNA expression levels (as fold difference) of (a) PECAM-1, (b) VE-Cadherin, (c) vWF, in 0.5 % and (d) PECAM-1, (e) VE-Cadherin, (f) vWF in 1 % KLD, KLD-V1, KLD-V2, and Biogelx after HUVEC/hMSC encapsulation and incubation in vasculogenic medium for up to 7 days. The error bars indicate the mean SE (n = 3) of the data. [One-way ANOVA was used to assess significant differences.] [$*p < 0.05$, $**p < 0.01$, $***p < 0.001$] Newman–Keuls multiple contrast test]

5.3.4 In vitro Angiogenesis Assay

The pro-angiogenic activity of laminin-derived peptide conjugated KLD SAP scaffolds after 7 d was evaluated by an *in vitro* tube formation assay (see Figure 5.8).

hMSCs/HUVECs (1:1) were seed onto SAP cell culture dishes and the angiogenic response measured on the capillary-like network formed after 7 d incubation with the parameters of mean mesh size, total meshes area, number of meshes, total length, number of junctions, number of nodes. Each parameter of the capillary-like network was higher in the KLD-V2 group compared to KLD-V1, Biogelx, and KLD groups.

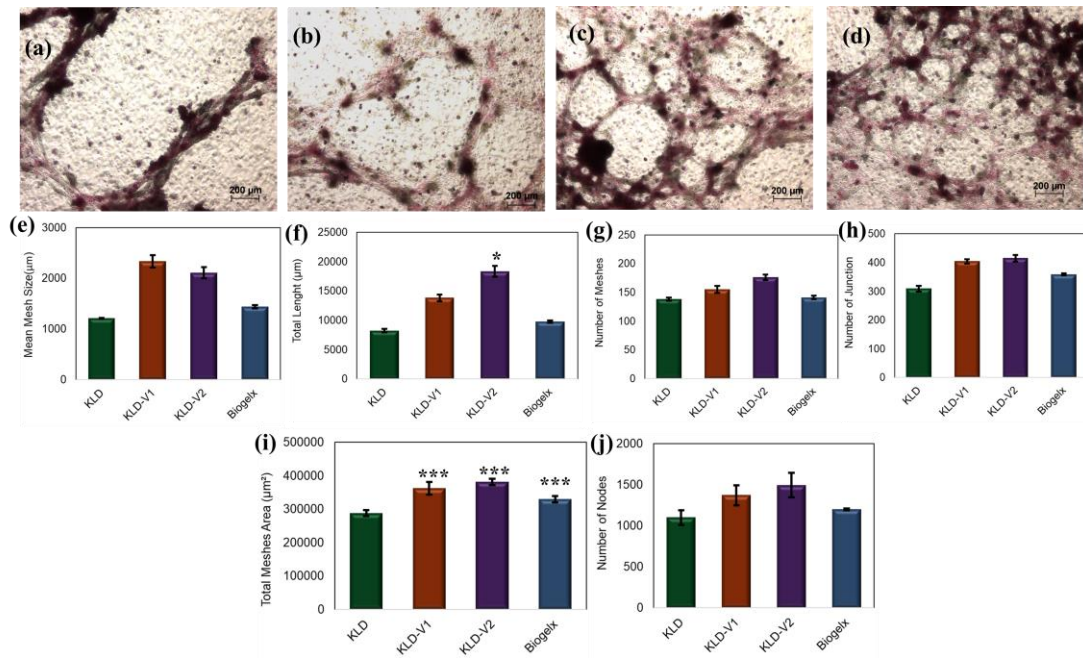


Figure 5.7: Capillary-like tube formation assay. Representative microscopic images of the capillary network of 1 % (a) KLD, (b) KLD-V1, (c) KLD-V2, (d) Biogelx after HUVEC/hMSC encapsulation and incubation in vasculogenic medium for up to 7 days. (Scale bar represents 200 µm). Histogram representing (e) Mesh mean size (f) Total tube length (g) Number of meshes (h) Number of junctions (i) Total mesh area (J) Number of nodes of the capillary-like network as calculated from image the analysis. The error bars indicate the mean SE (n = 3) of the data. [One-way ANOVA was used to assess significant differences.] [$*p<0.05$, $**p<0.01$, $***p<0.001$) Newman–Keuls multiple contrast test]

5.3.5 Immunofluorescent Staining

Immunostaining images of HUVEC/MSC encapsulated in 1% KLD, KLD-V1, KLD-V2, and Biogelx are shown in Figure 5.9 a-d which represents the groups of Biogelx as a positive control (a), KLD as negative control (b), KLD-V1 (c) and KLD-V2 (d) respectively stained with PECAM-1(red) and, vWF (green). The expression of these

vasculogenic related proteins was drastically higher for HUVEC/hMSC on KLD-V2 than those on KLD-V1, Biogelx, and KLD, respectively. KLD group showed weak staining for both markers while vasculogenic epitope containing groups showed moderate to strong staining for vasculogenic markers PECAM-1, and vWF. Immunofluorescence staining of differentiated HUVEC/MSC also confirmed q-PCR results. The expression pattern of PECAM-1, and vWF in HUVEC/hMSC were determined by immunofluorescent staining at day 7 and the results were consistent with q-PCR results.

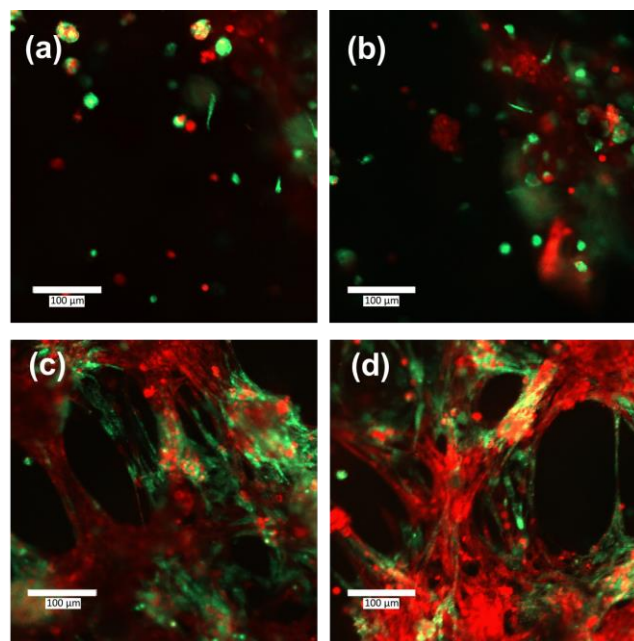


Figure 5.8: Expression pattern of vasculogenic markers PECAM-1(red), and vWF (green) for HUVEC/hMSC encapsulated in 1% (a) Biogelx, (b) KLD, (c) KLD-V1 (d) KLD-V2 after 7 days incubation in vasculogenic medium. (Scale bar represents 100 μm).

5.4 Discussion

In a cell-based engineered tissue construct, the ability to accomplish mass transfer is critical to increasing the availability of nutrient and oxygen supply. Well-orchestrated interactions between the ECM and cells have involved the formation of the vascular network in tissues and are affected by biochemical and mechanical cues. Synthetic

scaffolds have been tailored to resemble the micro-environment of cells and microvascular structure. Short SAPs hydrogel scaffolds which are being integrated into biological processes, can be designed with functional sequences to improve cellular response. For instance, KLD as a short SAP has been utilized due to self-assembling property and functionalization capability for tissue engineering applications [246]. To mimic the laminin in native ECM, we designed SAP hydrogel functionalized with laminin-derived short peptides which are IKVAV (V1) and YIGSR (V2). To the best of our knowledge, it is the first-time approach for a combination of short KLD hydrogel and two short and bioactive peptides resulting in improved vasculogenesis. Our objective was to improve vasculogenesis with SAP hydrogels with controlled mechanical properties thereby the hydrogels also enable to support nutrient and oxygen delivery. We have designed two SAP which are KLD-V1 and KLD-V2 and produced the hydrogels in 0.5% and 1% concentrations. The results revealed that the self-assembling process was not affected by the addition of laminin-derived residues to KLD and increasing peptide concentration affected mechanical properties of KLD-V1 and KLD-V2 hydrogels. Furthermore, the addition of laminin-derived peptides to KLD significantly improved proliferation and vasculogenesis of hMSC/HUVEC co-culture by inducing PECAM-1, VE-cadherin, and vWF genes and proteins expression.

The self-assembly process of SAP hydrogels is intermolecular and spontaneous and the balance between hydrophilicity and hydrophobicity of a peptide often plays a significant role to form a hydrogel structure and affects the solubility of SAPs [215]. Although the functionalization of SAPs with bioactive epitope is used as an approach to direct cell behavior, the functionalization of SAP hydrogels by the addition of functional peptide group charge at the N-terminus of the peptide can affect hydrogel formation by self-assembling into nanofibers in water. Herein, the addition of hydrophobic IKVAV, as well as hydrophilic YIGSR to KLD sequence to the N-terminus of KLD, the hydrogel formation ability of the SAP, was not affected and the hydrogel formation of KLD-V2, KLD-V1, and KLD was confirmed by AFM and SEM. In a previous study, Jain *et al.* designed collagen inspired peptide sequence with a combination of the collagen with Nap-FF (naphthoxy-diphenylalanine) and aromatic dipeptide gelator and functionalized with IKVAV and YIGSR by attachment to the N-terminal [235]. However, these functionalized peptides were reported as insoluble in

water due to the extensive hydrophobicity and intermolecular interaction which avoids forming an organized network structure in water, and peptides were solved in 10% DMSO in DI water. Further, since DMSO concentrations above 1% can decrease cell proliferation significantly [247], solvent exchange methods for post-gelation were performed to avoid the toxic effect of DMSO.

SAP hydrogels gained importance as a potential scaffold for vascularization [248]. By increasing peptide concentration, variable SAP hydrogel stiffness could be obtained to control cell attachment, proliferation, and differentiation [249]. Herein, the equilibrium hydrogel modulus changed depending on concentration and vasculogenic epitopes and KLD hydrogels containing V1 and V2 epitopes showed similar rheological gel properties. At higher concentrations, KLD self-assembled nanofibers further assemble into a fibrillar hydrogel network, different vasculogenic epitopes (V1 and V2) did not significantly affect the rheological properties of the gels. The impact of higher concentration (1%) on equilibrium gel modulus was fundamentally attributed to intense network topology and results in higher storage modulus. Previous studies have demonstrated that hydrogels with improved mechanical properties enhance both cell proliferation and vascularization [250, 251]. Lee *et al.* produced hydrogels that contained gelatin–hydroxyphenyl propionic acid (GH) which can be cross-linked to enhance the angiogenic potential of MSCs and reported that GH hydrogels with increased mechanical properties supported functional vascularization of MSCs [250]. Similarly, Lee *et al.* improved mechanical stiffness by using hydrogen peroxide and speculate that the GH with a more effective biomechanical structure increased cell viability and subsequently maintained vascularization of hMSCs [251]. Herein, since KLD-V1 and KLD-V2 possess similar mechanical features, the effect of mechanical properties of hydrogels was eliminated on cell proliferation and vascularization.

The degradation rate of SAP hydrogels is changed depending on the charge of hydrogel components and confirms the stability of hydrogels during vascularization. Rapid degradation by proteases commonly limits the effectiveness of hydrogels in long-term cell culture, while peptides can be easily incorporated within the hydrogels [252]. The hydrogels should allow degradation at a rate similar to tissue formation for secretion of ECM [253]. The degradation profile of KLD hydrogel without any epitope was previously reported [237] and the degradation profile of KLD-V1 and KLD-V2

compared with KLD. The degradation time of 0.5% and 1% KLD hydrogels were 35, and 42, respectively and there is no significant difference between KLD and laminin-derived peptide containing KLD groups. Additionally, the degradation duration to confirm the stability of designed KLD hydrogels *in vivo* can be considered adequate to support *in-situ* tissue formation such as skin, skeletal muscle, and bone tissues [254-256].

The cell number of laminin-derived peptide anchored groups (KLD-V1 and KLD-V2) were significantly higher than the groups in which laminin-derived peptide mixed groups (KLD+V1 and KLD+V2) at each time point. These results highlighted the importance of anchoring peptides onto SAP hydrogel. MTT assay depicted that increased SAP hydrogel concentration and the addition of laminin-derived peptides resulted in increased cell number and. Increased vasculogenesis due to the addition of IKVAV and YIGSR has demonstrated the potential of these two-laminin-derived peptides on adhesion, differentiation of ECs [236, 257]. Herein, the effect of IKVAV(V1) and YIGSR(V2) laminin-derived peptides on proliferation was determined based on MTT assay. MTT assay results revealed that KLD-V2 and KLD-V1 facilitated the proliferation of HUVEC/hMSC significantly compared to Biogelx, and KLD throughout the 7 days of the incubation period. These findings suggest that the addition of laminin derived peptides induces cell proliferation. Furthermore, KLD-V2 consists of YIGSR was found more effective on HUVEC/hMSC proliferation compared to KLD-V1 consist of IKVAV. Our results are consistent with an early report that showed YIGSR conjugated poly(ethylene glycol) diacrylate (PEGDA) had a better influence on endothelial cell adhesion compared to IKVAV conjugated PEGDA [236]. However, Ali et al. conjugated IKVAV and YIGSR peptides to PEGDA synthetic polymers and formed hydrogel structure by cross-linking procedure consists of UV exposure and N-vinyl-2-pyrrolidone (NVP) crosslinker which is toxic for the cells [258]. Therefore, SAP hydrogels which are crosslinked physically like natural proteins in ECM, are ideal candidates for tissue engineering scaffold compared to synthetic polymeric hydrogels such as PEGDA, which need the chemical cross-linking procedure. This toxic effect may have inhibited the effect on cell proliferation and vasculogenic differentiation of the conjugated bioactive isotopes. However, SAP hydrogels which are crosslinked physically like natural proteins in ECM might be an alternative to photoinitiated polymerization of biomaterials in terms of ease of

fabrication, the capability of biofunctionalization, and superior biocompatibility properties. Herein, the addition of IKVAV and YIGSR at the N-terminus of KLD peptide did not affect the water solubility of SAP and a similar trend was observed when the effect of YIGSR and IKVAV on proliferation and endothelial vascular formation. ECs binding to collagen IV and laminin is facilitated by integrins and affects the adhesion and proliferation of cells by the $\alpha v \beta 3$ integrin and $\alpha v \beta 3$ integrin enhance ECs attachment in response to IKVAV and YIGSR peptides. Ali et al. demonstrated the deposition of collagen IV and laminin is higher in YIGSR conjugated PEGDA compared to IKVAV conjugated PEGDA throughout 28 days. Herein, the more expression of ECM proteins such as laminin and collagen IV in KLD-V2 might provide more attachment points for $\alpha v \beta 3$ integrin compared to KLD-V1.

Vascularization of tissue constructs is important for clinical application. The scaffolds should support endothelial cells to maintain new vessel formation. During vessel formation, endothelial cells secrete vascular endothelial growth factors, angiogenic growth factors, and angiopoietins insignificant levels to improve early capillary network formation [259]. HUVECs have been known to form capillary-like networks by expressing mature endothelial cell markers such as PECAM-1 (CD31), vWF, and VE-cadherin *in vitro* [260]. Gene expression results showed V1 and V2 laminin-derived peptides containing KLD hydrogels improved vasculogenic differentiation in HUVECs/hMSCs compared to KLD hydrogel. Nevertheless, the expression of PECAM, Ve-cadherin, and vWf mRNA in KLD-V2 is higher compared to KLD-V2 at each time point. However, it is interesting to remark on the enhanced expression of PECAM, Ve-cadherin, and vWf mRNA in increased hydrogel concentration for each time point. PECAM-1, which is a cell adhesion molecule from trans-membrane glycoprotein member of the Ig superfamily, expressed in endothelial cells at the cell-cell interface, and the expression of PECAM is used to specify the microcapillary-like structure or lumina [246, 261]. HUVECs secrete PECAM-1 for vessel formation and maintenance [262]. Our results showed that strong PECAM-1 expression can be observed on KLD-V1 and KLD-V2. The ability of HUVECs to form lumina depends on the properties of the ECM, which can influence the migration of HUVECs [263]. Nevertheless, the continuous PECAM-1 expression by the HUVECs was not observed. On day 7, PECAM-1 expression was decreased, whereas the continuous trend was observed up to day 4 for all groups. It is generally considered that MSCs generally

affect negatively PECAM expression [264]. However, VE-cadherin and vWF expression was increased up to 7 days for all groups. VE-cadherin is present at endothelial adherent junctions and plays an important role in the intercellular adhesion, differentiation, growth, and migration of HUVECs [265]. The expression of VE-cadherin can be regulated depending on the mechanical properties of the environment around endothelial cells [266] and bioactive molecules [267]. In this study, increased concentration of SAP hydrogels and addition of bioactive peptides (V1 and V2) resulted in increased Ve-cadherin expression which regulated depending on mechanical and biological properties of the matrices around the cells. VWF is a multifunctional glycoprotein that regulates blood formation. VWF is expressed in ECs to regulate the levels of $\alpha v\beta 3$ and its internalization. The cell-binding motifs presented IKVAV, and YIGSR is commonly used as a cell adhesion motif that is known to bind through $\alpha v\beta 3$ [268]. Herein, $\alpha v\beta 3$ internalization of IKVAV and YIGSR in KLD-V1 and KLD-V2, respectively can be related increased VWF expression.

Laminin-derived peptide containing SAP hydrogels could significantly enhance the expression of PECAM-1, and vWF proteins, which is of great importance for vascularization because of the multifunction of these factors in different stages of nerve regeneration. 1% Biogelx and KLD showed moderate staining for vasculogenic proteins such as PECAM, and vWF, while 1% KLD-V2 and KLD-V1 hydrogel groups showed strong staining for the vasculogenic proteins. This pattern is probably due to the increased HUVECs/hMSCs population found by cell proliferation analysis and probably decreased HUVECs/hMSCs population in control groups led to the inability of HUVECs to contact and form a microcapillary-like structure. The bioactivity of scaffolds to induce vasculogenesis was usually assessed by evaluating the ability of scaffolds to release vasculogenic growth factors from endothelial cells such as PECAM, and vWF. The expression of these vasculogenesis-related proteins such as PECAM, and vWF was drastically higher for hMSCs in KLD-V2 than those in KLD-V1, Biogelx, and KLD, respectively. In consistent with real-time PCR results, HUVECs/hMSCs on KLD-V1 showed higher expression of these markers compared to those on KLD, highlighting the vasculogenic inductive effect of laminin-derived peptides. Based on these protein expression trends, we suggest that it may be that HUVECs/hMSCs can benefit from laminin-derived peptides for 7 days while the cells

are adapting to their environment and release paracrine signals which are vital during the early stages of vasculogenesis.

5.5 Conclusion

In summary, KLD hydrogel was successfully functionalized with laminin-derived peptides through direct solid-phase synthesis extension at the amino terminal. SAP hydrogels were successfully formed and laminin-derived peptide-functionalized improved the vasculogenesis potential of the KLD hydrogels. Moreover, YIGSR(V2) containing KLD sharply increased proliferation compared to IKVAV(V1) peptide containing KLD. Our findings revealed that KLD hydrogel functionalized with YIGSR templated peptides had more potential on inducing vasculogenesis and these laminin-derived peptides could improve the blood vessel formation in the tissue construct. Improving vascularization can recompense the loss of function in tissues or organs by promoting the survival of transplanted cells [269].

Chapter 6

Self-assembled peptide Hydrogel for Accelerating the Osseointegration Period of Dental Implants

6.1 Introduction

Since the 1980s, dental implants have become an integral part of the treatment of partially and completely edentulous patients due to improved grafting materials [270, 271]. However, the issues that lead to osseointegration failures, such as insufficient bone formation around the implant and the development of direct implant-bone interaction, have been continuing to be the most difficult obstacles to the clinical effectiveness of oral implants [272, 273]. Biomechanical integration, as well as biological interactions via biochemical bonding, are needed for the osseointegration of bone tissues. Researchers have recently concentrated on methods to enhance osseointegration by biological mediators and coating methods [274].

Hydrogels have a 3-D and interrelated structure, which can provide a biocompatible ECM environment for the cells to attach and proliferate while supporting bone formation at the defect area [275]. Injectable hydrogels should be capable of non-invasively filling irregularly-shaped spaces as a less invasive alternative bone tissue engineering strategy to the painful and long invasive surgery [276]. Hydrogels used as a bone filler substitute should induce osseointegration by allowing the growth factors to release and enhancing osteogenesis. Hydrogel solutions containing biomolecules or/and cells are introduced to the defect area can resemble the surrounding environment [277]. Self-assembling peptide hydrogels (SAP) with structural and

functional properties similar to bone tissue have significant potential for applications in bone tissue engineering. SAP hydrogels are emerging biomaterials for bone regeneration because they develop spontaneously in the absence of chemical crosslinkers or physical stimuli such as heat or UV irradiation. By functionalizing with different peptide epitopes, SAP hydrogels can not only form a temporary 3D network but also guide bone regeneration and increase the bioactivity of the matrix [207]. In our previous work, we developed injectable five glutamic acids templated KLD (KLDLKLKLDL) SAP hydrogel which improved the osteoinductive capacity of KLD SAP hydrogels [237].

In dental applications, both achieving an optimal cell response at the implant-tissue interface and penetration of the implant into the surrounding tissue affect the ultimate performance of implants [278]. In several physiological conditions such as bone growth and fracture cure, as well as bone regeneration and the osseointegration of implanted implants, angiogenesis is an important mechanism for the formation of new vascular capillaries [279]. The implant materials should promote peri-implant bone formation and angiogenesis. Blood vessel development *in vivo* is a dynamic mechanism that requires the coordination of multiple growth factors and events. PECAM-1, vWF, and Ve-cadherin are among several known growth factors that contribute to the initiation and regulation of angiogenesis around the implant site [280]. The involvement of vascular networks regulates bone growth and regeneration since bone is a highly vascularized tissue [281].

The objective of the study is to develop and characterize *in situ* multifunctional SAP hydrogels, which can support osteogenic and vasculogenic differentiation and determine the efficacy of multifunctional SAP hydrogel on the dental implant osseointegration process (see Figure 6.1). The novelty of this study is to develop multifunctional SAP hydrogels that induce both osteogenic and vasculogenic differentiation of MSCs and HUVECs with their functional epitopes and develop multifunctional SAP hydrogels on dental implant osseointegration. Herein, SAP hydrogels that can induce both osteogenesis and vasculogenesis were developed. The effect of epitopes that were added to SAP structure on inducing osteogenesis and vasculogenesis of hMSC cocultured with HUVEC were evaluated by biochemical, immunostaining, and gene expression analysis. The efficacy of using multifunctional

SAP hydrogel on dental implant osseointegration was determined with resonance frequency analysis, reverse torque testing, right after *in vitro* studies. Multifunctional SAP hydrogel enhanced both osteogenesis and vasculogenesis *in vitro*. Furthermore, SAP hydrogels improved the mechanical stability of titanium implants *in vivo* studies using a tibial defect rabbit model. Injectable multifunctional scaffolds that were developed in this study could be used in clinics to accelerate dental implant osseointegration.



Figure 6.1: Schematic illustration of multifunctional self-assembled peptide (SAP) hydrogel for dental implant osseointegration

6.2 Materials and Methods

6.2.1 Peptide Synthesis

Ac-Lys-Leu-Asp-Leu-Lys-Leu-Asp-Leu-Lys-Leu-Asp-Leu-NH₂ (KLD), KLD-EEEE (KLD-Glu-Glu-Glu-Glu-Glu-NH₂), KLD-YIGSR (KLD-Tyr-Ile-Gly-Ser-Arg-NH₂) were synthesized on MBHA resin as described in Chapter 2 by using the automated peptide synthesis device. Briefly, all amino acids were coupled by removing the Fmoc-protecting group of amino acids. For each coupling step, the amine groups which were not reacted were acetylated. Each deprotection and coupling reaction was monitored by the Kaiser test. The peptides were separated from resin. The peptides were purified via preparative HPLC system and mass spectrums of KLD,

KLD-EEEE (KLD-O), and KLD-YIGSR (KLD-V) peptides were characterized (see liquid chromatography and mass spectra for KLD, KLD-O2, and KLD-V2 in Figure S1 and 2 and Table S1, Supporting Information).

6.2.2 Self-assembled Hydrogel Fabrication

2% w/v multifunctional SAP hydrogel (KLD-O-V) were prepared by mixing KLD-O and KLD-V at the same molar ratio. 2% KLD-O-V, KLD, and Biogelx (Biogelx Inc., Scotland, UK) were produced by dissolving in di water and mixed with sterilized DMEM with 25 mM 4-(2-hydroxyethyl)-1-piperazineethanesulfonic acid (HEPES) buffer containing no FBS. The highest concentration for KLD-O-V, KLD-O, KLD, Biogelx was selected as 2% w/v due to the complete solubility problem of peptides over 2% w/v in di water.

6.2.3 In vitro Cell Differentiation

6.2.3.1 Cell Seeding and Proliferation Analysis

hMSCs and HUVECs were cultivated in containing FBS (10%), penicillin-streptomycin (100 units/mL). Fresh medium was added to cultures at intervals of 2 days. 5×10^6 cells/ml hMSCs and HUVEC/ hMSCs (1:1) co-culture were encapsulated in SAP hydrogels by using basal medium. After 24 h, the medium was replaced with a mixture of osteogenic medium and vasculogenic medium (1:1). The osteogenic medium contains basal medium supplemented with 50 $\mu\text{g/mL}$ ascorbic acid, 100 nM dexamethasone, 10 mM β -glycerophosphate. The vasculogenic medium was prepared by using EGM-2 (Lonza, Walkersville, USA) contained ascorbic acid, hydrocortisone, insulin-like growth factor (R3-IGF-1), fibroblast growth factor (hFGF-B), epidermal growth factor (hEGF), gentamicin, amphotericin-B, heparin with 10% FBS. Cells for osteogenic differentiation and vasculogenic differentiation were cultured at 5% CO_2 for 28 d, and 7 d, respectively.

For the cell proliferation analysis of HUVECs/MSCs that were encapsulated into the hydrogels, 3-(4, 5-dimethylthiazol-2-yl)-2, 5-diphenyltetrazolium bromide (MTT) (Vybrant® MTT Cell Proliferation Assay Kit, Invitrogen, Waltham, MA, USA) assay

was performed at 1., 4. and 7. days of the culture as previously described [173]. First, the cell medium was removed and 10% MTT dye in the culture medium was added to each sample. The procedures with MTT were carried out in the dark. Encapsulated cells were incubated in the MTT dye for 4 hours at 37°C and 5% CO₂. Then, MTT dye was removed from the samples, and 500 µl dimethyl sulfoxide (DMSO, Sigma-Aldrich, Steinheim, Germany) was added for dissolving formazan crystals. Hydrogel structures were smashed by pipetting and the absorbance was measured at 570 nm using a microplate reader (Biotek Synergy HTX, Winooski, VT, USA).

6.2.3.2 Osteogenic differentiation in multifunctional hydrogels

At each time point (7, 14, 21, and 28 d), double-stranded DNA content, ALPase activity, and calcium content of the samples of cell-encapsulated hydrogels were rinsed with PBS. 10 mM Tris containing 0.2% triton in PBS was used to take lysate for measurement of DNA content, ALPase activity, and calcium content. [201]. DNA Quantification Kit was purchased from Sigma Aldrich (St. Louis, MO, USA), and ALPase assay and Calcium Assay were purchased from Bioassay Systems (Hayward, CA, USA). Briefly, bisBenzimide H 33258 Solution was prepared and added on lysed samples in a 96-well plate. Fluorescence (excited at a wavelength of 360 nm) was measured using a spectrophotometer (BioTek, Winooski, VT, USA) at an emission wavelength of 460 nm, at ambient temperature. ALP activity was measured by *p*-nitrophenylphosphate (*p*NPP) at 405 nm in alkaline solution using ALP kit. Briefly, 50 µL of lysed sample to 200 µL total reaction volume were used for initiating the reaction by the addition of assay buffer, 5 mM magnesium acetate, and 10 mM *p*NPP in a 96-well plate. Optical density (OD) in 405 nm was measured at initial time ($t=0$) and after 4 min ($t=4$ min) on multi-plate reader (BioTek, Winooski, VT, USA). The calcium content of hydrogels was measured by adding 50 µL of the suspension to 150 µL of the working solution. The wavelength of 612 nm was used to measure absorbance. A calibration curve was created with reference calcium solutions and the intensity values were associated with the equivalent calcium values. The calcium deposit and ALP activity were calculated by normalizing by dividing DNA content at each time point.

Total cellular RNA was isolated at 7 d, 14 d, 21 d, and 28 d for q-PCR analysis. Briefly, SAP hydrogels were rinsed with PBS and incubated in trypsin. Then, the samples were centrifuged at 850 rpm for 5 min. RNA isolation Kit (Geneaid, Sijhih City, Taiwan) was applied to all samples according to the manufacturer's instruction. The samples were reacted with reaction buffer for lysis. RNAs were collected in RNase Free Water after washing with W1, wash buffer solution, respectively. The RNA sample concentration was measured with nanodrop (Nanodrop 2000, Thermo Scientific, Wilmington, DE) and stored at -20°C. After total cellular RNA was resuspended in water (nuclease-free) and remaining genomic DNA contaminations were digested by TURBO DNase (Ambion, Austin, TX) by incubating for 30 min at 37°C and incubated in DNase Inactivation Reagent for 5 min at 37°C. RNAs were centrifuged in 10000 RCF for 2 min to precipitate DNA molecules. cDNA converted by cDNA Synthesis Kit Protocol (Biomatiks, K5147). Briefly, after 1 µl Oligo dT (10 µM), 1 µl Random Primer (10 µM), 1 µl dNTP Mix, 14.5 µl Nuclease Free Water were added into 1 ng-2 µg/rxn RNA incubated at 65°C for 5 min. RNase Inhibitor, RT Buffer, M-MuLV Reverse Transcriptase were mixed and all components (20 µl) were collected by brief centrifugation and incubated at 25°C for 10 min, at 42°C 50 min, at 85°C for 5 min. and stored at -20°C. Forward and reverse primers including glyceraldehyde 3-phosphate dehydrogenase (GAPDH), alkaline phosphatase (ALP), Collagen type I (COL-1), osteocalcin (OCN), and osteopontin (OPN) purchased from Sentegen Biotechnology (Ankara, TURKEY), shown in Table 3.1 in Chapter 3. Power SYBR Green PCR Master Mix (Applied Biosystems, Foster City, USA) and Step One Plus Real-time PCR system (Applied Biosystems, Foster City, USA) were used to quantifying ALP, COL-1, OPN, and OCN. GAPDH differential expression is used for housekeeping gene and other primers were normalized according to GAPDH. Briefly, 200 nmol primers (0,1mM), SYBR Master Mix, cDNA was mixed and diluted 1:10 ratio with water. qPCR was formed with the following stages: Holding Stage at 95°C for 10 min., Cycling Stage at 95 °C for 15 sec. and at 64,4 °C for 1 min, Cycling Stage includes at 64,4 °C, Melt Curve Stage at 95 °C 15 sec, at 60 °C and 95°C for 15 sec. The Ct values obtained from experiments (n=6) were classified by the $2^{(-\Delta\Delta Ct)}$ method.

Immunofluorescence staining was carried out to observe protein expression and nuclei in hMSCs by using primary and secondary antibodies and phalloidin and 4',6-Diamidino-2-Phenylindole (DAPI), respectively [197]. Cell-encapsulated KLD SAP

hydrogels and Biogelx were rinsed with PBS. The fixation was performed by 4% paraformaldehyde. 0.1% Triton X-100 in PBS was used to permeabilize to allow DAPI and antibodies to access intracellular epitopes. 1.5% bovine serum albumin (BSA) in PBS was used to eliminate unspecific binding within the cell. Then, samples were incubated in primary antibodies in PBS containing 1% BSA overnight at 4°C. Primary antibodies (Santa Cruz Biotechnology Inc., Santa Cruz, California, USA) were used included mouse monoclonal antibody against COL-1 (cat. no sc-59772; 1:50), mouse monoclonal against OPN antibody (cat. no. sc-21742; 1:50), and mouse monoclonal antibody against OCN (cat. no. sc-365797; 1:500). Fluorescence secondary antibodies (Santa Cruz Biotechnology Inc., Santa Cruz, California, USA) included m-IgG kappa BP-FITC (cat. no. sc-516140; 1:200) and m-IgG kappa BP-PE (cat. no. sc-21742; 1:200) were diluted with 1% BSA. The fluorescent microscope (Olympus CKX41, Tokyo, Japan) was used for imaging.

Calcium deposition on hMSCs encapsulated hydrogels over 28 d were evaluated by Alizarin Red staining (Alizarin Red S, Sigma Aldrich, St. Louis, MO, USA). Briefly, hMSCs were fixed for 15 minutes using 4 % PFA followed by wash steps using PBS (1x), and the staining solution (1% Alizarin Red S in ddH₂O) was applied for 30 minutes followed by imaging using the inverted microscope (Olympus CKX41, Tokyo, Japan).

6.2.3.3 Vasculogenic differentiation of in multifunctional hydrogels

The RT-qPCR analysis was performed in each sample was isolated at each time point (1, 4, and, 7d) as described in the osteogenic differentiation part. Forward and reverse primers for RT-qPCR, shown in Table 4.1 in Chapter 4, including platelet/endothelial cell adhesion molecule-1 (PECAM-1) [241], von Willebrand factor (vWF) [242], vascular endothelial cadherin (VE-cadherin) [241], and glyceraldehyde 3-phosphate dehydrogenase (GAPDH) were purchased from Sentegen Biotechnology (Ankara, TURKEY) and used to evaluate gene expression [209]. The differential expression of genes PECAM-1, vWF, and VE-cadherin was quantified by StepOne Software v2.3 and Ct values were classified by the $2^{(-\Delta\Delta Ct)}$ method described elsewhere [210, 243]. Every group was experimented with in qPCR as doublet and repeated as triplicate (n = 6).

Immunofluorescence staining was carried out to observe protein expression and nuclei in HUVEC/hMSC by using primary and secondary antibodies and phalloidin and 4',6-Diamidino-2-Phenylindole (DAPI), respectively [197]. Cell-encapsulated KLD SAP hydrogels and Biogelx were rinsed with PBS. The fixation was performed by 4% paraformaldehyde. 0.1% Triton X-100 in PBS was used to permeabilize to allow DAPI and antibodies to access intracellular epitopes. 1.5% bovine serum albumin (BSA) in PBS was used to eliminate unspecific binding within the cell. Then, samples were incubated in primary antibodies in PBS containing 1% BSA overnight at 4°C. Primary antibodies (Santa Cruz Biotechnology Inc., Santa Cruz, California, USA) were used included mouse monoclonal antibody against PECAM-1 (cat. no. sc-376764; 1:50), and mouse monoclonal antibody against vWF antibody (cat. no. sc-365712; 1:50). Fluorescence secondary antibodies (Santa Cruz Biotechnology Inc., Santa Cruz, California, USA) included m-IgG kappa BP-FITC (cat. no. sc-516140; 1:200) and m-IgG kappa BP-PE (cat. no. sc-21742; 1:200) were diluted with 1% BSA. The fluorescent microscope (Olympus CKX41, Tokyo, Japan) was used for imaging.

6.2.4 In vivo Evaluation

6.2.4.1 Replacement of the Dental Implants

9 months old adult male New Zealand rabbits with an average weight of 3-3.5 kg were used for implantation. The control group consists of rabbits in which only dental implants were placed and no injection was made afterward. In Figure 6.2, the placement of dental implants is schematized. Titanium dental implants with a diameter of 4 mm and a length of 6 mm with SLA (Sandblasted, Large-grit, Acid-etched) surface were placed in the tibia bone of rabbits (2 implants to each tibia). Surgical procedures required for cell isolation and dental implant placement were carried out under the supervision of the veterinarian and performed according to an animal study protocol approved by the Ege University Local Ethics Committee of Animal Experiments (approval no 2019-110). All surgical procedures were performed at Ege University Center for Research on Laboratory Animals (EGEHAYMER) under sterile surgical conditions by paying attention to asepsis, antisepsis, and sterilization rules. Animals fasted before surgery and 40 mg/kg Ketamine HCl (Alfamine®, Egevet, Turkey), and 5 mg/kg Xylazine (Alfazine®, Egevet, Turkey) were injected into muscle

for general anesthesia. After the skin in the proximal regions of the tibia bone on both sides was shaved, hemostasis and local anesthetics containing articaine HCl (Ultrac DS Fort Aventis Pharma, Turkey) for postoperative pain control were injected. The surgical field was cleaned with the antiseptic solution following intramuscular prophylactic antibiotic and prophylactic antibiotic (50 mg/kg Cefazolin) and analgesic drug 1 mg/kg Tramadol HCl injections. Subcutaneous and muscle layers were passed through by blunt dissection following the 2 cm skin incision extending from medial to distal from the proximal metaphysis of the tibia. After the tibia metaphyseal bone surface was reached by the periosteal incision, the implant nests were prepared with the driller in the implant system. Multifunctional SAP was injected into the area between the dental implant and the bone surface for modeling the osseointegration process. The implant nests were replaced at 2/3 coronal with a gap of at least 2.5 mm and at the 1/3 apical in the vestibule area of the implant to ensure the stability of the implants.

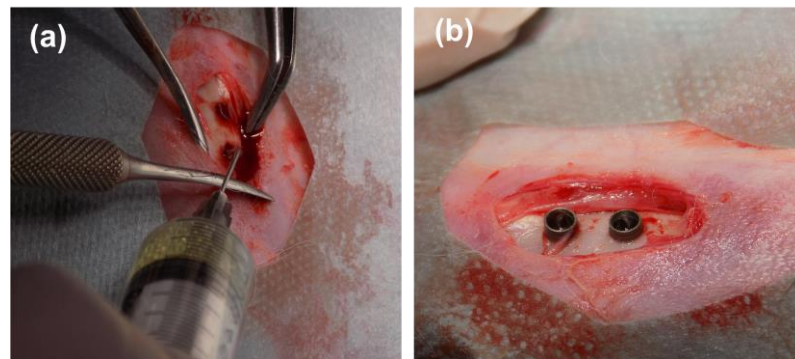


Figure 6.2: Implantation of titanium into the tibia of a New Zealand. (a) SAP hydrogel insertion, (b) installation of titanium dental implants into the tibia

6.2.4.2 Resonance Frequency Analysis

Resonance Frequency Analysis (RFA) was performed to determine the degree of osseointegration biomechanically (see Figure 6.3a). Osstell® (Osstell AB, Göteborg, Sweden) device was used for RFA method. Measurements were carried out at two different periods such as the first placement and sacrifice periods. The measurement results were recorded in terms of ISQ (implant stability quotient) at values between 0-100. These values obtained were compared statistically. After

sacrificiation, the implants were resected with 3-4 mm of bone around them and these samples were fixed in an acrylic mold. The bone blocks in the acrylic mold obtained were fixed to the standard test setup to be formed.

6.2.4.3 Reverse Torque Test

Reverse torque tests (RTT) were performed to determine the degree of osseointegration biomechanically (see Figure 6.3 b). After the digital torque meter (Checkline MTT03 10Z, NY, USA) probe was fixed on the implant bearing parts, an anti-clockwise extraction force was applied slowly and gradually. The procedure is completed when the implant begins to rotate in the bone socket. The highest torque value recorded on the graph and digital screen and obtained at the moment of the break was recorded in N.cm. The values obtained were compared statistically.

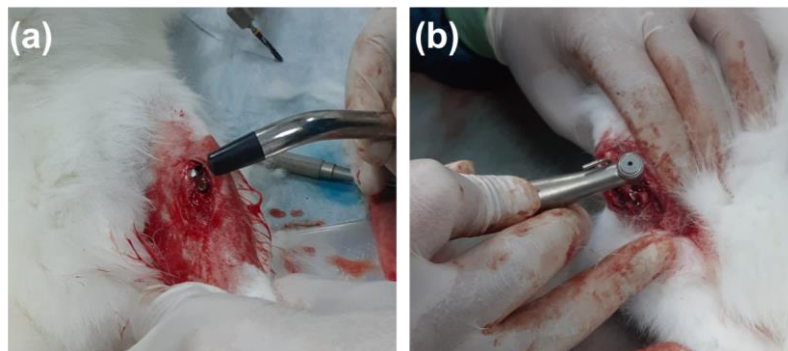


Figure 6.3: (a) Resonance frequency analysis (b) Reverse torque measurements of dental implants before the removal

6.2.5 Statistical Analysis

All the data that are obtained, were statistically analyzed with two-way ANOVA (SPSS 12.0, SPSS GmbH, Germany) and the Student-Newman-Keuls technique as a post hoc test. At least three samples from all experimental groups were tested ($n = 3$) and experiments were at least three replicates. Average values, standard deviations, and standard error values of all results were determined. Meaningful distinctions among groups were defined at p values ($***p < 0.001$, $**p < 0.01$, $*p < 0.05$).

6.3 Results

6.3.1 Proliferation of HUVEC/hMSC in SAP Hydrogels

The viability and proliferation of HUVEC/hMSCs in hydrogels were evaluated by MTT assay with respect to incubation time of 3, 7, 14, 21, and 28 d (see Figure 6.4). The cell number of KLD, KLD-O, KLD-O/KLD-V, and Biogelx increased slightly with incubation time. The cell number for KLD-O/KLD-V was significantly higher than that of KLD, KLD-O, and Biogelx at all each time point. Cell numbers in all groups suggested that the self-assembled hydrogels did not have a toxic effect on the encapsulated cells and the increase in cell number was related to hydrogel concentration and glutamic acid (see the Discussion section). At Day 28, the ratio of cell number in KLD-O/KLD-V was $19,566,666 \pm 814,452$ while $17,733,333 \pm 814,452$ ($p^* < 0,05$), $17,166,666 \pm 680,685$ ($p^{**} < 0,01$), and $15,633,333 \pm 321,455$ ($p^{***} < 0,001$) in KLD-O, Biogelx and KLD, respectively.

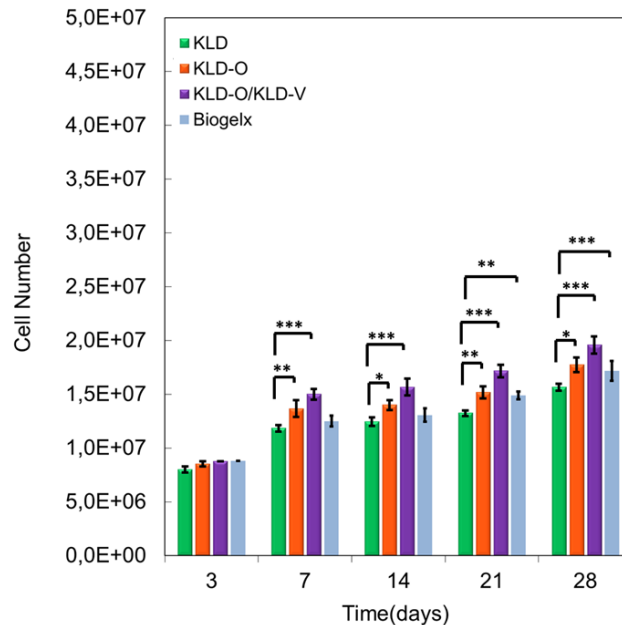


Figure 6.4: Cell number of HUVEC/hMSC encapsulated in KLD, KLD-O, KLD-O/KLD-V, and Biogelx and incubated in osteogenic/vasculogenic (1:1) medium for up to 28 days. The error bars indicate the mean SE (n = 3) of the data. [One-way ANOVA was used to assess significant differences.] [$*p < 0.05$, $**p < 0.01$, $***p < 0.001$] Newman–Keuls multiple contrast test]

6.3.2 Osteogenic Differentiation in Multifunctional Hydrogels

HUVEC/hMSCs were encapsulated and incubated in KLD, KLD-O, KLD-O/KLD-V, and Biogelx for 7, 14, 21, 28 d for osteogenic differentiation. DNA content, ALP activity, and calcium deposition over 28 d were quantified. The measured ALP activities and calcium contents were normalized to cell numbers by dividing them into DNA contents at each time point. The DNA content was correlated with cell number (see Figure 6.5 a). All other groups incubated in the osteogenic medium had their ALP activity peak after 14 days and then return to baseline by day 28, which is consistent with previous reports (see Figure 6.5 b) [201]. The ALP activity increased significantly with the increased concentration and glutamic acid in peptide hydrogels. For example, peak ALP activity of KLD, Biogelx, and KLD-O increased to $1509,46 \pm 34,89$, $1784,71 \pm 88,88$, $5042,98 \pm 69,82$ IU/mg DNA, respectively, while that of KLD-O/KLD-V was $6435,91 \pm 291,60$ IU/mg ($p^{***} < 0.001$). The extent of mineralization of the hMSCs increased gradually from day 7 to day 28, with KLD-O/KLD-V having the highest mineralization after 28 d of incubation in osteogenic medium, as shown in Figure 6.5 c. The calcium content of the hMSCs in KLD-O/KLD-V, KLD-O, Biogelx, and KLD incubated in an osteogenic medium increased slightly with time. For example, the calcium content of hMSCs encapsulated KLD-O/KLD-V after 28 d was $68596,63 \pm 718,26$ mg/mg DNA, while those of KLD-O, Biogelx and KLD were $46801,13 \pm 1640,84$, $31199,37 \pm 756,12$, and $25275,39 \pm 592,08$ mg/mg DNA ($p^{***} < 0.001$), respectively.

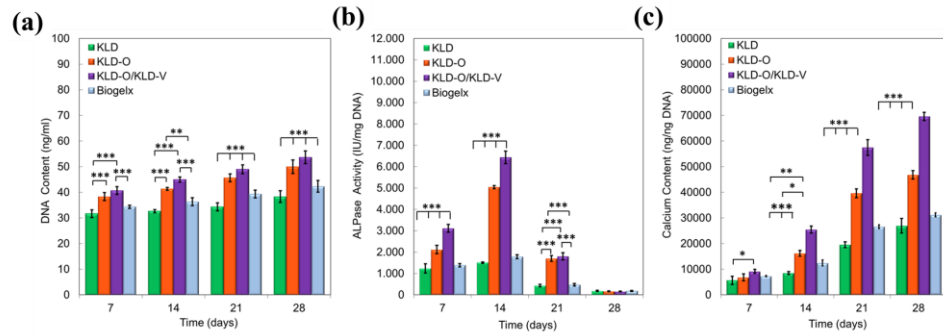


Figure 6.5: (a) DNA content, (b) ALP activity, (c) Calcium content of HUVEC/hMSCs encapsulated in KLD, KLD-O, KLD-O/KLD-V, and Biogelx and incubated in osteogenic/vasculogenic (1:1) medium for up to 28 days. The error bars indicate the mean SE ($n = 3$) of the data. [One-way ANOVA was used to assess significant differences.] [$*p < 0.05$, $**p < 0.01$, $***p < 0.001$] Newman–Keuls multiple contrast test]

Expression of osteogenic markers ALP, Col-1, OPN, and OCN with incubation time for MSC-encapsulated peptide hydrogels is shown in Figures 6.6 a-d, respectively. For the KLD control group, expression of ALP, Col-1, OPN, and OCN was significantly less than for all groups. ALP mRNA expression for all groups followed their corresponding ALP activity, peaking at day 14 and returning to the baseline level at day 28. mRNA expression for OPN, OCN, and Col-1 increased gradually with incubation time. Expression of osteogenic markers ALP, Col-1, OPN, and OCN increased with all groups. ALP, Col-1, OPN, and OCN expression were highest for KLD-O/KLD-V in each time point. For example, Col-1 expression for KLD-O/KLD-V at day 28 was $186,808 \pm 7,154$ while that for KLD, Biogelx and KLD-O were $118,516 \pm 5,783$, $131,686 \pm 9,933$, and $145,700 \pm 6,244$ ($p^{***} < 0.001$) respectively; OPN expression for KLD-O/KLD-V at day 28 was $217,269 \pm 12,507$ while that for KLD, Biogelx and KLD-O were $78,646 \pm 2,496$, $80,326 \pm 2,907$, $132,383 \pm 9,164$ and ($p^{***} < 0.001$) respectively; and OCN expression for KLD-O/KLD-V at day 28 was $199,325 \pm 2,475$ while that for KLD, Biogelx and KLD-O were $147,430 \pm 9,489$, $7,6 \pm 1,23$ and $94,369 \pm 2,392$ ($p^{***} < 0.001$) respectively; expression of ALP for KLD-O/KLD-V at day 14 was $173,280 \pm 7,308$ while that for KLD, Biogelx and KLD-O were $94,730 \pm 0,642$, $62,042 \pm 1,829$, and $134,372 \pm 2,483$ ($p^{***} < 0.001$) respectively.

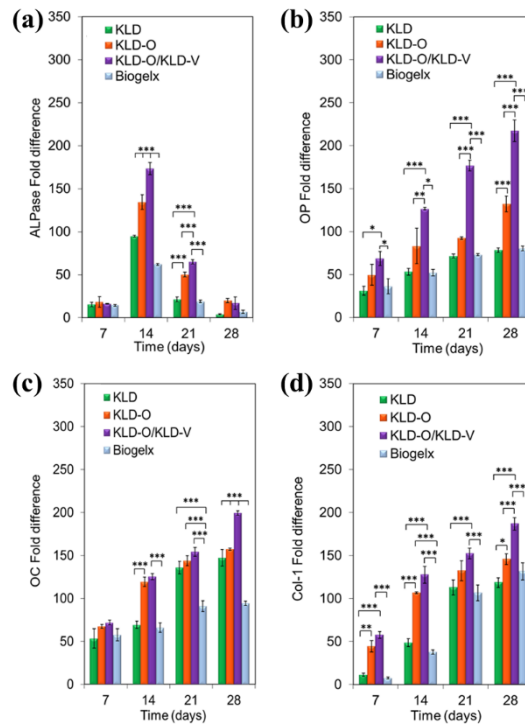


Figure 6.6: The mRNA expression levels (as fold difference) of (a) alkaline phosphatase (ALPase), (b) type 1 collagen (COL-1), (c) osteopontin (OP), (d) osteocalcin (OC) for HUVEC/hMSCs encapsulated in KLD, KLD-O, KLD-O/KLD-V and Biogelx and incubated in osteogenic/vasculogenic (1:1) medium for up to 28 days. The error bars indicate the mean SE ($n = 3$) of the data. [One-way ANOVA was used to assess significant differences.] [$*p < 0.05$, $**p < 0.01$, $***p < 0.001$) Newman–Keuls multiple contrast test]

Immunostaining images of HUVEC/MSC encapsulated in KLD-O/KLD-V, KLD-O, KLD and Biogelx are shown in Figure 6.7 a-d which represents the groups of KLD-O/KLD-V (a), KLD-O (b), KLD as negative control (c) and Biogelx as a positive control (d) respectively stained with COL-I (green), OPN (red) and, OCN (green). The expression of these osteogenic related proteins was drastically higher for HUVEC/hMSC on KLD-O/KLD-V than those on KLD-O, Biogelx, and KLD, respectively. KLD group showed weak staining for three markers while osteogenic epitope containing groups showed moderate to strong staining for osteogenic markers COL-I, OPN, and OCN. Immunofluorescence staining of differentiated HUVEC/MSC also confirmed q-PCR results. The expression pattern of COL-1, OPN, and OCN in HUVEC/hMSC was determined by immunofluorescent staining at day 28 and the results were consistent with q-PCR results.

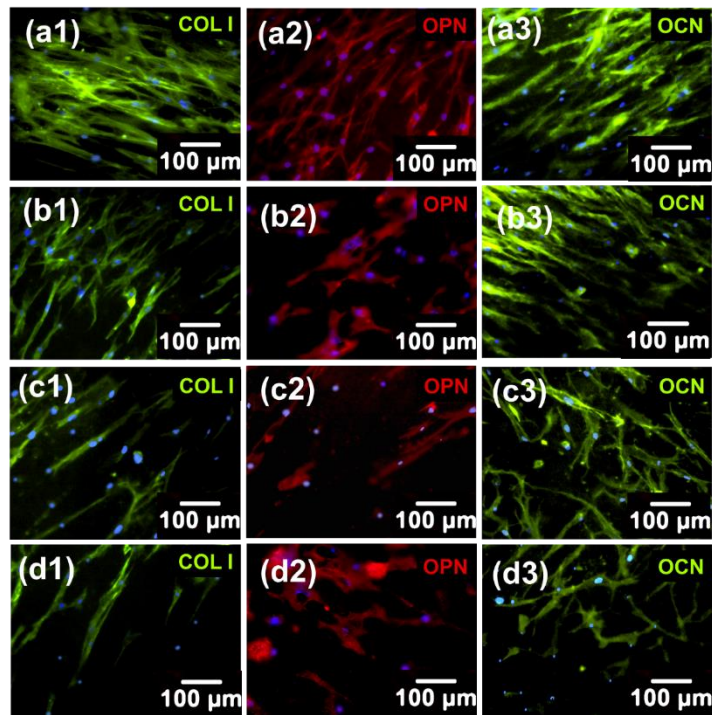


Figure 6.7: Expression pattern of osteogenic markers type 1 collagen (COL-I) (green, first column), osteopontin (OP) (red, second column) and osteocalcin (OC) (green, third column) for HUVEC/hMSCs encapsulated in (a) KLD-O/KLD-V (a 1-3), (b) KLD-O (b1-3), (c) KLD (1-3) and (d) Biogelx (d 1-3) after 28 days' incubation in osteogenic/vasculogenic (1:1) medium. Cell nuclei in the images are stained with 4',6-diamidino-2-phenylindole (DAPI; blue) (Scale bar represents 100 μm)

Sections of the hydrogel's culture matrix on day 28 showed matrix nodules stained with Alizarin Red and markedly mineralized (see Figure 6.8). Although the sign of mineralization in control cultures is less than in the other groups, the color intensity in the KLD-O/KLD-V group shows that the mineralization is more than in the other groups. Overall, the KLD-O/KLD-V group showed the greatest staining for Alizarin Red.

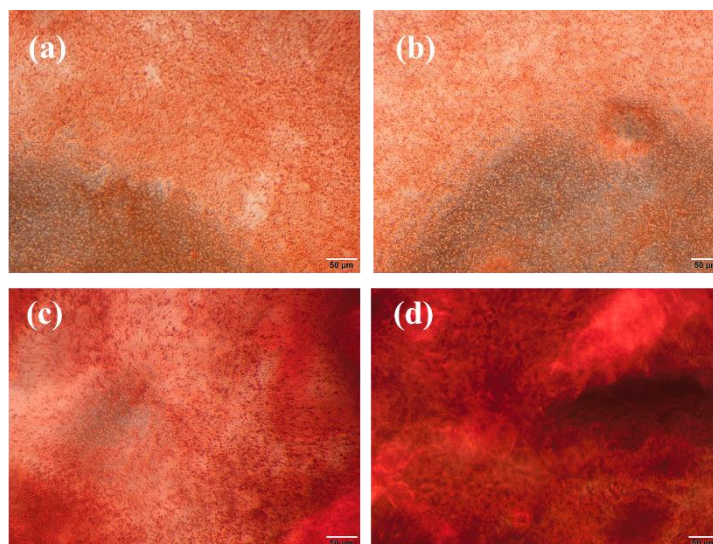


Figure 6.8: Alizarin red staining for mineral deposition of HUVEC/hMSCs encapsulated in (a) Biogelx, (b) KLD, (c) KLD-O (C), and KLD-O/KLD-V (D) after 28 days incubation in osteogenic/vasculogenic (1:1) medium. (Scale bar represents 50 μm)

6.3.3 Vasculogenic Differentiation of SAP Hydrogels

Expression of vasculogenic markers VE-Cad, VWF, and Pecam-1 with incubation time for MSC-encapsulated peptide hydrogels is shown in Figures 6.9 a-c, respectively. For the KLD control group, expression of VE-Cad, VWF, and Pecam-1 was significantly less than for all groups. mRNA expression for VE-Cad, VWF, and Pecam-1 increased gradually with incubation time. Expression of vasculogenic markers VE-Cad, VWF, and Pecam-1 increased with all groups. Furthermore, VE-Cad, VWF, and Pecam-1 expression were highest for KLD-O/KLD-V in each time point. For example, VE-Cad expression for KLD-O/KLD-V at day 7 was $306,446 \pm 19,745$ while that for KLD, Biogelx and KLD-O was $139,800 \pm 4,471$, $151,053 \pm 3,885$, and $176,710 \pm 7,963$ ($p^{***} < 0.001$) respectively; VWF expression for KLD-O/KLD-V at day 7 was $218,186 \pm 13,692$ while that for KLD, Biogelx and KLD-O was $158,430 \pm 11,824$, $160,730 \pm 13,925$, $172,609 \pm 9,498$ and ($p^{***} < 0.001$) respectively; and Pecam-1 expression for KLD-O/KLD-V at day 28 was $305,234 \pm 14,134$ while that for KLD, Biogelx and KLD-O was $207,063 \pm 8,383$, $183,167 \pm 28,325$ and $258,921,94 \pm 25,648$ ($p^{***} < 0.001$) respectively.

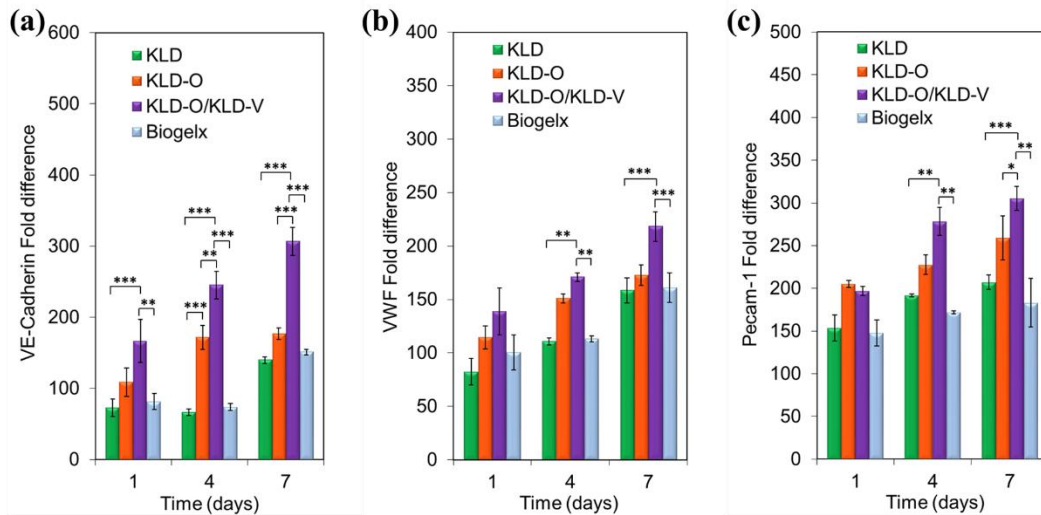


Figure 6.9: The mRNA expression levels (as fold difference) of (a) Ve-Cadherin, (b) vWF, (c) Pecam-1 for HUVEC/hMSCs encapsulated in KLD, KLD-O, KLD-O/KLD-V, and Biogelx and incubated in osteogenic/vasculogenic (1:1) medium for up to 28 days. The error bars indicate the mean SE (n = 3) of the data. [One-way ANOVA was used to assess significant differences.] [$*p < 0.05$, $**p < 0.01$, $***p < 0.001$] Newman–Keuls multiple contrast test]

Immunostaining images of HUVEC/hMSC encapsulated in KLD-O/KLD-V, KLD-O, KLD, and Biogelx are shown in Figure 6.10 a to d which represents the groups of KLD-O/KLD-V (a), KLD-O (b), KLD as negative control (c) and Biogelx as a positive control (d) respectively stained with PECAM-1 (red) and vWF (green). The expression of these vasculogenic related proteins was drastically higher for HUVEC/hMSC on KLD-O/KLD-V than those on KLD-O, Biogelx, and KLD, respectively. KLD group showed weak staining for both markers while vasculogenic epitope containing groups showed moderate to strong staining for vasculogenic markers PECAM-1, and vWF. Immunofluorescence staining of differentiated HUVEC/MSK also confirmed q-PCR results. The expression pattern of PECAM-1, and vWF in HUVEC/hMSC were determined by immunofluorescent staining at day 7 and the results were consistent with q-PCR results.

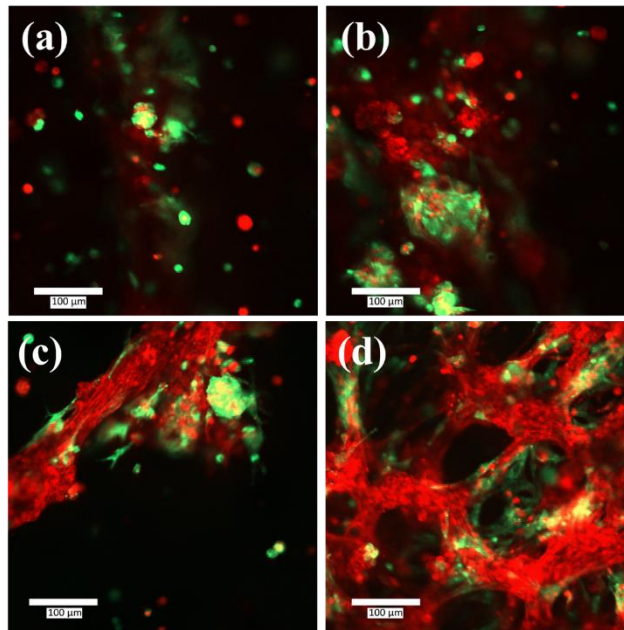


Figure 6.10: Expression pattern of vasculogenic markers PECAM-1(red), and vWF (green) for HUVEC/hMSC encapsulated in (a) Biogelx, (b) KLD, (c) KLD-V1, (d) KLD-V2 after 7 days incubation in osteogenic/vasculogenic (1:1) medium. (Scale bar represents 100 μm)

6.3.4 In vivo Evaluation

Implant stability quotient values (ISQ) for both control and test groups increased after 8 weeks of healing (see Figure 6.11 a). ISQ values for control implants increased from 37 ± 3 to 60 ± 4 ($p < 0.01$), while multifunctional KLD-O/KLD-V hydrogel treated implant increased from 51 ± 2 to 71 ± 2 ($p < 0.01$) and ISQ values were higher for test implants compared to control implants 8 weeks after surgery.

After the subjects were sacrificed, the highest torque values obtained during the removal of the relevant implants were calculated in N.cm. Reverse torque values for both control and test groups increased after 8 weeks of healing (see Figure 6.11 b). Reverse torque values for control implants increased from 41 ± 3 to 60 ± 5 ($p < 0.01$), while multifunctional KLD-O/KLD-V hydrogel treated implant increased from 51 ± 2 to 81 ± 2 ($p < 0.01$), and reverse torque values were higher for test implants compared to control implants 8 weeks after surgery.

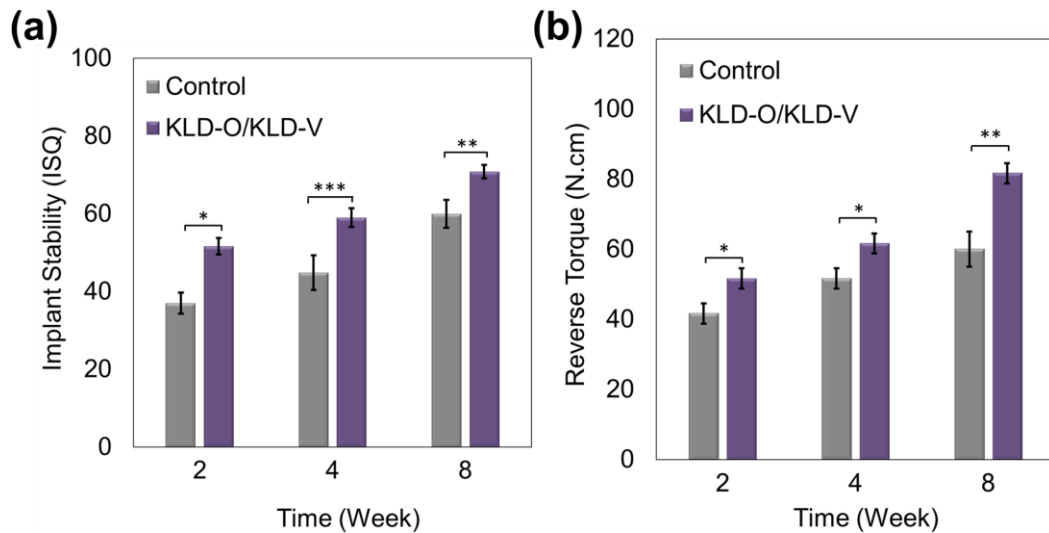


Figure 6.11: (a) Resonance frequency analysis (RFA) (b) Reverse Torque values comparing control and KLD-O/KLD-V hydrogel treated implants at surgery and after 8 weeks healing

6.4 Discussion

Implanted biomaterials with good biocompatibility and containing bioactive molecules to enhance osteogenesis can integrate well with host bone tissue and provide fast fixation, long-term stabilization, and eventually stable implantation [282]. Due to their superior biocompatibility and mechanical properties, titanium implants have shown considerable promise as an embedded biomaterial in dental applications [283]. However, since titanium is bioinert, it prevents successful osteogenesis and osseointegration [284]. Many attempts have been made to improve the bioreactivity of titanium to facilitate osteogenic activity and osseointegration, such as the use of bioactive fillers and surface modification. Among the synthetic bone substitutes as a bone filler material to enhance osseointegration, bioactive hydrogels are considered a promising candidate. However, using synthetic hydrogels alone has a negligible impact on bone ingrowth and osseointegration. The ability of bone graft substitutes to facilitate both rapid osteogenesis and vascularization is considered the gold standard. Herein, we demonstrated that SAP hydrogel scaffold containing both vasculogenic and osteogenic differentiation inducing bioactive peptides had excellent biocompatibility, osteogenic and vasculogenic potential. These encouraging *in vitro* findings laid the groundwork for *in vivo* studies performed on rabbit femur model based on the usage

of multifunctional SAP as a filler between titanium implant the bone tissue and showed promising results for enhancement of osseointegration.

hMSC differentiation to osteogenic lineage is a dynamic mechanism involving the spreading, differentiation, maturation, and mineralization [285]. The first stage in bone regeneration is cell proliferation which affects directly the maturation and mineralizing processes. Bone-mimetic peptide sequences can regulate proliferation and osteogenic differentiation and thus bioinert synthetic SAP hydrogel can become osteoinductive by the addition of these bioactive sequences. In our previous study, we demonstrated that five repetitive glutamic acid epitope containing KLD SAP (KLD-O) increased proliferation and osteogenic differentiation of hMSCs due to the role of glutamic acid in integrin-binding motif [237]. Herein, five repetitive glutamic acid-containing KLD SAP were mixed with a laminin-derived peptide containing KLD SAP (KLD-V) which was previously demonstrated as an effective hydrogel on vasculogenic differentiation to develop multifunctional hydrogels. Accelerated proliferation and osteogenic differentiation of HUVEC/hMSC was observed with the addition of KLD-V to KLD-O SAP hydrogel compared to bare KLD-O. Enhanced osteogenic differentiation can be accomplished through addition of laminin derived peptide which enhanced proliferation and vasculogenesis of HUVECs. MSCs–HUVECs co-culture is an efficient method for achieving osteogenic differentiation [286]. The involvement of ECs with MSCs is deeply influenced by their development, differentiation, and consequent angiogenesis and osteogenesis. The potential of KLD-O/KLD-V in osteogenesis can be related to the presence and more influential role of laminin derived peptides in increased vasculogenic differentiation and biological cues of HUVECs.

One of the most significant barriers to using synthetic bone substitutes to enhance osseointegration of implants is their slow neovascularization after implantation [287]. A robust microvascular network delivers oxygen and nutrients to the surrounding bone tissue around the implant, allowing them to expand, differentiate, and function properly [288]. To enhance bone ingrowth and osseointegration, functional vascularization is particularly important for osseointegration. Despite rapid advances, osteogenesis and vascularization of bone grafts remain a significant obstacle to the clinical implementation of bone substitutes or tissue engineering scaffolds. For instance, Tomlinson *et al.* demonstrated that a single local simvastatin/poloxamer 407

injection induces autogenous expression of BMP-2 and VEGF and increases bone growth [288]. However, the injectable thermosensitive hydrogel poloxamer 407 does have low mechanical properties, preventing its use as a bone replacement. Lyu *et al.* implanted rhBMP-2 into mandibular defects of dental implants with porous β -TCP microsphere-hyaluronate powder base gel composite and the hydrogel promoted new bone formation in the mandible bone defect and improved osseointegration between the host tissue and dental implant [289]. It has been suggested that BMP-2 has potential in neovascularization and improved osseointegration could be related to both induced vasculogenesis and osteogenesis at the implant site due to BMP-2 [290]. In our previous work, we demonstrated that glutamic acid-containing KLD SAP induced osteogenesis of hMSC. Herein, YIGSR which is one of the most effective laminin-derived peptide sequences on vasculogenesis was added to glutamic acid-containing KLD SAP and HUVEC/hMSC encapsulated into this multifunctional hydrogel. Although KLD-O was an effective SAP hydrogel on osteogenic differentiation, KLD-O/KLD-V was performed improved characteristics on bone formation. Although KLD-O is an effective SAP hydrogel on osteogenic differentiation, KLD-O/KLD-V is more effective in bone formation. KLD-O/KLD-V SAP hydrogel promoted new bone formation around the dental implant and improved osseointegration between the host tissue and dental implant. The improved osseointegration is considered due to both induced bone formation caused by GLU and improved vasculogenesis caused by the YIGSR sequence.

The efficiency of the ISQ and reverse torque values are critical for the evaluation of early osseointegration [291]. Some studies have shown that low RFA and reverse torque values after surgery could be a signal for elevated risk for a potential implant failure [292]. The simulation of short-term healing times in implants might be related to higher initial ISQ and reverse torque values. Herein, resonance frequency and reverse torque values have evaluated the quantitative assessment of bone tissue-implant integration. Although, ISQ and reverse torque values are increased in both the control and test group, multifunctional SAP hydrogel increased both ISQ and reverse torque values compared to the control group.

6.5 Conclusion

The osteogenic and vasculogenic epitope containing multifunctional SAP hydrogel can promote osseointegration by enhancing bone and vascular formation between the dental implant and host tissue. *In vitro* studies confirmed that the developed multifunctional SAP showed excellent biocompatibility, osteogenic activity, and vascular formation, demonstrating great potential for orthopedic applications. The *in vivo* study conducted in a rabbit femoral cavity defect model showed that multifunctional SAP had the greatest reverse torque and implant stability values, indicating the significantly promoted osteogenesis and osseointegration after surface modification. In conclusion, multifunctional SAP hydrogel as a dental implant filler has demonstrated its ability to actively modulate cellular responses and osseointegration.

Chapter 7

Peptide Conjugated Nanofiber Reinforced Self-assembled peptide Hydrogel for Bone Regeneration

7.1 Introduction

Bone tissue transplantation applications are widely used to treat bone cancer, skeletal trauma, and bone loss due to infection, bone fractures, and congenital deformities. Extensive bone injuries are commonly treated by autograft and allograft procedures. These methods have many limitations, such as immune system response, damage to the tissue removal area, and limited graft availability [293, 294]. Therefore, 3D bone grafts have been developed with tissue engineering techniques. Bone grafts fabricated with tissue engineering approaches need to mimic the bone extracellular matrix (ECM) that supports the attachment of cells and their functions during bone formation [295, 296].

Hydrogels with a three-dimensional interconnected porous surface and a high-water content have been widely used in bone tissue engineering [297]. Hydrogels are classified into two types: natural and synthetic. Due to the lack of bioactive factors, natural hydrogels are unable to promote cell adhesion, proliferation, and differentiation into complex lineage osteogenesis. Therefore, there is a strong desire to create a bioactive synthetic hydrogel scaffold capable of inducing osteogenesis. Self-assembling peptide hydrogels (SAP) with structural and functional similarities with the bone tissue have significant potential for bone tissue engineering applications. SAP hydrogels are emerging biomaterials for bone regeneration due to spontaneous self-

assembling without chemical crosslinkers or physical stimuli such as heat or UV exposure [298]. However, the ability to interact with a large amount of water and the tendency to swell makes SAP hydrogels mechanically insufficient for bone tissue engineering applications. Both the biological value of improved ECM rigidity and mechanical problems of SAP hydrogels in clinic application for bone regeneration, mechanical properties of SAP hydrogels are enhanced by increasing the peptide concentrations, changing the ionic strength of the gelation environment, or stiffening which can be accomplished over weeks through natural ECM secretion by cells in culture [204, 299, 300]. However, each of these methods has disadvantages such as solubility problem, the addition of chemicals that affect the self-assembling process, and taking a long time.

Current tissue engineering approaches rarely return damaged tissue to its natural state due to the limited capacity to reconstruct the anisotropic composition and function of native bone tissue. The cellular phenotypes, extracellular matrix (ECM) structure, fibrous architectures, and mechanical properties of native bone tissue vary spatially. The bone structure consists of aligning collagen nanofiber (NF) structures coated with HA [298, 299]. Electrospinning is commonly used to manufacture NF from natural and synthetic polymers to produce bone ECM mimetic scaffolds. The properties of electrospun NF can be easily tuned to mimic the natural structure of a bone with ideal physical properties, such as high porosity and broad surface area, which can improve cellular behaviors including cell adhesion, proliferation, and differentiation [301]. Non-collagenous bone proteins contain the 2 to 10 repetitive glutamic acid (GLU) residues that are known to act as a nucleation point for calcium phosphate (CaP) mineralization. Sarvestani *et al.* used six repeat sequences of glutamic acid as the binding agent to poly (lactic ethylene oxide fumarate) (PLEOF) hydrogel structure and observed that GLU entered the hydrogel structure and interacted with HA crystals resulting in increased mechanical properties [189]. By incorporating GLU peptide conjugated highly porous electrospun PLGA NF with well-controlled 3D architecture hydrogels, the mechanical properties of SAP hydrogels can be improved.

Tissue engineering approaches for highly vascularized tissues such as bone often fail due to insufficient vascularization to reconstruct large skeletal defects [301]. The oxygen and nutrient transfer are required to maintain tissue viability and functionality

[302]. The maximum distance between capillaries should be 200 μ m to maintain the viability of bone tissue due to oxygen and nutrient diffusion restrictions in the body [303]. Providing vascularization within the tissue scaffolds increases the diffusion area and provides optimum nutrient/waste transfer. Co-cultivation of endothelial cells (ECs) and mesenchymal stem cells (MSCs) into designed tissue scaffolds have been shown to effectively increase vascularization [304]. Several laminin-derived peptides, including YIGSR sequences, have been studied for their ability to modulate cell attachment and migration to the surrounding ECM in the microvascular matrix during physiological vasculogenesis. Many researchers focused on the incorporation of laminin-derived peptides into synthetic scaffolds to achieve widespread vascularization as an alternative path to protein loading, since these functional peptides are precisely designed to activate major regulatory cascades by binding to the same receptor as their originating protein [235, 236].

One of the major challenges in the reconstruction of bone defects is the inadequate ability to design biomimetic scaffolds that induces differentiation of osteoprogenitor cells by cell-matrix interaction at the nanoscale, as well as ensuring microvascular structure. Due to the inadequate mechanical properties, there are only a few studies on building bone matrix mimetic scaffolds by SAP hydrogels. Therefore, there is still a tremendous need for new approaches and strategies for developing vascularized bone tissue. In this study, GLU conjugated NFs and SAP hydrogel functionalized with YIGSR that can induce osteogenesis and vasculogenesis developed. The mechanical properties of the NF reinforced SAP hydrogels were evaluated by rheological measurements and the effect of motifs that added to SAP structure on inducing osteogenesis vasculogenesis were evaluated by biochemical, immunostaining, and gene expression analysis (see Figure 7.1). The mechanical properties of SAP hydrogels were improved and GLU conjugated NFs reinforced SAP hydrogel functionalized with YIGSR enhanced both osteogenic and vasculogenic differentiation. The scaffold that was developed in this study could be used in clinics for bone regeneration.

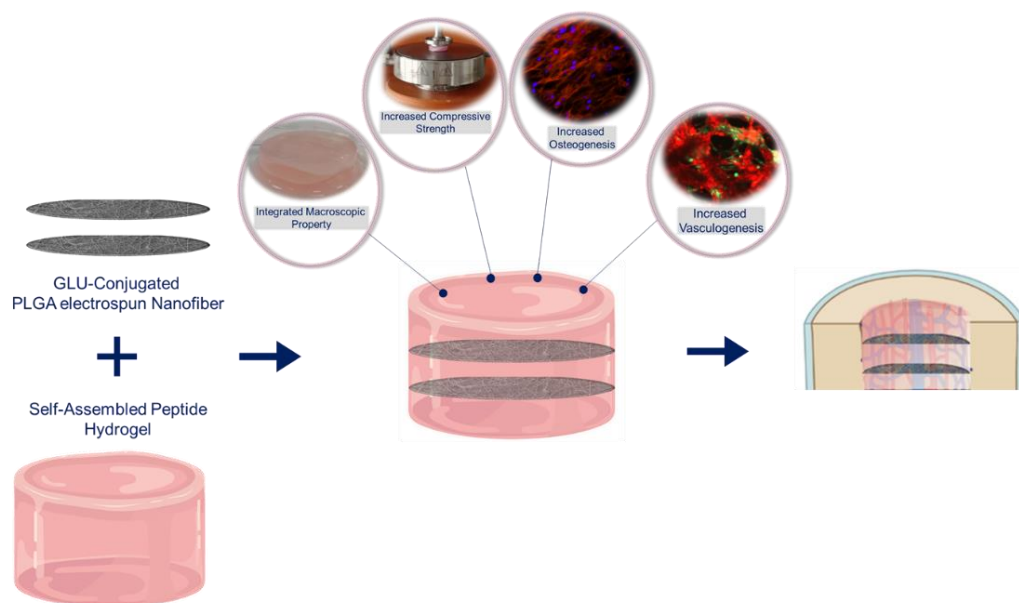


Figure 7.1: Schematic diagram of PLGA electrospun nanofiber reinforced self-assembled hydrogel with increased mechanical properties, osteogenesis, and vascularization

7.2 Materials and Methods

7.2.1 Peptide Synthesis

KLD-YIGSR (Ac-Lys-Leu-Asp-Leu-Lys-Leu-Asp-Leu-Lys-Leu-Asp-Leu-Tyr-Ile-Gly-Ser-Arg-NH₂), EEEEEEC (Glu-Glu-Glu-Glu-Glu-Cys) were synthesized as previously described in Chapter 2. Synthesized peptide sequences were purified by high-performance liquid chromatography (Agilent Technologies, Agilent 1200), and their characterization was performed by using mass spectrometry.

7.2.2 Fabrication and Characterization of Nanofibers

The lyophilized EEEEEEC peptide was conjugated to poly (lactide) acrylate (PLAA, MA = 4000 Da) by Michael's addition reaction between the acryl group of PLAA and the sulfhydryl group of the cysteine amino acid in the peptide structure [152]. The peptide-PLAA polymer mixture (2: 1 molar ratio) was dissolved in DMF-distilled water (1: 1 volumetric ratio) and reacted at 30 C° for 24 h in an orbital shaker. Then

the mixture was dialyzed in di water and the remaining mixture was lyophilized [152]. Electrospinning solution was prepared by dissolving PLGA (7wt%) and PLAA-EEEEEC conjugate (1.5% of the PLGA amount) in HFIP as previously explained [152]. The polymer solution was transferred to a 5 ml syringe through a 21-gauge needle and replaced with a syringe pump. The needle was connected to a high-voltage power supply with the positively charged electrode and an aluminum rotating wheel powered by a high-speed DC motor was connected to the ground electrode. PLGA/PLA-GLU fibers hereafter denoted GLU-NF were produced with previously optimized electrospinning conditions such as a flow rate of a distance of 15 cm, 20 kV electrical potential, 1.0 ml/h, and rotation speed of 1200 rpm and 38 mm diameter samples were cut with the help of cork borer which is a round-shaped cutting tool.

7.2.3 Fabrication of Nanofiber Reinforced Hydrogels

2 wt % KLD-YIGSR hydrogels were prepared by dissolving 0.5 mg peptide in 100 μ l deionized water. The self-assembling process was initiated by the addition of an equal volume of Dulbecco's Modified Eagle's Medium (DMEM) cell culture medium with 25 mM 4-(2-hydroxyethyl)-1-piperazineethanesulfonic acid (HEPES) buffer without Fetal Bovine Serum (FBS). For the self-assembling process, 200 μ l peptide solution were being poured into a 5 ml syringe, and 38 mm in diameter NF was added to the solution. This process was repeated until three layers of SAP solution and two layers of NF are placed in the syringe.

7.2.4 Mechanical Properties

Mechanical properties of the hydrogels were determined by using a discovery hybrid rheometer-2 (HR2, TA Instruments, New Castle, DE). The elastic modulus was calculated from the toe (0–50% strain) and linear regions (200–250% strain) of the stress-strain curve. The fractured stress and strain were also determined from the stress-strain curve. Compressive properties were determined by subjecting the samples to a crosshead speed of 0.01 mm/s by using a 20 mm parallel plate geometry at room temperature (22 °C). Compressive modulus was calculated by determining the slope from the initial region (0–10% strain) of the stress-strain curve. Recovery was calculated by dividing the unloading curve by the loading curve.

7.2.5 Cell Culture

Human bone marrow-derived mesenchymal stem cells (hMSCs) (HMSC-AD-500, CLS cell lines Service, Lot#102, Eppelheim, Germany) and HUVECs (kindly donated from Ege University Research Group of Animal Cell Culture and Tissue Engineering Laboratory) were cultured at 37 °C and 5% CO₂ with DMEM containing FBS (10%), penicillin-streptomycin (100 units/mL), amphotericin-B (250 ng/mL), and gentamicin (50 µg/mL). The cells at passage three were used by keeping in exponential phase.

NFs were sterilized by ultraviolet (UV) radiation for 1 hour and immersed in 70% ethanol for 30 minutes as described previously for cell seeding [173]. After sterilization, NFs were conditioned in basal medium containing FBS (10%), penicillin-streptomycin (100 units/ml) for 1 hour. 1×10^5 cells/cm² hMSCs were seeded on the NF and incubated for 2 hours to attach on the NF surface. The hMSCs suspension was encapsulated in hydrogel (5×10^6 cells/ml) in a basal medium. For the self-assembling process, 200 µl cell encapsulated peptide solution was be poured into a 5 ml syringe and 38 mm in diameter, and cell-seeded NF were added to the solution. This process was repeated until three layers of SAP solution and two layers of NF are placed in the syringe. After incubation for 24 hours for cell adhesion, the medium has replaced the mixture of osteogenic medium and vasculogenic medium (1:1). The osteogenic medium contains basal medium supplemented with 50 µg/mL ascorbic acid, 100 nM dexamethasone, 10 mM β-glycerophosphate. The vasculogenic medium was prepared by using EGM-2 (Lonza, Walkersville, USA) contained ascorbic acid, hydrocortisone, insulin-like growth factor (R3-IGF-1), fibroblast growth factor (hFGF-B), epidermal growth factor (hEGF), gentamicin, amphotericin-B, heparin with 10% FBS. Cells for osteogenic differentiation and vasculogenic differentiation were cultured at 5% CO₂ for 28 d, and 7 d, respectively. MSCs and HUVECs encapsulated KLD incubated in the mixture of osteogenic medium and vasculogenic medium (1:1) was used as the negative control group.

7.2.6 In vitro Osteogenic Differentiation

At each time point (7, 14, 21, and 28 d), double-stranded DNA content, ALPase activity and calcium content of the samples of NF reinforced cell-encapsulated

hydrogels were rinsed with PBS. 10 mM Tris containing 0.2% triton in PBS was used to take lysate for measurement of DNA content, ALPase activity, and calcium content. [201]. DNA Quantification Kit was purchased from Sigma Aldrich (St. Louis, MO, USA), and ALPase assay and Calcium Assay were purchased from Bioassay Systems (Hayward, CA, USA). Briefly, bisBenzimide H 33258 Solution was prepared and added on lysed samples in a 96-well plate. Fluorescence (excited at a wavelength of 360 nm) was measured using a spectrophotometer (BioTek, Winooski, VT, USA) at an emission wavelength of 460 nm, at ambient temperature. ALP activity was measured by p-nitrophenylphosphate (*p*NPP) at 405 nm in alkaline solution using ALP kit. Briefly, 50 μ L of lysed sample to 200 μ L total reaction volume were used for initiating the reaction by the addition of assay buffer, 5 mM magnesium acetate, and 10 mM *p*NPP in a 96-well plate. Optical density (OD) in 405 nm was measured at initial time ($t=0$) and after 4 min ($t=4$ min) on multi-plate reader (BioTek, Winooski, VT, USA). The calcium content of hydrogels was measured by adding 50 μ L of the suspension to 150 μ L of the working solution. The wavelength of 612 nm was used to measure absorbance. A calibration curve was created with reference calcium solutions and the intensity values were associated with the equivalent calcium values. The calcium deposit and ALP activity were calculated by normalizing by dividing DNA content at each time point.

7.2.7 Quantitative Real-time PCR Analysis

Total cellular RNA was isolated at 7 d, 14 d, 21 d, and 28 d for q-PCR analysis. Briefly, SAP hydrogels were rinsed with PBS and incubated in trypsin. Then, the samples were centrifuged at 850 rpm for 5 min. RNA isolation Kit (Geneaid, Sijhih City, Taiwan) was applied to all samples according to the manufacturer's instruction. The samples were reacted with reaction buffer for lysis. RNAs were collected in RNase Free Water after washing with W1, wash buffer solution, respectively. The RNA sample concentration was measured with nanodrop (Nanodrop 2000, Thermo Scientific, Wilmington, DE) and stored at -20°C . After total cellular RNA was resuspended in water (nuclease-free) and remaining genomic DNA contaminations were digested by TURBO DNase (Ambion, Austin, TX) by incubating for 30 min at 37°C and incubated in DNase Inactivation Reagent for 5 min at 37°C . RNAs were centrifuged in 10000 RCF for 2 min to precipitate DNA molecules. cDNA converted by cDNA

Synthesis Kit Protocol (Biomatiks, K5147). Briefly, after 1 μ l Oligo dT (10 μ M), 1 μ l Random Primer (10 μ M), 1 μ l dNTP Mix, 14.5 μ l Nuclease Free Water were added into 1 ng-2 μ g/rxn RNA incubated at 65°C for 5 min. RNase Inhibitor, RT Buffer, M-MuLV Reverse Transcriptase were mixed and all components (20 μ l) were collected by brief centrifugation and incubated at 25°C for 10 min, at 42°C 50 min, at 85°C for 5 min. and stored at -20°C. Forward and reverse primers including glyceraldehyde 3-phosphate dehydrogenase (GAPDH), alkaline phosphatase (ALP), Collagen type I (COL-1), osteocalcin (OCN), and osteopontin (OPN), (PECAM-1), von Willebrand factor (vWF), vascular endothelial cadherin (VE-cadherin) were purchased from Sentegen Biotechnology (Ankara, TURKEY), shown in Table 6.1. Power SYBR Green PCR Master Mix (Applied Biosystems, Foster City, USA) and Step One Plus Real-time PCR system (Applied Biosystems, Foster City, USA) were used to quantifying ALP, COL-1, OPN, OCN, PECAM-1, vWF, VE-cadherin. GAPDH differential expression is used for housekeeping gene and other primers were normalized according to GAPDH. Briefly, 200 nmol primers (0,1mM), SYBR Master Mix, cDNA was mixed and diluted 1:10 ratio with water. qPCR was formed with the following stages: Holding Stage at 95°C for 10 min., Cycling Stage at 95 °C for 15 sec. and at 64,4 °C for 1 min, Cycling stage includes at 64,4 °C, Melt Curve Stage at 95 °C 15 sec, at 60 °C and at 95°C for 15 sec. The Ct values obtained from experiments (n=6) were classified by the $2^{(-\Delta\Delta C_t)}$ method.

7.2.8 Immunofluorescence Staining

For immunofluorescence staining, cell-encapsulated hydrogels were rinsed twice in PBS and fixed with 4% paraformaldehyde (Sigma Aldrich, St. Louis, MO, USA) at 4°C for 30 minutes. Next, samples were immersed with 0.1% Triton X-100 in PBS for 1 hour and blocked with 1.5% Bovine Serum Albumin (BSA) in PBS for 2 hours. Then, samples were incubated with primary antibodies in PBS containing 1% BSA overnight at 4°C according to the manufacturer's instructions. Primary antibodies (Santa Cruz Biotechnology Inc., Santa Cruz, California, USA) were used included mouse monoclonal antibody against COL-1 (cat. no sc-59772; 1:50), mouse monoclonal against OPN antibody (cat. no. sc-21742; 1:50), and mouse monoclonal antibody against OCN (cat. no. sc-365797; 1:500). Fluorescence secondary antibodies (Santa Cruz Biotechnology Inc., Santa Cruz, California, USA) included m-IgG kappa

BP-FITC (cat. no. sc-516140; 1:200) and m-IgG kappa BP-PE (cat. no. sc-21742; 1:200) were diluted with 1% BSA. It should be noted that each sample was stained with 4,6-diamidino-2-phenylindole (DAPI, Sigma Aldrich, St. Louis, MO, USA) to image the cell nuclei and one of the antibodies for COL-I, OCN, and OPN. The expression pattern of COL-1, OPN, and OCN with the same exposure time and light intensity were characterized via capturing images using an inverted fluorescence microscope (Olympus CKX41, Tokyo, Japan).

7.2.9 Statistical Analysis

All the data that are obtained, were statistically analyzed with two-way ANOVA (SPSS 12.0, SPSS GmbH, Germany) and the Student-Newman-Keuls technique as a post hoc test. At least three samples from all experimental groups were tested ($n = 3$) and experiments were at least three replicates. Average values, standard deviations, and standard error values of all results were determined. Meaningful distinctions among groups were defined at p values ($***p < 0.001$, $**p < 0.01$, $*p < 0.05$).

7.3 Results

7.3.1 Characterization of Fiber Reinforced Hydrogels

SEM imaging was used to confirm self-assembled hydrogels (see Figure 7.2a). The SEM photomicrograph of PGLA electrospun NF is given in Figure 7.2b. The confirmation of peptide conjugation was characterized via observing FITC intensity by using a fluorescence microscope. FITC labeled GLU peptides were used to show the NF surface coverage with peptides. As shown in Figure 7.2c-d, the fluorescence was observed with GLU-NF and NF only were used as a negative control, and as expected no fluorescence was observed, which confirms that the fluorescence observed in GLU-NF images came from the label FITC.

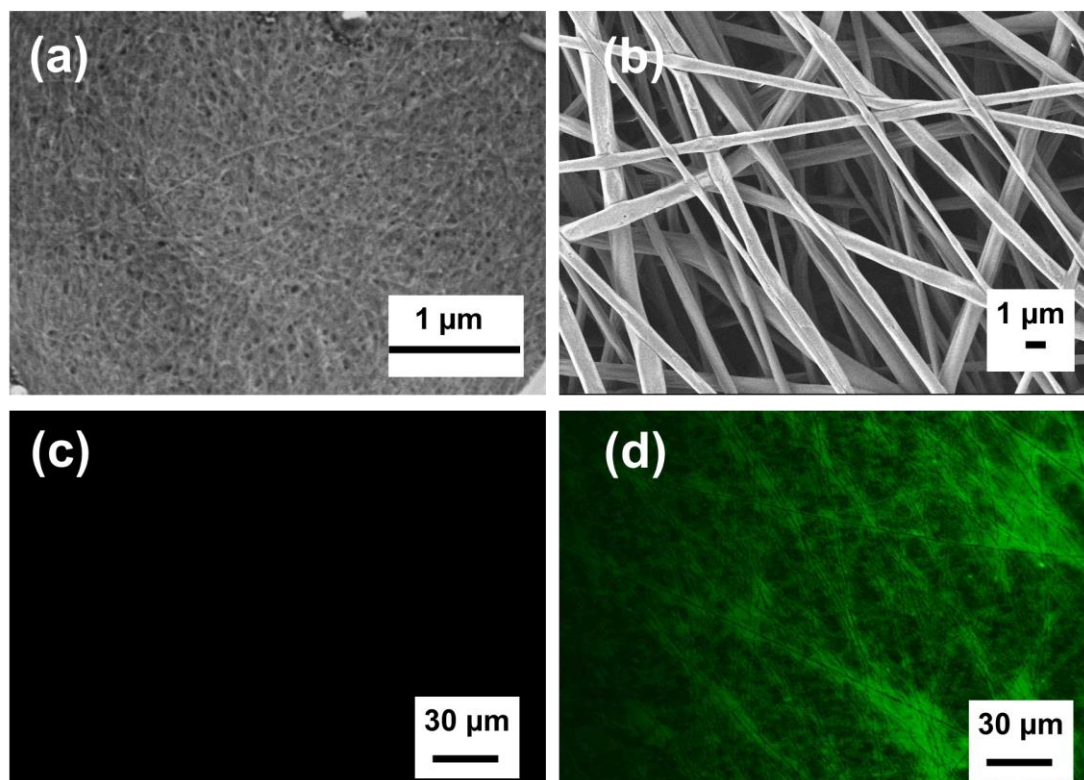


Figure 7.2: Scanning electron microscopy images of (a) KLD-V self-assembled peptide (SAP) (b) electrospun PLGA nanofiber (NF) Fluorescent microscopy images of (c) PLGA NF (d) fluorescein isothiocyanate (FITC) labeled glutamic acid peptide conjugated NF (GLU-NF)

The PLGA electrospun NF reinforced SAP hydrogels fabricated from laminin-derived peptide YIGSR containing KLD (KLD-V2) maintain the cylindrical shape of the mold as integrated after removal from the mold, indicating good mechanical stability (see Figure 7.3a). Young's modulus of KLD-V, KLD-V/NF, and KLD-V/GLU-NF hydrogels were significantly different under compression (see Figure 7.3b). The young's modulus of KLD-V, KLD-V/NF, and KLD-V/GLU-NF was 1.16 ± 0.10 Pa, 2.19 ± 0.41 Pa ($p < 0.001$), and 5.04 ± 0.41 ($p < 0.05$), respectively. The compression tests showed that the KLD-V/GLU-NF had the highest compressive strength of 7.7×10^{-4} MPa at 77 % compression strain (see Figure 7.3c), which is higher than that of KLD-V/NF hydrogel, and KLD-V. The compressive strength of KLD-V/NF was 1.5×10^{-4} MPa at 55 % compression strain (see Figure 7.3d), while the compressive strength of KLD-V was 8×10^{-5} MPa at 32 % compression strain (see Figure 7.3e).

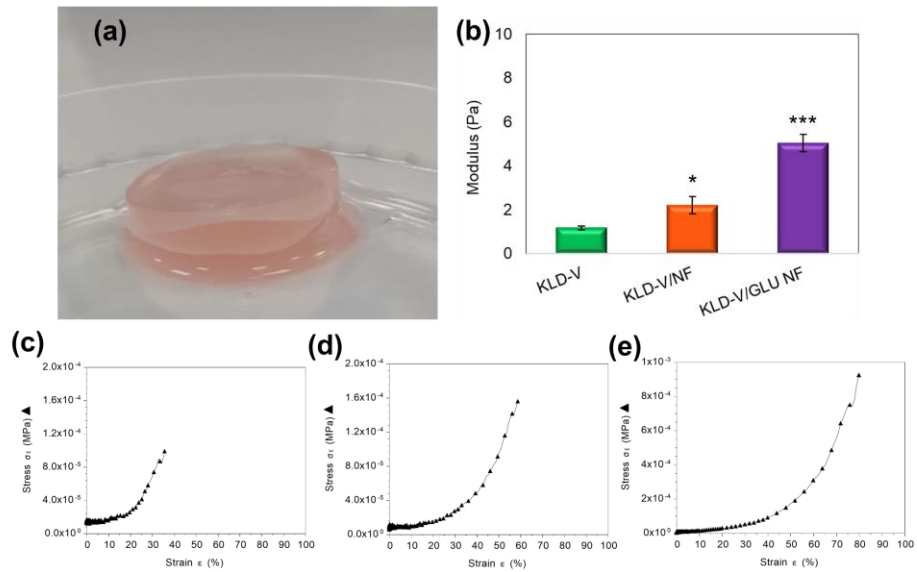


Figure 7.3: (a) Picture of electrospun PLGA nanofiber (NF) reinforced SAP hydrogel (d=38 mm, h=20 mm) (b) Young's modulus of hydrogels under compression, (c) Compression stress-strain curves of KLD-V, (d) KLD-V/NF (e) KLD-V/ GLU-NF hydrogels

The biodegradation of hydrogels was calculated every 7 days (see Figure 7.4). The duration required for complete degradation was similar in KLD-V/ NF, and KLD-V/GLU-NF. KLD-V/ NF and KLD-V/GLU-NF completely degraded after 49 d, while KLD-V completely degraded after 42d.

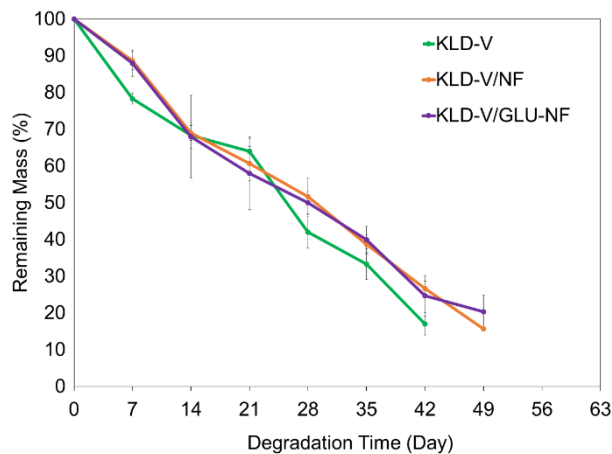


Figure 7.4: Biodegradation of KLD-V, KLD-V/NF, and KLD-V/GLU-NF hydrogels (Periods: 7,14,21,28, 35,42,49)

7.3.2 Osteogenic Differentiation in Hydrogels

hMSCs seeded and HUVEC encapsulated KLD-V, KLD-V/NF, and KLD-V/GLU-NF hydrogels incubated in osteogenic/vasculogenic (1:1) medium for 7, 14, 21, 28 d for osteogenic differentiation. DNA content, ALP activity, and calcium deposition over 28 d were quantified. The measured ALP activities and calcium contents were normalized to cell numbers by dividing them into DNA contents at each time point. The DNA content was correlated with cell number (Figure 7.5a). The ALP activity of all other groups incubated in osteogenic/vasculogenic (1:1) medium peaked after 14 d and returned to baseline level at day 28 (Figure 7.5b). The ALP activity increased significantly with the increased concentration and glutamic acid in peptide hydrogels. For example, peak ALP activity of KLD-V and KLD-V/NF increased to $1,735.32 \pm 194.39$, and $4,422.97 \pm 101.93$ IU/mg DNA, respectively, while that of KLD-V/GLU-NF was $5,669.95 \pm 84.77$ IU/mg ($p^{***} < 0.001$). The extent of mineralization of the HUVEC/hMSCs increased gradually from day 7 to day 28, with KLD-V/GLU-NF having the highest mineralization after 28 d of incubation in osteogenic/vasculogenic (1:1) medium, as shown in Figure 7.5c. The calcium content of the HUVEC/hMSCs in KLD-V, KLD-V/NF, and KLD-V/GLU-NF incubated in osteogenic/vasculogenic (1:1) medium increased slightly with time. For example, the calcium content of hMSCs encapsulated KLD-V after 28 d was $28,454.04 \pm 612.27$ mg/mg DNA, while those of KLD-V/NF, and KLD-V/GLU-NF were $51,196.88 \pm 1,015.47$, and $76,863.50 \pm 1,346.42$ mg/mg DNA ($p^{***} < 0.001$), respectively.

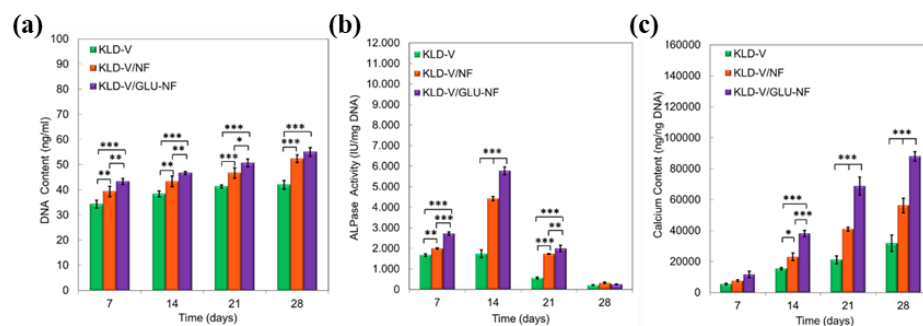


Figure 7.5: (a) DNA content (b) ALP activity (c) Calcium content of HUVEC/hMSCs encapsulated in KLD-V, KLD-V/NF, KLD-V/GLU-NF incubated in osteogenic/vasculogenic (1:1) medium for up to 28 days. The error bars indicate the mean SE ($n = 3$) of the data. [One-way ANOVA was used to assess significant differences.] [$*p < 0.05$, $**p < 0.01$, $***p < 0.001$) Newman–Keuls multiple contrast test]

Expression of osteogenic markers ALP, Col-1, OP, and OC with incubation time for HUVEC encapsulated, hMSC seeded hydrogels is shown in Figures 7.6a-d, respectively. For the KLD-V control group, expression of ALP, Col-1, OP, and OC was significantly less than for all groups. ALP mRNA expression for all groups followed their corresponding ALP activity, peaking at day 14 and returning to the baseline level at day 28. mRNA expression for OP, OC, and Col-1 increased gradually with incubation time. Expression of osteogenic markers ALP, Col-1, OP, and OC increased with all groups. Furthermore, ALP, Col-1, OP, and OC expression were highest for KLD-V/GLU-NF at each time point. For example, Col-1 expression for KLD-V/GLU-NF at day 28 was 961.17 ± 60.65 while that for KLD-V and KLD-V/NF was 163.94 ± 36.28 , and 394.80 ± 75.99 ($p^{***} < 0.001$) respectively; OP expression for KLD-V/GLU-NF at day 28 was 605.39 ± 17.12 while that for KLD-V and KLD-V/NF 148.59 ± 36.28 , and 210.82 ± 58.95 ($p^{***} < 0.001$) respectively; and OC expression for KLD-V/GLU-NF at day 28 was $5,408.08 \pm 110.31$ while that for KLD-V and KLD-V/NF $2,365.25 \pm 583.51$, and $3,350.00 \pm 666.53$ ($p^{***} < 0.001$) respectively; expression of ALP for KLD-V/GLU-NF at day 14 was 91.89 ± 0.73 while that for KLD-V and KLD-V/NF 21.01 ± 0.47 , and 43.09 ± 0.14 ($p^{***} < 0.001$) respectively.

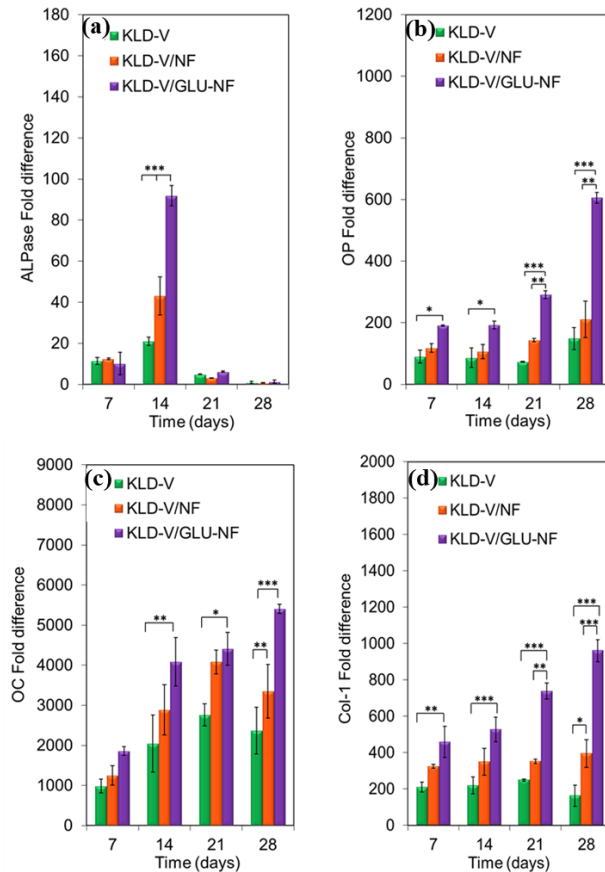


Figure 7.6: The mRNA expression levels (as fold difference) of (a) alkaline phosphatase (ALPase) (b) type 1 collagen (COL-1) (c) osteopontin (OP) (d) osteocalcin (OC) (D) for HUVEC/hMSCs encapsulated in KLD-V, KLD-V/NF, KLD-V/GLU-NF and incubated in osteogenic/vasculogenic (1:1) medium for up to 28 days. The error bars indicate the mean SE (n = 3) of the data. [One-way ANOVA was used to assess significant differences.] [($p < 0.05$, $p < 0.01$, $p < 0.001$) Newman–Keuls multiple contrast test]

Immunostaining images of hMSCs seeded and HUVEC encapsulated KLD-V, KLD-V/NF, and KLD-V/GLU-NF hydrogels are shown in Figure 7.7 a to c which represents the groups of KLD-V/GLU-NF (A), KLD-V/NF (B), KLD-V as negative control (C) respectively stained with COL-I (green), OPN (red) and, OCN (green). The expression of these osteogenic related proteins was drastically higher for HUVEC/hMSC on KLD-V/GLU-NF than those on KLD-V/NF, and KLD-V, respectively. KLD-V group showed weak staining for three markers while the osteogenic epitope containing group (KLD-V/GLU NF) showed moderate to strong staining for osteogenic markers COL-I, OPN, and OCN. Immunofluorescence staining of differentiated HUVEC/MS also confirmed q-PCR results. The expression pattern of COL-1, OPN, and OCN in

HUVEC/hMSC was determined by immunofluorescent staining at day 28 and the results were consistent with q-PCR results.

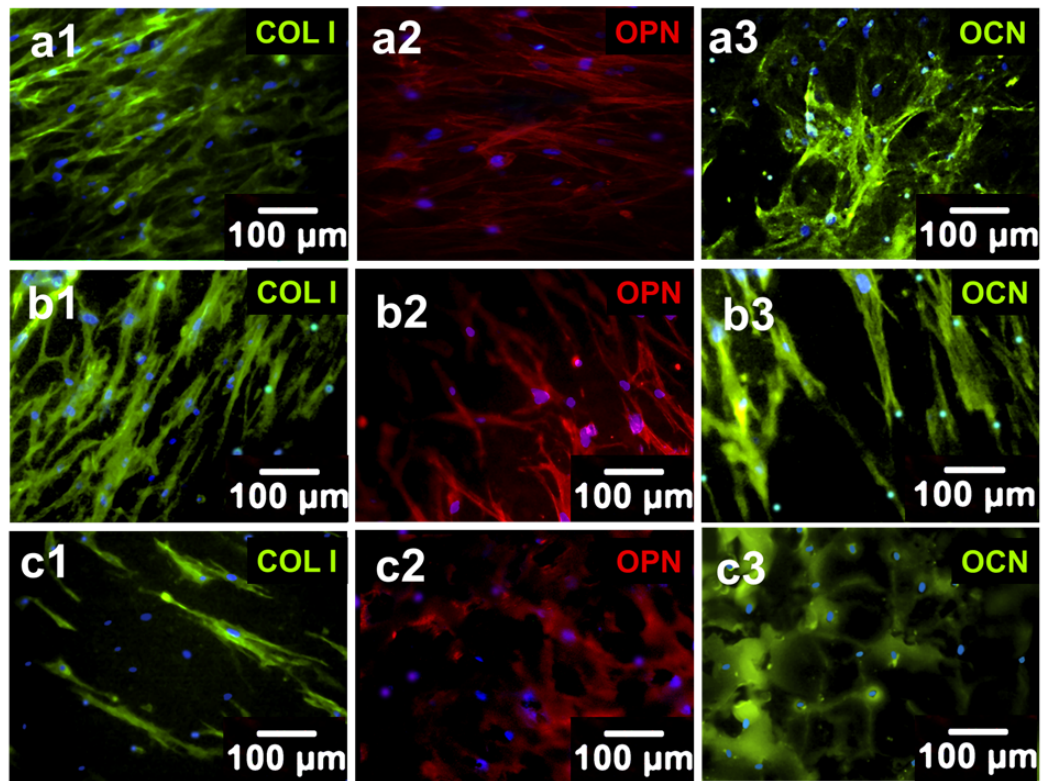


Figure 7.7: Expression pattern of osteogenic markers type 1 collagen (COL-I)(green, first column), osteopontin (OP) (red, second column), and osteocalcin (OC) (green, third column) for HUVEC/hMSCs encapsulated in KLD-V/GLU-NF (AI-III), KLD-V/NF (BI-III), KLD (CI-III) after 28 days incubation in osteogenic/vasculogenic (1:1) medium. Cell nuclei in the images are stained with 4',6-diamidino-2-phenylindole (DAPI; blue) (Scale bar represents 100 μ m)

7.3.3 Vasculogenic Differentiation in Hydrogels

Expression of vasculogenic markers VE-Cad, VWF, and Pecam-1 with incubation time for hMSCs seeded and HUVEC encapsulated KLD-V, KLD-V/NF, and KLD-V/GLU-NF hydrogels are shown in Figures 7.8 a to d, respectively. For the KLD-V control group, expression of VE-Cad, VWF, and Pecam-1 was significantly less than for all groups. mRNA expression for VE-Cad, VWF, and Pecam-1 increased gradually with incubation time. Expression of vasculogenic markers VE-Cad, VWF, and Pecam-1 increased with all groups. Furthermore, VE-Cad, VWF, and Pecam-1 expression

were highest for KLD-V/GLU-NF in each time point. For example, VE-Cad expression for KLD-V/GLU-NF at day 7 was 89.02 ± 1.99 while that for KLD-V and KLD-V/NF was 42.21 ± 8.86 , and 59.54 ± 10.38 ($p^{***} < 0.001$) respectively; VWF expression for KLD-V/GLU-NF V at day 7 was 223.08 ± 5.71 while that for KLD-V and KLD-V/NF 132.14 ± 5.54 , and 155.16 ± 0.67 ($p^{***} < 0.001$) respectively; and Pecam-1 expression for KLD-V/GLU-NF at day 7 was $2,802.34 \pm 283.35$ while that for KLD-V and KLD-V/NF $2,070.63 \pm 372.50$, and $2,589.21 \pm 256.48$ ($p^{***} < 0.001$) respectively.

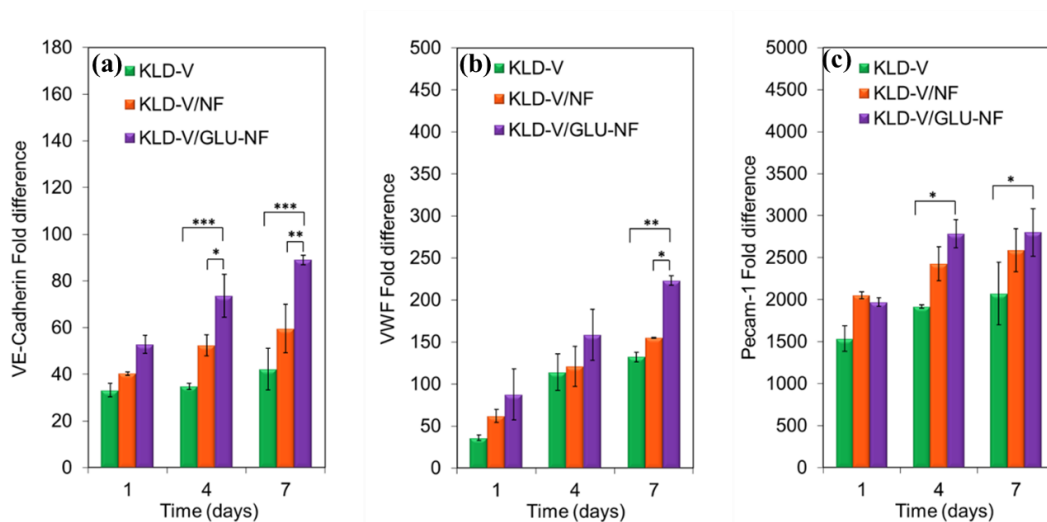


Figure 7.8: The mRNA expression levels (as fold difference) of (a) Ve-Cadherin (b) vWF (c) osteopontin (OP) Pecam-1 for HUVEC/hMSCs encapsulated in KLD-V, KLD-V/NF, KLD-V/GLU-NF and incubated in osteogenic/vasculogenic (1:1) medium for up to 28 days. The error bars indicate the mean SE (n = 3) of the data. [One-way ANOVA was used to assess significant differences.] [(*)p<0.05, (**p<0.01, ***p<0.001) Newman–Keuls multiple contrast test]

Immunostaining images of HUVEC encapsulated hMSC seeded KLD-V, KLD-V/NF, KLD-V/GLU-NF are shown in Figure 7.9 a-c which represents the groups of KLD-V/GLU-NF (a), KLD-V/NF (b), KLD-V (c), respectively stained with PECAM-1 (red) and, vWF (green). The expression of these vasculogenic related proteins was drastically higher for HUVEC/hMSC on KLD-V/GLU-NF than those on KLD-V/NF, and KLD-V, respectively. KLD-V group showed weak staining for both markers while NF containing groups showed moderate to strong staining for vasculogenic markers PECAM-1, and vWF. Immunofluorescence staining of differentiated HUVEC/MS

also confirmed q-PCR results. The expression pattern of PECAM-1, and vWF in HUVEC/hMSC were determined by immunofluorescent staining at day 7 and the results were consistent with q-PCR results.

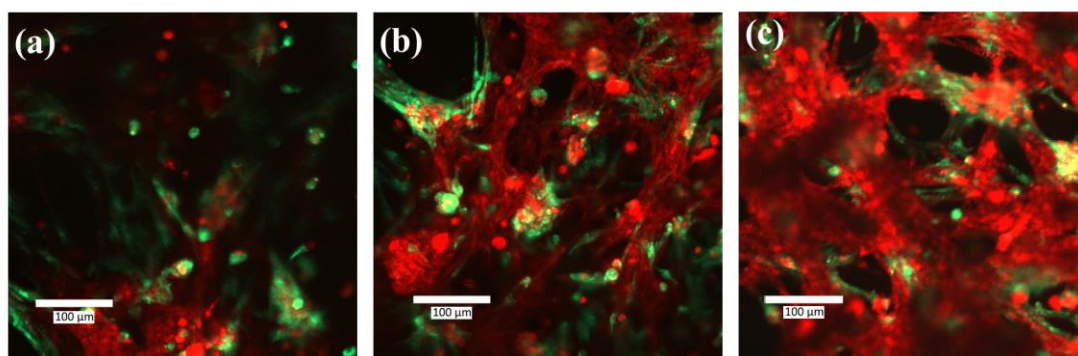


Figure 7.9: Expression pattern of vasculogenic markers PECAM-1(red), and vWF (green) for HUVEC/hMSC encapsulated in (a) KLD-V/GLU-NF (b) KLD-V/NF (c) KLD-V (C) after 7 days incubation in osteogenic/vasculogenic (1:1) medium (Scale bar represents 100 µm)

7.4 Discussion

SAP hydrogels are emergent biomaterials for bone regeneration since they can be functionalized with different peptide epitopes to provide a temporary 3D network, as well as direct bone repair and increase matrix bioactivity [203]. To successfully regenerate bone tissue, the SAP hydrogel scaffold must allow for long-term tissue development and integration with surrounding tissue *in vivo*. However, SAP hydrogels mechanically insufficient for bone tissue engineering applications. Due to the inadequate mechanical properties, there are only a few studies on building bone matrix mimetic scaffolds by SAP hydrogels. Additionally, there is still a tremendous need for new approaches and strategies for developing vascularized bone tissue. Herein, a vascularized bone tissue model by using GLU peptide conjugated stem cell-laden electrospun NF reinforced SAP hydrogels with a vasculogenic epitope (YIGSR), which can support osteogenic and vasculogenic differentiation *in vitro* was proposed for bone defects.

SAP hydrogel self-assembly is an intermolecular and spontaneous process, and the balance of a peptide's hydrophilicity and hydrophobicity often plays a key role in forming hydrogel structure and affecting SAP solubility [215]. While functionalization of SAPs with bioactive epitopes is used to direct cell behavior, functionalization of SAP hydrogels by adding functional peptide group charge at the N-terminus of the peptide has a huge impact on hydrogel formation by self-assembling into nanofibers in water. Previously, we reported that the addition of hydrophobic YIGSR to KLD sequence to the N-terminus of KLD, the hydrogel formation ability of the SAP was not affected and the hydrogel formation of KLD-V was confirmed by AFM and SEM. However, these functionalized peptides were reported soluble in water instead of organic toxic solvents such as DMSO [247]. Herein, we also confirmed the hydrogel formation of KLD-V by SEM. GLU peptide conjugated PLGA electrospun NF was integrated into the hydrogel structure for both reinforcing YIGSR conjugated SAP hydrogels and improving osteogenic differentiation via GLU residues. The GLU peptide was conjugated via a reaction of Ac-PLA conjugated PLGA by Michael's addition reaction between acrylate groups on the PLGA and the cysteine's sulphhydryl group on the GLU peptide. Even though we previously used EDC and NHS chemistry for effective conjugation, this method did not allow to functionalize NFs without attaching to a glass slide to avoid shrinking of the NF area. The use of a glass slide made it difficult to separate the NF from the glass surface before using the NFs as hydrogel reinforcement. Previously, Karaman *et al.* confirmed –Cys containing GLU peptides were successfully conjugated to PLGA surface [152]. We also confirmed the efficacy of peptide conjugation by observing the fluorescence intensity of FITC conjugated GLU peptides via a fluorescence microscope. FITC labeled GLU peptides were used to show the NF surface coverage with peptides. The images were then compared to those of NF. No fluorescence on NF without GLU conjugation which was used as a negative control was detected as expected, which confirms that the fluorescence observed in the GLU-peptide came from the label FITC.

Native bone tissue is subjected to considerable mechanical forces; thus, the mechanical characteristics of bone scaffolds must endure the same stresses. The ECM of bone is stratified, including collagen-rich areas and non-collagenous proteins. This layered structure contributes to the phenotype's heterogeneity. Previous research has discovered that the compressive pressures exerted during bone movement are

distributed differently [305]. Our composite approach mimics the heterogeneous structure of native bone tissue by recapitulating the collagenous layers via the fibrous GLU conjugated PLGA NFs, which offers mechanical strength, while also providing a 3D ECM-like structure via YIGSR containing SAP hydrogels. The cells can remodel this model to generate a diverse bone phenotype. Herein, we reported that the mechanical properties of SAP hydrogels were enhanced with the addition of two layers of NFs. Furthermore, GLU conjugated nanofiber contributed to the reinforcement of SAP hydrogels more compared to bare NF. The difference in mechanical endurance can be explained by increased strength caused by the addition of GLU peptides to PLGA. Kim *et al.* reported that nanofibrous scaffolds are mechanically reinforced with the conjugation with mussel adhesive proteins [306].

To maintain SAP hydrogel stability during tissue regeneration, the degradation rate of SAP hydrogels, which is governed by the charge of hydrogel matrices, should be comparable to the production rate of new bone tissue-specific ECM for ECM secretion [253]. Bioactive hydrogels for bone regeneration, as previously reported in the literature, stimulate bone layer growth *in vivo* within 28 to 42 days [307]. Herein, the degradation times of KLD-V hydrogels were 42 days, while KLD-V/NF and KLD-GLU-NF degraded in 49 days. We hypothesize that KLD-V/NF and KLD-V/PLGA-NF degraded slower due to the addition of PLGA NFs. Furthermore, the degradation time required to assure the stability of hydrogels *in vivo* is sufficient to sustain bone regeneration.

During osteogenesis, calcium ions turn into calcium phosphate on collagen type I mineralizes and mineralized structure accounts for approximately 70% of bone matrix, whereas ALP enzyme, OP, and OC proteins facilitate calcium phosphate crystal nucleation and stabilization [217]. One of the crucial enzymes in the bone ECM is ALP that delivers free phosphate ions to mineral nucleation sites by cleaving organic phosphate esters [218]. The ALP expression trend is often associated with a surge during the early differentiation of progenitor cells into immature osteoblasts. Increasing ALP levels until the 14th-day aids in bone growth and osteoblast activation. ALP levels normally drop in mature progenitor cells, while COL-1, OP, and OC expression increases, indicating a late-osteoblast condition [219]. The expressions of COL-1, OP, and OC are expected to rise during the 28-day incubation period in the

bone mineralization stage. Herein, osteogenic differentiation was assessed in terms of the expression of osteogenic markers such as ALP, COL-1, OP, and OC via q-PCR and immunofluorescent staining. The findings showed that KLD-V/GLU-NF considerably increased the expression of these markers when compared to KLD-V/NF and KLD, showing that a GLU peptide conjugated on the NF contributed to osteogenic differentiation of hMSCs. The expression of all markers on KLD-V was the lowest, showing that PLGA nanofibers have an impact on bone mineralization. According to Nudelman et al., negatively charged glutamic acid peptides operate as calcium ion nucleation locations in collagen nanofibers during biomineralization and greatly increase contact with positively charged calcium ions [221]. Ca^{2+} ions can bind to amino acids with varied affinity depending on pH and stabilized more CaP. The increased calcium amount indicated that GLU on the PLGA NF stabilized more CaP, resulting in enhanced ALP activity, Ca content, and osteogenic gene marker expression [221]. We previously investigated that five glutamic acid sequences after conjugation on PLGA NFs aided mineralization and dramatically enhanced gene expression and secretion of COL-I, OC, and OP [201]. The contribution of GLU peptide on the NF reinforced SAP hydrogel system increased the bioactivity on osteogenic differentiation and rendered the model more effective for bone replacement.

The expression of vasculogenic markers PECAM-1, vWF, and VE-cadherin increased with incubation time in all HUVEC/MSC-containing SAP hydrogel groups. However, the expression of PECAM-1, vWF, and VE-cadherin was significantly lower in the KLD-V control group than in the KLD-V/NF and KLD-V/GLU-NF groups. KLD-V/GLU-NF had higher levels of the vasculogenic markers PECAM-1, vWF, and VE-cadherin. Vascularization of bone tissue constructs is critical for clinical applications. Endothelial cells should be supported by the scaffolds to maintain new vessel creation. Endothelial cells release considerable amounts of vascular endothelial growth factors, angiogenic growth factors, and angiopoietins during vessel formation to promote early capillary network creation [259]. In vitro expression of mature endothelial cell markers such as PECAM-1 (CD31), vWF, and VE-cadherin by HUVECs has been shown to create capillary-like networks [260]. Previously, we demonstrated that YIGSR (V) laminin-derived peptides incorporating KLD hydrogels increased vasculogenic development in HUVECs/hMSCs compared to IKVAV containing KLD and bare

KLD hydrogels [308]. Although, KLD-V showed promising results on vasculogenesis the contribution of GLU-NF and NF integration to KLD-V provided more efficient results. Enhanced vasculogenic differentiation can be related to increased osteogenic differentiation of hMSCs and released growth factors as a result of osteogenesis. Co-culture of MSCs and HUVECs is an effective technique for inducing osteogenic differentiation [286]. The involvement of MSCs with HUVECs is deeply influenced to the development, differentiation, and consequent angiogenesis and osteogenesis. The potential of KLD-V-GLU-NF in vasculogenesis can be related to the presence and more influential role of GLU peptide in increased osteogenic differentiation and biological cues of hMSCs.

7.5 Conclusion

This study is a significant step towards the growth of highly tunable NF fiber-reinforced bioactive SAP by integrating highly porous PLGA electrospun NF and conjugating bioactive GLU peptides. The stiffness of the engineered SAP hydrogels was dramatically increased with the reinforcement with PLGA NF, and this reinforcing effect can be modulated by conjugating GLU peptides on PLGA NFs. The cell-response, significantly higher mineralization rates, osteogenic and vasculogenic gene expressions were observed with the fiber-reinforced SAP hydrogels. The engineered scaffolds could be a promising bone mimetic approach for clinical applications.

Chapter 8

Concluding Remarks

The main goal of the thesis is to produce peptide-based scaffolds for creating an appropriate matrix for bone tissue engineering applications. Bone tissue engineering aims to develop bone-mimetic structures functionalized with biomimetic peptides and integrated with MSCs to restore bone defects. Biomimetic peptides were used as a tool to facilitate the bioactivity of engineered synthetic scaffolds for bone tissue engineering applications due to the advantages such as functioning with the minimum immunological response, high resistance to pH or temperature changes, and precise control over the chemical composition. For this purpose, biomimetic peptides were synthesized by the solid-phase peptide synthesis method according to the desired bioactivity such as osteogenic and vasculogenic differentiation. The effect of these peptides was examined after integrating the scaffolds produced with different fabrication techniques. Furthermore, tissue-engineered structures for bone regeneration need to be gained certain properties such as ease of implantation, suitable mechanical and physical features, biodegradability, osteoconductivity, and biocompatibility. Since tissue-engineered constructs are intended to be used for treating complex bone defects, scaffolds should have bone ECM mimetic structure and function. It should also contain a central microvascular channel structure to ensure proper nutrient/waste transport to the bone tissue. Considering all these needs, we designed different scaffolds in five different studies. In the first part, we implied that NTAP application and GLU peptide conjugation can be a potentially promising method to develop efficient CaP nucleated NF for bone tissue engineering applications. In the second part, the results revealed that KLD SAP functionalized with EEEEE templated peptides had more potential for inducing osteogenesis. In the third part, we found that KLD hydrogel functionalized with YIGSR templated peptides had more potential on inducing vasculogenesis and these laminin-derived peptides could

improve the blood vessel formation in the bone tissue construct. Improving vascularization with this potential model can recompense the loss of function in bone tissue by promoting the survival of transplanted cells. In the fourth part, multifunctional SAP hydrogel as a dental implant filler has demonstrated its ability to actively modulate cellular responses such as vasculogenic and osteogenic differentiation and osseointegration *in vivo*. In the last part, the cell-response, higher mineralization rates, osteogenic and vasculogenic gene expressions were observed with the fiber-reinforced SAP hydrogel model and this engineered scaffold could be a promising bone mimetic approach for clinical applications. Overall, promising results were obtained for the clinical use of these materials as engineering scaffolds. As an ongoing study, it is planning to evaluate *in vivo* studies with an animal model such as femoral defect. Scaffolds will be cultured in a bioreactor after integrating with MSCs/ECs and implanted into a critically sized bone defect. Immunohistochemical analysis will be used for the determination of the bone tissue regeneration and quantitatively determine the bioactivity of scaffolds. In this thesis, the potential of bone-mimetic scaffolds for bone regeneration will be useful for clinical applications.

References

- [1] Ralston SH. Bone structure and metabolism. *Medicine* 2017; 45(9): 560-564.
- [2] Buckwalter J, Glimcher M, Cooper R, Recker R. Bone biology. I: Structure, blood supply, cells, matrix, and mineralization. *Instructional Course Lectures* 1996; 45: 371.
- [3] Gordeladze J, Haugen H, Lyngstadaas S, Reseland J. Bone Tissue Engineering: State of the Art, Challenges, and Prospects: Regenerative Medicine, Smart Diagnostics and Personalized Medicine. Ed.: Hasan A. *Tissue Engineering for Artificial Organs*. Wiley; 2017. 525-551.
- [4] Feng X. Chemical and biochemical basis of cell-bone matrix interaction in health and disease. *Current Chemical Biology* 2009; 3(2): 189-196.
- [5] Bhattacharjee P, Kundu B, Naskar D, Kim HW, Maiti TK, Bhattacharya D, et al. Silk scaffolds in bone tissue engineering: An overview. *Acta Biomaterialia* 2017; 63: 1-17.
- [6] McNamara LM. *Comprehensive Biomaterials*, 1st ed. Elsevier; 2017.
- [7] Frankel VH, Nordin M. *Biomechanics of Bone*. Ed.: Frankel VH, Nordin M. *Basic Biomechanic of Musculoskeletal System*. Wolters Kluwer; 2001. 27.
- [8] Korkusuz F, Tomin E, Yetkinler DN, Timuçin M, Öztürk A, Korkusuz P. Synthetic bone grafts. *TOTBİD Dergisi* 2011; 10(2): 134-142.
- [9] Gao C, Peng S, Feng P, Shuai C. Bone biomaterials and interactions with stem cells. *Bone Research* 2017; 5: 17059.
- [10] Clarke B. Normal bone anatomy and physiology. *Clinical Journal of the American Society of Nephrology : CJASN* 2008; 3(3): 131-139.
- [11] Hubbell JA, Massia SP, Desai NP, Drumheller PD. Endothelial cell-selective materials for tissue engineering in the vascular graft via a new receptor. *Biotechnology* 1991; 9(6): 568-572.

- [12] Tortora G, Derrickson B. Principles of Anatomy and Physiology, 12th ed. Wiley; 2008.
- [13] Jayakumar P, Di Silvio L. Osteoblasts in bone tissue engineering. Proceedings of the Institution of Mechanical Engineers, Part H: Journal of Engineering in Medicine 2010; 224(12): 1415-1440.
- [14] Florencio-Silva R, Sasso GR, Sasso-Cerri E, Simoes MJ, Cerri PS. Biology of bone tissue: Structure, function, and factors that influence bone cells. BioMed Research International 2015; 2015: 421746.
- [15] Damoulis PD, Hauschka PV. Nitric oxide acts in conjunction with proinflammatory cytokines to promote cell death in osteoblasts. Journal of Bone and Mineral Research 1997; 12(3): 412-422.
- [16] Capulli M, Paone R, Rucci N. Osteoblast and osteocyte: Games without frontiers. Archives of Biochemistry and Biophysics 2014; 561: 3-12.
- [17] Roodman GD. Cell biology of the osteoclast. Experimental Hematology 1999; 27(8): 1229-1241.
- [18] Hollinger JO, Einhorn TA, Doll B, Sfeir C. Bone Tissue Engineering, 1st ed. CRC Press; 2004.
- [19] Laurencin CT, Khan Y. Regenerative Engineering, 1st ed. CRC Press; 2013.
- [20] Marieb EN, Hoehn K. Human Anatomy & Physiology, 1st ed. Pearson Education; 2007.
- [21] Meyer U, Meyer T, Wiesmann HP. Bone and Cartilage Engineering, 1st ed. Springer Berlin Heidelberg; 2006.
- [22] Gilbert SF. Developmental Biology, 1st ed. Palgrave Macmillan; 2000.
- [23] Horton WA. The Biology of Bone Growth. Lancet 1990; 6(2): 1-3.
- [24] Bailey FR, Miller AM. Text-book of Embryology, 3rd ed. Wentworth Press; 2016.

- [25] Schroeder A, van der Zypen E, Stich H, Sutter F. The reactions of bone, connective tissue, and epithelium to endosteal implants with titanium-sprayed surfaces. *Journal of Oral and Maxillofacial Surgery* 1981; 9(1): 15-25.
- [26] Terheyden H, Lang NP, Bierbaum S, Stadlinger B. Osseointegration--communication of cells. *Clinical Oral Implants Research* 2012; 23(10): 1127-1135.
- [27] Kusumbe AP, Ramasamy SK, Adams RH. Coupling of angiogenesis and osteogenesis by a specific vessel subtype in bone. *Nature* 2014; 507(7492): 323-328.
- [28] Chen Q, Thouas GA. Metallic implant biomaterials. *Materials Science and Engineering R: Reports* 2015; 87: 1-57.
- [29] Bauer S, Schmuki P, von der Mark K, Park J. Engineering biocompatible implant surfaces: Part i: Materials and surfaces. *Progress in Materials Science* 2013; 58(3): 261-326.
- [30] Domanska A, Boczkowska A. Biodegradable polyurethanes from crystalline prepolymers. *Polymer Degradation and Stability* 2014; 108: 175-181.
- [31] Dos Santos V, Brandalise RN, Savaris M. *Engineering of Biomaterials*, 1st ed. Springer International Publishing; 2017.
- [32] Vert M, Doi Y, Hellwich K-H, Hess M, Hodge P, Kubisa P, et al. Terminology for biorelated polymers and applications (iupac recommendations 2012). *Pure and Applied Chemistry* 2012; 84(2): 377-410.
- [33] Zeugolis DI, Pandit A. Biofunctional biomaterials – the next frontier. *Bioconjugate Chemistry* 2015; 26(7): 1157-1157.
- [34] Service IFI. *Ifis Dictionary of Food Science and Technology*, 2nd ed. John Wiley & Sons; 2009.
- [35] Katz SH, Weaver WW. *Encyclopedia of Food and Culture*, 2nd ed. Scribner; 2003.

- [36] Moldoveanu SC, David V. RP-HPLC Analytical Columns. Ed.: Moldoveanu SC, David V. Selection of the HPLC Method in Chemical Analysis. Elsevier; 2017. 279-328.
- [37] Kondyurin A, Bilek M. Wetting. Ed.: Kondyurin A, Bilek M. Ion Beam Treatment of Polymers. Elsevier; 2015. 129-143.
- [38] Kyriakides TR. Molecular Events at Tissue–Biomaterial Interface. Ed.: Badylak SF. Host Response to Biomaterials. Academic Press; 2015. 81-116.
- [39] Nikola Slepickova Kasalkova PS, Zdenka Kolska and Vaclav Svorcik. Wettability and Other Surface Properties of Modified Polymers. Ed.: Aliofkhazraei M. Wetting and Wettability. IntechOpen; 2015.
- [40] Wang H-ICaY. Cell Responses to Surface and Architecture of Tissue Engineering Scaffolds. Ed.: Eberli D. Regenerative Medicine and Tissue Engineering - Cells and Biomaterials. IntechOpen; 2011.
- [41] Choudhury SK, Chinchankar S. Finish Machining of Hardened Steel. Ed.: Hashmi MSJ. Comprehensive Materials Finishing. Elsevier; 2017. 47-92.
- [42] Anseth KS, Klok H-A. Click chemistry in biomaterials, nanomedicine, and drug delivery. *Biomacromolecules* 2016; 17(1): 1-3.
- [43] Hench LL, Wilson J. Surface-active biomaterials. *Science* 1984; 226(4675): 630-636.
- [44] Tomazic-Jezic VJ, Merritt K, Umbreit TH. Significance of the type and the size of biomaterial particles on phagocytosis and tissue distribution. *Journal of Biomedical Materials Research* 2001; 55(4): 523-529.
- [45] Roosa SMM, Kemppainen JM, Moffitt EN, Krebsbach PH, Hollister SJ. The pore size of polycaprolactone scaffolds has limited influence on bone regeneration in an in vivo model. *Journal of Biomedical Materials Research Part A* 2010; 92A(1): 359-368.

- [46] Bhat G, Kandagor V. Synthetic Polymer Fibers and Their Processing Requirements. Ed.: Zhang D. *Advances in Filament Yarn Spinning of Textiles and Polymers*. Woodhead Publishing; 2014. 3-30.
- [47] Grynepas M. The crystallinity of bone mineral. *Journal of Materials Science* 1976; 11(9): 1691-1696.
- [48] Hearn EJ. Simple Stress and Strain. Ed.: Hearn EJ. *Mechanics of Materials 1*. Butterworth-Heinemann; 1997. 1-26.
- [49] Saini M, Singh Y, Arora P, Arora V, Jain K. Implant biomaterials: A comprehensive review. *World Journal of Clinical Cases* 2015; 3(1): 52-57.
- [50] Chattopadhyay R. Artificial Neural Networks in Yarn Property Modeling. Ed.: Majumdar A. *Soft Computing in Textile Engineering*. Woodhead Publishing; 2011. 105-125.
- [51] Hughes SE. Materials and Their weldability. Ed.: Hughes SE. *A Quick Guide to Welding and Weld Inspection*. Woodhead Publishing; 2009. 36-48.
- [52] Topçu IB, Uygunoglu T. Sustainability of Using Waste Rubber in Concrete. Ed.: Khatib JM. *Sustainability of Construction Materials*. Woodhead Publishing; 2016. 597-623.
- [53] Acevedo C, Stadelmann V, Pioletti D, Alliston T, Ritchie R. Fatigue as the missing link between bone fragility and fracture. *Nature Biomedical Engineering* 2018; (2): 62–71.
- [54] Yasuda I. The classic: Fundamental aspects of fracture treatment. *Clinical Orthopaedics and Related Research* 1977; (124): 5-8.
- [55] Park B, Kim YK. Metallic biomaterials. *Balance* 2003; 1:50.
- [56] Alvarez K, Nakajima H. Metallic scaffolds for bone regeneration. *Materials* 2009; 2(3): 790-832.
- [57] Tschernitschek H, Borchers L, Geurtsen W. Nonalloyed titanium as a bioinert metal-a review. *Quintessence International* 2005; 36(7).

- [58] Pouilleau J, Devilliers D, Garrido F, Durand-Vidal S, Mahé E. Structure and composition of passive titanium oxide films. *Materials Science and Engineering: B* 1997; 47(3): 235-243.
- [59] Odman J, Lekholm U, Jemt T, Branemark PI, Thilander B. Osseointegrated titanium implants-a new approach in orthodontic treatment. *European Journal of Orthodontics* 1988; 10(2): 98-105.
- [60] Al-Nawas B, Bragger U, Meijer HJ, Naert I, Persson R, Perucchi A, et al. A double-blind randomized controlled trial (RCT) of titanium-13zirconium versus titanium grade iv small-diameter bone level implants in edentulous mandibles--results from a 1-year observation period. *Clinical Implant Dentistry and Related Research* 2012; 14(6): 896-904.
- [61] Romeo E, Lops D, Amorfini L, Chiapasco M, Ghisolfi M, Vogel G. Clinical and radiographic evaluation of small-diameter (3.3-mm) implants followed for 1-7 years: A longitudinal study. *Clinical Oral Implants Research* 2006; 17(2): 139-148.
- [62] Zinsli B, Sagesser T, Mericske E, Mericske-Stern R. Clinical evaluation of small-diameter iti implants: A prospective study. *The International Journal of Oral & Maxillofacial Implants* 2004; 19(1): 92-99.
- [63] Schwarz MS. Mechanical complications of dental implants. *Clinical Oral Implants Research* 2000; 11(1): 156-158.
- [64] Kubasiewicz-Ross P, Dominiak M, Gedrange T, Botzenhart UU. Zirconium: The material of the future in modern implantology. *Advances in Clinical And Experimental Medicine: Official Organ Wroclaw Medical University* 2017; 26(3): 533-537.
- [65] Dubok VA. Bioceramics-yesterday, today, tomorrow. *Powder Metallurgy and Metal Ceramics* 2000; 39(7-8): 381-394.
- [66] Thomas S, Balakrishnan P, Sreekala MS. *Fundamental biomaterials: Ceramics*. Woodhead Publishing; 2018.

- [67] Hayashi K, Inadome T, Tsumura H, Mashima T, Sugioka Y. Bone-implant interface mechanics of in vivo bio-inert ceramics. *Biomaterials* 1993; 14(15): 1173-1179.
- [68] De Aza A, Chevalier J, Fantozzi G, Schehl M, Torrecillas R. Crack growth resistance of alumina, zirconia and zirconia toughened alumina ceramics for joint prostheses. *Biomaterials* 2002; 23(3): 937-945.
- [69] Mahyudin F, Widhiyanto L, Hermawan H. *Biomaterials in Orthopaedics*. Ed.: Rodriguez-Gonzalez FA. *Biomaterials and Medical Devices*. Springer; 2016. 161-181.
- [70] Salinas AJ, Vallet-Regí M. Bioactive ceramics: From bone grafts to tissue engineering. *RSC Advances* 2013; 3(28): 11116-11131.
- [71] Suchanek W, Yashima M, Kakihana M, Yoshimura M. Processing and mechanical properties of hydroxyapatite reinforced with hydroxyapatite whiskers. *Biomaterials* 1996; 17(17): 1715-1723.
- [72] Uemura T, Dong J, Wang Y, Kojima H, Saito T, Iejima D, et al. Transplantation of cultured bone cells using combinations of scaffolds and culture techniques. *Biomaterials* 2003; 24(13): 2277-2286.
- [73] Alaribe FN, Manoto SL, Motaung SC. Scaffolds from biomaterials: Advantages and limitations in bone and tissue engineering. *Biologia* 2016; 71(4): 353-366.
- [74] Singh H, Sharma C, Dhasmana A, Gupta S, Purohit SD, Mishra N, et al. *Bone Regeneration: Emerging Paradigms and Existing Snags*, 1st ed; 2018.
- [75] Noori A, Ashrafi SJ, Vaez-Ghaemi R, Hatamian-Zaremi A, Webster TJ. A review of fibrin and fibrin composites for bone tissue engineering. *International Journal of Nanomedicine* 2017; 12: 4937-4961.
- [76] Kaplan DL. Fibrous proteins—silk as a model system. *Polymer Degradation and Stability* 1998; 59(1-3): 25-32.

- [77] Shen X, Zhang Y, Gu Y, Xu Y, Liu Y, Li B, et al. Sequential and sustained release of sdf-1 and bmp-2 from silk fibroin-nanohydroxyapatite scaffold for the enhancement of bone regeneration. *Biomaterials* 2016; 106: 205-216.
- [78] Ferreira AM, Gentile P, Chiono V, Ciardelli G. Collagen for bone tissue regeneration. *Acta Biomaterialia* 2012; 8(9): 3191-3200.
- [79] Ahmed TA, Dare EV, Hincke M. Fibrin: A versatile scaffold for tissue engineering applications. *Tissue Engineering Part B* 2008; 14(2): 199-215.
- [80] Watanabe K, Nakamura M, Okano H, Toyama Y. Establishment of three-dimensional culture of neural stem/progenitor cells in collagen type-1 gel. *Restorative Neurology and Neuroscience* 2007; 25(2): 109-117.
- [81] Venkatesan J, Vinodhini PA, Sudha PN, Kim SK. Chitin and chitosan composites for bone tissue regeneration. *Advances in Food and Nutrition Research* 2014; 73: 59-81.
- [82] Marsich E, Bellomo F, Turco G, Travan A, Donati I, Paoletti S. Nano-composite scaffolds for bone tissue engineering containing silver nanoparticles: Preparation, characterization and biological properties. *Journal of Materials Science: Materials in Medicine* 2013; 24(7): 1799-1807.
- [83] Kolambkar YM, Dupont KM, Boerckel JD, Huebsch N, Mooney DJ, Hutmacher DW, et al. An alginate-based hybrid system for growth factor delivery in the functional repair of large bone defects. *Biomaterials* 2011; 32(1): 65-74.
- [84] Renier D, Bellato P, Bellini D, Pavesio A, Pressato D, Borriero A. Pharmacokinetic behaviour of acp gel, an autocrosslinked hyaluronan derivative, after intraperitoneal administration. *Biomaterials* 2005; 26(26): 5368-5374.
- [85] Kim J, Kim IS, Cho TH, Lee KB, Hwang SJ, Tae G, et al. Bone regeneration using hyaluronic acid-based hydrogel with bone morphogenic protein-2 and human mesenchymal stem cells. *Biomaterials* 2007; 28(10): 1830-1837.

- [86] Diker N, Koroglu T, Gulsever S, Akcay EY, Oguz Y. Effects of hyaluronic acid and alloplastic bone graft combination on bone regeneration. *International Journal of Oral and Maxillofacial Surgery* 2015; 44: e55.
- [87] Solchaga LA, Gao J, Dennis JE, Awadallah A, Lundberg M, Caplan AI, et al. Treatment of osteochondral defects with autologous bone marrow in a hyaluronan-based delivery vehicle. *Tissue Engineering* 2002; 8(2): 333-347.
- [88] Okamoto M, John B. Synthetic biopolymer nanocomposites for tissue engineering scaffolds. *Progress in Polymer Science* 2013; 38(10): 1487-1503.
- [89] Vats A, Tolley NS, Polak JM, Gough JE. Scaffolds and biomaterials for tissue engineering: A review of clinical applications. *Clinical Otolaryngology* 2003; 28(3): 165-172.
- [90] Mulinti P, Brooks JE, Lervick B, Pullan JE, Brooks AE. Strategies to Improve the Hemocompatibility of Biodegradable Biomaterials. Ed.: Siedlecki CA. *Hemocompatibility of Biomaterials for Clinical Applications*. Woodhead Publishing; 2018. 253-278.
- [91] Zakharova L, Pashirova T, Kashapov R, Gabdrakhmanov D, Sinyashin O. Drug Delivery Mediated by Confined Nanosystems: Structure-Activity Relations and Factors Responsible for the Efficacy of Formulations. Ed.: Andronescu E, Grumezescu AM. *Nanostructures for drug delivery*. Elsevier; 2017. 749-806.
- [92] Gentile P, Chiono V, Carmagnola I, Hatton PV. An overview of poly(lactic-co-glycolic) acid (PLGA)-based biomaterials for bone tissue engineering. *International Journal of Molecular Sciences* 2014; 15(3): 3640-3659.
- [93] Engineer C, Parikh J, Raval A. Review on hydrolytic degradation behavior of biodegradable polymers from controlled drug delivery system. *Trends in Biomaterials & Artificial Organs* 2011; 25(2).
- [94] Lee J-H, Kim H-W. Emerging properties of hydrogels in tissue engineering. *Journal of Tissue Engineering* 2018; 9: 20-41.

- [95] Gökteş M. Bioactive porous peg-peptide composite hydrogels with tunable mechanical properties (master's thesis). Ankara: Bilkent University; 2014.
- [96] Stancu IC, Lungu A, Iovu H. Hydrogels for Bone Regeneration. Ed.: Dubruel P, Van Vlierberghe S. Biomaterials for Bone Regeneration. Woodhead Publishing; 2014. 62-86.
- [97] Nune M, Kumaraswamy P, Maheswari Krishnan U, Sethuraman S. Self-assembling peptide nanofibrous scaffolds for tissue engineering: Novel approaches and strategies for effective functional regeneration. *Current Protein and Peptide Science* 2013; 14(1): 70-84.
- [98] Toksöz S, Guler MO. Self-assembled peptidic nanostructures. *Nano Today* 2009; 4(6): 458-469.
- [99] Cui H, Webber MJ, Stupp SI. Self-assembly of peptide amphiphiles: From molecules to nanostructures to biomaterials. *Peptide Science: Original Research on Biomolecules* 2010; 94(1): 1-18.
- [100] Subia B, Kundu J, Kundu S. Biomaterial Scaffold Fabrication Techniques for Potential Tissue Engineering Applications. Ed.: Eberli D. *Tissue Engineering*. IntechOpen; 2010.
- [101] Eltom A, Zhong G, Muhammad A. Scaffold Techniques and Designs in Tissue Engineering Functions and Purposes: A review, 1st ed; 2019.
- [102] Prasad A, Sankar MR, Katiyar V. State of art on solvent casting particulate leaching method for orthopedic scaffolds fabrication. *Materials Today: Proceedings* 2017; 4(2, Part A): 898-907.
- [103] Garg T, Singh O, Arora S, Rayasa M. Scaffold: A novel carrier for cell and drug delivery. Ed.: Birchall J. *Critical reviews in therapeutic drug carrier systems*; 2012. 1-63.
- [104] Sachlos E, Czernuszka JT. Making tissue engineering scaffolds work. Review: The application of solid freeform fabrication technology to the production of tissue engineering scaffolds. *European Cells & Materials* 2003; 5: 29-39.

- [105] Sofokleous P, Chin MHW, Day R. Phase-Separation Technologies for 3D Scaffold Engineering. Ed.: Deng Y, Kuiper J. Functional 3D Tissue Engineering scaffolds. Woodhead Publishing; 2018. 101-126.
- [106] Abdelaal O. Review of Rapid Prototyping Techniques for Tissue Engineering Scaffolds Fabrication. Ed.: Lucas ÖA, da Silva FM, Altenbach H. Characterization and Development of Biosystems and Biomaterials. Springer; 2013. 33-54.
- [107] Pham QP, Sharma U, Mikos AG. Electrospinning of polymeric nanofibers for tissue engineering applications: A review. *Tissue Engineering* 2006; 12(5): 1197-1211.
- [108] Bhardwaj N, Kundu SC. Electrospinning: A fascinating fiber fabrication technique. *Biotechnology Advances* 2010; 28(3): 325-347.
- [109] Erkal TS. Self-assembly of peptide nanofibers and their mechanical properties (master's thesis). Ankara: Bilkent University; 2012.
- [110] Dikecoglu FB, Topal AE, Ozkan AD, Tekin ED, Tekinay AB, Guler MO, et al. Force and time-dependent self-assembly, disruption and recovery of supramolecular peptide amphiphile nanofibers. *Nanotechnology* 2018; 29(28): 285701.
- [111] Zhang S, Marini DM, Hwang W, Santoso S. Design of nanostructured biological materials through self-assembly of peptides and proteins. *Current Opinion in Chemical Biology* 2002; 6(6): 865-871.
- [112] Rajagopal K, Schneider JP. Self-assembling peptides and proteins for nanotechnological applications. *Current Opinion in Structural Biology* 2004; 14(4): 480-486.
- [113] Iscen A, Schatz GC. Peptide amphiphile self-assembly. *Europhysics Letters* 2017; 119(3): 38002.
- [114] Zhang S. Emerging biological materials through molecular self-assembly. *Biotechnology Advances* 2002; 20(5-6): 321-339.

- [115] Dana A, Tekinay AB, Tekin ED. A comparison of peptide amphiphile nanofiber macromolecular assembly strategies. *The European Physical Journal E* 2019; 42(5): 63.
- [116] Ustun Yaylaci S, Sardan Ekiz M, Arslan E, Can N, Kilic E, Ozkan H, et al. Supramolecular gag-like self-assembled glycopeptide nanofibers induce chondrogenesis and cartilage regeneration. *Biomacromolecules* 2016; 17(2): 679-689.
- [117] Toksöz S. Electrostatic effects on the self-assembly mechanism of peptide amphiphiles (master's thesis). Ankara: Bilkent University; 2010.
- [118] Webber MJ, Berns EJ, Stupp SI. Supramolecular nanofibers of peptide amphiphiles for medicine. *Israel Journal of Chemistry* 2013; 53(8): 530-554.
- [119] Çakmak S. Kemik doku onarımı için hidroksiapatit peptid amfil bazlı nanokompozit doku İskelelerinin geliştirilmesi. *International Journal of Multidisciplinary Studies and Innovative Technologies* 2015.
- [120] Arslan E, Guler MO, Tekinay AB. Glycosaminoglycan-mimetic signals direct the osteo/chondrogenic differentiation of mesenchymal stem cells in a three-dimensional peptide nanofiber extracellular matrix mimetic environment. *Biomacromolecules* 2016; 17(4): 1280-1291.
- [121] Hosseinkhani H, Hong P-D, Yu D-S. Self-assembled proteins and peptides for regenerative medicine. *Chemical Reviews* 2013; 113(7): 4837-4861.
- [122] Zhang A, Addou F, Duguet T, Caussé N, Vahlas C. Adaptation of a dry metalorganic chemical vapor deposition metallization process to a wet chemical pretreatment of polymers. *Journal of Vacuum Science & Technology A* 2017; 35(6): 61-101.
- [123] Abu-Isa IA. Iodine treatment of nylon: Effect on metal plating of the polymer. *Journal of Applied Polymer Science* 1971; 15(11): 2865-2876.
- [124] Regis S, Jassal M, Mukherjee N, Bayon Y, Scarborough N, Bhowmick S. Altering surface characteristics of polypropylene mesh via sodium hydroxide

- treatment. *Journal of Biomedical Materials Research Part A* 2012; 100A(5): 1160-1167.
- [125] Michaljaničová I, Slepíčka P, Rimpelová S, Slepíčková Kasálková N, Švorčík V. Regular pattern formation on surface of aromatic polymers and its cytocompatibility. *Applied Surface Science* 2016; 370: 131-141.
- [126] Teixeira AI, Nealey PF, Murphy CJ. Responses of human keratocytes to micro- and nanostructured substrates. *Journal of Biomedical Materials Research Part A* 2004; 71(3): 369-376.
- [127] Ko T-J, Jo W, Lee HJ, Oh KH, Moon M-W. Nanostructures formed on carbon-based materials with different levels of crystallinity using oxygen plasma treatment. *Thin Solid Films* 2015; 590: 324-329.
- [128] Gomez E, Rani DA, Cheeseman CR, Deegan D, Wise M, Boccaccini AR. Thermal plasma technology for the treatment of wastes: A critical review. *Journal of Hazardous Materials* 2009; 161(2-3): 614-626.
- [129] Choi EH, Uhm HS, Kaushik NK. Plasma bioscience and its application to medicine. *AAPPS Bulletin* 2021; 31(1): 10.
- [130] Monchaux E, Vermette P, J. Doillon C. *Development of Bioactive Surfaces to Control Cell Behaviour - Use of Polymer and Biomolecule Arrays*, 1st ed; 2006.
- [131] Shakesheff K, Cannizzaro S, Langer R. Creating biomimetic micro-environments with synthetic polymer-peptide hybrid molecules. *Journal of Biomaterials Science, Polymer Edition* 1998; 9(5): 507-518.
- [132] Rahmany MB, Van Dyke M. Biomimetic approaches to modulate cellular adhesion in biomaterials: A review. *Acta Biomaterialia* 2013; 9(3): 5431-5437.
- [133] Özdemir ZÖ, Mustafaeva Z. Development of polyelectrolyte based bioconjugates using with synthetic viral peptides. *Sigma* 2011; 29: 65-89.
- [134] Jaradat DM. Thirteen decades of peptide synthesis: Key developments in solid phase peptide synthesis and amide bond formation utilized in peptide ligation. *Amino Acids* 2018; 50(1).

- [135] Meienhofer J. Peptide synthesis: A Review of the Solid-Phase Method. Ed.: Hao Li C. Hormonal Proteins and Peptides. Elsevier; 1973. 45-267.
- [136] Pires DAT, Bemquerer MP, do Nascimento CJ. Some mechanistic aspects on fmoc solid phase peptide synthesis. *International Journal of Peptide Research and Therapeutics* 2014; 20(1): 53-69.
- [137] Amblard M, Fehrentz J-A, Martinez J, Subra G. Methods and protocols of modern solid phase peptide synthesis. *Molecular Biotechnology* 2006; 33(3): 239-254.
- [138] Xu Y, Xia D, Han J, Yuan S, Lin H, Zhao C. Design and fabrication of porous chitosan scaffolds with tunable structures and mechanical properties. *Carbohydrate Polymers* 2017; 177: 210-216.
- [139] Lu G, Liu S, Lin S, Kaplan DL, Lu Q. Silk porous scaffolds with nanofibrous microstructures and tunable properties. *Colloids and Surfaces B: Biointerfaces* 2014; 120: 28-37.
- [140] Tampieri A, Landi E, Valentini F, Sandri M, D'alessandro T, Dediu V, et al. A conceptually new type of bio-hybrid scaffold for bone regeneration. *Nanotechnology* 2010; 22(1): 015104.
- [141] Lin Z, Solomon KL, Zhang X, Pavlos NJ, Abel T, Willers C, et al. In vitro evaluation of natural marine sponge collagen as a scaffold for bone tissue engineering. *International Journal of Biological Sciences* 2011; 7(7): 968.
- [142] Hoyer B, Bernhardt A, Heinemann S, Stachel I, Meyer M, Gelinsky M. Biomimetically mineralized salmon collagen scaffolds for application in bone tissue engineering. *Biomacromolecules* 2012; 13(4): 1059-1066.
- [143] Gutiérrez-Hernández JM, Escobar-García DM, Escalante A, Flores H, González FJ, Gatenholm P, et al. In vitro evaluation of osteoblastic cells on bacterial cellulose modified with multi-walled carbon nanotubes as scaffold for bone regeneration. *Materials Science and Engineering: C* 2017; 75: 445-453.

- [144] Zhao X, Han Y, Li J, Cai B, Gao H, Feng W, et al. Bmp-2 immobilized plga/hydroxyapatite fibrous scaffold via polydopamine stimulates osteoblast growth. *Materials Science and Engineering: C* 2017; 78: 658-666.
- [145] Karaman O. Mineralized Nanofibers for Bone Tissue Engineering. Ed.: Khosrow M. *Biomedical Engineering: Concepts, Methodologies, Tools, and Applications*. IGI Global; 2018. 461-475.
- [146] Karaman O, Celik C, Urkmez AS. Self-Assembled Biomimetic Scaffolds for Bone Tissue Engineering. Ed.: Khosrow M. *Biomedical Engineering: Concepts, Methodologies, Tools, and Applications*. IGI Global; 2018. 476-504.
- [147] Xie J, Zhong S, Ma B, Shuler FD, Lim CT. Controlled biomineralization of electrospun poly (ϵ -caprolactone) fibers to enhance their mechanical properties. *Acta Biomaterialia* 2013; 9(3): 5698-5707.
- [148] Leszczak V, Place LW, Franz N, Popat KC, Kipper MJ. Nanostructured biomaterials from electrospun demineralized bone matrix: A survey of processing and crosslinking strategies. *ACS Applied Materials & Interfaces* 2014; 6(12): 9328-9337.
- [149] Kim H, Che L, Ha Y, Ryu W. Mechanically-reinforced electrospun composite silk fibroin nanofibers containing hydroxyapatite nanoparticles. *Materials Science and Engineering: C* 2014; 40: 324-335.
- [150] Gao Y, Shao W, Qian W, He J, Zhou Y, Qi K, et al. Biomineralized poly (l-lactic-co-glycolic acid)-tussah silk fibroin nanofiber fabric with hierarchical architecture as a scaffold for bone tissue engineering. *Materials Science and Engineering: C* 2018; 84: 195-207.
- [151] Liu W, Yeh Y-C, Lipner J, Xie J, Sung H-W, Thomopoulos S, et al. Enhancing the stiffness of electrospun nanofiber scaffolds with a controlled surface coating and mineralization. *Langmuir* 2011; 27(15): 9088-9093.
- [152] Karaman O, Kumar A, Moeinzadeh S, He XZ, Cui T, Jabbari E. Effect of surface modification of nanofibres with glutamic acid peptide on calcium phosphate

nucleation and osteogenic differentiation of marrow stromal cells. *Journal of Tissue Engineering and Regenerative Medicine* 2016; 10(2): 132-146.

- [153] Kawata M, Azuma K, Izawa H, Morimoto M, Saimoto H, Ifuku S. Biom mineralization of calcium phosphate crystals on chitin nanofiber hydrogel for bone regeneration material. *Carbohydrate Polymers* 2016; 136: 964-969.
- [154] Maiti S, Jana S, Jana S. *Biocomposites in Therapeutic Application: Current Status and Future*. Ed.: Jana S, Maiti S, Jana S. *Biopolymer-Based Composites*. Woodhead Publishing; 2017. 1-29.
- [155] Abdellaoui H, Bouhfid R, Qaiss AEK. *Lignocellulosic Fibres Reinforced Thermoset Composites: Preparation, Characterization, Mechanical and Rheological Properties*. Ed.: Kalia S. *Lignocellulosic Composite Materials*. Springer International Publishing; 2018. 215-270.
- [156] Zhang H, Mao X, Zhao D, Jiang W, Du Z, Li Q, et al. Three dimensional printed polylactic acid-hydroxyapatite composite scaffolds for prefabricating vascularized tissue engineered bone: An in vivo bioreactor model. *Scientific Reports* 2017; 7(1): 15255.
- [157] Xie L, Qian W, Sun J, Zou B. *Engineering nanobiomaterials for improved tissue regeneration*. *Nanobiomaterials: Classification, Fabrication and Biomedical Applications* 2017.
- [158] Krajina BA, Proctor AC, Schoen AP, Spakowitz AJ, Heilshorn SC. Biotemplated synthesis of inorganic materials: An emerging paradigm for nanomaterial synthesis inspired by nature. *Progress in Materials Science* 2018; 91: 1-23.
- [159] Bas O, D'Angella D, Baldwin JG, Castro NJ, Wunner FM, Saidy NT, et al. An integrated design, material, and fabrication platform for engineering biomechanically and biologically functional soft tissues. *ACS Applied Materials & Interfaces* 2017; 9(35): 29430-29437.

- [160] Jordan AM, Viswanath V, Kim S-E, Pokorski JK, Korley LTJ. Processing and surface modification of polymer nanofibers for biological scaffolds: A review. *Journal of Materials Chemistry B* 2016; 4(36): 5958-5974.
- [161] Wang Q, Wang X, Tian L, Cheng Z, Cui F. In situ remineralization of partially demineralized human dentine mediated by a biomimetic non-collagen peptide. *Soft Matter* 2011; 7(20): 9673-9680.
- [162] Barati D, Walters JD, Pajoum Shariati SR, Moeinzadeh S, Jabbari E. Effect of organic acids on calcium phosphate nucleation and osteogenic differentiation of human mesenchymal stem cells on peptide functionalized nanofibers. *Langmuir* 2015; 31(18): 5130-5140.
- [163] Kurokawa N, Endo F, Maeda T, Hotta A. *Electrospinning and Surface Modification Methods for Functionalized Cell Scaffolds*. Ed.: Ficiu Denisa, Grumezescu AM. *Nanostructures for Novel Therapy*. Elsevier; 2017. 201-225.
- [164] Bertrand O, Gohy J-F. *Photo-responsive polymers: Synthesis and applications*. *Polymer Chemistry* 2017; 8(1): 52-73.
- [165] Liu F, Wang W, Mirihanage W, Hinduja S, Bartolo P. A plasma-assisted bioextrusion system for tissue engineering. *CIRP Annals* 2018.
- [166] Fabbri P, Messori M. *Surface Modification of Polymers: Chemical, Physical, and Biological Routes*. Ed.: Jasso-Gastinel CF, Kenny JM. *Modification of Polymer Properties*. Elsevier; 2017. 109-130.
- [167] Sorkio A, Porter PJ, Juuti-Uusitalo K, Meenan BJ, Skottman H, Burke GA. Surface modified biodegradable electrospun membranes as a carrier for human embryonic stem cell-derived retinal pigment epithelial cells. *Tissue Engineering Part A* 2015; 21(17-18): 2301-2314.
- [168] Karaman O, Kelebek S, Demirci EA, İbiş F, Ulu M, Ercan UK. Synergistic effect of cold plasma treatment and rgd peptide coating on cell proliferation over titanium surfaces. *Tissue Engineering and Regenerative Medicine* 2018; 15(1): 13-24.

- [169] Kan C-W, Man W-S. Surface characterisation of atmospheric pressure plasma treated cotton fabric-effect of operation parameters. *Polymers* 2018; 10(3): 250.
- [170] Golda M, Brzychczy-Wloch M, Faryna M, Engvall K, Kotarba A. Oxygen plasma functionalization of parylene c coating for implants surface: Nanotopography and active sites for drug anchoring. *Materials Science and Engineering: C* 2013; 33(7): 4221-4227.
- [171] Puliyalil H, Cvelbar U. Selective plasma etching of polymeric substrates for advanced applications. *Nanomaterials* 2016; 6(6): 108.
- [172] Kokubo T, Kushitani H, Ohtsuki C, Sakka S, Yamamuro T. Chemical reaction of bioactive glass and glass-ceramics with a simulated body fluid. *Journal of Materials Science: Materials in Medicine* 1992; 3(2): 79-83.
- [173] Onak G, Karaman O. Accelerated mineralization on nanofibers via non-thermal atmospheric plasma assisted glutamic acid templated peptide conjugation. *Regenerative Biomaterials* 2019; 6(4): 231-240.
- [174] Kim HW, Song JH, Kim HE. Nanofiber generation of gelatin–hydroxyapatite biomimetics for guided tissue regeneration. *Advanced Functional Materials* 2005; 15(12): 1988-1994.
- [175] Sailaja GS, Ramesh P, Vellappally S, Anil S, Varma HK. Biomimetic approaches with smart interfaces for bone regeneration. *Journal of Biomedical Science* 2016; 23(1): 77-77.
- [176] Polo-Corrales L, Latorre-Esteves M, Ramirez-Vick JE. Scaffold design for bone regeneration. *Journal of Nanoscience and Nanotechnology* 2014; 14(1): 15-56.
- [177] Chan BP, Leong KW. Scaffolding in tissue engineering: General approaches and tissue-specific considerations. *European Spine Journal* 2008; 17(4): 467-479.
- [178] Amini AR, Laurencin CT, Nukavarapu SP. Bone tissue engineering: Recent advances and challenges. *Critical Reviews in Biomedical Engineering* 2012; 40(5): 363-408.

- [179] Abdal-hay A, Vanegas P, Hamdy AS, Engel FB, Lim JH. Preparation and characterization of vertically arrayed hydroxyapatite nanoplates on electrospun nanofibers for bone tissue engineering. *Chemical Engineering Journal* 2014; 254: 612-622.
- [180] Kim Y, Kim G. Highly roughened polycaprolactone surfaces using oxygen plasma-etching and in vitro mineralization for bone tissue regeneration: Fabrication, characterization, and cellular activities. *Colloids and Surfaces B: Biointerfaces* 2015; 125: 181-189.
- [181] Rezaei F, Abbasi-Firouzjah M, Shokri B. Investigation of antibacterial and wettability behaviours of plasma-modified pmma films for application in ophthalmology. *Journal of Physics D: Applied Physics* 2014; 47(8): 085401.
- [182] Yang H, Fung S-Y, Pritzker M, Chen P. Modification of hydrophilic and hydrophobic surfaces using an ionic-complementary peptide. *PLoS One* 2007; 2(12): 1325.
- [183] Man Z, Yin L, Shao Z, Zhang X, Hu X, Zhu J, et al. The effects of co-delivery of bmsc-affinity peptide and rhtgf- β 1 from coaxial electrospun scaffolds on chondrogenic differentiation. *Biomaterials* 2014; 35(19): 5250-5260.
- [184] Deng Y, Yang Y, Wei S. Peptide-decorated nanofibrous niche augments in vitro directed osteogenic conversion of human pluripotent stem cells. *Biomacromolecules* 2017; 18(2): 587-598.
- [185] De Geyter N, Morent R, Leys C, Gengembre L, Payen E. Treatment of polymer films with a dielectric barrier discharge in air, helium and argon at medium pressure. *Surface Coatings Technology* 2007; 201(16-17): 7066-7075.
- [186] Cui W, Li X, Xie C, Zhuang H, Zhou S, Weng J. Hydroxyapatite nucleation and growth mechanism on electrospun fibers functionalized with different chemical groups and their combinations. *Biomaterials* 2010; 31(17): 4620-4629.
- [187] Sarvestani AS, He X, Jabbari E. Osteonectin-derived peptide increases the modulus of a bone-mimetic nanocomposite. *European Biophysics Journal* 2008; 37(2): 229-234.

- [188] Mavis B, Demirtaş TT, Gümüşdereliolu M, Gündüz G, Çolak Ü. Synthesis, characterization and osteoblastic activity of polycaprolactone nanofibers coated with biomimetic calcium phosphate. *Acta Biomaterialia* 2009; 5(8): 3098-3111.
- [189] Deng H, Wang S, Wang X, Du C, Shen X, Wang Y, et al. Two competitive nucleation mechanisms of calcium carbonate biomineralization in response to surface functionality in low calcium ion concentration solution. *Regenerative Biomaterials* 2015; 2(3): 187-195.
- [190] Tavafoghi M, Brodusch N, Gauvin R, Cerruti M. Hydroxyapatite formation on graphene oxide modified with amino acids: Arginine versus glutamic acid. *Journal of the Royal Society Interface* 2016; 13(114): 20150986.
- [191] Deng X, Hao J, Wang C. Preparation and mechanical properties of nanocomposites of poly(d,l-lactide) with Ca-deficient hydroxyapatite nanocrystals. *Biomaterials* 2001; 22(21): 2867-2873.
- [192] Zhang Y, Venugopal JR, El-Turki A, Ramakrishna S, Su B, Lim CT. Electrospun biomimetic nanocomposite nanofibers of hydroxyapatite/chitosan for bone tissue engineering. *Biomaterials* 2008; 29(32): 4314-4322.
- [193] Ramalingam M, Jabbari E, Ramakrishna S, Khademhosseini A. *Micro and Nanotechnologies in Engineering Stem Cells and Tissues*, 1st ed. John Wiley & Sons; 2013.
- [194] Sheikh FA, Ju HW, Moon BM, Park HJ, Kim JH, Lee OJ, et al. A novel approach to fabricate silk nanofibers containing hydroxyapatite nanoparticles using a three-way stopcock connector. *Nanoscale Research Letters* 2013; 8(1): 303-303.
- [195] Siddiqa AJ, Maji S, Chaudhury K, Adhikari B. A facile route to develop hydrophilicity on the polyolefin surface for biomedical applications. *Advances in Polymer Technology* 2017.
- [196] Birhanu G, Akbari Javar H, Seyedjafari E, Zandi-Karimi A, Dusti Telgerd M. An improved surface for enhanced stem cell proliferation and osteogenic differentiation using electrospun composite PLLA/P123 scaffold. *Artificial Cells, Nanomedicine, and Biotechnology* 2018; 46(6): 1274-1281.

- [197] Rana D, Ramasamy K, Leena M, Jimenez C, Campos J, Ibarra P, et al. Surface functionalization of nanobiomaterials for application in stem cell culture, tissue engineering, and regenerative medicine. *Biotechnology Progress* 2016; 32(3): 554-567.
- [198] Dimitriou R, Mataliotakis GI, Calori GM, Giannoudis PVJBm. The role of barrier membranes for guided bone regeneration and restoration of large bone defects: Current experimental and clinical evidence. *BMC Medicine* 2012; 10(1): 81.
- [199] Gungormus M, Branco M, Fong H, Schneider JP, Tamerler C, Sarikaya M. Self assembled bi-functional peptide hydrogels with biomineralization-directing peptides. *Biomaterials* 2010; 31(28): 7266-7274.
- [200] García-García A, Martín I. Extracellular matrices to modulate the innate immune response and enhance bone healing. *Frontiers in Immunology* 2019; 10(2256).
- [201] Onak G, Şen M, Horzum N, Ercan UK, Yaralı ZB, Garipcan B, et al. Aspartic and glutamic acid templated peptides conjugation on plasma modified nanofibers for osteogenic differentiation of human mesenchymal stem cells: A comparative study. *Scientific Reports* 2018; 8(1): 17620.
- [202] Xu J, Feng Q, Lin S, Yuan W, Li R, Li J, et al. Injectable stem cell-laden supramolecular hydrogels enhance in situ osteochondral regeneration via the sustained co-delivery of hydrophilic and hydrophobic chondrogenic molecules. *Biomaterials* 2019; 210: 51-61.
- [203] He B, Ou Y, Zhou A, Chen S, Zhao W, Zhao J, et al. Functionalized d-form self-assembling peptide hydrogels for bone regeneration. *Drug Design, Development and Therapy* 2016; 10: 1379-1388.
- [204] Kisiday J, Jin M, Kurz B, Hung H, Semino C, Zhang S, et al. Self-assembling peptide hydrogel fosters chondrocyte extracellular matrix production and cell division: Implications for cartilage tissue repair. *Proceedings of the National Academy of Sciences* 2002; 99(15): 9996.

- [205] Sung Eun K, Dong Nyoung H, Jung Bok L, Jong Ryul K, Sang Hyuk P, Seong Ho J, et al. Electrospun gelatin/polyurethane blended nanofibers for wound healing. *Biomedical Materials* 2009; 4(4): 044106.
- [206] Kim SH, Hur W, Kim JE, Min HJ, Kim S, Min HS, et al. Self-assembling peptide nanofibers coupled with neuropeptide substance p for bone tissue engineering. *Tissue Engineering Part A* 2015; 21(7-8): 1237-1246.
- [207] Tsutsumi H, Kawamura M, Mihara H. Osteoblastic differentiation on hydrogels fabricated from ca(2+)-responsive self-assembling peptides functionalized with bioactive peptides. *Bioorganic & Medicinal Chemistry* 2018; 26(12): 3126-3132.
- [208] Bian L, Guvendiren M, Mauck RL, Burdick JA. Hydrogels that mimic developmentally relevant matrix and n-cadherin interactions enhance msc chondrogenesis. *Proc Natl Acad Sci U S A* 2013; 110(25): 10117-10122.
- [209] Kang Y, Kim S, Fahrenholtz M, Khademhosseini A, Yang Y. Osteogenic and angiogenic potentials of monocultured and co-cultured human-bone-marrow-derived mesenchymal stem cells and human-umbilical-vein endothelial cells on three-dimensional porous beta-tricalcium phosphate scaffold. *Acta Biomaterialia* 2013; 9(1): 4906-4915.
- [210] Schecke JH, Lehmann KE, Buschmann IR, Unger T, Funke-Kaiser H. Quantitative real-time RT-PCR data analysis: Current concepts and the novel “gene expression’s ctdifference” formula. *Journal of Molecular Medicine* 2006; 84(11): 901-910.
- [211] Li J, Xing R, Bai S, Yan X. Recent advances of self-assembling peptide-based hydrogels for biomedical applications. *Soft Matter* 2019; 15(8): 1704-1715.
- [212] Bairagi D, Biswas P, Basu K, Hazra S, Hermida-Merino D, Sinha DK, et al. Self-assembling peptide-based hydrogel: Regulation of mechanical stiffness and thermal stability and 3d cell culture of fibroblasts. *ACS Applied Bio Materials* 2019; 2(12): 5235-5244.

- [213] Sun J, Zheng Q, Wu Y, Liu Y, Guo X, Wu W. Biocompatibility of kld-12 peptide hydrogel as a scaffold in tissue engineering of intervertebral discs in rabbits. *Journal of Huazhong University of Science and Technology - Medical Science* 2010; 30(2): 173-177.
- [214] Whitesides GM, Mathias JP, Seto CT. Molecular self-assembly and nanochemistry: A chemical strategy for the synthesis of nanostructures. *Science* 1991; 254(5036): 1312-1319.
- [215] Aldilla VR, Chen R, Martin AD, Marjo CE, Rich AM, Black DS, et al. Anthranilamide-based short peptides self-assembled hydrogels as antibacterial agents. *Scientific Reports* 2020; 10(1): 770.
- [216] Elgersma SV, Ha M, Yang J-LJ, Michaelis VK, Unsworth LD. Charge and peptide concentration as determinants of the hydrogel internal aqueous environment. *Materials (Basel, Switzerland)* 2019; 12(5): 832.
- [217] Marie PJ, Fromigué O. Osteogenic differentiation of human marrow-derived mesenchymal stem cells. *Regenerative Medicine* 2006; 1(4): 539-548.
- [218] Orimo H, Shimada T. The role of tissue-nonspecific alkaline phosphatase in the phosphate-induced activation of alkaline phosphatase and mineralization in saos-2 human osteoblast-like cells. *Molecular and Cellular Biochemistry* 2008; 315(1-2): 51-60.
- [219] Jafary F, Hanachi P, Gorjipour K. Osteoblast differentiation on collagen scaffold with immobilized alkaline phosphatase. *International Journal of Organ Transplantation Medicine* 2017; 8(4): 195-202.
- [220] Chen Y, Huang Z, Li X, Li S, Zhou Z, Zhang Y, et al. In vitro biocompatibility and osteoblast differentiation of an injectable chitosan/nano-hydroxyapatite/collagen scaffold. *Journal of Nanomaterials* 2012; 2012: 401084.
- [221] Nudelman F, Lausch AJ, Sommerdijk NA, Sone ED. In vitro models of collagen biomineralization. *Journal of Structural Biology* 2013; 183(2): 258-269.

- [222] Rademakers T, Horvath JM, van Blitterswijk CA, LaPointe VLS. Oxygen and nutrient delivery in tissue engineering: Approaches to graft vascularization. *Journal of Tissue Engineering and Regenerative Medicine* 2019; 13(10): 1815-1829.
- [223] Sarker MD, Naghieh S, Sharma NK, Chen X. 3d biofabrication of vascular networks for tissue regeneration: A report on recent advances. *Journal of Pharmaceutical Analysis* 2018; 8(5): 277-296.
- [224] Rouwkema J, Khademhosseini A. Vascularization and angiogenesis in tissue engineering: Beyond creating static networks. *Trends in Biotechnology* 2016; 34(9): 733-745.
- [225] Moon JJ, Saik JE, Poché RA, Leslie-Barbick JE, Lee S-H, Smith AA, et al. Biomimetic hydrogels with pro-angiogenic properties. *Biomaterials* 2010; 31(14): 3840-3847.
- [226] Nikolova MP, Chavali MS. Recent advances in biomaterials for 3d scaffolds: A review. *Bioactive materials* 2019; 4: 271-292.
- [227] Liu J, Chuah YJ, Fu J, Zhu W, Wang D-A. Co-culture of human umbilical vein endothelial cells and human bone marrow stromal cells into a micro-cavitary gelatin-methacrylate hydrogel system to enhance angiogenesis. *Materials Science and Engineering: C* 2019; 102: 906-916.
- [228] Böhrnsen F, Schliephake H. Supportive angiogenic and osteogenic differentiation of mesenchymal stromal cells and endothelial cells in monolayer and co-cultures. *International Journal of Oral Science* 2016; 8(4): 223-230.
- [229] Heo DN, Hospodiuk M, Ozbolat IT. Synergistic interplay between human mscs and huvecs in 3D spheroids laden in collagen/fibrin hydrogels for bone tissue engineering. *Acta Biomaterialia* 2019; 95: 348-356.
- [230] Simon-Assmann P, Orend G, Mammadova-Bach E, Spenle C, Lefebvre O. Role of laminins in physiological and pathological angiogenesis. *The International Journal of Developmental Biology* 2011; 55(4-5): 455-465.

- [231] Hohenester E, Yurchenco PD. Laminins in basement membrane assembly. *Cell Adhesion & Migration* 2013; 7(1): 56-63.
- [232] Kao G, Huang C, Hedgecock EM, Hall DH, Wadsworth WG. The role of the laminin β subunit in laminin heterotrimer assembly and basement membrane function and development in *C. Elegans*. *Developmental Biology* 2006; 290(1): 211-219.
- [233] Grant DS, Kinsella JL, Fridman R, Auerbach R, Piasecki BA, Yamada Y, et al. Interaction of endothelial cells with a laminin α chain peptide (sikvav) in vitro and induction of angiogenic behavior in vivo. *Journal of Cellular Physiology* 1992; 153(3): 614-625.
- [234] Jun HW, West J. Development of a yigrs-peptide-modified polyurethaneurea to enhance endothelialization. *Journal of Biomaterials Science, Polymer Edition* 2004; 15(1): 73-94.
- [235] Jain R, Roy S. Designing a bioactive scaffold from coassembled collagen–laminin short peptide hydrogels for controlling cell behaviour. *RSC Advances* 2019; 9(66): 38745-38759.
- [236] Ali S, Saik JE, Gould DJ, Dickinson ME, West JL. Immobilization of cell-adhesive laminin peptides in degradable pegda hydrogels influences endothelial cell tubulogenesis. *BioResearch Open Access* 2013; 2(4): 241-249.
- [237] Onak G, Gökmen O, Yaralı ZB, Karaman O. Enhanced osteogenesis of human mesenchymal stem cells by self-assembled peptide hydrogel functionalized with glutamic acid templated peptides. *Journal of Tissue Engineering and Regenerative Medicine* 2020; 14(9): 1236-1249.
- [238] Harper MM, Connolly ML, Goldie L, Irvine EJ, Shaw JE, Jayawarna V, et al. *Biogelx: Cell culture on self-assembling peptide gels*. Ed.: Nilsson B, Doran T. Peptide self-assembly. Humana Press; 2018. 283-303.
- [239] Kokubo T, Takadama H. How useful is sbf in predicting in vivo bone bioactivity? *Biomaterials* 2006; 27(15): 2907-2915.

- [240] Barati D, Moeinzadeh S, Karaman O, Jabbari E. Time dependence of material properties of polyethylene glycol hydrogels chain extended with short hydroxy acid segments. *Polymer (Guildf)* 2014; 55(16): 3894-3904.
- [241] Yaralı ZB, Onak G, Karaman O. Effect of integrin binding peptide on vascularization of scaffold-free microtissue spheroids. *Tissue Engineering and Regenerative Medicine* 2020; 17(5): 595-605.
- [242] Wang C, Li Y, Yang M, Zou Y, Liu H, Liang Z, et al. Efficient differentiation of bone marrow mesenchymal stem cells into endothelial cells in vitro. *European Journal of Vascular and Endovascular Surgery* 2018; 55(2): 257-265.
- [243] Livak KJ, Schmittgen TD. Analysis of relative gene expression data using real-time quantitative pcr and the $2^{-\Delta\Delta Ct}$ method. *Methods* 2001; 25(4): 402-408.
- [244] Carpentier G, Berndt S, Ferratge S, Rasband W, Cuendet M, Uzan G, et al. Angiogenesis analyzer for image j - a comparative morphometric analysis of “endothelial tube formation assay” and “fibrin bead assay”. *Scientific Reports* 2020; 10(1): 11568.
- [245] Oliviero O, Ventre M, Netti PA. Functional porous hydrogels to study angiogenesis under the effect of controlled release of vascular endothelial growth factor. *Acta Biomaterialia* 2012; 8(9): 3294-3301.
- [246] Xiao X, Wang W, Liu D, Zhang H, Gao P, Geng L, et al. The promotion of angiogenesis induced by three-dimensional porous beta-tricalcium phosphate scaffold with different interconnection sizes via activation of pi3k/akt pathways. *Scientific Reports* 2015; 5(1): 9409.
- [247] Eljezi T, Pinta P, Richard D, Pinguet J, Chezal JM, Chagnon MC, et al. In vitro cytotoxic effects of dehp-alternative plasticizers and their primary metabolites on a 1929 cell line. *Chemosphere* 2017; 173: 452-459.
- [248] Mu X, Shi L, Pan S, He L, Niu Y, Wang X. A customized self-assembling peptide hydrogel-wrapped stem cell factor targeting pulp regeneration rich in vascular-like structures. *ACS Omega* 2020; 5(27): 16568-16574.

- [249] Kraehenbuehl TP, Zammaretti P, Van der Vlies AJ, Schoenmakers RG, Lutolf MP, Jaconi ME, et al. Three-dimensional extracellular matrix-directed cardioprogenitor differentiation: Systematic modulation of a synthetic cell-responsive peg-hydrogel. *Biomaterials* 2008; 29(18): 2757-2766.
- [250] Lee SH, Lee Y, Chun YW, Crowder SW, Young PP, Park KD, et al. In situ crosslinkable gelatin hydrogels for vasculogenic induction and delivery of mesenchymal stem cells. *Advanced Functional Materials* 2014; 24(43): 6771-6781.
- [251] Lee Y, Balikov DA, Lee JB, Lee SH, Lee SH, Lee JH, et al. In situ forming gelatin hydrogels-directed angiogenic differentiation and activity of patient-derived human mesenchymal stem cells. *International Journal of Molecular Sciences* 2017; 18(8): 1705.
- [252] Tokatlian T, Cam C, Segura T. Non-viral DNA delivery from porous hyaluronic acid hydrogels in mice. *Biomaterials* 2014; 35(2): 825-835.
- [253] Koch F, Müller M, König F, Meyer N, Gattlen J, Pieles U, et al. Mechanical characteristics of beta sheet-forming peptide hydrogels are dependent on peptide sequence, concentration and buffer composition. *Royal Society Open Science* 2018; 5(3): 171562-171562.
- [254] Vig K, Chaudhari A, Tripathi S, Dixit S, Sahu R, Pillai S, et al. Advances in skin regeneration using tissue engineering. *International Journal of Molecular Sciences* 2017; 18(4): 789.
- [255] Ju YM, Atala A, Yoo JJ, Lee SJ. In situ regeneration of skeletal muscle tissue through host cell recruitment. *Acta Biomaterialia* 2014; 10(10): 4332-4339.
- [256] Lin H, Tang Y, Lozito TP, Oyster N, Wang B, Tuan RS. Efficient in vivo bone formation by bmp-2 engineered human mesenchymal stem cells encapsulated in a projection stereolithographically fabricated hydrogel scaffold. *Stem Cell Research & Therapy* 2019; 10(1): 254-254.

- [257] Grant DS, Tashiro K, Segui-Real B, Yamada Y, Martin GR, Kleinman HK. Two different laminin domains mediate the differentiation of human endothelial cells into capillary-like structures in vitro. *Cell* 1989; 58(5): 933-943.
- [258] Lin Y, Singh A, Ebenso EE, Wu Y, Zhu C, Zhu H. Effect of poly(methyl methacrylate-co-n-vinyl-2-pyrrolidone) polymer on j55 steel corrosion in 3.5% nacl solution saturated with co2. *Journal of the Taiwan Institute Of Chemical Engineers* 2015; 46: 214-222.
- [259] Ucuzian AA, Gassman AA, East AT, Greisler HP. Molecular mediators of angiogenesis. *Journal of Burn Care & Research* 2010; 31(1): 158-175.
- [260] Goncharov NV, Nadeev AD, Jenkins RO, Avdonin PV. Markers and biomarkers of endothelium: When something is rotten in the state. *Oxidative Medicine and Cellular Longevity* 2017; 2017: 9759735-9759735.
- [261] O'Brien CD, Cao G, Makrigiannakis A, DeLisser HM. Role of immunoreceptor tyrosine-based inhibitory motifs of pecam-1 in pecam-1-dependent cell migration. *American Journal of Physiology-Cell Physiology* 2004; 287(4): 1103-1113.
- [262] Simon AM, McWhorter AR. Vascular abnormalities in mice lacking the endothelial gap junction proteins connexin37 and connexin40. *Developmental Biology* 2002; 251(2): 206-220.
- [263] Soucy PA, Romer LH. Endothelial cell adhesion, signaling, and morphogenesis in fibroblast-derived matrix. *Matrix Biology* 2009; 28(5): 273-283.
- [264] Lin C-S, Xin Z-C, Dai J, Lue TF. Commonly used mesenchymal stem cell markers and tracking labels: Limitations and challenges. *Histology and Histopathology* 2013; 28(9): 1109-1116.
- [265] Yamamoto K, Takahashi T, Asahara T, Ohura N, Sokabe T, Kamiya A, et al. Proliferation, differentiation, and tube formation by endothelial progenitor cells in response to shear stress. *Journal of Applied Physiology* 2003; 95(5): 2081-2088.

- [266] Noria S, Cowan DB, Gotlieb AI, Langille BL. Transient and steady-state effects of shear stress on endothelial cell adherens junctions. *Circulation Research* 1999; 85(6): 504-514.
- [267] Navaratna D, Maestas J, McGuire PG, Das A. Suppression of retinal neovascularization with an antagonist to vascular endothelial cadherin. *Archives of Ophthalmology* 2008; 126(8): 1082-1088.
- [268] Ruoslahti E. Rgd and other recognition sequences for integrins. *Annual Review of Cell and Developmental Biology* 1996; 12: 697-715.
- [269] Chen C-S, Chang J-H, Srimaneepong V, Wen J-Y, Tung O-H, Yang C-H, et al. Improving the in vitro cell differentiation and in vivo osseointegration of titanium dental implant through oxygen plasma immersion ion implantation treatment. *Surface and Coatings Technology* 2020; 399: 126125.
- [270] Cardoso R, Gerngross P, Dominici J, Kiat-Amnuay S. Survey of currently selected dental implants and restorations by prosthodontists. *The International Journal of Oral & Maxillofacial Implants* 2013; 28: 1017-1025.
- [271] Duncan WJ, Greer PFC, Lee M-H, Loch C, Gay JHA. Wool-derived keratin hydrogel enhances implant osseointegration in cancellous bone. *Journal of Biomedical Materials Research Part B: Applied Biomaterials* 2018; 106(6): 2447-2454.
- [272] Le Guéhennec L, Soueidan A, Layrolle P, Amouriq Y. Surface treatments of titanium dental implants for rapid osseointegration. *Dental Materials* 2007; 23(7): 844-854.
- [273] Novaes Jr AB, Souza SLSd, Barros RRMd, Pereira KKY, Iezzi G, Piattelli A. Influence of implant surfaces on osseointegration. *Brazilian Dental Journal* 2010; 21: 471-481.
- [274] Avila G, Misch K, Galindo-Moreno P, Wang H-L. Implant surface treatment using biomimetic agents. *Implant Dentistry* 2009; 18(1): 17-26.

- [275] Xu B, Ye J, Yuan F-Z, Zhang J-Y, Chen Y-R, Fan B-S, et al. Advances of stem cell-laden hydrogels with biomimetic microenvironment for osteochondral repair. *Front Bioeng Biotechnol* 2020; 8: 247.
- [276] Li D, Zhou J, Zhang M, Ma Y, Yang Y, Han X, et al. Long-term delivery of alendronate through an injectable tetra-peg hydrogel to promote osteoporosis therapy. *Biomaterials Science* 2020; 8(11): 3138-3146.
- [277] Ma R, Wang C, Mao S, Shao Y, Wang Z, Wang Y, et al. Luminescence in manganese (ii)-doped srzn2s2o crystals from multiple energy conversion. *Frontiers in Chemistry* 2020; 8(752).
- [278] Gasik M. Understanding biomaterial-tissue interface quality: Combined in vitro evaluation. *Science and Technology of Advanced Materials* 2017; 18(1): 550-562.
- [279] Senger DR, Davis GE. Angiogenesis. *Cold Spring Harbor Perspectives in Biology* 2011; 3(8): 5090-5090.
- [280] Breithaupt-Faloppa AC, de Lima WT, Oliveira-Filho RM, Kleinheinz J. In vitro behaviour of endothelial cells on a titanium surface. *Head & Face Medicine* 2008; 4: 14-14.
- [281] Pankajakshan D, Kansal V, Agrawal DK. In vitro differentiation of bone marrow derived porcine mesenchymal stem cells to endothelial cells. *Journal of Tissue Engineering and Regenerative Medicine* 2013; 7(11): 911-920.
- [282] Nuss KMR, von Rechenberg B. Biocompatibility issues with modern implants in bone - a review for clinical orthopedics. *The open orthopaedics journal* 2008; 2: 66-78.
- [283] W. Nicholson J. Titanium alloys for dental implants: A review. *Prosthesis* 2020; 2(2): 100-116.
- [284] Bosshardt DD, Chappuis V, Buser D. Osseointegration of titanium, titanium alloy and zirconia dental implants: Current knowledge and open questions. *Periodontology 2000* 2017; 73(1): 22-40.

- [285] Beiki B, Zeynali B, Taghiabadi E, Seyedjafari E, Kehtari M. Osteogenic differentiation of wharton's jelly-derived mesenchymal stem cells cultured on wj-scaffold through conventional signalling mechanism. *Artificial Cells, Nanomedicine, and Biotechnology* 2018; 46(sup3): S1032-S1042.
- [286] Kocherova I, Bryja A, Mozdziak P, Angelova Volponi A, Dyszkiewicz-Konwińska M, Piotrowska-Kempisty H, et al. Human umbilical vein endothelial cells (huvecs) co-culture with osteogenic cells: From molecular communication to engineering prevascularised bone grafts. *Journal of Clinical Medicine* 2019; 8(10): 1602.
- [287] Fernandez de Grado G, Keller L, Idoux-Gillet Y, Wagner Q, Musset A-M, Benkirane-Jessel N, et al. Bone substitutes: A review of their characteristics, clinical use, and perspectives for large bone defects management. *Journal of Tissue Engineering* 2018; 9: 20-41.
- [288] Tomlinson RE, Silva MJ. Skeletal blood flow in bone repair and maintenance. *Bone Research* 2013; 1(1): 311-322.
- [289] Lyu H-Z, Lee JH. The efficacy of rhbmp-2 loaded hydrogel composite on bone formation around dental implants in mandible bone defects of minipigs. *Biomaterials Research* 2020; 24(1): 5.
- [290] Langenfeld EM, Langenfeld J. Bone morphogenetic protein-2 stimulates angiogenesis in developing tumors. *Molecular Cancer Research* 2004; 2(3): 141-149.
- [291] Patil P, Nimbalkar-Patil S. Lost wax-bolus technique to process closed hollow obturator with uniform wall thickness using single flasking procedure. *Journal of the International Clinical Dental Research Organization* 2016; 8(1): 84-88.
- [292] Atsumi M, Park S-H, Wang H-L. Methods used to assess implant stability: Current status. *The International Journal of Oral & Maxillofacial Implants* 2007; 22: 743-754.

- [293] Damien CJ, Parsons JR. Bone graft and bone graft substitutes: A review of current technology and applications. *Journal of Applied Biomaterials* 1991; 2(3): 187-208.
- [294] Kretlow JD, Young S, Klouda L, Wong M, Mikos AG. Injectable biomaterials for regenerating complex craniofacial tissues. *Advanced Materials* 2009; 21(32-33): 3368-3393.
- [295] Burg KJ, Porter S, Kellam JF. Biomaterial developments for bone tissue engineering. *Biomaterials* 2000; 21(23): 2347-2359.
- [296] Frohlich M, Grayson WL, Wan LQ, Marolt D, Drobnic M, Vunjak-Novakovic G. Tissue engineered bone grafts: Biological requirements, tissue culture and clinical relevance. *Current Stem Cell Research & Therapy* 2008; 3(4): 254-264.
- [297] Yue Z, Wen F, Gao S, Ang MY, Pallathadka PK, Liu L, et al. Preparation of three-dimensional interconnected macroporous cellulosic hydrogels for soft tissue engineering. *Biomaterials* 2010; 31(32): 8141-8152.
- [298] Yue S, He H, Li B, Hou T. Hydrogel as a biomaterial for bone tissue engineering: A review. *Nanomaterials (Basel, Switzerland)* 2020; 10(8): 1511.
- [299] Caplan MR, Schwartzfarb EM, Zhang S, Kamm RD, Lauffenburger DA. Control of self-assembling oligopeptide matrix formation through systematic variation of amino acid sequence. *Biomaterials* 2002; 23(1): 219-227.
- [300] Caplan MR, Moore PN, Zhang S, Kamm RD, Lauffenburger DA. Self-assembly of a beta-sheet protein governed by relief of electrostatic repulsion relative to van der waals attraction. *Biomacromolecules* 2000; 1(4): 627-631.
- [301] Liu X, Chen W, Zhang C, Thein-Han W, Hu K, Reynolds MA, et al. Co-seeding human endothelial cells with human-induced pluripotent stem cell-derived mesenchymal stem cells on calcium phosphate scaffold enhances osteogenesis and vascularization in rats. *Tissue Engineering Part A* 2017; 23(11-12): 546-555.

- [302] Garvin KA, Dalecki D, Hocking DC. Vascularization of three-dimensional collagen hydrogels using ultrasound standing wave fields. *Ultrasound in Medicine & Biology* 2011; 37(11): 1853-1864.
- [303] Carmeliet P, Jain RK. Angiogenesis in cancer and other diseases. *Nature* 2000; 407(6801): 249-257.
- [304] Seebach C, Henrich D, Kähling C, Wilhelm K, Tami AE, Alini M, et al. Endothelial progenitor cells and mesenchymal stem cells seeded onto β -tcp granules enhance early vascularization and bone healing in a critical-sized bone defect in rats. *Tissue Engineering Part A* 2010; 16(6): 1961-1970.
- [305] Hart NH, Nimphius S, Rantalainen T, Ireland A, Siafarikas A, Newton RU. Mechanical basis of bone strength: Influence of bone material, bone structure and muscle action. *Journal of Musculoskeletal & Neuronal Interactions* 2017; 17(3): 114-139.
- [306] Kim BJ, Choi YS, Cha HJ. Reinforced multifunctionalized nanofibrous scaffolds using mussel adhesive proteins. *Angewandte Chemie International Edition* 2012; 51(3): 675-678.
- [307] Bai X, Gao M, Syed S, Zhuang J, Xu X, Zhang X-Q. Bioactive hydrogels for bone regeneration. *Bioactive materials* 2018; 3(4): 401-417.
- [308] Onak G, Gökmen O, Çevik ZB, Karaman O. Role of functionalized self-assembled peptide hydrogel on in vitro vasculogenesis. *Soft Matter* 2021.

Appendices

Appendix A

The Characterization Data of Peptides

Table A.1: Sequences, observed and calculated molecular weight of synthesized peptides

Name	Sequence	Calculated	Observed
GLU	EEEEEE	792.71	793.17
KLD	KLDLKLDLKLDL	1425,78	1422,68
KLD-O1	KLDLKLDLKLDL-EEGGC	1901,26	1900,08
KLD-O2	KLDLKLDLKLDL-EEEEEE	2071,35	2070,32
KLD-V1	KLDLKLDLKLDL-IKVAV	1936,45	1935,42
KLD-V2	KLDLKLDLKLDL-YIGSR	2002,43	2002,00

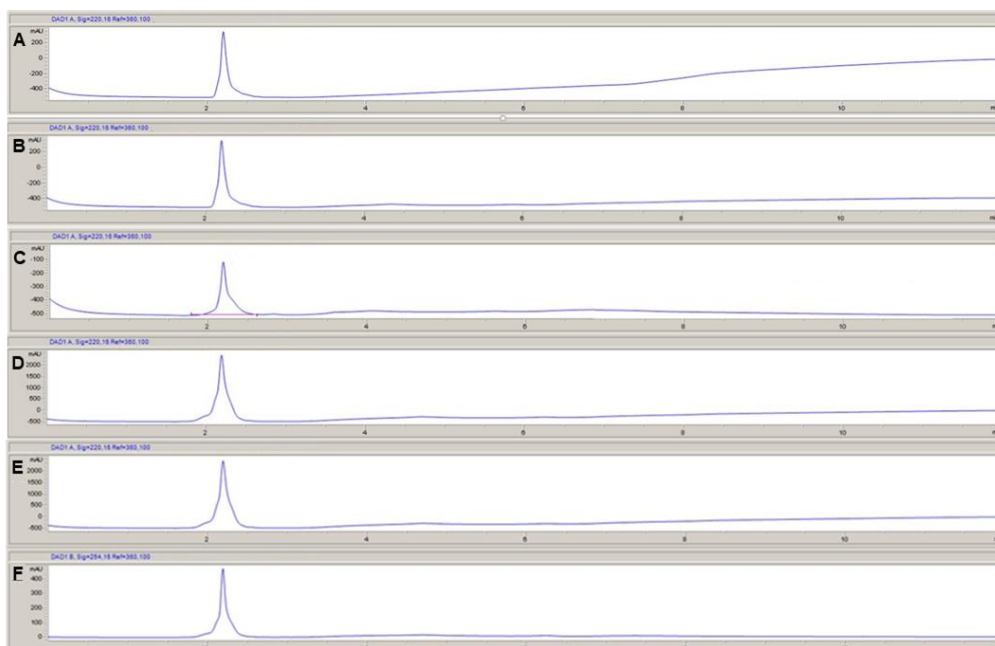


Figure A.1: Liquid chromatography spectra of A) GLU, B) KLD, C) KLD-O1, D) KLD-O2, E) KLD-V1, and F) KLD-V2

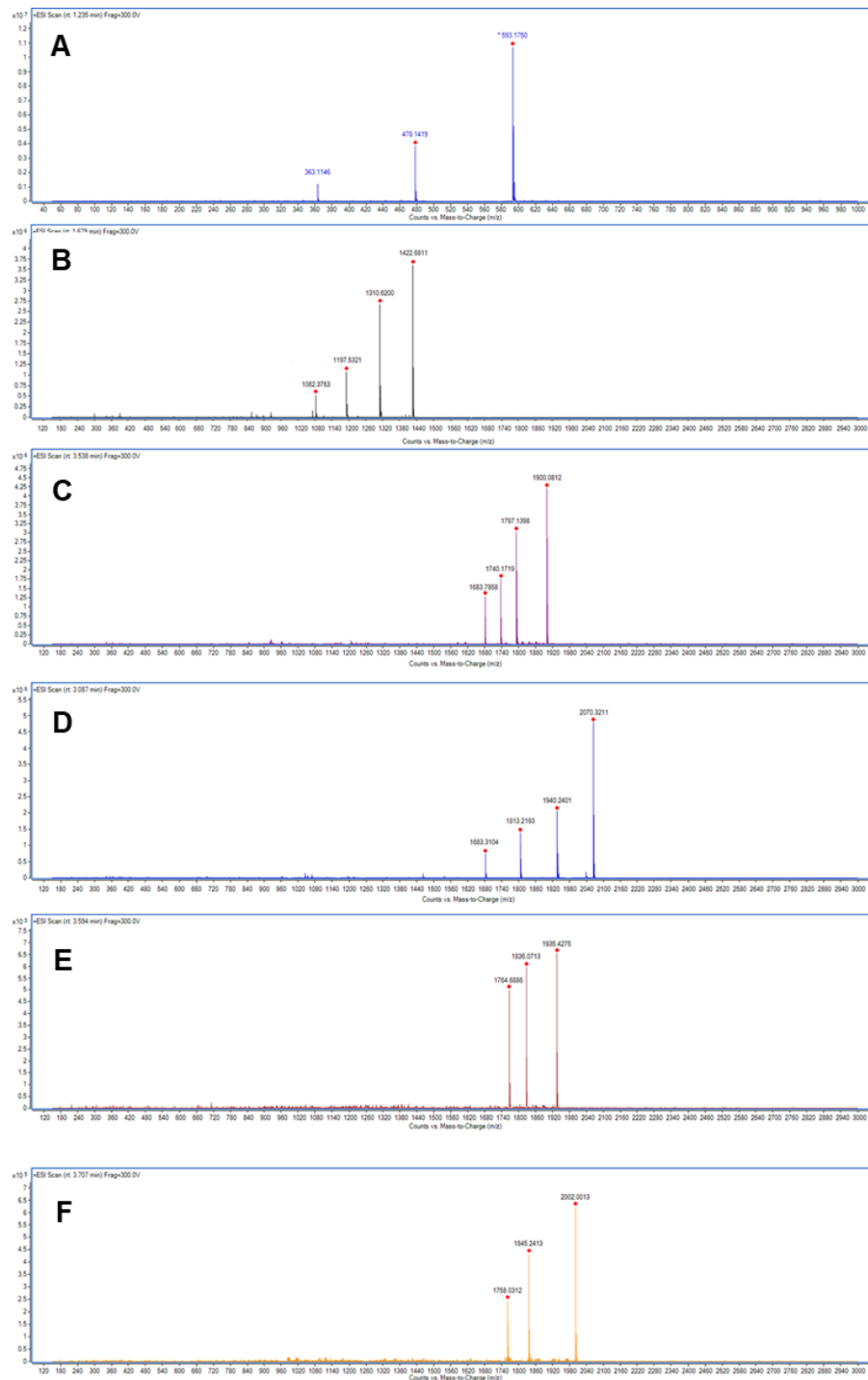


Figure A.2: Ionization mass spectra of A) GLU, B) KLD, C) KLD-O1, D) KLD-O2, E) KLD-V1, and F) KLD-V2

Appendix B

Publications from the Thesis

Conference Papers

1. Onak G., Gökmen O., Karaman O., Self-assembled peptide hydrogel for accelerating the osseointegration period of dental implants, TERMIS EU, Tissue Engineering and Regenerative Medicine European Chapter Meeting, 27-31 May 2019, Rhodes, GREECE (Oral Presentation)
2. Onak G., Ercan U.K, Şen M, Horzum Polat N., Garipcan B., Karaman O., Effective Surface Modification of Bone Sialoprotein Mimetic Peptide on Align Nanofibers with Cold Atmospheric Plasma, ICPM-7, 7th International Conference on Plasma Medicine, 17-22 June 2018, Philadelphia, USA (Oral Presentation)

Journal Articles

1. Onak G., Karaman O. “Accelerated mineralization on nanofibers via non-thermal atmospheric plasma assisted glutamic acid templated peptide conjugation”, *Regenerative Biomaterials*, 2019
2. Onak G., Gökmen O., Yaralı Z.B, Karaman O. “Enhanced Osteogenesis of Human Mesenchymal Stem Cells by Self-Assembled Peptide Hydrogel Functionalized with Glutamic Acid Templated Peptides”, *Journal of Tissue Engineering and Regenerative Medicine*, 2020
3. Onak G., Gökmen O., Yaralı Z.B, Karaman O. “Role of Functionalized Self-Assembled Peptide Hydrogel on In Vitro Vasculogenesis”, *Soft Matter*, 2021

Projects

1. Dental implantların osseointegrasyon süresinin hızlandırılması amaçlı çok işlevli kendiliğinden yapılanan peptid hidrojel geliştirilmesi ve etkinliğinin in vitro ve in vivo değerlendirilmesi (117S429 TÜBİTAK (The Scientific and Technological Research Council of Turkey))
2. Kemik Doku Uygulamaları için Peptit ile Modifiye Edilmiş Biyoaktif Malzemelerin Geliştirilmesi (Coordination Office of Scientific Research Projects through the Research Project 2021-TDR-FEBE-0001)

Appendix C

Ethical Committee Approval

EGE ÜNİVERSİTESİ
HAYVAN DENEYLERİ YEREL ETİK KURULU

SAYI: 2019-110
KONU: Onay

11.12.2019

Etik kurulumuza yapmış olduğunuz başvuru doğrultusunda "DENTAL İMPLANTLARIN OSSEOİNTEGRASYON SÜRESİNİN HIZLANDIRILMASI AMAÇLI ÇOK İŞLEVLİ KENDİLİĞİNDEN YAPILANAN PEPTİD HİDROJEL GELİŞTİRİLMESİ VE ETKİNLİĞİNİN *İN VİTRO* VE *İN VİVO* DEĞERLENDİRİLMESİ" isimli araştırma projeniz değerlendirilmiştir.

Yürütücü: Dr. Öğr. Üyesi. Ozan KARAMAN İKÇÜ Mühendislik Fak. Biyomedikal Mühendisliği AD.
Prof. Dr. Hafize Seda VATANSEVER CBÜ Tıp Fakültesi Histoloji ve Embriyoloji AD.
Doç. Dr. Murat ULU, İKÇÜ Diş Hekimliği Fakültesi Ağız, Diş ve Çene Cerrahisi AD.
Dr. Ömer ANKAYA, İKÇÜ Diş Hekimliği Fakültesi Ağız, Diş ve Çene Cerrahisi AD.

Proje başvuru formunuzda belirtildiği koşullarda olarak, 27 Yeni Zelanda Tavşanı deney hayvanları kullanarak araştırmayı gerçekleştirmeniz kurulumuz tarafından uygun bulunmuştur. Saygılarımla bilgilerinizi rica ederim.

Prof. Dr. Lokman OZTURK
(E.Ü. Hayvan Deneyleri Yerel Etik Kurulu Başkanı)

Prof. Dr. N. Ülkü KARABAY YAVAŞOĞLU

Prof. Dr. Hüseyin TEZEL

Prof. Dr. Haşmet ÇAĞIRGAN

Prof. Dr. Uğur KAYA

(KATILMADI)
Öğr. Gör. Dr. M. Ayberk OKTAY

Özcan NALBANTOĞLU

Prof. Dr. Aytül ÖNAL (KATILMADI)

Prof. Dr. Altuğ YAVAŞOĞLU

Prof. Dr. Figen KIRKPINAR (KATILMADI)

Dr. Öğr. Üyesi Sumru SÖZER KARADAĞLI

Vet. Hek. F. Enişah SOYLU

Figure C.1: Ethical Committee Approval

Curriculum Vitae

Name Surname : Günnur Pulat

E-mail (1) :

E-mail (2) :

Education:

2009–2013 Namık Kemal University, Dept. of Biomedical Eng. (B.S.)

2015–2019 Boğaziçi University, Dept. of Biomedical Eng. (M.S)

Work Experience:

2016 – Present Izmir Katip Çelebi University, Research Assistant

2015-2016 AstraZeneca, Long Term Internship

Publications

1. Onak G., Gökmen O., Yaralı Z.B, Karaman O. “Role of Functionalized Self-Assembled Peptide Hydrogel on In Vitro Vasculogenesis”, *Soft Matter*, 2021
2. Topaloğlu N, Yünlü M., Bakay E., “Induced photo-cytotoxicity on prostate cancer cells with the photodynamic action of toluidine Blue ortho” *Photodiagnosis and Photodynamic Therapy*, 2021
3. Onak G., Ercan U.K, Karaman O., “Antibacterial activity of antimicrobial peptide-conjugated nanofibrous membranes” *Biomedical Materials*, 2020
4. Topaloğlu N, Kadıköylü G., Onak G., Karaman O., “The effect of indocyanine green-based photodynamic therapy on healthy fibroblast and keratinocyte cells” *Photodiagnosis and Photodynamic Therapy*, 2020
5. Seven F., Gölcez T., Yaralı Z.B, Onak G., Karaman O., Şen M., “Guiding neural extensions of PC12 cells on carbon nanotube tracks dielectrophoretically formed in poly (ethylene glycol) dimethacrylate”, *RSC Advances*, 2020

6. Onak G., Gökmen O., Yaralı Z.B, Karaman O. “Enhanced Osteogenesis of Human Mesenchymal Stem Cells by Self-Assembled Peptide Hydrogel Functionalized with Glutamic Acid Templated Peptides”, *Journal of Tissue Engineering and Regenerative Medicine*, 2020
7. Yaralı Z.B, Onak G., Karaman O., “Effect of Integrin Binding Peptide on Vascularization of Scaffold-Free Microtissue Spheroids” *Tissue Engineering and Regenerative Medicine*, 2020
8. Onak G., Karaman O. “Accelerated mineralization on nanofibers via non-thermal atmospheric plasma assisted glutamic acid templated peptide conjugation”, *Regenerative Biomaterials*, 2019
9. Onak G., Şen M., Horzum Polat N., Ercan U.K, Yarali Z.B., Garipcan B., Karaman O. “Aspartic and Glutamic Acid Templated Peptides Conjugation on Plasma Modified Nanofibers for Osteogenic Differentiation of Human Mesenchymal Stem Cells: A Comparative Study”, *Scientific Reports*, 2018, 8
10. Onak G., and O. Karaman. "Osteogenic Differentiation of Human Mesenchymal Stem Cells on Osteopontin Mimetic Peptides Modified Electrospun Nanofibers." *Tissue Engineering Part A*. Vol. 23. 140 Huguenot Street, 3rd Fl, New Rochelle, Ny 10801 USA: Mary Ann Liebert, Inc, 2017.
11. Onak G., Demirci E.A., Kahraman E., Karaman O., "Integrin binding peptide promotes in vitro wound closure in the L929 mouse fibroblasts" *The European Research Journal*, 2017.